ELECTROCHEMISTRY AND SPECTROELECTROCHEMISTRY OF SAPPHYRINS, OPEN-CHAIN PENTAPYRROLES, COBALT CORROLES AND COBALT DIPYRRIN-BISPHENOLS

A Dissertation Presented to

the Faculty of the Department of Chemistry

University of Houston

In Partial Fulfillment

of the Requirements for the Degree

Doctor of Philosophy

By

Wenqian Shan

May 2019

ELECTROCHEMISTRY AND SPECTROELECTROCHEMISTRY OF SAPPHYRINS, OPEN-CHAIN PENTAPYRROLES, COBALT CORROLES AND COBALT DIPYRRIN-BISPHENOLS

Wenqian Shan

APPROVED:

Dr. Karl M. Kadish

Dr. Thomas S. Teets

Dr. Melissa L. Zastrow

Dr. Ognjen Miljanic

Dr. Tuan D. Phan

Dean, College of Natural Sciences and Mathematics

Dedication

This dissertation is dedicated to

my parents

Jialong Shan (单家龙) and Pin Zhou (周蘋)

Acknowledgements

I would like to thank my supervisor, Dr. Karl M. Kadish for his invaluable scientific guidance and support during my years in his laboratory.

I would like to express my sincere gratitude to my parents for their love, support and encouragement through my graduate years.

I would like to thank my collaborators, Professor Claude P. Gros and his colleagues from Institut de Chimie Moléculaire de l'Université de Bourgogne (ICMUB), in Dijon, France for their scientific comments and for providing the compounds investigated in this dissertation. I also would like to thank Professor Abhik Ghosh and Professor Jeanet Conradie for their contribution to the projects.

I wish to especially thank Dr. Zhongping Ou in our group for sharing his knowledge and giving me advice. I also appreciate the scientific discussions with Professor Muniappan Sankar, Professor Hong Wang, and Professor Dorota Gryko for sharing their knowledge and research experience with me during ICPP conferences and ECS Meeting.

I am gratefully acknowledge financial support provided by the Robert A. Welch Foundation.

Finally, I appreciate all of my colleagues and friends I have met at UH. This dissertation would not have been completed without every great person who helped me during my Ph. D. years.

ELECTROCHEMISTRY AND SPECTROELECTROCHEMISTRY OF SAPPHYRINS, OPEN-CHAIN PENTAPYRROLES, COBALT CORROLES AND COBALT DIPYRRIN-BISPHENOLS

A Dissertation Presented to

the Faculty of the Department of Chemistry

University of Houston

In Partial Fulfillment

of the Requirements for the Degree

Doctor of Philosophy

By

Wenqian Shan

May 2019

Abstract

For decades, pyrrolic complexes have attracted enormous scientific attention in various fields because of the potential applications in medicine and energy storage. In this thesis, about 31 pyrrolic compounds are studied, focusing on their spectroscopic and electrochemical properties along with characterizations by various other methods. The general introduction for the investigated pentapyrolic, tetrapyrrolic and dipyrolic complexes (Chapter 1), as well as the used experimental methods (Chapter 2), are given prior to the data and discussions.

Firstly, the spectral properties, protonation reactions, and electrochemistry of open-chain pentapyrroles and sapphyrins with various *meso*-tetraaryl substituents are discussed (Chapter 3 and 4) along with the protonation-initiated conversion of pentapyrroles to sapphyrins upon oxidation. The second part (Chapters 5, 6 and 7) is dedicated to a series of studies on electrochemistry and spectroelectrochemistry for the cobalt corroles axially ligated with bis(pyridine), mono(DMSO) and bis(ammonia). The last part (Chapter 8) presents the ligand noninnocence in cobalt dipyrrin-bisphenols as to their electrochemistry and spectroscopic properties in nonaqueous media. The potentials for each electrode reaction for all investigated pyrrolic complexes were measured by cyclic voltammetry and the electron-transfer mechanisms evaluated by analysis of the electrochemical data combined with UV−visible spectra of the neutral, electroreduced, and electroxidized forms of the investigated pyrrolic compounds.

Table of Contents

List of Abbreviations

Abbreviation	Meaning
A or Abs.	absorbance
CE	counter electrode
CH_2Cl_2	dichloromethane
Cor	corrole
CV	cyclic voltammetry
DFT	density functional theory
DMF	*N*, *N*-dimethylformamide
DMSO	dimethylsulfoxide
DPP	dipyrrin-bisphenol
$\Delta E_{1/2}$	difference in half-wave potentials between two redox reactions
$E_{1/2}$	half-wave potential (V)
E_p	peak potential (by cyclic voltammetry)
E_{pa}	anodic peak potential (by cyclic voltammetry)
E_{pc}	cathodic peak potential (by cyclic voltammetry)
eq.	equivalent
ε	molar absorptivity
EPR	electron paramagnetic resonance
HOMO	highest occupied molecular orbital
i_{pa}	anodic peak current (by cyclic voltammetry)
i_{pc}	cathodic peak current (by cyclic voltammetry)
LUMO	lowest unoccupied molecular orbital
λ_{max}	wavelength at a specific peak maximum
NMR	nuclear magnetic resonance

Ox 1 or 1st ox.	the first oxidation
PhCN	benzonitrile
PPy	open-chain pentapyrrole
Py	pyridine
RE	reference electrode
Red 1 or 1st red.	the first reduction
Red 2 or 2nd red.	the second reduction
Sap	sapphyrin
SCE	saturated calomel electrode
SI	supporting information
TBAP	tetra-*n*-butylammonium perchlorate
vs. or vs	versus
WE	working electrode

List of Charts

List of Figures

List of Tables

List of Schemes

1

Introduction

1.1 Sapphyrin and Open-Chain Pentapyrrole

1.1.1 Synthesis and Spectroscopic Characterizations

The pyrrolic macrocycle, sapphyrin, was initially discovered by Woodward more than 50 years ago.[1] As one of the first known 'expanded porphyrins', the sapphyrins were named after their intense blue-green color.[2] As originally formulated by Woodward, this 22π-electron pentapyrrolic macrocycle contains a single direct link and four methine bridges between the pyrrolic subunits (Figure 1-1a). The synthesis strategy for these β-pyrrole substituted sapphyrins (Figure 1-1c) in Woodward's work involves a MacDonald-type "3+2" condensation between bipyrrolic and tripyrroane precursors,[3] which was developed by Grigg and Johnson,[4] as well as by Sessler.[5, 6]

More efforts have contributed to sapphyrin synthesis. During the evaluation of the Rothethund synthesis by Latos-Grazynzki team,[7] they found tetraphenylsapphyrin as a minor byproduct during the synthesis of 'N-confused' porphyrin, which contains an inverted pyrrolic ring. In 2001, one *meso*-aryl sapphyrin was obtained with very high yield by oxidation of the corresponding open-chain pentapyrrole by iodine or oxygen.[8] Since then, the open-chain pentapyrroles (Figure 1-1b), first isolated as major side-products in the synthesis of corrole,[9] have attracted great attention as synthetic precursors for the respective *meso*-aryl sapphyrins.[8-15]

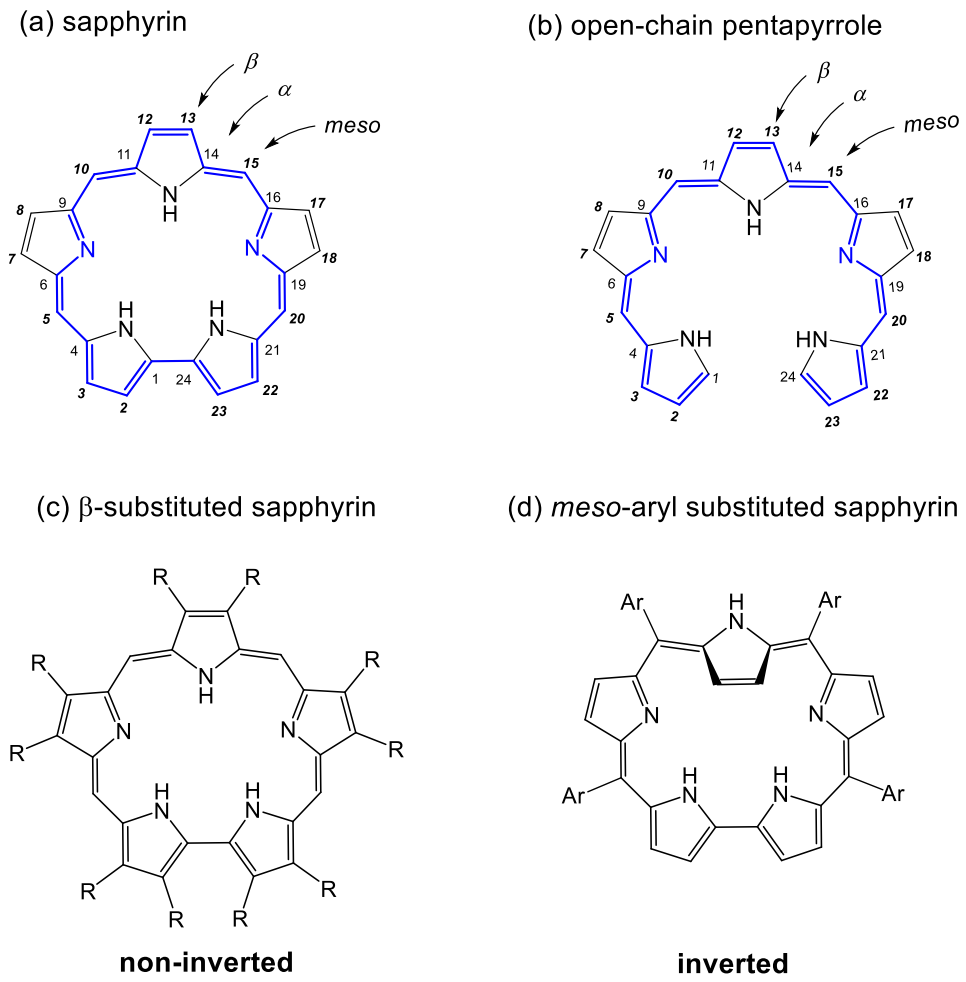

Figure 1-1. Structures of (a) sapphyrin and (b) open-chain pentapyrrole with IUPAC numbering system with the conjugated 22π-system given in blue and bold, as well as structures of (c) β-substituted sapphyrin and (d) *meso*-aryl substituted sapphyrin with inverted pyrrole ring.

As a typical porphyrinoid-type compound, sapphyrin shows an intense Soret band and a series of Q bands with lower intensity in their electronic spectrum, as well as for the mono- and diprotonated derivatives. For example, the electronic spectrum of tetraphenylsapphyrin displays split Soret bands at 439 and 518 nm, and four Q bands in the 640-790 nm spectral region.[7]

The characteristic ^{1}H-NMR signals for sapphyrin can come from *meso*-H on the methine and the β-H and NH groups on the subunit pyrroles. In the case of (decamethyl)sapphyrin,[6] for example, the signals assigned to the two sets of *meso*-H are well-resolved and appearing at 11.51 and 11.70 ppm, while the internal pyrrole NH groups exhibit broader signals at -5.46, -5.0 and -4.84 ppm in a 2:1:2 ratio.

The ^{1}H-NMR spectrum of the 'inverted sapphyrin', tetraphenylsapphyrin, differs from that of previously studied 'normal sapphyrin', in which signals of the exterior β-pyrrolic protons and the exterior NH proton appear at 9.0-10.2 and 12.2 ppm, while the β-pyrrolic protons and NH protons inside the core have signals at -1.5 and -2.58 ppm respectively.[7] The inverted pyrrolic ring of the sapphyrin will flip back to a planar conformation in acidic solution, which is confirmed by change in the upfield NH resonance pattern in ^{1}H-NMR. This conformational change upon protonation is considered as a property unique to *meso*-aryl substituted sapphyrins, which has also been reported by several following studies (Figure 1-1d).[12, 14]

Because of the expanded aromatic structure in sapphyrin as compared to porphyrin, a significant 30 to 60 nm red-shift for the Soret band is observed, while the ^{1}H

NMR spectra of sapphyrins sustain a large diamagnetic ring current with characteristic diatropic ring current effects. Both the optical and NMR data indicate that sapphyrins have a low-energy HOMO-LUMO gap, which will also be discussed in the latter section of electrochemistry.[2]

Three *meso*-aryl substituted sapphyrins will be described in Chapter 3 and 4, which were synthesized from corresponding open-chain pentapyrroles according to the method discussed above. The spectroscopic properties were also characterized for both the newly synthesized *meso*-aryl sapphyrins and a series of open-chain pentapyrroles. Also, two crystal structures of open-chain pentapyrroles will be given and compared with previous reported analogues. The results in Chapter 3 and 4 have been published in 2017 and 2019.[15, 16]

1.1.2 Acid-Base Properties and Related Reactions

In the free-base form, both pentapyrrolic derivatives, sapphyrin and open-chain pentapyrrole, contain three pyrrolic NH groups and two 'imine-type' nitrogens. The possible addition and abstraction of protons can be observed for both pentapyrrolic derivatives.

For the sapphyrin macrocycle, the two 'imine-type' nitrogens are more basic than the ones in porphyrin compounds, which can undergo step-wise protonations with two protons.[12, 15] The diprotonated derivatives are the most stable forms for sapphyrin complexes and imparts unusual anion binding properties via hydrogen bonding.[17, 18]

The deprotonation reaction is harder but also can occur on the pyrrole NH groups of sapphyrins, in which one proton will be abstracted from the sapphyrin.[13]

In the case of open-chain pentapyrrole, one-step-two-proton processes will occur for both the protonation and deprotonation reactions. The diprotonated open-chain pentapyrroles can undergo facile ring closure reactions, which can yield corresponding sapphyrins under O_2 or with certain oxidizing agent.[14-16]

Chapter 3 and 4 will discuss the protonation reactions of newly-synthesized sapphyrins and pentapyrroles and report the calculated equilibrium constants for both series of pentapyrrolic compounds. Moreover, the protonation-initiated ring closure reactions from open-chain pentapyrrole to corresponding sapphyrins will also be studied.

1.1.3 Electrochemistry

Enormous numbers of electrochemical studies have been reported for porphyrioid complexes, such as porphyrins and corroles.[19, 20] However, only few electrochemical characterizations can be found for sapphyrins or open-chain pentapyrroles in earlier work.[21] Detailed studies on electrochemistry of *meso*-aryl substituted sapphyrins and open-chain pentapyrroles has been reported in 2013 by our group,[12, 13] which give an insight of the electron transfer mechanism, HOMO-LUMO gap, as well as the dependency of solvents, substituents on the redox reactions for these pentapyrrolic compounds.

In Chapters 3 and 4, electrochemical data will be given and analyzed for all investigated sapphyrins and pentapyrroles, as to their solvent and substituents dependency, as well as comparison with porphyrins and corroles.

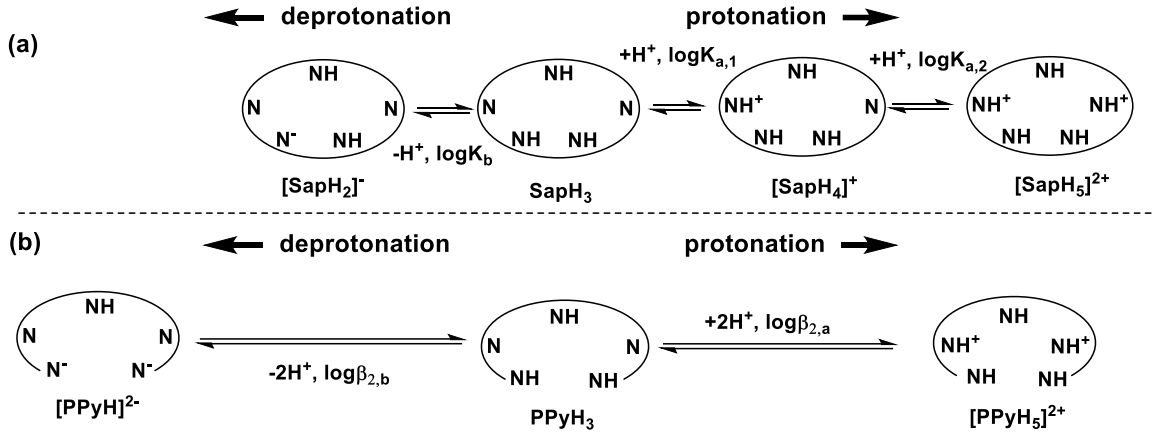

Scheme 1-1. Protonation and deprotonation reactions of (a) sapphyrin ($SapH_3$) and (b) open-chain pentapyrrole ($PPyH_3$).

1.2 Corroles

1.2.1 General Information of Corroles

Similar to 'well-known' porphyrins, corroles are also tetrapyrrolic macrocycle compounds containing four pyrrole subunits. The first corrole was reported in 1965,[22] which have been closely identified with porphyrins in recent decades. Because of the similarity to porphyrin and its unique properties, the number of publications on corrole chemistry has increased significantly over the last two decades. [20, 23-32]

Unlike porphyrin, there are only 19 carbons in corrole ring because two of the pyrroles are connected by one direct bond at their α-carbon positions (Figure 1-2a). The lack of C-20 in corrole results in the smaller cavity, reduced symmetry and nonplanarity of the macrocycle as compared to porphyrin. This structural difference also causes the corrole macrocycle to be trivalent as compared to divalent in the case of porphyrins, with steric strain forcing the corrole molecule slightly out of plane of the four nitrogen.[33, 34] In addition, corroles are structurally similar to corrins (Figure 1-2b), which include cobalamin, the major component of Vitamin B_{12} (Figure 1-2c).

The synthesis of corrole derivatives have been developed by different groups with substituents on the β-pyrrole positions, the *meso*-positions, or even on both positions in the cases of highly-substituted corroles (see Figure 2-1a).[30]

1.2.2 Redox-Active Metallocorroles

In a free-base corrole, three of the four pyrrole nitrogens have protons. The fully deprotonated corrole ligand has -3 charge, which can complex with numerous transition

and main-group metal ions with the oxidation states ranging from +1 to +6. The central metal ion is four-coordinate with the tetradentate corrole ligand, and it can be further ligated with one or two axial ligand(s) to form five- or six-coordinate complexes.

The corrole macrocycle possesses a highly conjugated π-ring system, which is an ideal location for the addition and abstraction of electrons. Most neutral corrole macrocycles can be oxidized by two electrons and reduced by one. Moreover, many metal-centered redox processes have been reported for corroles with electroactive central metal ions, such as nickle, copper, iron, cobalt, manganese, silver, gold, platinum, chromium, and ruthenium, etc. Recently, a review of electrochemistry of corroles has been published by our group,[20] which gives insight to the redox reactions of corroles and a better understanding of these molecules for their potential applications in the field of medicine and material science.

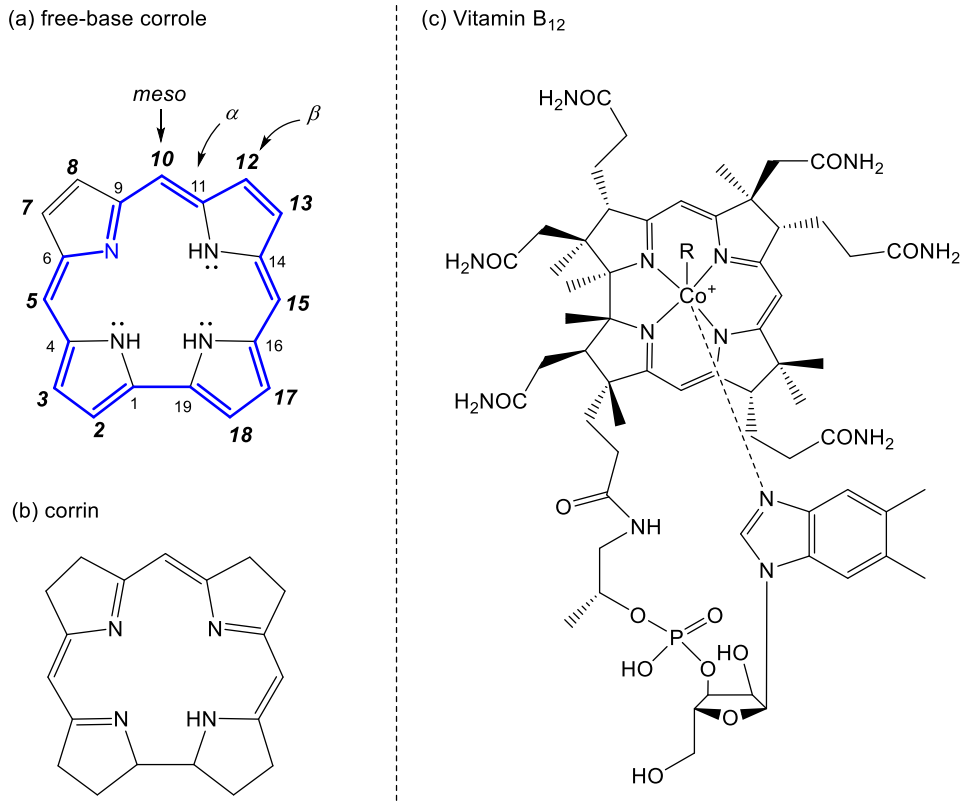

Figure 1-2. Structures of (a) free-base corrole with IUPAC numbering system with the conjugated 18π-system given in blue and bold, (b) corrin and (c) Vitamin B_{12}.

1.2.3 Cobalt Corroles

Cobalt corrole is one of most studied groups in metallocorroles for its rich redox chemistry,[20, 35, 36] as well as its possible use as a catalyst in a variety of reactions, such as oxygen reduction[32] and water oxidation.[37]

Multiple redox reactions can be observed for both β-substituted and *meso*-substituted cobalt corroles.[35, 36] The formal Co(III) in neutral cobalt corrole can undergo a facile reduction to generate Co(II) species, followed by a further reduction at more negative potential that may or may not generate Co(I) species.[36] Several oxidation processes also can be seen in various solvents. [35, 36] The dimerization behavior has been observed during the electrooxidations of the β-substituted cobalt corroles with dependency on solvent and substituents.[38] The existence of the large substituent groups on the *meso*-positions will decrease the planarity of the corrole, which weakens the π-π interactions. Meanwhile, the axial ligated coordinating solvent molecules enlarge the distance between two corrole molecules, which will eliminate the dimerization as well.[35]

The ligand noninnocence is an interesting property for corrole with various metal ions.[39] In the case of cobalt corrole, the ligand noninnocence also plays an important role for the studies on spectral properties and redox reactions.[40] Formally, the fully deprotonated corrole ligand (Cor) shows -3 charge and can be metallated with an M(III) ion to form a metallocorrole complex CorM. The corrole ligand can be innocent or noninnocent, depending upon the type and oxidation state of the central metal ion[29] and the axial ligand binding.[41-43]

In the case of cobalt corrole, the corrole ligand can be innocent as $Co^{III}Cor^{3-}$ and also can be noninnocent which can be described as containing a Co^{II} metal ion and a ligand radical, i.e., $Co^{II}Cor^{\bullet 2-}$. An equilibrium might exist between the two forms of the compounds as shown in Equation 1-1.

$$Co^{III}Cor^{3-} \rightleftharpoons Co^{II}Cor^{\bullet 2-} \qquad (1\text{-}1)$$

In Chapter 5 to 7, a series of cobalt corroles with one or two axial ligands including pyridine, DMSO, CO and NH_3 will be synthesized and characterized as to their spectroscopic and electrochemical properties. The innocence and noninnocence of the cobalt corroles will be discussed as a function of axial coordination. The effects of *meso*-substituents for both redox potentials and spectroscopic properties will be discussed with each axial ligand. The binding constants of several ligands to the central cobalt ion will be reported. The mechanisms of the electrode reactions for the studied cobalt corrole complexes, which can vary upon axial ligation will also be discussed in detail. The results in Chapter 5 to 7 were published in 2018.[41-43]

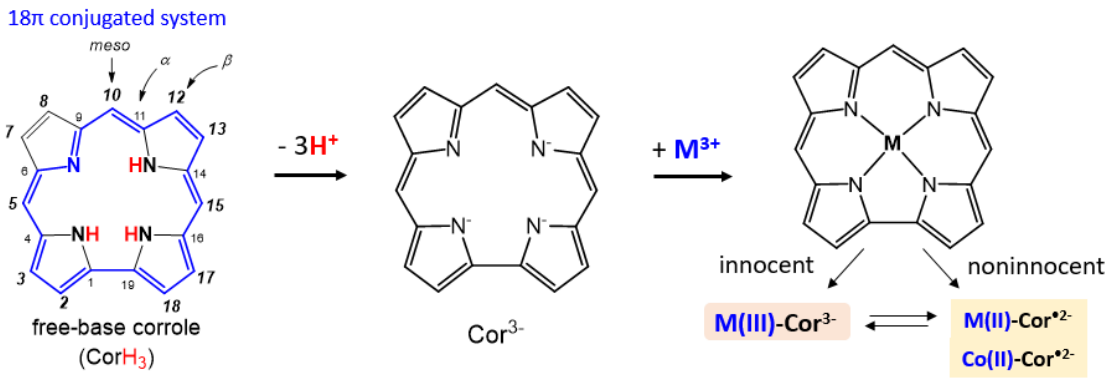

Figure 1-3. Corrole structures and innocence and noninnocence of the metallocorroles.

1.3 Dipyrrin-Bisphenols

1.3.1 Dipyrrins

Dipyrrin (or dipyrromethene) can be considered as half porphyrin, which contains two pyrrole rings bridged via a methine group and has a planar molecule structure with a conjugated π-system. (Figure 1-4a). The deprotonated form of dipyrrin can act as a monovalent and bidentate ligand (dipyrrinato ligand) that can ligate various cations. The most famous dipyrrin is the boron complexes (Figure 1-4b), BODIPY (boron dipyrromethene, 4,4-difluoro-4-bora-3a,4a-diaza-s-indacene), which has been studied over the past two decades as a popular fluorophore with applications in labeling, imaging and sensors.[44-46] The dipyrrinato ligand also can bind metal cations, such as Zn^{2+}, Cu^{2+}, Ni^{2+}, Fe^{2+}, and Co^{2+}, to form bis(dipyrrinato) and tri(pyrrinato) metal complexes (Figure 1-4c).[47]

Normally, like other porphyrinoid compounds, the dipyrrin structure can be substituted on β-positions of the two pyrrole rings or *meso*-position of the methine bridge. But, in this linear dipyrrin molecule, substituents can also be put on the α-positions of the two pyrrole rings. The bis(phenolate)-dipyrrin (dipyrrin-bisphenol, or N_2O_2-type dipyrrin)[48] and bis(2-aminophenyl)-dipyrrin[49] ligands have been developed with interesting properties and functions.

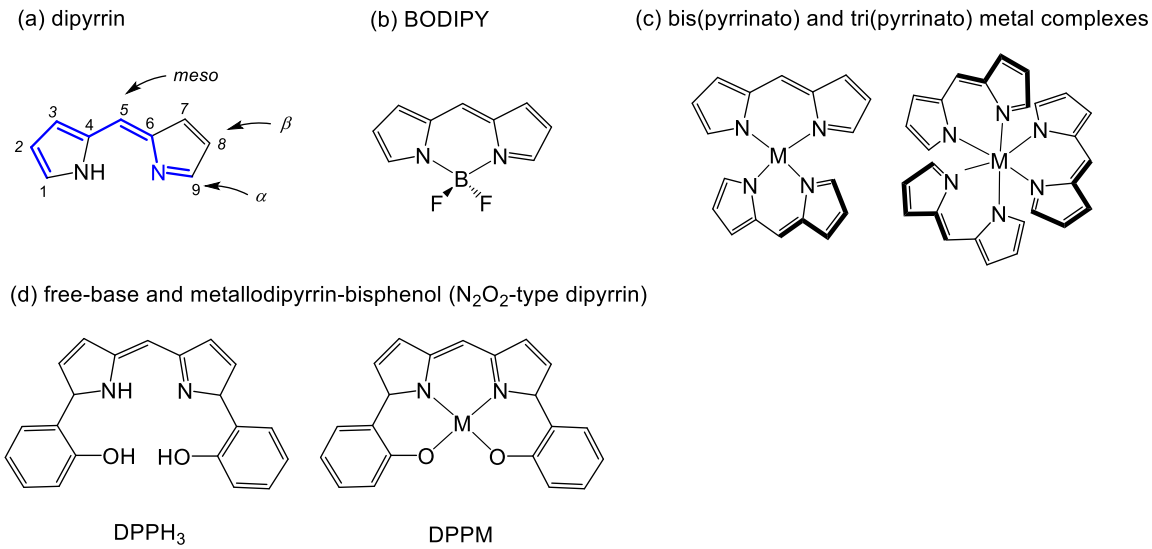

Figure 1-4. Structures of (a) dipyrrin with IUPAC numbering system with the conjugated π-system given in blue and bold, (b) BODIPY, (c) pyrrinato metal complexes and (d) free-base and metallodipyrrin-bisphenols ($DPPH_3$ and DPPM).

1.3.2 Cobalt Dipyrrin-Bisphenols

The first dipyrrin-bisphenol ligand and its boron complexes was reported in 1999 and is a fluorophore.[50] The free-base dipyrrin-bisphenol ($DPPH_3$) has two phenoxy groups at the 1,9-positions of the dipyrrin core (Figure 1-4d). The fully deprotonated dipyrrin-bisphenol has been described as N_2O_2-type dipyrrin ligand, which can behave as a tridentate or tetradentate ligand for main-group-element or metal complexes (DPPM) including B, Al, Ni, Co, Mn, Si, Ge, Sn, etc.[48]

Similar to corrole, the fully deprotonated DPP ligand shows -3 charge, as shown in Figure 1-5. Metallation of the dipyrrin-bisphenol ligand DPP^{3-} with a M(III) ion leads to a DPPM complex where the ligand can be innocent or noninnocent, depending on the type and oxidation state of the central metal ion[51] and the axial ligand binding.[52] The formal oxidation state of the cobalt metal ion in the neutral bis(phenolate)dipyrrin complexes is +3, but the dipyrrin ligand can be noninnocent in the nonbonding CH_2Cl_2 solvent with the investigated compounds in Chapter 8, then being described as containing a Co^{II} metal ion and a ligand radical, i.e., $Co^{II}L^{\bullet 2-}$. An equilibrium might exist between the two forms of the compounds as shown in Equation 1-2.

$$Co^{III}DPP^{3-} \rightleftharpoons Co^{II}DPP^{\bullet 2-} \qquad (1\text{-}2)$$

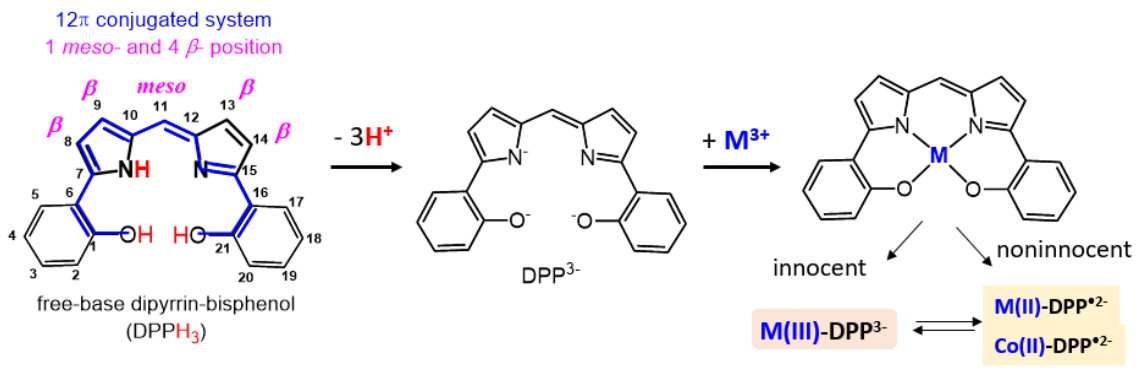

Figure 1-5. Dipyrrin-bisphenol structures and innocence and noninnocence of the metallodipyrrin-bisphenols.

Chapter 8 will present three newly-synthesized cobalt dipyrrin-bisphenol complexes (DPPCo) with different *meso*-aryl groups, and characterized as to their electrochemistry and spectroscopic properties, along with the axial ligation of DPPCo and noninnocence of this DPP ligand. The results in Chapter 8 have been published in 2019.[52]

1.4 References

[1] R. B. Woodward, *Presented in the Aromaticity Conference* **1966**.

[2] A. Jasat, D. Dolphin, Expanded Porphyrins and Their Heterologs, *Chem. Rev.* **1997**, *97*, 2267-2340.

[3] V. J. Bauer, D. L. J. Clive, D. Dolphin, J. B. Paine, III, F. L. Harris, M. M. King, J. Loder, S. W. C. Wang, R. B. Woodward, Sapphyrins: novel aromatic pentapyrrolic macrocycles, *J. Am. Chem. Soc.* **1983**, *105*, 6429-6436.

[4] M. J. Broadhurst, R. Grigg, A. W. Johnson, Synthesis of 22 π-electron macrocycles. Sapphyrins and related compounds, *J. Chem. Soc., Perkin Trans. 1* **1972**, 2111-2116.

[5] J. L. Sessler, M. J. Cyr, V. Lynch, E. McGhee, J. A. Ibers, Synthetic and structural studies of sapphyrin, a 22-π-electron pentapyrrolic "expanded porphyrin", *J. Am. Chem. Soc.* **1990**, *112*, 2810-2813.

[6] J. L. Sessler, M. Cyr, A. K. Burrell, Sapphyrins and heterosapphyrins, *Tetrahedron* **1992**, *48*, 9661-9672.

[7] P. J. Chmielewski, L. Latos-Grazynski, K. Rachlewicz, 5,10,15,20-Tetraphenylsapphyrin. Identification of a pentapyrrolic expanded porphyrin in the Rothemund synthesis, *Chem. Eur. J.* **1995**, *1*, 68-73.

[8] L. Simkhovich, S. Rosenberg, Z. Gross, Facile synthesis of a novel sapphyrin and its rhodium(I) complex, *Tetrahedron Lett.* **2001**, *42*, 4929-4931.

[9] Z. Gross, N. Galili, L. Simkhovich, I. Saltsman, M. Botoshansky, D. Blaeser, R. Boese, I. Goldberg, Solvent-Free Condensation of Pyrrole and Pentafluorobenzaldehyde: A Novel Synthetic Pathway to Corrole and Oligopyrromethenes, *Org. Lett.* **1999**, *1*, 599-602.

[10] L. Naumovski, M. Sirisawad, P. Lecane, J. Chen, J. Ramos, Z. Wang, C. Cortez, D. Magda, P. Thiemann, G. Boswell, D. Miles, G. Cho Dong, L. Sessler Jonathan, R. Miller, Tumor localization and antitumor efficacy of novel sapphyrin compounds, *Mol. Cancer Ther.* **2006**, *5*, 2798-2805.

[11] B. Koszarna, D. T. Gryko, Efficient Synthesis of meso-Substituted Corroles in a H2O-MeOH Mixture, *J. Org. Chem.* **2006**, *71*, 3707-3717.

[12] M. Yuan, Z. Ou, Y. Fang, S. Huang, Z. Xue, G. Lu, K. M. Kadish, Synthesis, Characterization, Protonation Reactions, and Electrochemistry of Substituted Open-Chain Pentapyrroles and Sapphyrins in Nonaqueous Media, *Inorg. Chem.* **2013**, *52*, 6664-6673.

[13] Z. Ou, D. Meng, M. Yuan, W. Huang, Y. Fang, K. M. Kadish, Deprotonation Reactions and Electrochemistry of Substituted Open-Chain Pentapyrroles and Sapphyrins in Basic Nonaqueous Media, *J. Phys. Chem. B* **2013**, *117*, 13646-13657.

[14] W. Huang, Z. Ou, X. Chen, Z. Xue, G. Lu, H. Wang, J. Xiao, Y. Fang, K. M. Kadish, A facile synthetic route to meso-tetraaryl substituted N-5 sapphyrins and first single crystal X-ray analysis confirming the pyrrole inverted structure, *J. Porphyrins Phthalocyanines* **2015**, *19*, 794-802.

[15] W. Shan, N. Desbois, V. Blondeau-Patissier, M. L. Naitana, V. Quesneau, Y. Rousselin, C. P. Gros, Z. Ou, K. M. Kadish, Synthesis, characterization and electrochemistry of open-chain pentapyrroles and sapphyrins with highly electron-withdrawing meso-tetraaryl substituents, *Chem. - Eur. J.* **2017**, *23*, 12833-12844.

[16] W. Shan, V. Quesneau, N. Desbois, V. Blondeau-Patissier, M. L. Naitana, Y. Rousselin, C. P. Gros, Z. Ou, K. M. Kadish, Synthesis, electrochemistry, protonation and X-ray analysis of meso-aryl substituted open-chain pentapyrroles, *J. Porphyrins Phthalocyanines* **2019**, *23*, 213-222.

[17] J. L. Sessler, M. Cyr, H. Furuta, V. Kral, T. Mody, T. Morishima, M. Shionoya, S. Weghorn, Anion binding: a new direction in porphyrin-related research, *Pure Appl. Chem.* **1993**, *65*, 393-398.

[18] J. L. Sessler, A. Andrievsky, J. W. Genge, Anion binding by sapphyrins, *Adv. Supramol. Chem.* **1997**, *4*, 97-142.

[19] K. M. Kadish, E. Van Caemelbecke, G. Royal, Electrochemistry of metalloporphyrins in nonaqueous media, **2000**, *8*, 1-114.

[20] Y. Fang, Z. Ou, K. M. Kadish, Electrochemistry of Corroles in Nonaqueous Media, *Chem. Rev.* **2017**, *117*, 3377-3419.

[21] A. Srinivasan, S. K. Pushpan, M. R. Kumar, S. Mahajan, T. K. Chandrashekar, R. Roy, P. Ramamurthy, meso-Aryl sapphyrins with heteroatoms; synthesis, characterization, spectral and electrochemical properties, *J. Chem. Soc., Perkin Trans. 2* **1999**, 961-968.

[22] A. W. Johnson, I. T. Kay, Corroles. I. Synthesis, *J. Chem. Soc.* **1965**, 1620-1629.

[23] R. Paolesse, *Syntheses of corroles, Vol. 2*, Academic Press, **2000**, pp. 201-232.

[24] C. Erben, S. Will, K. M. Kadish, *Metallocorroles: Molecular structure, spectroscopy and electronic states, Vol. 2*, Academic Press, **2000**, pp. 233-300.

[25] R. Guilard, J.-M. Barbe, C. Stern, K. M. Kadish, in *The Porphyrin Handbook, Vol. 18* (Eds.: K. M. Kadish, K. M. Smith, R. Guilard), World Scientific Publishing Co. Pte. Ltd., Singapore, **2003**, pp. 303-349.

[26] I. Aviv, Z. Gross, Corrole-based applications, *Chem. Commun.* **2007**, 1987-1999.

[27] L. Flamigni, D. T. Gryko, Photoactive corrole-based arrays, *Chem. Soc. Rev.* **2009**, *38*, 1635-1646.

[28] K. E. Thomas, A. B. Alemayehu, J. Conradie, C. M. Beavers, A. Ghosh, The Structural Chemistry of Metallocorroles: Combined X-ray Crystallography and Quantum Chemistry Studies Afford Unique Insights, *Acc. Chem. Res.* **2012**, *45*, 1203-1214.

[29] A. Ghosh, Electronic Structure of Corrole Derivatives: Insights from Molecular Structures, Spectroscopy, Electrochemistry, and Quantum Chemical Calculations, *Chem. Rev.* **2017**, *117*, 3798-3881.

[30] R. Orlowski, D. Gryko, D. T. Gryko, Synthesis of Corroles and Their Heteroanalogs, *Chem. Rev.* **2017**, *117*, 3102-3137.

[31] R. D. Teo, J. Y. Hwang, J. Termini, Z. Gross, H. B. Gray, Fighting Cancer with Corroles, *Chem. Rev.* **2017**, *117*, 2711-2729.

[32] A. Mahammed, Z. Gross, Metallocorroles as Electrocatalysts for the Oxygen Reduction Reaction (ORR), *Isr. J. Chem.* **2016**, *56*, 756-762.

[33] D. C. Hodgkin, H. R. Harrison, O. J. R. Hodder, Crystal and molecular structure of 8,12-diethyl-2,3,7,13,17,18-hexamethylcorrole, *J. Chem. Soc. B* **1971**, 640-645.

[34] B. F. Anderson, T. J. Bartczak, D. C. Hodgkin, Crystal and molecular structure of 8,12-diethyl-2,3,7,13,17,18-hexamethylcorrole hydrobromide, *J. Chem. Soc., Perkin Trans. 2* **1974**, 977-980.

[35] K. M. Kadish, J. Shao, Z. Ou, C. P. Gros, F. Bolze, J.-M. Barbe, R. Guilard, Alkyl- and Aryl-Substituted Corroles. 4. Solvent Effects on the Electrochemical and Spectral Properties of Cobalt Corroles, *Inorg. Chem.* **2003**, *42*, 4062-4070.

[36] K. M. Kadish, J. Shen, L. Fremond, P. Chen, M. El Ojaimi, M. Chkounda, C. P. Gros, J.-M. Barbe, K. Ohkubo, S. Fukuzumi, R. Guilard, Clarification of the Oxidation State of Cobalt Corroles in Heterogeneous and Homogeneous Catalytic Reduction of Dioxygen, *Inorg. Chem.* **2008**, *47*, 6726-6737.

[37] B. Mondal, K. Sengupta, A. Rana, A. Mahammed, M. Botoshansky, S. G. Dey, Z. Gross, A. Dey, Cobalt Corrole Catalyst for Efficient Hydrogen Evolution Reaction from H_2O under Ambient Conditions: Reactivity, Spectroscopy, and Density Functional Theory Calculations, *Inorg. Chem.* **2013**, *52*, 3381-3387.

[38] K. M. Kadish, V. A. Adamian, E. Van Caemelbecke, E. Gueletii, S. Will, C. Erben, E. Vogel, Electrogeneration of oxidized corrole dimers. Electrochemistry of (OEC)M Where M = Mn, Co, Ni, or Cu and OEC is the trianion of 2,3,7,8,12,13,17,18-octaethylcorrole, *J. Am. Chem. Soc.* **1998**, *120*, 11986-11993.

[39] A. Ghosh, T. Wondimagegn, A. B. J. Parusel, Electronic Structure of Gallium, Copper, and Nickel Complexes of Corrole. High-Valent Transition Metal Centers versus Noninnocent Ligands, *J. Am. Chem. Soc.* **2000**, *122*, 5100-5104.

[40] S. Ganguly, D. Renz, L. J. Giles, K. J. Gagnon, L. J. McCormick, J. Conradie, R. Sarangi, A. Ghosh, Cobalt- and Rhodium-Corrole-Triphenylphosphine Complexes Revisited: The Question of a Noninnocent Corrole, *Inorg. Chem.* **2017**, *56*, 14788-14800.

[41] V. Quesneau, W. Shan, N. Desbois, S. Brandes, Y. Rousselin, M. Vanotti, V. Blondeau-Patissier, M. Naitana, P. Fleurat-Lessard, E. Van Caemelbecke, K. M. Kadish,

C. P. Gros, Cobalt Corroles with Bis-Ammonia or Mono-DMSO Axial Ligands. Electrochemical, Spectroscopic Characterizations and Ligand Binding Properties, *Eur. J. Inorg. Chem.* **2018**, *2018*, 4265-4277.

[42] X. Jiang, M. L. Naitana, N. Desbois, V. Quesneau, S. Brandes, Y. Rousselin, W. Shan, W. R. Osterloh, V. Blondeau-Patissier, C. P. Gros, K. M. Kadish, Electrochemistry of Bis(pyridine)cobalt (Nitrophenyl)corroles in Nonaqueous Media, *Inorg. Chem.* **2018**, *57*, 1226-1241.

[43] X. Jiang, W. Shan, N. Desbois, V. Quesneau, S. Brandes, E. Van Caemelbecke, W. R. Osterloh, V. Blondeau-Patissier, C. P. Gros, K. M. Kadish, Mono-DMSO ligated cobalt nitrophenylcorroles: electrochemical and spectral characterization, *New J. Chem.* **2018**, *42*, 8220-8229.

[44] A. Loudet, K. Burgess, BODIPY dyes and their derivatives: Syntheses and spectroscopic properties, *Chem. Rev.* **2007**, *107*, 4891-4932.

[45] N. Boens, V. Leen, W. Dehaen, Fluorescent indicators based on BODIPY, *Chem. Soc. Rev.* **2012**, *41*, 1130-1172.

[46] A. Kamkaew, S. H. Lim, H. B. Lee, L. V. Kiew, L. Y. Chung, K. Burgess, BODIPY dyes in photodynamic therapy, *Chem. Soc. Rev.* **2013**, *42*, 77-88.

[47] R. Sakamoto, Bottom-up creation of functional low-dimensional materials based on metal complexes, *Bull. Chem. Soc. Jpn.* **2017**, *90*, 272-278.

[48] T. Nabeshima, M. Yamamura, G. J. Richards, T. Nakamura, Design and synthesis of dipyrrin complexes bearing unique structures, properties and functions, *Yuki Gosei Kagaku Kyokaishi* **2015**, *73*, 1111-1119.

[49] J. Moutet, C. Philouze, A. du Moulinet d'Hardemare, N. Leconte, F. Thomas, Ni(II) Complexes of the Redox-Active Bis(2-aminophenyl)dipyrrin: Structural, Spectroscopic, and Theoretical Characterization of Three Members of an Electron Transfer Series, *Inorg. Chem.* **2017**, *56*, 6380-6392.

[50] H. Kim, A. Burghart, M. B. Welch, J. Reibenspies, K. Burgess, Synthesis and spectroscopic properties of a new 4-bora-3a,4a-diaza-s-indacene (BODIPY) dye, *Chem. Commun.* **1999**, 1889-1890.

[51] M. Yamamura, H. Takizawa, Y. Gobo, T. Nabeshima, Stable neutral radicals of planar N2O2-type dipyrrin platinum complexes: hybrid radicals of the delocalized organic π-orbital and platinum d-orbital, *Dalton Trans* **2016**, *45*, 6834-6838.

[52] W. Shan, N. Desbois, S. Pacquelet, B. Stephane, Y. Rousselin, J. Conradie, A. Ghosh, C. P. Gros, K. M. Kadish, Ligand Noninnocence in Cobalt Dipyrrin-Bisphenols: Spectroscopic, Electrochemical, and Theoretical Insights Indicating an Emerging Analogy with Corroles, *Inorg. Chem.* **2019**, Ahead of Print. (DOI: 10.1021/acs.inorgchem.8b03006)

2

Experimental Methods

2.1 Chemicals

Dichloromethane (CH_2Cl_2, 99.8%) from EMD Chemicals Inc. was used for electrochemistry without further purification. Benzonitrile (PhCN) was purchased from Sigma-Aldrich Chemical Co. and distilled over P_2O_5 under vacuum prior to use. Dimethyl sulfoxide (DMSO), pyridine (Py, HPLC) and tetra-n-butylammonium perchlorate (TBAP), used as supporting electrolyte, were purchased from Sigma-Aldrich Chemical Co.. High purity N_2 or argon gas from Trigas was used to deoxygenate the solution before each electrochemical or spectroelectrochemical experiment. Trifluoroacetic acid (TFA) was obtained from Sigma-Aldrich Chemical Co. and used as received.

2.2 Studied Compounds

All compounds characterized in this dissertation were obtained from our collaborators, Dr. Claude P. Gros from Institut de Chimie Moléculaire de l'Université de Bourgogne (ICMUB), in Dijon, France. The UV-visible spectrum of each compound was measured before carrying out experiments in Houston and our spectral data were compared to that provided by our collaborator or published in the literature.

2.3 Instrumentation

2.3.1 UV-Visible Spectroscopy

UV-visible spectra of investigated compounds under electrochemical conditions (at 10^{-3} M, with 0.1 M TBAP, in certain solvent) in this dissertation were measured in a pair of 0.1 mm round quartz cells. The volume of the solution for this

experiment is about 50 μL.

For other UV-visible spectral measurements, such as spectroscopically monitored titrations, the concentration of the each investigated compound in this dissertation is about 10^{-5} M in the specified solvent. The experiments were carried out in a 1.0 cm path length glass or quartz cell and the measurement of the neat solvent as the background is needed before measuring the investigated compounds. The volume of the solution for each measurement should be 2 to 3.5 mL.

All UV-visible spectra were recorded with a Hewlett-Packard Model 8453 diode array spectrophotometer.

2.3.2 Electrochemistry

Cyclic voltammetry was used for all electrochemical characterization in this dissertation and was carried out with an EG&G model 173 potentiostat/galvanostat at room temperature (22 ± 1 °C in most of the cases). A homemade three-electrode system with a special electrochemistry cell was used, consisting of glassy carbon working electrode (diameter = 3 mm), a platinum wire counter electrode, and a homemade saturated calomel reference electrode (SCE) (See Figure 2-1). The SCE was separated from the bulk of the solution by a fritted glass bridge of low porosity, which contained the solvent/supporting electrolyte mixture. All potentials measured by cyclic voltammetry are referenced to the SCE. High purity N_2 from Trigas was used to deoxygenate the solution and was kept over the solution during each experiment.

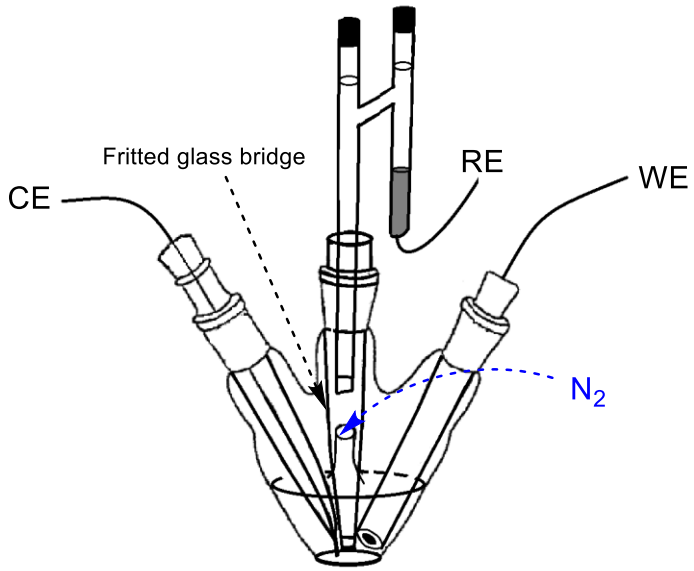

Figure 2-1. Schematic illustration of the utilized electrochemical cell. WE, CE, and RE represent for the working electrode, counter electrode and reference electrodes.

Cyclic voltammetry (CV) is a useful and popular electrochemical technique for studying the reduction and oxidation processes of inorganic molecules.[1] The applied potential for the cyclic voltammetry measurement is ramped linearly versus time, and is measured against a reference electrode, which is SCE in this dissertation. Once it reached the end potential set in a CV experiment, the applied potential will go in the reverse direction to return the initial potential. This potential cycle can be repeated many times.

For example, as shown in Figure 2-2, the potential is initially scanned in a negative value for a reduction reaction, from the start point **A** at 0.0 V to the end point **C** at -2.0 V, and then it will go back to the initial potential 0.0 V at point **E** in the figure. The scan rate $\Delta E/\Delta t$ can range from 20 mV/s to 500 mV/s for the EG&G model 173 potentiostat/galvanostat. All cyclic voltammograms reported in this dissertation were recorded at 100 mV/s unless otherwise noted.

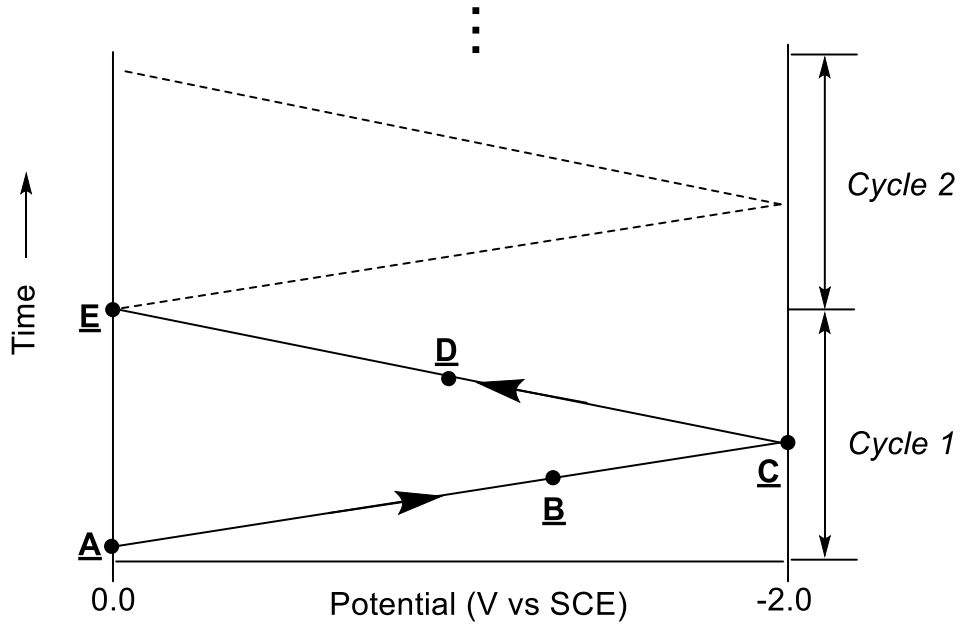

Figure 2-2. Schematic illustration of cyclic voltammetry excitation signal.

The curve shown in Figure 2-3 is cyclic voltammogram, which can be plotted from the current at the working electrode versus the applied potential. The compounds in this case undergoes a reversible one-electron reduction, which shows a 'duck' shape well-defined voltammogram as shown in the figure.[1] This redox process can be written as Equation 2-1.

$$M^+ + e^- \rightleftharpoons M \qquad (2\text{-}1)$$

When the potential applied at point **C** (in Figure 2-2), the cathodic (reduction) peak current i_{pc} has achieved, while the reoxidation peak current is given by i_{pa} when applied potential is at point **D**. Correspondingly, the cathodic (reduction) peak potential is labeled as E_{pc} while the anodic (oxidation) peak potential as E_{pa}, as shown in the Figure 2-3.

The factors which can affect the current in a voltammogram can be described by Ransdles-Sevcik equation,[2, 3] which is given in Equation 2-2:

$$i_P = (2.69 \times 10^5) n^{3/2} A C D^{1/2} v^{1/2} \qquad (2\text{-}2)$$

where i_P is the peak current in μA, n is the number of electrons transferred, A is the electrode area in cm^2, D is the diffusion coefficient of the species in cm^2/s and C is the bulk concentration of the species in mol/cm^3. For the compounds described in this thesis, n was almost always 1, while the value of D was about 10^{-6} cm^2/s.

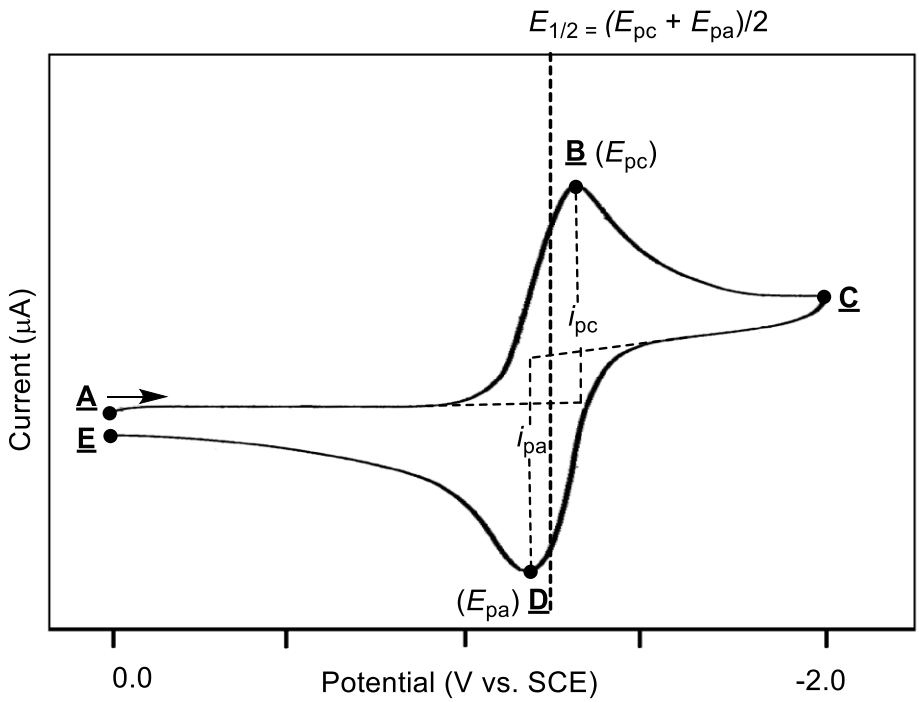

Figure 2-3. Schematic illustration of cyclic voltammogram.

2.3.3 Spectroelectrochemistry

Thin-layer UV-visible spectroelectrochemical experiments were carried out with the commercial Honeycomb spectrochemical cell purchased from Pine Research Instrumentation. In this three-electrode system, a platinum or gold working electrode and counter electrode are designed on a "honeycomb" electrode card and working together with a miniature Ag/AgCl reference electrode.

The patterned "honeycomb" electrode card that mounts easily inside a thin layer quartz cuvette. The path length of the electrode/slot is 1.7 mm. The volume of the cell is 1.5 mL. A special cuvette cap securely holds the honeycomb electrode card and a separate reference electrode in the proper position within the cuvette. The working electrode is perforated with a honeycomb pattern of holes, which allow light to pass through the electrode. The active surface of the working electrode includes a metal coating along the inner walls of the holes.

Potentials were applied and monitored with an EG&G PAR Model 173 Potentiostat. Time-resolved UV-visible spectra were recorded with a Hewlett-Packard Model 8453 diode array spectrophotometer. Argon gas from Trigas was used to deoxygenate the solution and was kept over the solution during each experiment.

2.4 Titration Techniques

Equilibrium constants for the binding of axial ligands to compounds can be determined using both spectral and electrochemical titration methods. A set of titrants in a range of concentrations were prepared for the specific ligand, and were quantitatively added to the investigated compound solution. UV-visible absorbance changes or the half-wave potential changes by cyclic voltammetry were recorded as a function of the free ligand concentration in the solution using methods described in the following section to obtain equilibrium constants and the coordination number.

Equilibrium constants for the loss or addition of protons to the investigated compounds were determined by monitoring the spectral changes in CH_2Cl_2 during titrations of the compounds with trifluoroacetic acid (TFA) in CH_2Cl_2. The acid titration reagents were prepared in CH_2Cl_2 with different concentrations of TFA. 10-100 Microliters of the reagents was added gradually to a 4.0 mL stock solution (~10^{-5} M) of the investigated compounds in CH_2Cl_2 and changes in the UV-vis spectra during the titration were analyzed as a function of the concentration of added acid using the Hill equation[4] ($K < 10^6$) or the Molar Ratio method[5] ($K \geq 10^6$) to calculate the equilibrium constants for proton addition.

2.4.1 Spectral Titration[4]

For the ligand binding reaction: $M + pL = ML_p$, the relationship between the concentration of the species in solution and the equilibrium constant, log K, is given by equation (2-1).

$$\log([ML_p]/[M]) = \log K + p \log [L] \quad (2\text{-}3)$$

Where [M] and $[ML_p]$ are the concentration of the unligated and ligated metalloporphyrin species and [L] is the free-ligand concentration in solution. If M and ML_p have different spectra, then we have:

$A_0 = \varepsilon_M b C_M$

$A_f = \varepsilon_{MLp} b C_{MLp}$

$A_i = \varepsilon_M b [M] + \varepsilon_{MLp} b [ML_p]$

Where C_M and C_{MLp} are the total concentration of M or ML_p, ε is the molar absorptivity and b is the path length, A_0 and A_f are the initial and final absorbance at a given wavelength (λ_{max}) for the species M and ML_p and A_i is the absorbance at λ_{max} at any point during the titration as shown in Figure 2-6.

According to the mass balance equation: $C_M = C_{MLp} = [M] + [ML_p]$, we have:

$A_i = \varepsilon_M b [M] + \varepsilon_{MLp} b [ML_p]$

$= \varepsilon_M b (C_M-[ML_p]) + \varepsilon_{MLp} b [ML_p]$

$= \varepsilon_M b C_M - \varepsilon_M b [ML_p] + \varepsilon_{MLp} b [ML_p]$

$= A_0 + (\varepsilon_{MLp} b - \varepsilon_M b) [ML_p]$

or

$A_i = \varepsilon_M b [M] + \varepsilon_{MLp} b [ML_p]$

$= \varepsilon_M b [M] + \varepsilon_{MLp} b (C_{MLp} - [M])$

$= \varepsilon_M b [M] + \varepsilon_{MLp} b C_{MLp} - \varepsilon_{MLp} b [M]$

$[M] = (A_f - A_i)/(\varepsilon_{MLp} b - \varepsilon_M b)$

Substituting the values of [M] and [ML_p] into Equation 2-3 gives a useful result:

$$\log((A_i - A_0)/(A_f - A_i)) = \log K + p \log [L] \quad (2\text{-}4)$$

A graph of $\log((A_i - A_0)/(A_f - A_i))$ versus log [L] should be a straight line whose slope should be equal to the number of ligands (p) axially bound to the metalloporphyrin and the intercept will give the formation constant (logK). The multiple step coordination is defined as $\log\beta_n$ which related to logK as: $\log\beta_n = \log K_1 \cdot \log K_2 \ldots \log K_n$.

2.4.2 Electrochemical Titration[6, 7]

For a reversible n electron transfer reaction which is coupled with a ligand binding reaction such as $M + p\ L \rightleftharpoons (MLp)^{n-}$, the half-wave potentials will shift with changes of the free-ligand concentration according to Equation 2-5.

$$(E_{1/2})_c = (E_{1/2})_s + RT/nF\ (\log K + p \log[L]) \quad (2\text{-}5)$$

Where $(E_{1/2})_c$ and $(E_{1/2})_s$ are the half-wave potentials for the electron transfer reaction of the axial ligated and unligated metal complexes, respectively. The term RT/F is equal to 59 mV at 25 °C. The number of electrons transferred in the reaction is given by n. The meaning of K and pare the same as described in Equation 2-4. A plot of $(E_{1/2})_c$ vs. log[L] should give a straight line and both p and K can then be calculated from the slope and intercept of this straight line.

If both the oxidized and reduced forms of the complex can bind ligands, the calculation of stability constants will become more complicated and the relevant electrochemical equation (at 25 °C) is expressed in Equation 2-6, where K_{MLP} = ligand

binding constant of oxidized form and $K_{(MLP)^-}$ = ligand binding constant of reduced form.

$$(E_{1/2})_c = (E_{1/2})_s + 0.059 \log(K_{MLP}/K_{(MLP)^-}) + (p-q)\ 0.059 \log[L] \quad (2\text{-}6)$$

In this case p and q represent the number of ligands bound to the oxidation form (M) and the reduction form $(M)^-$, respectively. When the ligand concentration equals to 1.0 M or in the case of $p = q$, the half-wave potential changes thus are only related with the ratio of the stability constants of the two oxidation states.

2.5 Other Experimental Methods

2.5.1 Gassing the solution

High purity N_2 gas was used to deoxygenate the solutions for about 3 minutes before each electrochemical experiment and a positive nitrogen pressure was maintained above the solution throughout the experiment.

CO gas and NH_3 gas were used as source of the axial ligated molecules for cobalt corrole complexes. Each gas was bubbled for about 3 minutes before related experiments and was maintained above the solution throughout the experiment.

2.5.2 Temperature control

All experiments are performed at room temperature (22±1 °C) unless otherwise noted. A dry ice and acetone mixture was used to obtain low temperature that varied from 22 to -75 °C. The exact temperature was monitored using a mercury thermometer and the cell was centered in a slush bath of the dry ice and acetone.

2.6 References

[1] N. Elgrishi, K. J. Rountree, B. D. McCarthy, E. S. Rountree, T. T. Eisenhart, J. L. Dempsey, A Practical Beginner's Guide to Cyclic Voltammetry, *J. Chem. Educ.* **2018**, *95*, 197-206.

[2] A. J. Bard, L. R. Faulkner, *Electrochemical Methods: Fundamentals and Applications*, Wiley, **1980**, p. 718 pp.

[3] P. Zanello, *Inorganic Electrochemistry: Theory, Practice and Application*, Royal Society of Chemistry, **2003**, p. 615 pp.

[4] D. Brault, M. Rougee, Ferrous porphyrins in organic solvents. I. Preparation and coordinating properties, *Biochemistry* **1974**, *13*, 4591-4597.

[5] B. W. Budesinsky, Limits of the molar-ratio method, *Talanta* **1974**, *21*, 323-326.

[6] K. M. Kadish, The electrochemistry of iron porphyrins in nonaqueous media, *Phys. Bioinorg. Chem. Ser.* **1983**, *2*, 161-249.

[7] D. R. Crow, J. V. Westwood, The study of complexed metal ions by polarographic methods, *Quart. Rev. (London)* **1965**, *19*, 57-76.

3

Electrochemistry, Spectroscopic Characterization and Protonation Reactions of Open-Chain Pentapyrroles and Sapphyrins with Highly Electron-Withdrawing *Meso*-Tetraaryl Substituents

3.1 Introduction

Sapphyrins are 22-π aromatic pentapyrrolic macrocycles containing one direct link and four bridging methine groups between five pyrrole subunits.[1] This macrocycle is an early member of the group of "expanded porphyrins"[2-11] and was first discovered in the early 1960s as a byproduct in the synthesis of corroles.[12] Since then, sapphyrins have remained a topic of high interest,[13-16] in part because of their potential applications in the area of photodynamic therapy and their structural similarity to the well-known porphyrin and corrole macrocycles,[10, 11, 17-21] and in part because of their unique properties as a receptor of neutral and anionic substrates.[22-28]

A large number of studies have characterized different sapphyrin derivatives, including β-alkylated sapphyrins,[29-32] core-modified sapphyrins with heteroatoms (O, S or Se),[33-49] *N*-fused/*N*-confused sapphyrins,[50-53] and *meso*-tetraaryl substituted sapphyrins.[54-60] Sapphyrins containing four *meso*-aryl substituents can serve as favorable building blocks for the further design of molecules which are similar to *meso*-aryl substituted porphyrins, whose redox properties and chemical reactions can be finely tuned.[54] Although *meso*-tetraaryl sapphyrins can be isolated as side-products of the Rothemund reaction[54], or synthesized from the self-coupling reaction of dipyrromethane,[55] they can also be easily prepared from the respective open-chain pentapyrroles by acid catalyzed oxidative coupling.[15, 56, 57, 59, 60]

Open-chain pentapyrroles (or pentapyrrotetramethene) with *meso*-tetraaryl substituents were first isolated as the major side-products in corrole synthesis with a high

yield (11%, the same as the target product),[61] and later attracted greater attention as synthetic precursors for the respective sapphyrins.[56-61]

Our own interest in sapphyrins and open-chain pentapyrroles has involved in large part the characterization of their electrochemistry and acid-base properties in nonaqueous solvents.[58-60] The pentapyrroles previously examined in our laboratory were shown to undergo two reversible one-electron reductions and two reversible one-electron oxidations,[59] with an average HOMO-LUMO gap of 1.34 ± 0.04 V in CH_2Cl_2. However, as described in the current manuscript, the reversibility is dependent upon the solvent and type of substituent on the *meso*-aryl groups. The structurally related sapphyrins were also shown to exhibit two or sometimes three reversible one-electron oxidations,[59] but this is not the case for reduction where deprotonation follows the first one-electron addition leading to an overall irreversible redox process, similar to what has been reported in the case of corroles.[62, 63]

Corroles are easily protonated and deprotonated in nonaqueous media[62-65] and this is also the case for sapphyrins which can lose one pyrrole nitrogen proton or gain two pyrrole protons in nonaqueous media under the same solution conditions. Open-chain pentapyrroles can also gain or lose protons from the pyrrole nitrogen atoms,[58, 59] with the extent of these reactions being related to both the properties of the nonaqueous solvent and the type of *meso*-substituents on the compounds. The stability of the electrooxidized and electroreduced forms of pentapyrroles and the related sapphyrins, as well as the known conversion of pentapyrroles to sapphyrins upon oxidation,[57, 60] should also

depend upon the type of electron-withdrawing substituents on the *meso*-positions of the macrocycle.

This is investigated in the present paper where a series of newly synthesized open-chain pentapyrroles and sapphyrins containing *meso*-phenyl groups with highly electron-withdrawing substituents are characterized together with their spectral and electrochemical properties in CH_2Cl_2, benzonitrile (PhCN) and/or pyridine (Py), as well as their protonation reaction. The investigated compounds are shown in Chart 3-1 and are represented as $(Ar)_4PPyH_3$ and $(Ar)_4SapH_3$ where PPy and Sap = the trianion of the open chain pentapyrrole and sapphyrin, respectively, and Ar = PhCN, $PhCF_3$ or $PhCO_2Me$.

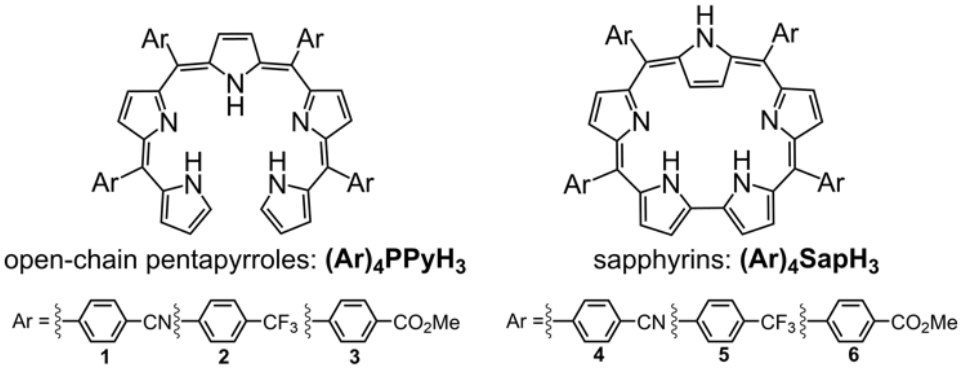

Chart 3-1. Structures of investigated compounds.

3.2 Synthesis and Characterization

The open-chain pentapyrroles **1**-**3** were isolated from synthesis of the corresponding corroles as shown in Scheme 3-1 and tested as starting materials for conversion to the corresponding sapphyrins **4**-**6**.

The data obtained from ^{1}H NMR, mass spectrometry (MS MALDI-TOF) and high-resolution mass spectrometry (HR-MS MALDI-TOF) are given in supporting information in the reference,[66] which confirm structures of the newly synthesized open-chain pentapyrroles and sapphyrins. The newly synthesized sapphyrins were fully characterized and showed C_2 symmetry by ^{1}H NMR spectroscopy.

The structure of open-chain pentapyrrole (*p*-CF_3Ph)$_4$PPyH_3 **2** was determined by single crystal X-ray diffraction analysis, as given in the reference.[66] This compound, which crystallizes in a centrosymmetric C2/*c* symmetry, has an original right or left helix shape. The conformation of this compound is imposed by intramolecular hydrogen bonds between nitrogen atoms from the pyrrole groups. The stacking of the crystal is also imposed by some π-π stacking interactions.

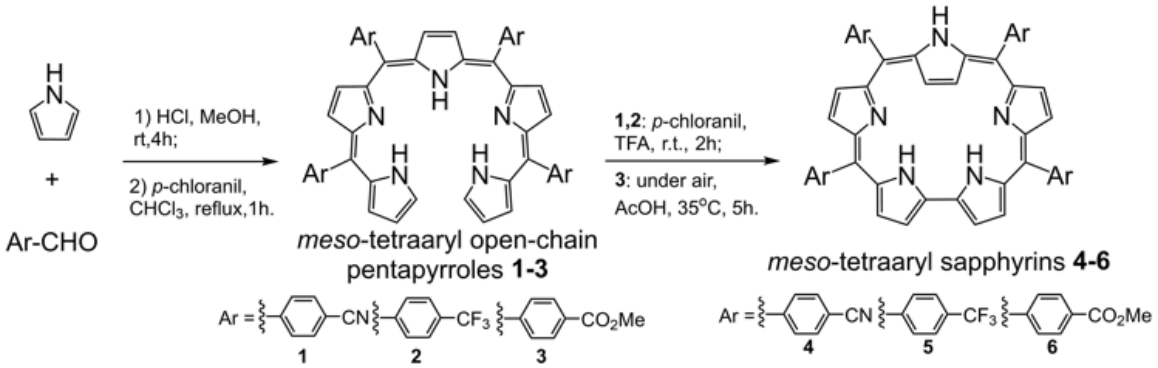

Scheme 3-1. Synthesis of investigated pentapyrroles and sapphyrins.

3.3 UV-Visible Spectra

UV−visible spectra of the open-chain pentapyrroles **1-3** and sapphyrins **4-6** were measured in CH_2Cl_2, PhCN and pyridine (Py) containing 0.1 M TBAP. The spectra in CH_2Cl_2 are shown in Figure 3-1 and the data for each investigated compound are summarized in Tables 3-1 and 3-2.

The pentapyrroles are characterized by two intense absorption bands at 378-388 and 503-509 nm and two to three moderate intensity Q bands between 695 and 894 nm. These spectra differ from that of the structurally related sapphyrins (Figure 3-1b) which are characterized by an intense split Soret band at 494-525 nm and four Q bands between 635 and 806 nm. Solvent independent spectral patterns are seen for each compound in the two series, a feature unlike corroles with similar substituents which are known to deprotonate in basic solvents such as pyridine.[62, 63]

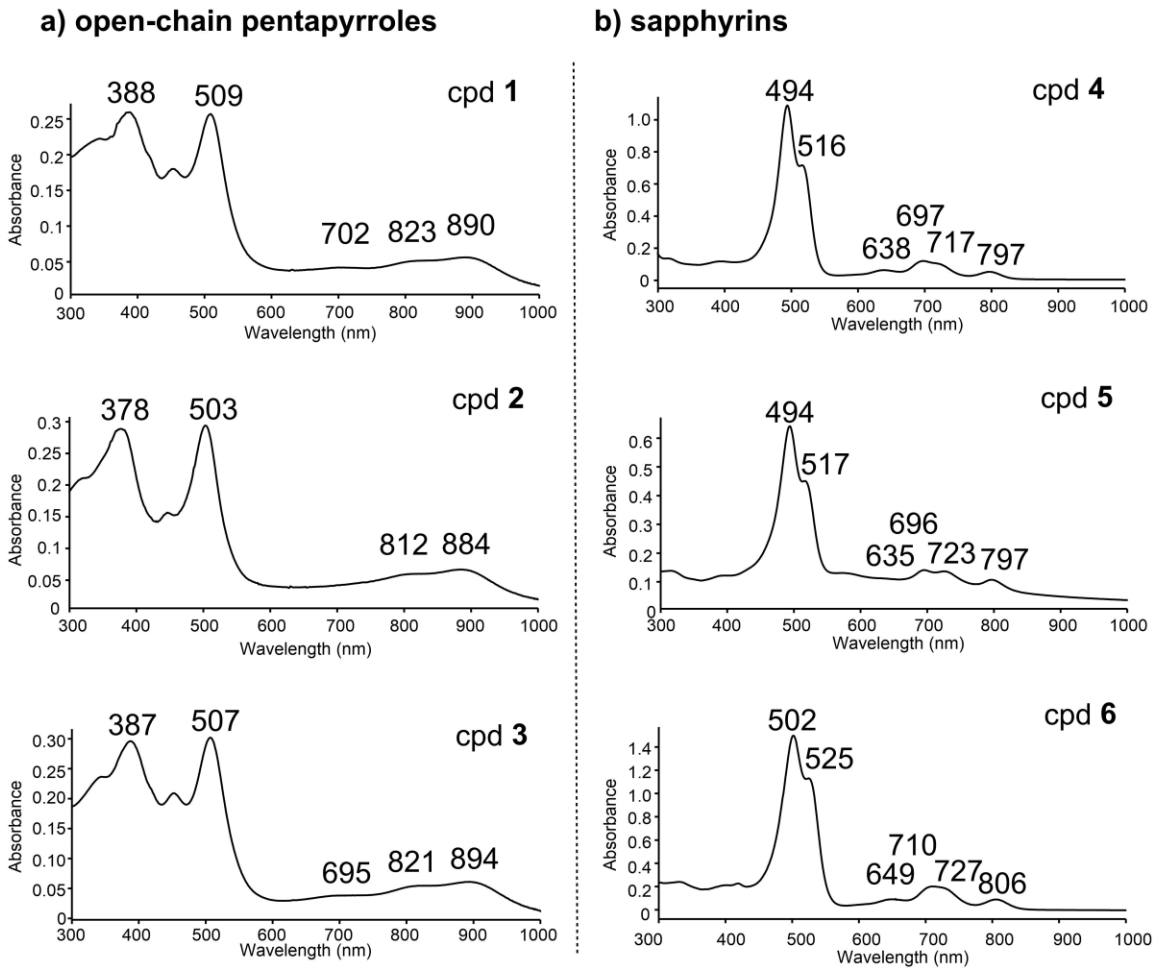

Figure 3-1. UV-vis spectra of open-chain pentapyrroles and corresponding sapphyrins in CH_2Cl_2 containing 0.1 M TBAP.

Table 3-1. UV-vis spectral data of open-chain pentapyrroles **1-3** in CH_2Cl_2, PhCN and Py containing 0.1 M TBAP.

solvent	compound	λ_{max}, nm ($\varepsilon \times 10^{-4}$ M^{-1} cm^{-1})					
		Soret region			visible region		
CH_2Cl_2	(*p*-CNPh)$_4$PPyH$_3$ **1**	388 (4.1)	453 (2.8)	509 (4.0)	702 (0.7)	823 (0.8)	890 (0.9)
	(*p*-CF$_3$Ph)$_4$PPyH$_3$ **2**	378 (5.4)	447 (2.9)	503 (5.5)	-	812 (1.1)	884 (1.3)
	(*p*-CO$_2$MePh)$_4$PPyH$_3$ **3**	387 (3.5)	454 (2.5)	507 (3.6)	695 (0.4)	821 (0.6)	894 (0.7)
PhCN	(*p*-CNPh)$_4$PPyH$_3$ **1**	390 (5.6)	458 (4.2)	512 (5.8)	707 (0.9)	834 (1.1)	900 (1.2)
	(*p*-CF$_3$Ph)$_4$PPyH$_3$ **2**	383 (3.9)	453 (2.0)	507 (4.2)	-	825 (0.7)	898 (0.9)
	(*p*-CO$_2$MePh)$_4$PPyH$_3$ **3**	389 (3.9)	456 (2.9)	510 (4.3)	718 (0.4)	837 (0.6)	907 (0.8)
Py	(*p*-CNPh)$_4$PPyH$_3$ **1**	392 (3.0)	458 (2.2)	513 (3.2)	720 (0.5)	829 (0.6)	893 (0.6)
	(*p*-CF$_3$Ph)$_4$PPyH$_3$ **2**	385 (5.3)	450 (2.8)	507 (5.4)	-	815 (1.1)	888 (1.2)
	(*p*-CO$_2$MePh)$_4$PPyH$_3$ **3**	392 (4.0)	456 (3.0)	511 (4.4)	727 (0.4)	831 (0.5)	895 (0.6)

Table 3-2. UV-vis spectral data of sapphyrins **4-6** in CH_2Cl_2, PhCN and Py containing 0.1 M TBAP.

solvent	compound	λ_{max}, nm ($\varepsilon \times 10^{-4}$ M^{-1} cm^{-1})					
		Soret region		visible region			
CH_2Cl_2	(*p*-CNPh)$_4$SapH$_3$ **4**	494 (15.2)	516 (10.0)	638 (0.9)	697 (1.7)	717 (1.8)	797 (0.7)
	(*p*-CF$_3$Ph)$_4$SapH$_3$ **5**	494 (12.1)	517 (8.3)	635 (1.6)	696 (2.2)	723 (2.1)	797 (1.5)
	(*p*-CO$_2$MePh)$_4$SapH$_3$ **6**	502 (19.2)	525 (14.5)	649 (1.2)	710 (2.6)	727 (2.4)	806 (1.1)
PhCN	(*p*-CNPh)$_4$SapH$_3$ **4**	498 (16.5)	522 (11.3)	646 (0.8)	706 (1.9)	718 (1.9)	797 (0.8)
	(*p*-CF$_3$Ph)$_4$SapH$_3$ **5**	498 (10.5)	523 (7.8)	661 (1.8)	699 (2.3)	726 (2.5)	797 (1.8)
	(*p*-CO$_2$MePh)$_4$SapH$_3$ **6**	506 (16.0)	530 (12.6)	656 (1.0)	-	727 (2.6)[a]	806 (1.2)
Py	(*p*-CNPh)$_4$SapH$_3$ **4**	496 (16.2)	519 (10.5)	647 (0.5)	-	712 (1.8)[a]	795 (0.7)
	(*p*-CF$_3$Ph)$_4$SapH$_3$ **5**	496 (17.0)	521 (11.1)	649 (0.5)	-	716 (1.9)[a]	797 (0.7)
	(*p*-CO$_2$MePh)$_4$SapH$_3$ **6**	504 (9.6)	527 (7.2)	656 (0.4)	-	725 (1.4)[a]	805 (0.5)

[a]Overlapped absorption peaks.

3.4 Protonation

The known protonation reactions of corroles, sapphyrins and pentapyrroles are schematically shown in Scheme 3-2. Two protons can be added stepwise to the neutral sapphyrins to give $[(Ar)_4SapH_4]^+$ and $[(Ar)_4SapH_5]^{2+}$, respectively, while the open-chain pentapyrroles can add two protons in a single step to give $[(Ar)_4PPyH_5]^{2+}$ as shown in Scheme 3-2.

These protonation reactions are given by Equations 3-1 to 3-3 and the measured equilibrium constants are summarized in Table 3-3.

$$(Ar)_4PPyH_3 + 2H^+ \overset{\beta_2}{\rightleftharpoons} [(Ar)_4PPyH_5]^{2+} \quad (3\text{-}1)$$

$$(Ar)_4SapH_3 + H^+ \overset{K_1}{\rightleftharpoons} [(Ar)_4SapH_4]^+ \quad (3\text{-}2)$$

$$[(Ar)_4SapH_4]^+ + H^+ \overset{K_2}{\rightleftharpoons} [(Ar)_4SapH_5]^{2+} \quad (3\text{-}3)$$

The spectral changes recorded during the protonation of compounds **1-3** with TFA in CH_2Cl_2 are given in Figure 3-2. The neutral pentapyrroles are characterized by two major bands at 376-388 nm and 502-509 nm in CH_2Cl_2, while the doubly protonated pentapyrrole products also have two bands at 405-413 nm and 532-539 nm, in addition to a broad band located between 800-1000 nm (Table 3-3).

As shown in Figure 3-2, multiple isosbestic points are obtained during the titration with TFA, indicating both the lack of a spectrally detectable mono-protonated pentapyrrole intermediate and the absence of a spectrally detectable protonated sapphyrin product on the timescale of the pentapyrrole protonation. This latter point is

important because ring closure of the pentapyrrole will occur with formation of the sapphyrin on longer timescales as described on the following pages.

The spectral changes which occur during the stepwise two proton addition to the related sapphyrin derivatives with TFA in CH_2Cl_2 are given in Figure 3-3. The initial spectrum is characterized by two bands in the Soret region and four bands in the visible region, and this converts to a spectrum with a single intense Soret band and two visible bands after the addition of 1.0 equivalent TFA (Figure 3-3a). Much higher concentrations of acid are needed to generate the doubly protonated sapphyrins $[(Ar)_4SapH_5]^{2+}$ which have a split Soret band and three visible bands as shown in Table 3-4 and Figure 3-3b.

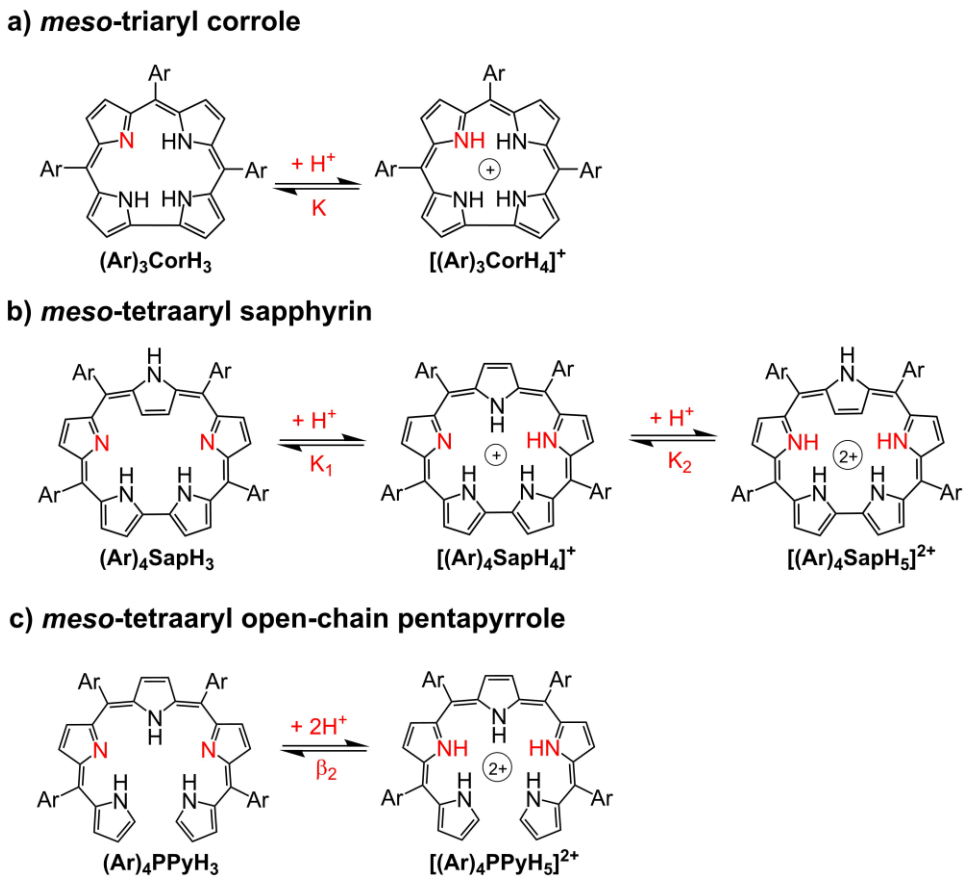

Scheme 3-2. Protonation reactions of *meso*-aryl corroles, sapphyrins and pentapyrroles in nonaqueous media.

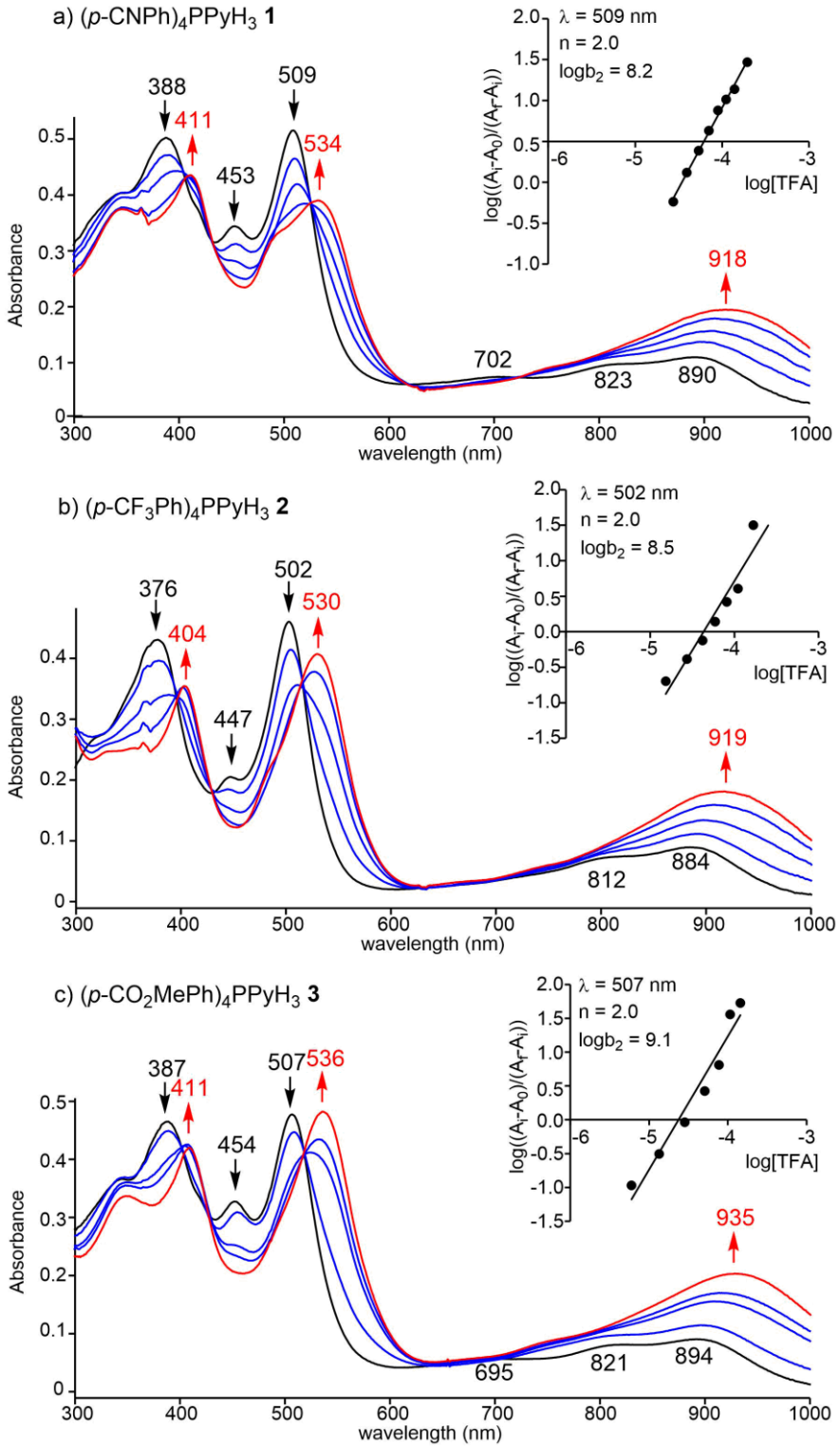

Figure 3-2. UV-visible spectral changes during the protonation of open-chain pentapyrrole **1-3** in CH_2Cl_2 with TFA.

Table 3-3. UV-vis spectral data of the protonated open-chain pentapyrroles, $[(Ar)_4PPyH_5]^{2+}$, and the protonation constants in CH_2Cl_2 with TFA.

Ar	$4\sigma^a$	wavelength: λ_{max}, nm ($\varepsilon \times 10^{-4}$ $M^{-1}\cdot cm^{-1}$)			protonation constant[b]
		Soret region	visible region		
p-CNPh **1**	2.64	413 (3.9)	539 (4.1)	943 (2.3)	$\log\beta_2 = 8.2$
p-CF_3Ph **2**	2.16	405 (4.6)	532 (6.4)	931 (3.4)	$\log\beta_2 = 8.5$
p-CO_2MePh **3**	1.80	409 (3.2)	536 (3.9)	928 (2.0)	$\log\beta_2 = 9.1$

[a]Values of σ for the *p*-CN, CF_3 and CO_2Me groups were taken from reference [69]. [b]Equilibrium constants for proton addition according to Equation 3-1 were calculated from the Hill equation (see text).

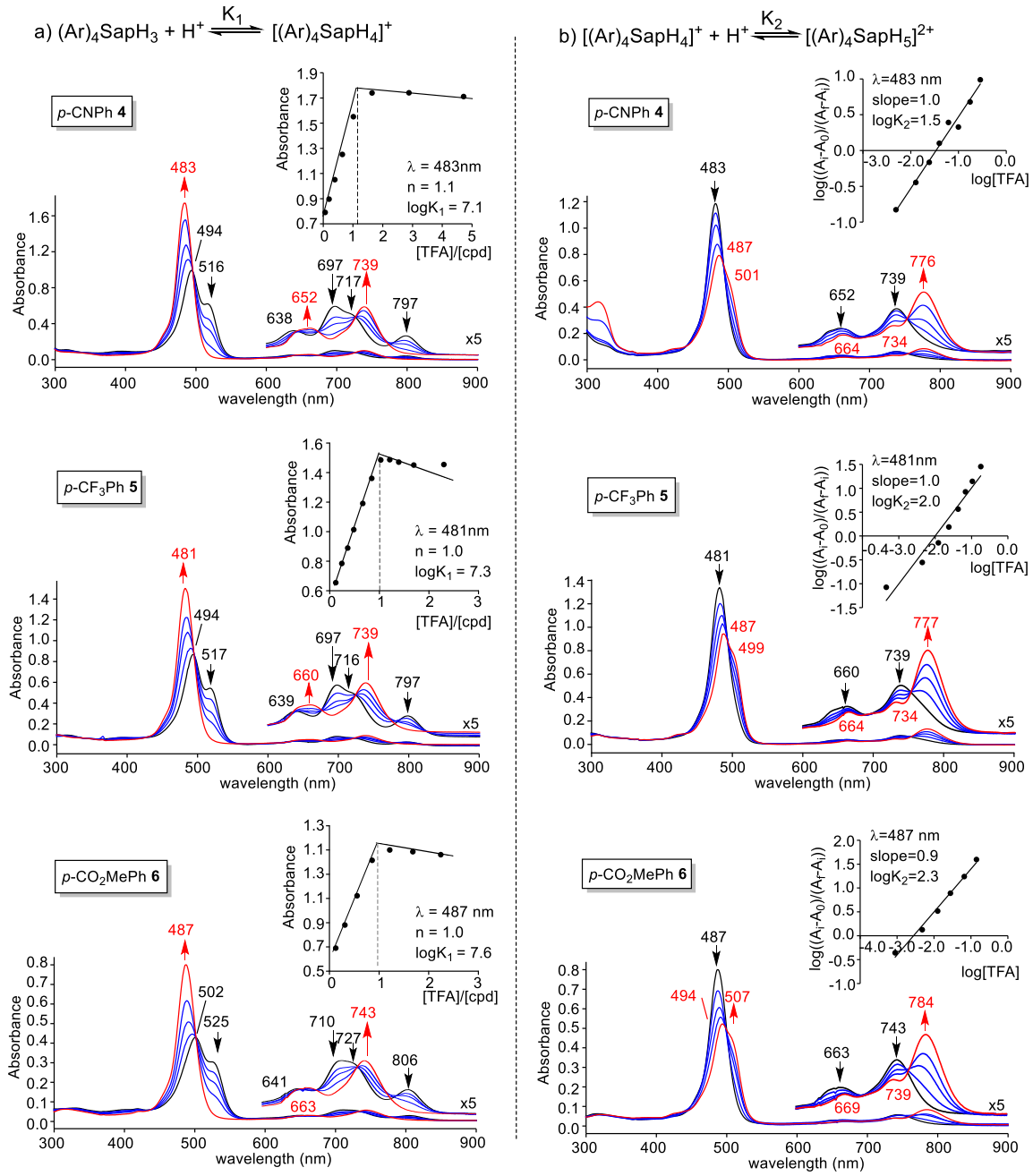

Figure 3-3. UV-visible spectral changes during a) the first and b) the second proton addition to the sapphyrins **4-6** in CH_2Cl_2 with TFA. Plots for calculating the equilibrium constants are shown as inserts.

Table 3-4. UV-vis spectral data of the protonated sapphyrins, $[(Ar)_4SapH_4]^+$ and $[(Ar)_4SapH_5]^{2+}$, and calculated protonation constants in CH_2Cl_2 with TFA.

protonated form	Ar	$4\sigma^a$	wavelength: λ_{max}, nm ($\varepsilon \times 10^{-4}$ $M^{-1}\cdot cm^{-1}$)					$logK^b$
			Soret region		visible region			
$[(Ar)_4SapH_4]^+$	*p*-CNPh **4**	2.64	483 (26.3)	-	654 (0.7)	739 (1.4)	-	$logK_1 = 7.1$
	p-CF_3Ph **5**	2.16	481 (31.2)	-	653 (1.0)	739 (1.8)	-	$logK_1 = 7.3$
	p-CO_2MePh **6**	1.80	487 (35.4)	-	663 (1.4)	743 (2.6)	-	$logK_1 = 7.6$
$[(Ar)_4SapH_5]^{2+}$	*p*-CNPh **4**	2.64	487 (17.3)	501 (13.3)	664 (2.0)	734 (0.7)	776 (1.9)	$logK_2 = 1.5$
	p-CF_3Ph **5**	2.16	487 (19.6)	499 (16.4)	664 (0.7)	734 (1.0)	777 (2.7)	$logK_2 = 2.0$
	p-CO_2MePh **6**	1.80	494 (22.8)	507 (19.8)	669 (0.8)	739 (1.4)	784 (3.4)	$logK_2 = 2.3$

[a]Values of σ were taken from reference [69]. [b]Equilibrium constants for proton addition were calculated according to Equations 3-2 and 3-3 using the Hill equation and the Molar Ratio method (see text).

3.5 Conversion of $[(Ar)_4PPyH_5]^{2+}$ to $[(Ar)_4SapH_4]^+$

The oxidative conversion of pentapyrroles to sapphyrins in a nonaqueous solvent containing I_2 and TFA has been reported and was proposed to proceed via a bis-protonated pentapyrrole intermediate $[(Ar)_4PPyH_5]^{2+}$ as shown in Scheme 3-3 for derivatives with sterically hindered *meso*-aryl substituents.[60] We wished to know if a pentapyrrole to sapphyrin conversion would also occur for the newly synthesized pentapyrroles after protonation in CH_2Cl_2 and if so, we wished to elucidate the mechanism and possibly evaluate the kinetics of this conversion.

The protonation of $(Ar)_4PPyH_3$ to $[(Ar)_4PPyH_5]^{2+}$ is shown in Figure 3-2 for the CF_3 derivative. The doubly protonated pentapyrrole is relatively unstable in CH_2Cl_2 and a conversion to the sapphyrin is observed when spectroscopically monitoring the solution as a function of time. An example of the resulting spectral changes for compound **2** in CH_2Cl_2 containing 23 eq. TFA over a period of 48 hours is given in Figure 3-4. Almost no spectral changes are seen between 4 and 48 hours and the spectra at this point are characterized by a species with an intense Soret band at 483 nm and two Q bands at 655 and 738 nm. The broad band associated with $[(Ar)_4PPyH_5]^{2+}$ at ~900 nm is no longer present, and the final spectrum is virtually identical to that of singly protonated $[(p\text{-}CF_3Ph)_4SapH_4]^+$, which is characterized by bands at 482, 652 and 739 nm (Figure 3-3a). The spectral changes monitored in Figure 3-4 were taken in CH_2Cl_2 containing 23 eq. of TFA, an acid concentration not large enough to completely generate the doubly protonated sapphyrin which has a $\log K_2$ of 2.0 and requires a large (10^5) excess of TFA. Thus, under

the examined solution conditions, only the mono-protonated sapphyrin can be observed as a final product of the ring closure reaction under these conditions. The reactants and products in the ring closure reaction are shown in Scheme 3-3 and involve a conversion of $[(Ar)_4PPyH_5]^{2+}$ to $[(Ar)_4SapH_4]^+$.

A similar conversion from the fully protonated pentapyrrole to the mono-protonated sapphyrin also occurred for compounds **1** and **3**, and the progress of this reaction was examined by plotting the measured absorbance changes (% conversion) vs. time at wavelengths corresponding to the peak of maximum absorbance for the formation of each $[(Ar)_4SapH_4]^+$ derivative. These plots are shown in Figure 3-5 for compounds **1**, **2** and **3** in CH_2Cl_2 containing 25 eq. TFA.

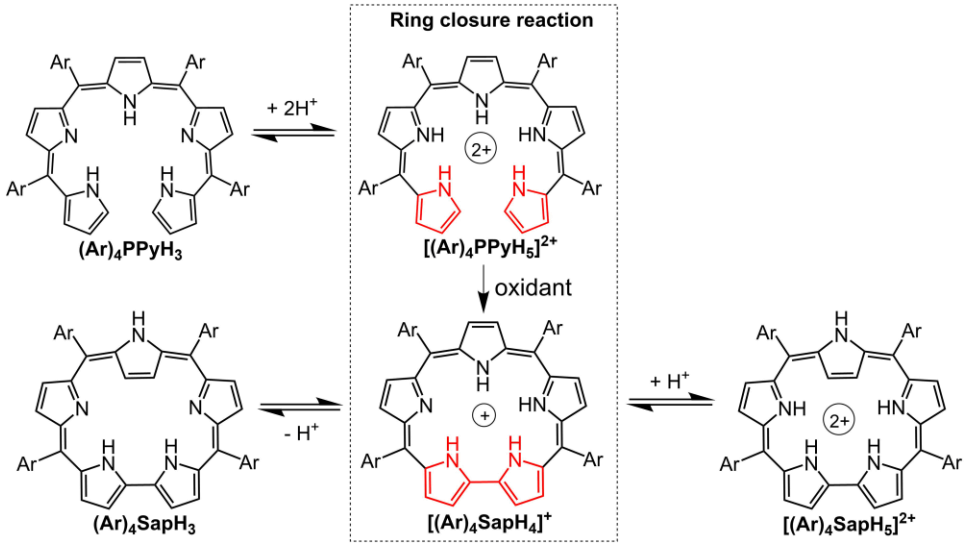

Scheme 3-3. Proposed mechanism for the conversion of open-chain pentapyrrole to the corresponding sapphyrin.

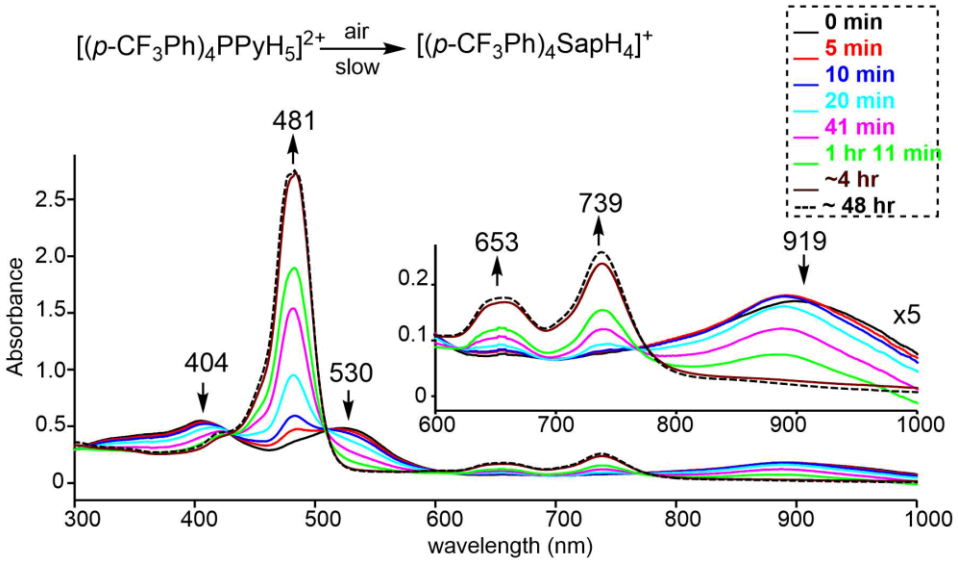

Figure 3-4. UV-visible spectral changes monitored during the conversion of protonated pentapyrrole **2** $[(p\text{-}CF_3Ph)_4PPyH_5]^{2+}$ to mono-protonated sapphyrin **5** $[(p\text{-}CF_3Ph)_4SapH_4]^+$ in CH_2Cl_2 containing 23 eq. TFA.

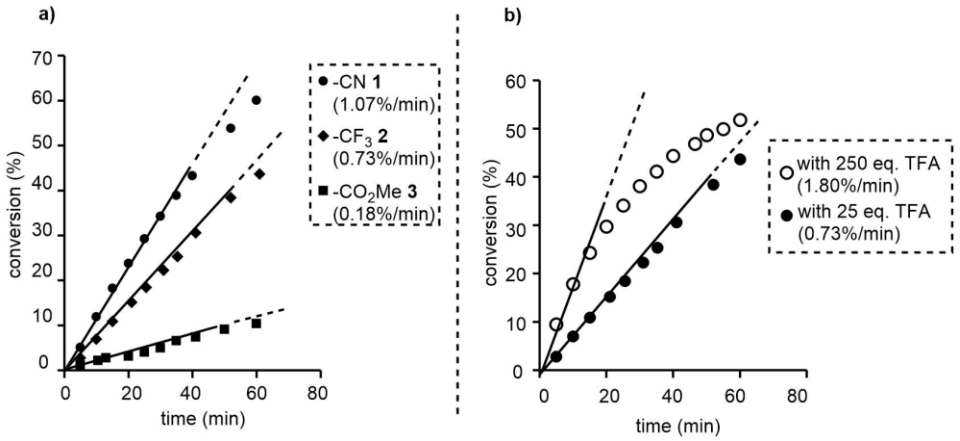

Figure 3-5. Relationship between percentage conversion of the doubly protonated pentapyrrole to the mono-protonated sapphyrin ($[[SapH_4]^+]/[[PPyH_5]^{2+}]$ %) and reaction time (min) a) with different substituents containing 25 eq. TFA and b) the pentapyrroles **3** (Ar = *p*-CF_3Ph) containing different equivalence TFA in CH_2Cl_2 (see text and Figure 3-4).

3.6 Electrochemistry and Substituent Effects on Redox Properties of Open-Chain Pentapyrroles

The electrochemistry of the three newly-synthesized pentapyrroles was characterized by cyclic voltammetry in CH_2Cl_2, PhCN and Py. Examples of the cyclic voltammograms in CH_2Cl_2 are given in Figure 3-6 and a summary of the measured half-wave potentials for reduction and oxidation in the three solvents is given in Table 3-5.

Earlier examined $(Ar)_4PPyH_3$ derivatives with *p*-FPh, *p*-ClPh *and* *p*-Cl_2Ph *meso*-substituents were characterized by two reversible reductions, two reversible oxidations and an average HOMO/LUMO gap of 1.34 ± 0.04 V.[59] A similar HOMO-LUMO gap is seen for the currently studied open-chain pentapyrroles, i.e., 1.32 ± 0.03 V in CH_2Cl_2, 1.23 ± 0.02 V in PhCN and 1.07 ± 0.01 V in pyridine.

The effect of phenyl ring substituents on the open-chain pentapyrroles can be related to the measured $E_{1/2}$ values by plots of the type shown in Figure 3-7 using the relationship in Equation 3-4[67] where ρ is the slope of the line correlating the measured half-wave potentials and the values of σ are taken from the literature.[68]

$$\Delta E_{1/2} = 4\sigma\rho \qquad (3\text{-}4)$$

There are four *meso*-aryl groups on open-chain pentapyrrole $(Ar)_4PPyH_3$ and 4σ is used in the plots which includes both data on compounds **1-3** from the current study and data from the literature on derivatives of $(p\text{-FPh})_4PPyH_3$ and $(p\text{-ClPh})_4PPyH_3$.[59]

As shown in Figure 3-7 and Table 3-5, the average HOMO-LUMO gap of $(Ar)_4PPyH_3$ is 1.32 ± 0.03 V while the potential difference between the first and second

redox processes ranges from 0.18 to 0.22 V for oxidation of compounds **1-3** and 0.21 to 0.25 V for reduction of the same species in CH_2Cl_2. Larger separations between $E_{1/2}$ values for the stepwise reductions or oxidations of **1-3** are observed in PhCN and pyridine as seen by the data in Table 3-5.

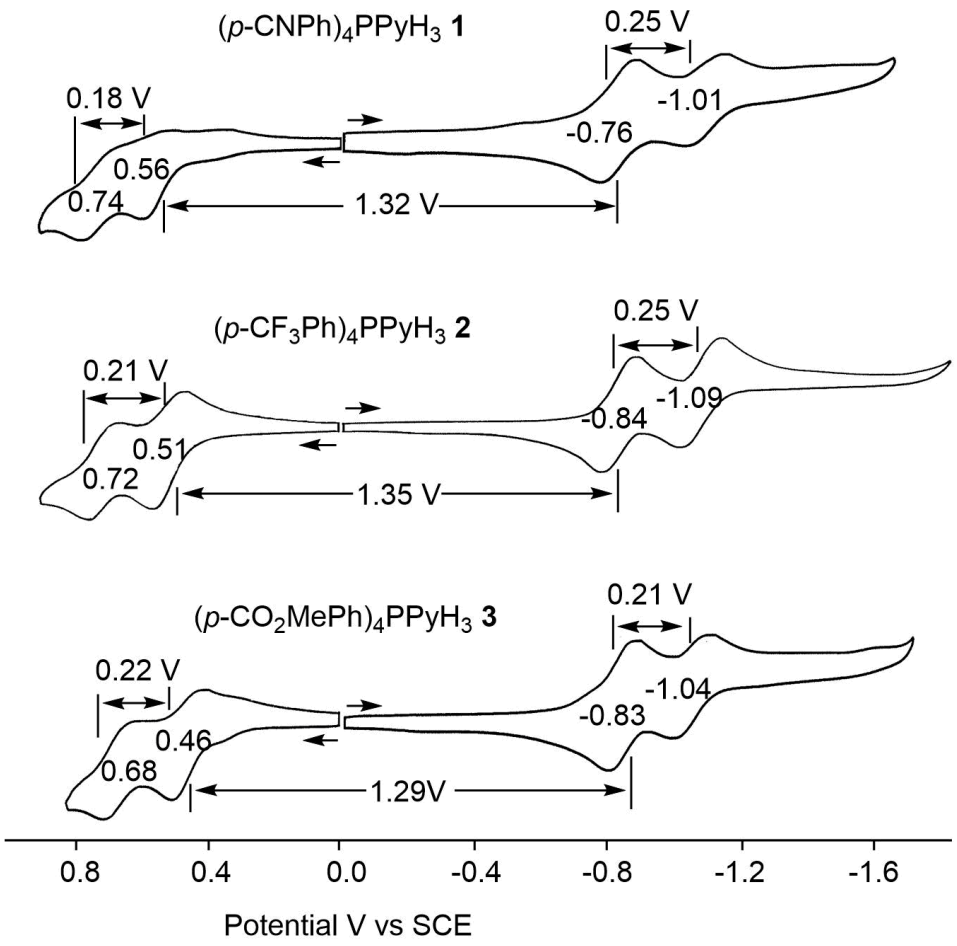

Figure 3-6. Cyclic voltammogram of open-chain pentapyrroles **1-3** in CH_2Cl_2 containing 0.1 M TBAP.

Table 3-5. Half-wave potentials ($E_{1/2}$, V vs SCE) of open-chain pentapyrroles **1-3** in CH_2Cl_2, PhCN and pyridine containing 0.1 M TBAP.

solvent	compound	$4\sigma^a$	oxidation			reduction			
			1st ox	2nd ox	ΔE_o[b]	1st red	2nd red	ΔE_r[b]	H-L[c]
CH_2Cl_2	(*p*-CNPh)$_4$PPyH$_3$ **1**	2.64	0.56	0.74	**0.18**	-0.76	-1.01	**0.25**	**1.32**
	(*p*-CF$_3$Ph)$_4$PPyH$_3$ **2**	2.16	0.51	0.72	**0.21**	-0.84	-1.09	**0.25**	**1.35**
	(*p*-CO$_2$MePh)$_4$PPyH$_3$ **3**	1.80	0.46	0.68	**0.22**	-0.83	-1.04	**0.21**	**1.29**
PhCN	(*p*-CNPh)$_4$PPyH$_3$ **1**	2.64	0.51	0.70	**0.19**	-0.71	-0.99	**0.28**	**1.22**
	(*p*-CF$_3$Ph)$_4$PPyH$_3$ **2**	2.16	0.48	0.70	**0.22**	-0.77	-1.07	**0.30**	**1.25**
	(*p*-CO$_2$MePh)$_4$PPyH$_3$ **3**	1.80	0.43	0.68	**0.25**	-0.80	-1.06	**0.26**	**1.23**
Py	(*p*-CNPh)$_4$PPyH$_3$ **1**	2.64	0.41[d]	0.73	**0.32**	-0.66	-0.93	**0.27**	**1.07**
	(*p*-CF$_3$Ph)$_4$PPyH$_3$ **2**	2.16	0.37[d]	0.71	**0.34**	-0.71	-1.02	**0.31**	**1.08**
	(*p*-CO$_2$MePh)$_4$PPyH$_3$ **3**	1.80	0.33[d]	0.66	**0.33**	-0.74	-1.01	**0.27**	**1.07**

[a]Values of σ were taken from reference [69]. [b]ΔE_o = Potential difference between 1st oxidation and 2nd oxidation, ΔE_r = Potential difference between 1st reduction and 2nd reduction. [c]H-L = HOMO-LUMO gap (the potential difference $\Delta E_{1/2}$ between 1st oxidation and 1st reduction). [d]Second scan potential.

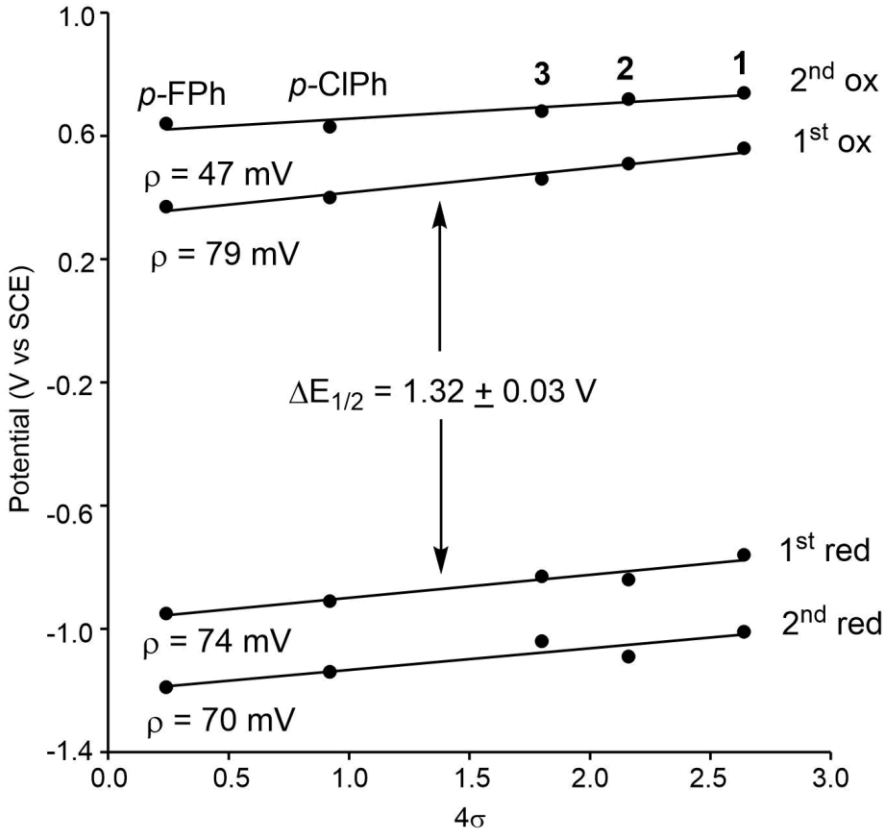

Figure 3-7. Plots of half-wave potentials vs. Hammett substituents constants (4σ) for the two reversible oxidations and two reversible reductions of $(Ar)_4PPyH_3$ in CH_2Cl_2 containing 0.1 M TBAP. Values of $E_{1/2}$ for $(p\text{-ClPh})_4PPyH_3$ and $(p\text{-FPh})_4PPyH_3$ are taken from reference [60] and the values of σ for the *para*-phenyl substituents are taken from reference [69].

3.7 Electrochemistry and Substituent Effects on Redox Properties of Sapphyrins

Earlier studies of *meso*-tetraaryl sapphyrins showed the compounds to exhibit an irreversible reduction in all solvents due to the loss of a pyrrole proton following electron addition.[58, 59] This is also the case for the currently investigated compounds whose reduction was not investigated in further detail. The first oxidation of sapphyrins is also irreversible in pyridine,[58] but this is not the case in CH_2Cl_2 or PhCN where two or three reversible oxidations are obtained as shown by the cyclic voltammograms in Figure 3-8 for compounds **4**, **5** and **6** where the processes were monitored in PhCN containing 0.1 M TBAP.

The first one-electron oxidation of the sapphyrins **4-6** is harder than the first one-electron oxidation of the related pentapyrroles **1-3** by an average of 120 mV ($E_{1/2}$ (avg.) = 0.47 V for $(Ar)_4PPyH_3$ and 0.59 V for $(Ar)_4SapH_3$ in PhCN) as seen in Table 3-5 and Figure 3-8, while the second oxidation of $(Ar)_4SapH_3$ is more difficult than the corresponding oxidation of $(Ar)_4PPyH_3$ by an average of 310 mV ($E_{1/2}$ (avg.) = 0.69 V for $(Ar)_4PPyH_3$ and 1.00 V for $(Ar)_4SapH_3$ in PhCN).

The potential separation ($\Delta E_{1/2}$) between the first and second oxidation of the sapphyrins **4-6** ranges from 0.40 to 0.42 V in PhCN (Figure 3-8a) and is larger than the potential separation between the two reversible oxidations of the corresponding $(Ar)_4PPyH_3$ derivatives **1-3** which ranges from 0.19 to 0.25 V in the same solvent (Table 3-5). Compound **1,** with CN substituents, has the smallest $\Delta E_{1/2}$ among the three pentapyrroles (Table 3-5) while the related compound **4** also has the smallest $\Delta E_{1/2}$ among

the three investigated sapphyrins (Figure 3-8a). This is as expected on the basis of the slopes of the $E_{1/2}$ vs. 4σ plots in Figures 3-7 and 3-8.

As seen in Figure 3-8b, the slope (ρ) of the $E_{1/2}$ vs. 4σ plot (Equation 3-4) is equal to 71 mV for the first oxidation of the sapphyrins and 54 mV for the second in PhCN. These slopes are not significantly different than slopes for the same oxidations of the related pentapyrroles in CH_2Cl_2, 79 mV and 47 mV respectively (Figure 3-7). However, it must be noted that the electrochemical values of ρ are solvent-dependent[70] and they also depend upon the specific site of electron transfer. In this regard, it should be pointed out that the second oxidation of the pentapyrroles and sapphyrins are both less sensitive to the substituents than the first oxidation when measured in PhCN or CH_2Cl_2.

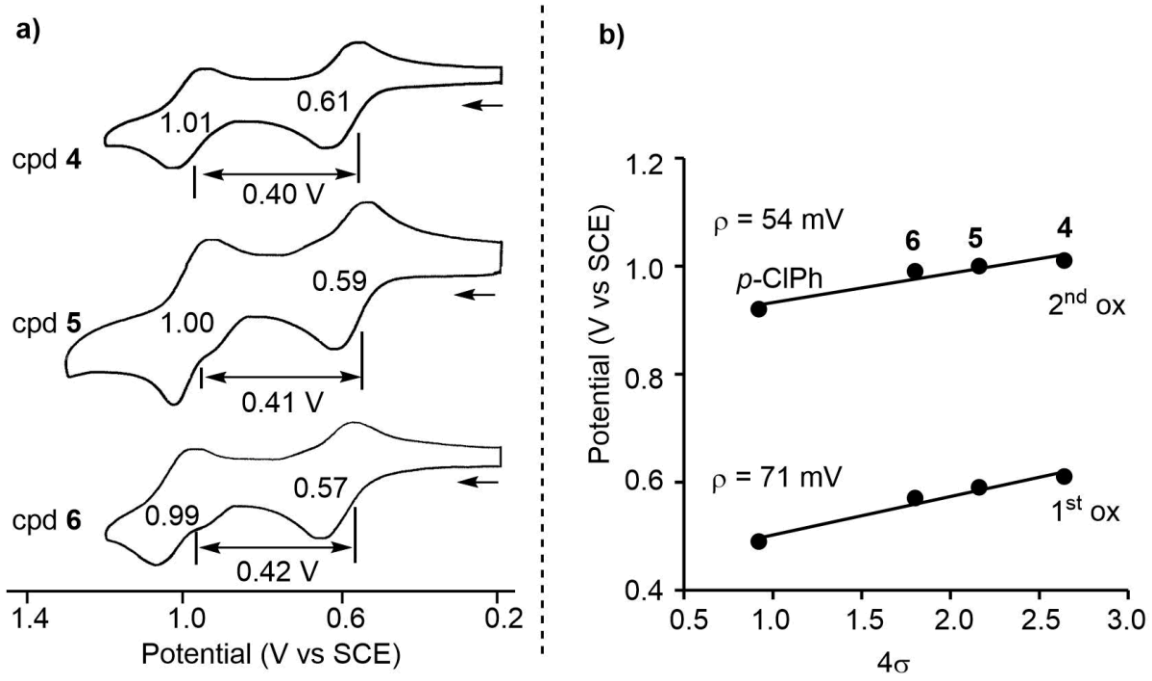

Figure 3-8. a) Cyclic voltammograms showing the first two oxidations of sapphyrins **4-6** in PhCN containing 0.1 M TBAP and b) plots of half-wave potentials vs. the sum of Hammett substituent constants of electron-withdrawing groups on the *meso*-phenyl rings. Also included in the figure are $E_{1/2}$ values of (*p*-ClPh)$_4$SapH$_3$ taken from reference [60]. Values of σ for the *para*-phenyl substituents are taken from reference [69].

3.8 Comparison of Substituent Effects with Related Macrocycles

Reversible oxidations are seen for most free-base *meso*-substituted tetraarylporphyrins[71] and the effect of *meso*-substituents on these electrode reactions can be compared to that of the sapphyrins and pentapyrroles. Such a comparison is given in Figure 3-9 which plots $E_{1/2}$ for the first one-electron oxidation of the related *meso*-aryl sapphyrins, pentapyrroles and porphyrins vs. the sum of the Hammett substituent constants on the *meso*-phenyl groups. Also included in this plot are values of the measured peak potentials (E_p) for the first irreversible oxidation of related triaryl-corroles having the same type of electron-withdrawing substituents on the *meso*-phenyl rings.

As seen by the structures in Scheme 3-2, the corroles have three *meso*-aryl groups as compared to four *meso*-aryl groups for the sapphyrins, pentapyrroles and porphyrins (not shown in scheme).

Thus, the data in Figure 3-9 provides a good indication of how the *meso*-substituents will affect the $E_{1/2}$ values for oxidation of three free-base macrocycles and a related free-base open-chain pentapyrrole. As seen in this figure, there is not a significant difference in the magnitude of the substituent effect for the first one electron oxidation of the porphyrins, sapphyrins or open-chain pentapyrroles as measured by the slope of the $\Delta E_{1/2}/\Delta\Sigma\sigma$ plots which are defined in Equation 3-4 and given in mV. The values of the slopes (ρ) in Figure 3-9 range from 50 mV for the open-chain pentapyrroles to 67 mV for the porphyrins and 71 mV for the sapphyrins. This suggests a very similar inductive effect of the four *meso*-aryl groups on the HOMO of the sapphyrin and porphyrin macrocycles,

but a smaller effect on the π system of the open-chain pentapyrroles. A larger substituent effect is seen for the corroles (ρ = 115 mV) but because these electrode reactions are irreversible and involve coupled chemical reactions,[62, 63] care must be taken when comparing the non-thermodynamic values of peak potentials with the more meaningful thermodynamic $E_{1/2}$ values.

The first one-electron oxidations of the free-base porphyrins, sapphyrins and pentapyrroles are reversible, and thus thermodynamically meaningful comparisons can be made between redox potentials for these three types of compounds having the same set of *meso*-substituents. For example, the measured $E_{1/2}$ values are 1.22 V for (*p*-CNPh)$_4$PorH$_2$[71] and 0.56 V for (*p*-CNPh)$_4$PPyH$_3$ in CH_2Cl_2, and 0.61 V for (*p*-CNPh)$_4$SapH$_3$ in PhCN. Despite the difference in solvents, it is clear that the larger π system of compounds **1-6** which have five linked pyrroles is easier to oxidize than that of the corresponding porphyrins with four linked pyrroles.

The first one-electron reductions of the pentapyrroles and related free-base porphyrins are also reversible and comparisons can be made between $E_{1/2}$ values for these processes. For example, the reduction of (*p*-CNPh)$_4$PorH$_2$ occurs at $E_{1/2}$ = -1.00 V in CH_2Cl_2[71], and this value can be compared to an $E_{1/2}$ = -0.76 V for (*p*-CNPh)$_4$PPyH$_3$ under the same solution conditions (See Figure 3-6). Thus, a shift of 240 mV towards an easier reduction is seen for the open-chain pentapyrroles with five ring systems. Combining the easier 240 mV reduction of (Ar)$_4$PPyH$_3$ with the easier 680 mV oxidation of the same compound leads to a decrease in the HOMO-LUMO gap of 920 mV, as graphically shown

in Figure 3-7 where the average $\Delta E_{1/2}$ = 1.32 V. This as compare to an average 2.2 V HOMO-LUMO gap for the related porphyrin derivative having CN groups, i.e. (*p*-CNPh)$_4$PorH$_2$.

The potentials for oxidations of the sapphyrins and open-chain pentapyrroles can also be related to the protonation constants and such a comparison is given in Figure 3-10. In the case of sapphyrins, there is a significant dependence of logK$_1$ for proton additions on the para substituents and the same dependence is seen on the half-wave potential as shown in Figure 3-9. Thus, the plot of logK$_1$ vs $E_{1/2}$ is linear, with the values of logK$_1$ for (Ar)$_4$SapH$_3$ ranging from 7.1 for Ar = *p*-CNPh to 9.8 for Ar = *p*-FPh. A much smaller effect is seen for the second proton addition to the same sapphyrins where the logK$_2$ values ranges from 1.5 for Ar = *p*-CNPh to 2.7 for Ar = *p*-ClPh.

The slope of the $\Delta\log\beta_2/\Delta E_{1/2}$ plot for the sapphyrins in Figure 3-10 indicates a decrease of 2.3 $\log\beta_2$ units for every 100 mV change in potential towards a harder oxidation as compared to a much smaller decrease of 1.2 $\log\beta_2$ units for every 100 mV change in potential for oxidation of the open-chain pentapyrroles **1-3**. Thus, the stronger the electron-withdrawing groups on the four *meso*-positions of the investigated compounds, the more positive is the charge on the π-system and pyrrole nitrogens which leads to smaller values of logK or $\log\beta_2$ for proton addition.

An increased positive charge on the π-system and pyrrole nitrogens of the pentapyrroles also leads to an enhanced conversion to the related sapphyrins as shown in Figure 3-5, where the most rapid pentapyrrole to sapphyrin conversion was obtained for the CN derivative (compound **1**) and the slowest for the CO_2Me species (compound **3**).

This might at first suggest that open-chain pentapyrroles with electron-withdrawing groups on both the *meso*- and β-pyrrole positions would exhibit a further enhanced conversion to the related sapphyrins but one must also consider the expected decreased magnitude of protonation constants which might have an opposite effect and lead to more stable pentapyrroles under mild acid condition. Further studies are needed to verify if this is the case.

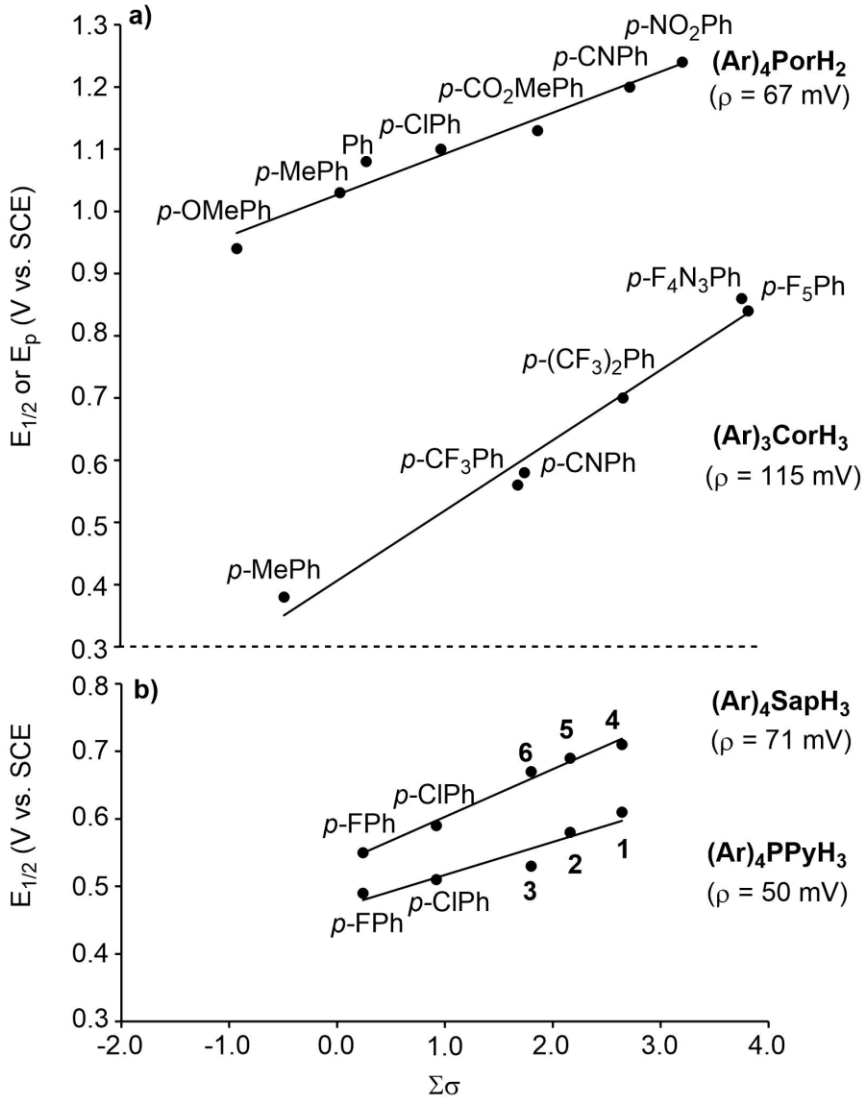

Figure 3-9. Plots of first oxidation potential of porphyrins (in CH_2Cl_2), corroles, sapphyrins and pentapyrroles vs. Σσ in PhCN containing 0.1 M TBAP. The data in part a) are for porphyrins[71] and corroles[62, 63] while those in part b) are for sapphyrins and pentapyrroles.[59] Potentials used in the plots are given in SI in reference.[66]

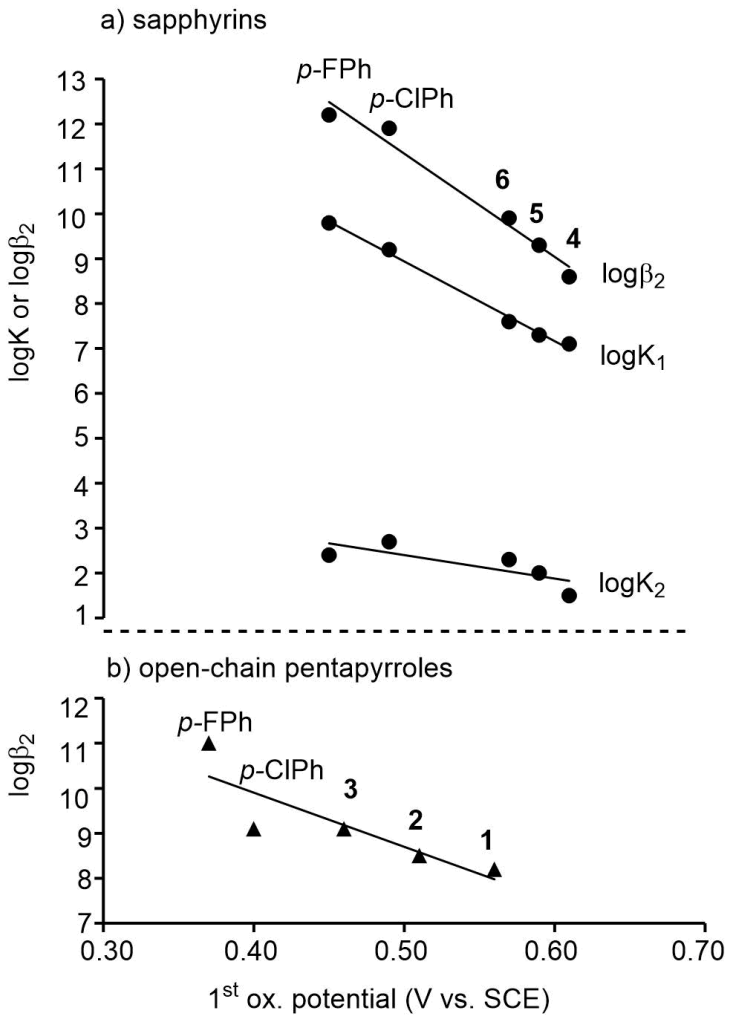

Figure 3-10. Plots of log (protonation constants) vs. the first oxidation potentials of a) sapphyrins **4-6**, (*p*-ClPh)$_4$SapH$_3$ and (*p*-FPh)$_4$SapH$_3$ and b) open-chain pentapyrroles **1-3**, (*p*-ClPh)$_4$PPyH$_3$ and (*p*-FPh)$_4$PPyH$_3$ in CH_2Cl_2. The data used in the plots are given in SI of the reference.[66]

3.9 References

[1] V. J. Bauer, D. L. J. Clive, D. Dolphin, J. B. Paine, III, F. L. Harris, M. M. King, J. Loder, S. W. C. Wang, R. B. Woodward, Sapphyrins: novel aromatic pentapyrrolic macrocycles, *J. Am. Chem. Soc.* **1983**, *105*, 6429-6436.

[2] J. L. Sessler, D. Seidel, Synthetic expanded porphyrin chemistry, *Angew. Chem. Int. Ed.* **2003**, *42*, 5134-5175.

[3] R. Misra, K. Chandrashekar Tavarekere, Structural diversity in expanded porphyrins, *Acc. Chem. Res.* **2008**, *41*, 265-279.

[4] A. Ghosh, A perspective of one-pot pyrrole-aldehyde condensations as versatile self-assembly processes, *Angew. Chem. Int. Ed.* **2004**, *43*, 1918-1931.

[5] J. L. Sessler, S. Camiolo, P. A. Gale, Pyrrolic and polypyrrolic anion binding agents, *Coord. Chem. Rev.* **2003**, *240*, 17-55.

[6] S. K. Pushpan, T. K. Chandrashekar, Aromatic core-modified expanded porphyrinoids with meso-aryl substituents, *Pure Appl. Chem.* **2002**, *74*, 2045-2055.

[7] J. L. Sessler, A. Andrievsky, J. W. Genge, Anion binding by sapphyrins, *Adv. Supramol. Chem.* **1997**, *4*, 97-142.

[8] J. L. Sessler, W. E. Allen, Anion carriers: New tools for crossing membranes, *Chem. Tech.* **1999**, *29*, 16-24.

[9] Y. Pareek, M. Ravikanth, T. K. Chandrashekar, Smaragdyrins: Emeralds of Expanded Porphyrin Family, *Acc. Chem. Res.* **2012**, *45*, 1801-1816.

[10] J.-Y. Shin, K. S. Kim, M.-C. Yoon, J. M. Lim, Z. S. Yoon, A. Osuka, D. Kim, Aromaticity and photophysical properties of various topology-controlled expanded porphyrins, *Chem. Soc. Rev.* **2010**, *39*, 2751-2767.

[11] J. L. Sessler, J. M. Davis, Sapphyrins: Versatile Anion Binding Agents, *Acc. Chem. Res.* **2001**, *34*, 989-997.

[12] R. B. Woodward, *Presented in the Aromaticity Conference* **1966**.

[13] T. Chatterjee, A. Srinivasan, M. Ravikanth, T. K. Chandrashekar, Smaragdyrins and Sapphyrins Analogues, *Chem. Rev.* **2017**, *117*, 3329-3376.

[14] F. Figueira, A. S. F. Farinha, A. C. Tome, J. A. S. Cavaleiro, A. M. S. Silva, J. P. C. Tome, I. Marques, V. Felix, I. Marques, V. Felix, J. Sessler, J. P. C. Tome, Unprecedented Double aza-Michael Addition within a Sapphyrin Core, *Chem. Eur. J.* **2016**, *22*, 14349-14355.

[15] J.-i. Setsune, 2,2'-Bipyrrole-Based Porphyrinoids, *Chem. Rev.* **2017**, 3044-3101.

[16] Y. M. Sung, J. Oh, W.-Y. Cha, W. Kim, J. M. Lim, M.-C. Yoon, D. Kim, Control and Switching of Aromaticity in Various All-Aza-Expanded Porphyrins: Spectroscopic and Theoretical Analyses, *Chem. Rev.* **2017**, 2257-2312.

[17] S. Saito, A. Osuka, Expanded Porphyrins: Intriguing Structures, Electronic Properties, and Reactivities, *Angew. Chem. Int. Ed.* **2011**, *50*, 4342-4373.

[18] J. L. Sessler, S. Weghorn, *Expanded, Contracted & Isomeric Porphyrins, Vol. 15*, Elsevier, **1997**, p. 520 pp.

[19] A. Jasat, D. Dolphin, Expanded Porphyrins and Their Heterologs, *Chem. Rev.* **1997**, *97*, 2267-2340.

[20] R. Bonnett, Photosensitizers of the porphyrin and phthalocyanine series for photodynamic therapy, *Chem. Soc. Rev.* **1995**, *24*, 19-33.

[21] L. Naumovski, M. Sirisawad, P. Lecane, J. Chen, J. Ramos, Z. Wang, C. Cortez, D. Magda, P. Thiemann, G. Boswell, D. Miles, G. Cho Dong, L. Sessler Jonathan, R. Miller, Tumor localization and antitumor efficacy of novel sapphyrin compounds, *Mol. Cancer Ther.* **2006**, *5*, 2798-2805.

[22] J. L. Sessler, D. A. Ford, M. J. Cyr, H. Furuta, Enhanced transport of fluoride anion effected using protonated sapphyrin as a carrier, *J. Chem. Soc., Chem. Commun.* **1991**, 1733-1735.

[23] V. Kral, J. L. Sessler, H. Furuta, Synthetic sapphyrin-cytosine conjugates: carriers for selective nucleotide transport at neutral pH, *J. Am. Chem. Soc.* **1992**, *114*, 8704-8705.

[24] J. Sessler, E. A. Brucker, The first "crowned" expanded porphyrin, *Tetrahedron Lett.* **1995**, *36*, 1175-1176.

[25] M. Shionoya, H. Furuta, V. Lynch, A. Harriman, J. L. Sessler, Diprotonated sapphyrin: a fluoride selective halide anion receptor, *J. Am. Chem. Soc.* **1992**, *114*, 5714-5722.

[26] J. L. Sessler, M. J. Cyr, A. K. Burrell, Sapphyrins: new life for an old "expanded porphyrin", *Synlett* **1991**, 127-134.

[27] J. L. Sessler, M. J. Cyr, V. Lynch, E. McGhee, J. A. Ibers, Synthetic and structural studies of sapphyrin, a 22-π-electron pentapyrrolic "expanded porphyrin", *J. Am. Chem. Soc.* **1990**, *112*, 2810-2813.

[28] B. L. Iverson, K. Shreder, V. Kral, J. L. Sessler, Phosphate recognition by sapphyrin. A new approach to DNA binding, *J. Am. Chem. Soc.* **1993**, *115*, 11022-11023.

[29] J. L. Sessler, J. Lisowski, K. A. Boudreaux, V. Lynch, J. Barry, T. J. Kodadek, Synthesis and characterization of diaryl sapphyrins prepared under Lindsey-type conditions, *J. Org. Chem.* **1995**, *60*, 5975-5978.

[30] Z. S. Yoon, D.-G. Cho, K. S. Kim, J. L. Sessler, D. Kim, Nonlinear Optical Properties as a Guide to Aromaticity in Congeneric Pentapyrrolic Expanded Porphyrins: Pentaphyrin, Sapphyrin, Isosmaragdyrin, and Orangarin, *J. Am. Chem. Soc.* **2008**, *130*, 6930-6931.

[31] P. J. Boul, D.-G. Cho, G. M. A. Rahman, M. Marquez, Z. Ou, K. M. Kadish, D. M. Guldi, J. L. Sessler, Sapphyrin-Nanotube Assemblies, *J. Am. Chem. Soc.* **2007**, *129*, 5683-5687.

[32] P. K. Panda, Y.-J. Kang, C.-H. Lee, A benzodipyrrole-derived sapphyrin, *Angew. Chem., Int. Ed.* **2005**, *44*, 4053-4055.

[33] S. J. Narayanan, B. Sridevi, T. K. Chandrashekar, A. Vij, R. Roy, Novel Core-Modified Expanded Porphyrins with meso-Aryl Substituents: Synthesis, Spectral and Structural Characterization, *J. Am. Chem. Soc.* **1999**, *121*, 9053-9068.

[34] S. J. Narayanan, B. Sridevi, T. K. Chandrashekar, A. Vij, R. Roy, Sapphyrin Supramoleculess through C-H...S and C-H...Se Hydrogen Bond: First Structural

Caracteristion fo meso-ArylSapphyrins with Heteroatoms, *Angew. Chem. Int. Ed.* **1998**, *37*, 3394-3397.

[35] L. Szterenberg, L. Latos-Grazynski, Geometry and tautomerism of sapphyrin-DFT studies, *J. Mol. Struct.* **1999**, *490*, 33-46.

[36] A. Srinivasan, S. K. Pushpan, M. R. Kumar, S. Mahajan, T. K. Chandrashekar, R. Roy, P. Ramamurthy, meso-Aryl sapphyrins with heteroatoms; synthesis, characterization, spectral and electrochemical properties, *J. Chem. Soc., Perkin Trans. 2* **1999**, 961-968.

[37] M. Rajeswara Rao, M. Ravikanth, Synthesis and Studies of Covalently Linked Porphyrin-Expanded Heteroporphyrin Dyads, *Eur. J. Org. Chem.* **2011**, 1335-1345.

[38] Y. Pareek, M. Ravikanth, Synthesis of Mono-Functionalized Core-Modified Expanded Porphyrin Building Blocks and Covalently Linked Expanded Porphyrin Dyads, *Eur. J. Org. Chem.* **2011**, *2011*, 5390-5399.

[39] V. S. Shetti, M. Ravikanth, Supramolecular Tetrads Containing Sn(IV) Porphyrin, Ru(II) Porphyrin, and Expanded Porphyrins Assembled Using Complementary Metal-Ligand Interactions, *Inorg. Chem.* **2011**, *50*, 1713-1722.

[40] J. D. Hooker, V. H. Nguyen, V. M. Taylor, D. L. Cedeno, T. D. Lash, M. A. Jones, S. M. Robledo, I. D. Velez, New application for expanded porphyrins: sapphyrin and heterosapphyrins as inhibitors of Leishmania parasites, *Photochem. Photobiol.* **2012**, *88*, 194-200.

[41] R. R. Malakalapalli, R. Mangalampalli, Synthesis of functionalized core-modified sapphyrins and covalently linked porphyrin-sapphyrin dyads, *Tetrahedron* **2012**, *68*, 1306-1314.

[42] J. M. Lim, I. Gupta, H. Furuta, D. Kim, Comparative photophysics of sapphyrin derivatives:: effects of confused and fused pyrrole rings, *J. Porphyrins Phthalocyanines* **2011**, *15*, 858-864.

[43] D.-G. Cho, P. Plitt, K. Kim Sung, V. Lynch, S.-J. Hong, C.-H. Lee, L. Sessler Jonathan, Dioxabenzosapphyrin: a new benzodifuran-derived sapphyrin analogue, *J. Am. Chem. Soc.* **2008**, *130*, 10502-10503.

[44] S.-D. Jeong, J. L. Sessler, V. Lynch, C.-H. Lee, Dithiabenzisapphyrin: A Core-Modified Sapphyrin Bearing Exocyclic Double Bonds at the meso-Positions, *J. Am. Chem. Soc.* **2008**, *130*, 390-391.

[45] S. Kang, H. Hayashi, T. Umeyama, Y. Matano, V. Tkachenko Nikolai, H. Lemmetyinen, H. Imahori, meso-3,5-Bis(trifluoromethyl)phenyl-substituted expanded porphyrins: synthesis, characterization, and optical, electrochemical, and photophysical properties, *Chem. Asian. J.* **2008**, *3*, 2065-2074.

[46] R. Lopez, M. I. Menendez, M. Santander-Nelli, G. I. Cardenas-Jiron, A theoretical investigation on the spectroscopic properties and photosensitizing capability of 5,10,15,20-tetraphenylsapphyrin and 5, 10, 15, 20-tetraphenyl-26,28-diheterosapphyrins with two O, S, or Se Atoms, *Theor. Chem. Acc.* **2010**, *127*, 475-484.

[47] M. Ishida, S. Karasawa, H. Uno, F. Tani, Y. Naruta, Protonation-Induced Formation of a Stable Singlet Biradicaloid Derived from a Modified Sapphyrin Analogue, *Angew. Chem. Int. Ed.* **2010**, *49*, 5906-5909.

[48] B. Sathyamoorthy, A. Axelrod, V. Farwell, S. M. Bennett, B. D. Calitree, J. B. Benedict, D. K. Sukumaran, M. R. Detty, Novel 21,23-Ditelluraporphyrins and the First 26,28-Ditellurasapphyrin and 30,33-Ditellurarubyrin, *Organometallics* **2010**, *29*, 3431-3441.

[49] T. Nakabuchi, Y. Matano, H. Imahori, Remarkable Effects of P-Perfluorophenyl Group on the Synthesis of Core-Modified Phosphaporphyrinoids and Phosphadithiasapphyrin, *Org. Lett.* **2010**, *12*, 1112-1115.

[50] I. Gupta, A. Srinivasan, T. Morimoto, M. Toganoh, H. Furuta, N-confused and N-fused meso-aryl sapphyrins, *Angew. Chem. Int. Ed.* **2008**, *47*, 4563-4567.

[51] S. K. Pushpan, A. Srinivasan, V. G. Anand, S. Venkatraman, T. K. Chandrashekar, B. S. Joshi, R. Roy, H. Furuta, N-Confused Expanded Porphyrin: First Example of a

Modified Sapphyrin with an Inverted N-Confused Pyrrole Ring, *J. Am. Chem. Soc.* **2001**, *123*, 5138-5139.

[52] S.-Y. Kee, J. M. Lim, S.-J. Kim, J. Yoo, J.-S. Park, T. Sarma, V. M. Lynch, P. K. Panda, J. L. Sessler, D. Kim, C.-H. Lee, Conformational and spectroscopic properties of π-extended, bipyrrole-fused rubyrin and sapphyrin derivatives, *Chem. Commun.* **2011**, *47*, 6813-6815.

[53] J. L. Sessler, D.-G. Cho, M. Stepien, V. Lynch, J. Waluk, Z. S. Yoon, D. Kim, Inverted Sapphyrin: A New Family of Doubly N-Confused Expanded Porphyrins, *J. Am. Chem. Soc.* **2006**, *128*, 12640-12641.

[54] P. J. Chmielewski, L. Latos-Grazynski, K. Rachlewicz, 5,10,15,20-Tetraphenylsapphyrin. Identification of a pentapyrrolic expanded porphyrin in the Rothemund synthesis, *Chem. Eur. J.* **1995**, *1*, 68-73.

[55] S. J. Narayanan, B. Sridevi, A. Srinivasan, T. K. Chandrashekar, R. Roy, One step synthesis of sapphyrin and N-confused porphyrin using dipyrromethane, *Tetrahedron Lett.* **1998**, *39*, 7389-7392.

[56] L. Simkhovich, S. Rosenberg, Z. Gross, Facile synthesis of a novel sapphyrin and its rhodium(I) complex, *Tetrahedron Lett.* **2001**, *42*, 4929-4931.

[57] B. Koszarna, D. T. Gryko, Efficient Synthesis of meso-Substituted Corroles in a H2O-MeOH Mixture, *J. Org. Chem.* **2006**, *71*, 3707-3717.

[58] Z. Ou, D. Meng, M. Yuan, W. Huang, Y. Fang, K. M. Kadish, Deprotonation Reactions and Electrochemistry of Substituted Open-Chain Pentapyrroles and Sapphyrins in Basic Nonaqueous Media, *J. Phys. Chem. B* **2013**, *117*, 13646-13657.

[59] M. Yuan, Z. Ou, Y. Fang, S. Huang, Z. Xue, G. Lu, K. M. Kadish, Synthesis, Characterization, Protonation Reactions, and Electrochemistry of Substituted Open-Chain Pentapyrroles and Sapphyrins in Nonaqueous Media, *Inorg. Chem.* **2013**, *52*, 6664-6673.

[60] W. Huang, Z. Ou, X. Chen, Z. Xue, G. Lu, H. Wang, J. Xiao, Y. Fang, K. M. Kadish, A facile synthetic route to meso-tetraaryl substituted N-5 sapphyrins and first single

crystal X-ray analysis confirming the pyrrole inverted structure, *J. Porphyrins Phthalocyanines* **2015**, *19*, 794-802.

[61] Z. Gross, N. Galili, L. Simkhovich, I. Saltsman, M. Botoshansky, D. Blaeser, R. Boese, I. Goldberg, Solvent-Free Condensation of Pyrrole and Pentafluorobenzaldehyde: A Novel Synthetic Pathway to Corrole and Oligopyrromethenes, *Org. Lett.* **1999**, *1*, 599-602.

[62] Y. Fang, Z. Ou, K. M. Kadish, Electrochemistry of Corroles in Nonaqueous Media, *Chem. Rev.* **2017**, *117*, 3377-3419.

[63] J. Shen, J. Shao, Z. Ou, W. E, B. Koszarna, D. T. Gryko, K. M. Kadish, Electrochemistry and Spectroelectrochemistry of meso-Substituted Free-Base Corroles in Nonaqueous Media: Reactions of (Cor)H3, [(Cor)H4]+, and [(Cor)H2], *Inorg. Chem.* **2006**, *45*, 2251-2265.

[64] J. Shen, Z. Ou, J. Shao, M. Galezowski, D. T. Gryko, K. M. Kadish, Free-base corroles: determination of deprotonation constants in non-aqueous media, *J. Porphyrins Phthalocyanines* **2007**, *11*, 269-276.

[65] Z. Ou, J. Shen, J. Shao, W. E, M. Galezowski, D. T. Gryko, K. M. Kadish, Protonated Free-Base Corroles: Acidity, Electrochemistry, and Spectroelectrochemistry of [(Cor)H4]+, [(Cor)H5]2+, and [(Cor)H6]3+, *Inorg. Chem.* **2007**, *46*, 2775-2786.

[66] W. Shan, N. Desbois, V. Blondeau-Patissier, M. L. Naitana, V. Quesneau, Y. Rousselin, C. P. Gros, Z. Ou, K. M. Kadish, Synthesis, characterization and electrochemistry of open-chain pentapyrroles and sapphyrins with highly electron-withdrawing meso-tetraaryl substituents, *Chem. - Eur. J.* **2017**, *23*, 12833-12844.

[67] M. Meot-Ner, A. D. Adler, Interpretation of linear Hammett constant correlations in substituted ms-tetraphenylporphins, *J. Am. Chem. Soc.* **1972**, *94*, 4763-4764.

[68] C. Hansch, A. Leo, R. W. Taft, A survey of Hammett substituent constants and resonance and field parameters, *Chem. Rev.* **1991**, *91*, 165-195.

[69] X. Q. Lin, K. M. Kadish, Vacuum-tight thin-layer spectroelectrochemical cell with a doublet platinum gauze working electrode, *Anal. Chem.* **1985**, *57*, 1498-1501.

[70] P. Zuman, *Substituents Effects in Organic Polarography* **1967**, *Plenum Press: New York*, pp. 23-41.

[71] K. M. Kadish, M. M. Morrison, Solvent and substituent effects on the redox reactions of para-substituted tetraphenylporphyrin, *J. Am. Chem. Soc.* **1976**, *98*, 3326-3328.

4

Electrochemistry and Protonation Reactions of *Meso*-aryl Substituted Open-chain Pentapyrroles

4.1 Introduction

Open-chain pentapyrroles (or pentapyrrotetramethene) with *meso*-tetraaryl substituents were first isolated as a major side-product in the synthesis of corroles, being obtained in high yield (11%, the same as the target product),[1] and these molecules have since attracted great attention as synthetic precursors for the related sapphyrin macrocycles.[1-8]

Our own interest in open-chain pentapyrroles has involved a characterization of their electrochemistry, spectroelectrochemistry and acid-base properties in nonaqueous media, as well as a study of their conversion to the corresponding sapphyrins [5-8]. The open-chain pentapyrroles were shown to undergo two reversible one-electron reductions in CH_2Cl_2, PhCN or pyridine, with the $E_{1/2}$ values for these processes varying only slightly with the utilized electrochemical solvent.[5, 6] However, in contrast to the well-defined reductions of open-chain pentapyrroles, the oxidation behavior of these compounds was shown to vary as a function of the selected solvent. Cations and dications of the pentapyrroles could be generated and characterized prior to sapphyrin formation in CH_2Cl_2 or PhCN[5] but this was not the case in pyridine where deprotonation was proposed to occur after the abstraction of one electron in the basic solvent.[6] Additional oxidation processes were also observed in the cyclic voltammograms of pentapyrroles with sterically hindered or highly electron-withdrawing groups, and it was suggested[5, 8] that this might be related to the products formed in a proton-induced conversion to the corresponding sapphyrins.

The acid-base properties of several open-chain pentapyrroles were previously examined in our laboratory and the equilibrium constants for proton addition to these compounds were determined utilizing spectroscopic monitoring of the reaction. Two protons could be easily added to the open-chain pentapyrroles with the measured $\log\beta_2$ for this reaction ranging from 8.1 to 11.0.[5, 8] Two protons could also be abstracted with $\log\beta_2$ values ranging from 5.1 to 6.4.[6] Detailed studies of the proton-induced conversion of pentapyrroles to the corresponding sapphyrins are described in the literature.[7, 8]

In the present paper, a new series of open-chain pentapyrroles containing different *meso*-aryl groups were synthesized and characterized as to their spectral and electrochemical properties in CH_2Cl_2, PhCN and pyridine (Py). Their protonation reactions were also investigated. A single crystal analysis of one compound is given in the present study and comparisons are made with an earlier reported open-chain pentapyrrole structure. The five newly investigated compounds are shown in Chart 4-1 and are represented as $(Ar)_4PPyH_3$ where Ar = *m,m*-F_2Ph **1**, *p*-BrPh **2**, Ph **3**, *m,m,p*-$(OMe)_3$Ph **4** or *p*-MePh **5**.

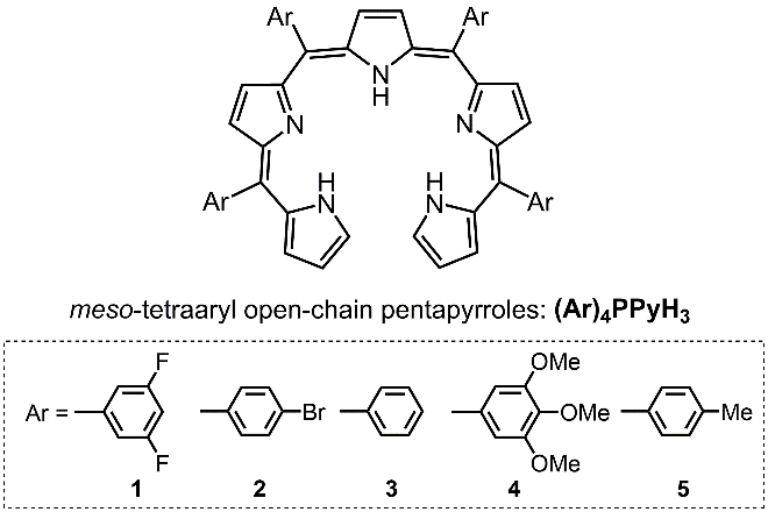

Chart 4-1. Structures of investigated compounds **1-5**.

4.2 Synthesis and Characterization

The five open-chain pentapyrroles in Chart 4-1 were isolated as side-products in the synthesis of structurally related triarylcorroles according to methods described in the literature.[5, 8] The newly synthesized compounds were then fully characterized by ^{1}H NMR spectroscopy, mass spectrometry (MS MALDI/TOF) and high-resolution mass spectrometry (HRMS MALDI/TOF).[9] The molecular weights of the compounds were determined by mass spectrometry and show, in each case, a perfect match with the calculated molar mass. Characteristic chemical shift data in the ^{1}H NMR spectra also confirmed the target compounds **1-5** to have the structures shown in Chart 4-1.

A plate-shaped crystal of compound **2** (*p*-BrPh)$_4$PPyH$_3$ was obtained and a single crystal X-ray diffraction experiment was carried out as given in the reference.[9] A comparison between the X-ray structure of compound **2** and the structures for three earlier reported pentapyrroles[8, 10, 11] are also given in this manuscript.

Absorption spectra of the compounds **1-5** were measured at a concentration of 10^{-3} M in CH_2Cl_2, PhCN and pyridine containing 0.1 M TBAP (Figure 4-1 and Table 4-1). Two or three intense bands (ε = ~10^4 cm^{-1}·M^{-1}) were present in the Soret region of the spectrum while one or two broad bands of lower intensity (ε = ~10^3 cm^{-1}·M^{-1}) are seen in the visible region.

The above spectroscopic properties are all consistent with previously reported spectral data for the similar compounds.[5, 7, 8] Additional detailed information on the synthesis and characterization are given in SI of reference.[9]

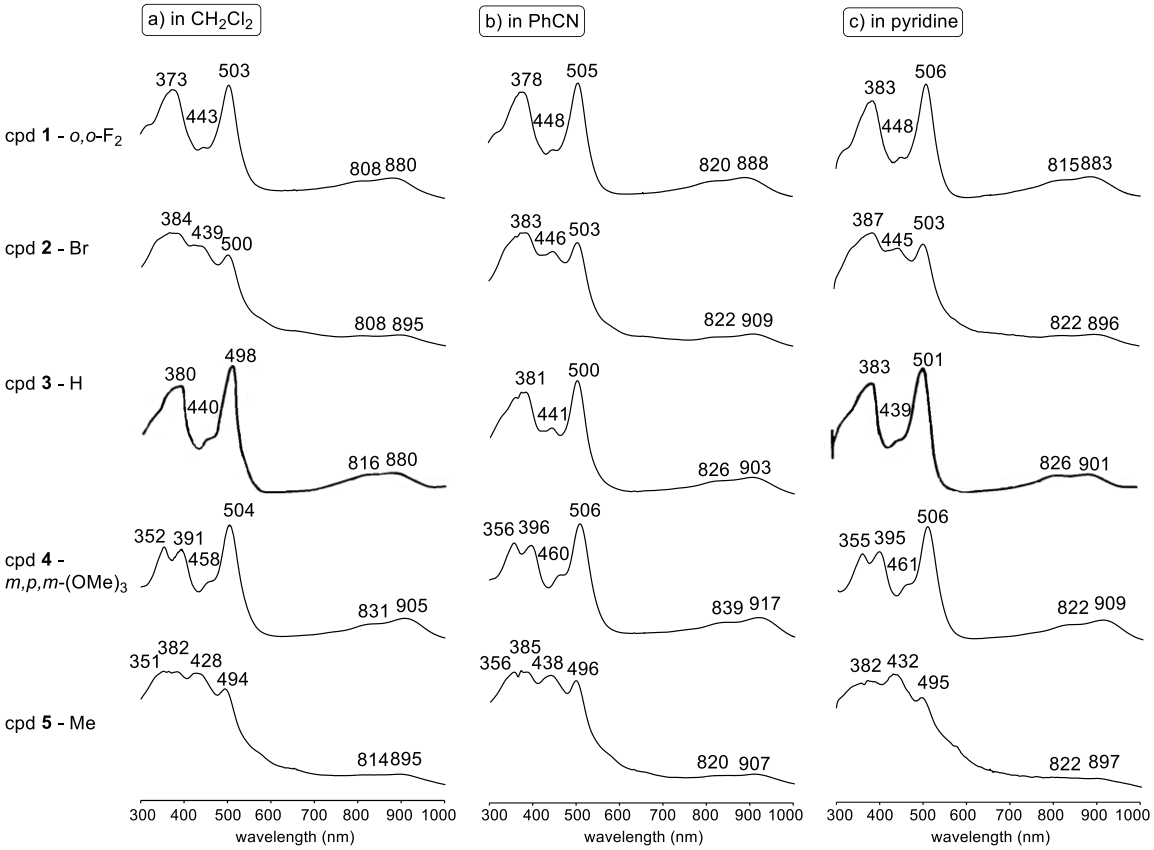

Figure 4-1. UV-visible spectra of compounds **1-5** in a) CH_2Cl_2, b) PhCN and c) pyridine containing 0.1 M TBAP.

Table 4-1. UV-visible spectral data of $(Ar)_4PPyH_3$ **1-5** (~10^{-3} M) in CH_2Cl_2, PhCN and pyridine containing 0.1 M TBAP.

Solvent	X (Ar = XPh)	wavelength: λ, nm (ε×10^{-4} $cm^{-1}\cdot M^{-1}$)				
		Soret region		visible region		
CH_2Cl_2	*m,m*-F_2 **1**	373 (4.4)	443 (2.2)	503 (4.6)	808 (0.9)	880 (1.0)
	p-Br **2**	384 (4.7)	439 (4.2)	500 (3.8)	808 (0.6)	895 (0.7)
	H **3**	380 (1.1)	440	498 (1.3)	816 (0.2)	880 (0.2)
	m,p,m-$(OMe)_3$ **4**	352 (4.3), 391 (4.2)	458 (2.7)	504 (5.5)	831 (0.8)	905 (1.0)
	p-Me **5**	351 (3.5), 382 (3.5)	428 (3.4)	494 (3.0)	814 (0.4)	895 (0.4)
PhCN	*m,m*-F_2 **1**	378 (3.4)	448 (1.6)	505 (3.7)	820 (0.6)	888 (0.7)
	p-Br **2**	383 (4.4)	446 (3.7)	503 (4.0)	822 (0.8)	909 (0.9)
	H **3**	381 (2.2)	441 (1.4)	500 (2.5)	826 (0.2)	903 (0.2)
	m,p,m-$(OMe)_3$ **4**	356 (3.7), 396 (3.6)	460 (2.5)	506 (4.3)	839 (0.8)	917 (1.0)
	p-Me **5**	356 (2.1), 385 (2.1)	438 (2.1)	496 (2.0)	820 (0.1)	907 (0.1)
pyridine	*m,m*-F_2 **1**	383 (2.8)	448 (1.1)	506 (3.3)	815 (0.5)	883 (0.6)
	p-Br **2**	387 (2.6)	445 (2.3)	503 (2.4)	822 (0.4)	896 (0.4)
	H **3**	383 (1.4)	439 (1.1)	501 (1.3)	826 (0.2)	901 (0.2)
	m,p,m-$(OMe)_3$ **4**	355 (4.4), 395 (4.5)	461 (2.9)	506 (5.7)	822 (0.9)	909 (1.1)
	p-Me **5**	382 (1.6)	432 (1.7)	495 (1.4)	822 (0.2)	897 (0.2)

4.3 Electrochemistry

The electrochemistry of compounds **1-5** was characterized by cyclic voltammetry in CH_2Cl_2, PhCN or pyridine containing 0.1 M TBAP. Examples of cyclic voltammograms for compound **4** in those three solvents containing 0.1 M TBAP are given in Figure 4-2 and a summary of the measured half-wave potentials for reductions and oxidations in each solvent are given in Table 4-2.

As shown in Figure 4-2, two reversible reductions occur in each solvent. Two reversible oxidations are also seen in CH_2Cl_2 and PhCN, but this is not the case in pyridine which reacts with the singly oxidized pentapyrrole as described previously [6]. Regardless of the solvent, two electrons can be abstracted from the conjugated π-system of the pentapyrrole under the given solution conditions.

The separation in $E_{1/2}$ between the two one-electron oxidations in CH_2Cl_2 or PhCN (0.22 V) are smaller than the separation in pyridine (0.30 V) as seen in Figure 4-2. Moreover, the electrochemical HOMO-LUMO gap (the potential difference between the first oxidation and first reduction) decreases upon going from CH_2Cl_2 to PhCN and then to pyridine. For example, in the case of compound **4** (Figure 4-2), the electrochemically measured HOMO-LUMO gap is 1.32 eV in CH_2Cl_2, 1.25 eV in PhCN and 1.13 eV in pyridine.

Cyclic voltammograms for all five pentapyrroles in each solvent containing 0.1 M TBAP are given in Figures 4-3 (in DCM), 4-4 (in PhCN) and 4-5 (in pyridine). As shown in Figure 4-3, the redox potentials are negatively shifted upon going from compound **1**

(which has two electron-withdrawing F atoms on the *meso*-phenyl rings) to compound **5**, which possesses *p*-Me electron-donating groups on the *meso*-phenyl rings. The HOMO-LUMO gap in CH_2Cl_2 averages 1.32 ± 0.04 V while the average gap in the other two solvents, PhCN and pyridine is 1.24 and 1.09 V, respectively.

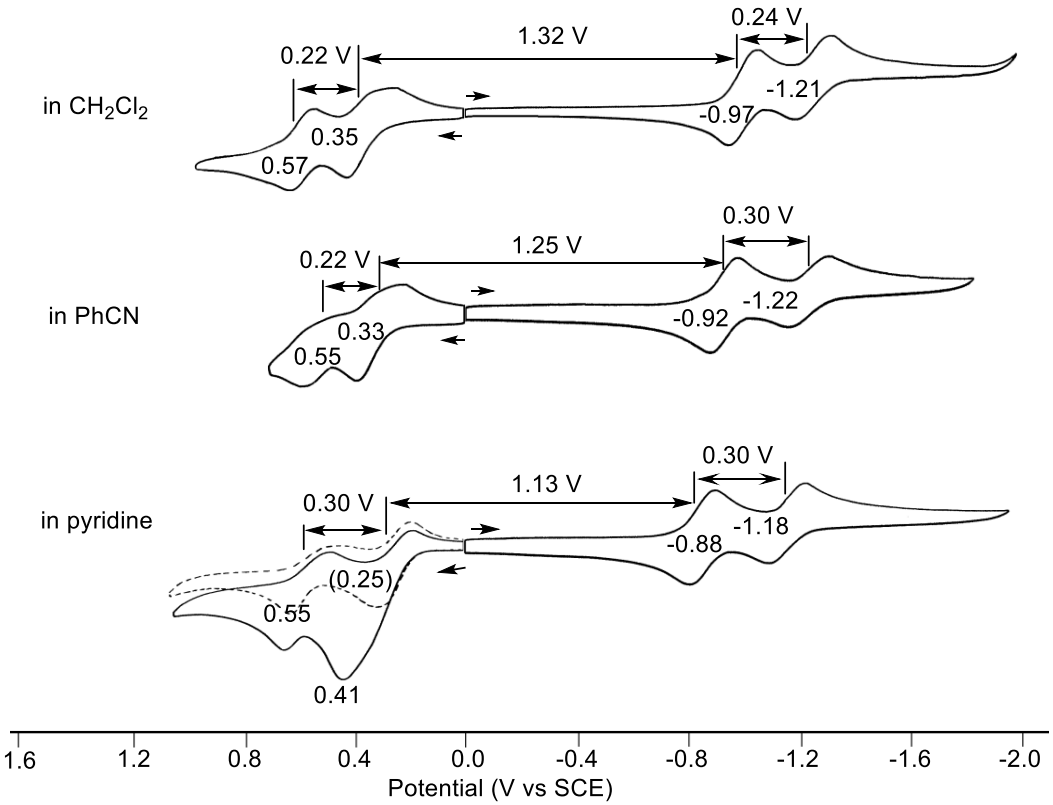

Figure 4-2. Cyclic voltammograms of (*m,p,m*-$(OMe)_3Ph)_4PPyH_3$ **4** in CH_2Cl_2, PhCN and pyridine containing 0.1 M TBAP. All current-voltage curves were obtained on the first potential scan except for the oxidation in pyridine which shows the first (solid line) and second (dashed line) potential scans.

Table 4-2. Half-wave potentials ($E_{1/2}$, V vs SCE) of $(Ar)_4PPyH_3$ derivatives **1-5** in CH_2Cl_2, PhCN and pyridine containing 0.1 M TBAP.

Solvent	X (Ar = XPh)	Σσ[a]	$E_{1/2}$ (V vs SCE)						H-L(eV)[b]
			Ox2	Ox1	ΔE_{ox}	Red1	Red2	ΔE_{red}	
CH_2Cl_2	*m,m*-F_2 **1**	2.72	0.77	0.57	0.20	-0.79	-1.05	0.26	1.36
	p-Br **2**	0.92	0.72	0.46	0.16	-0.88	-1.12	0.24	1.34
	H **3**	0.0	0.58	0.33	0.25	-0.98	-1.16	0.18	1.31
	m,p,m-$(OMe)_3$ **4**	-0.12	0.57	0.35	0.22	-0.97	-1.21	0.24	1.32
	p-Me **5**	-0.68	0.49	0.31	0.18	-0.99	-1.20	0.21	1.30
PhCN	*m,m*-F_2 **1**	2.72	0.77	0.56	0.21	-0.69	-0.99	0.30	1.25
	p-Br **2**	0.92	0.60	0.42	0.18	-0.83	-1.12	0.29	1.25
	H **3**	0.0	0.60	0.35	0.25	-0.89	-1.19	0.30	1.24
	m,p,m-$(OMe)_3$ **4**	-0.12	0.55	0.33	0.22	-0.92	-1.22	0.30	1.25
	p-Me **5**	-0.68	0.51	0.29	0.22	-0.94	-1.21	0.27	1.23
pyridine	*m,m*-F_2 **1**	2.72	0.73	0.42	0.31	-0.70	-1.00	0.30	1.12
	p-Br **2**	0.92	0.65	0.30	0.35	-0.78	-1.07	0.29	1.08
	H **3**	0.0	0.60	0.24	0.36	-0.85	-1.12	0.27	1.09
	m,p,m-$(OMe)_3$ **4**	-0.12	0.55	0.25	0.30	-0.88	-1.18	0.30	1.13
	p-Me **5**	-0.68	0.56	0.21[c]	0.35	-0.90	-1.13	0.23	1.11

[a]Values of σ were taken from reference [11]. [b]The HOMO-LUMO gap (potential difference between the first oxidation and first reduction). [c]Half-wave potentials for the first oxidation were obtained from the second scan.

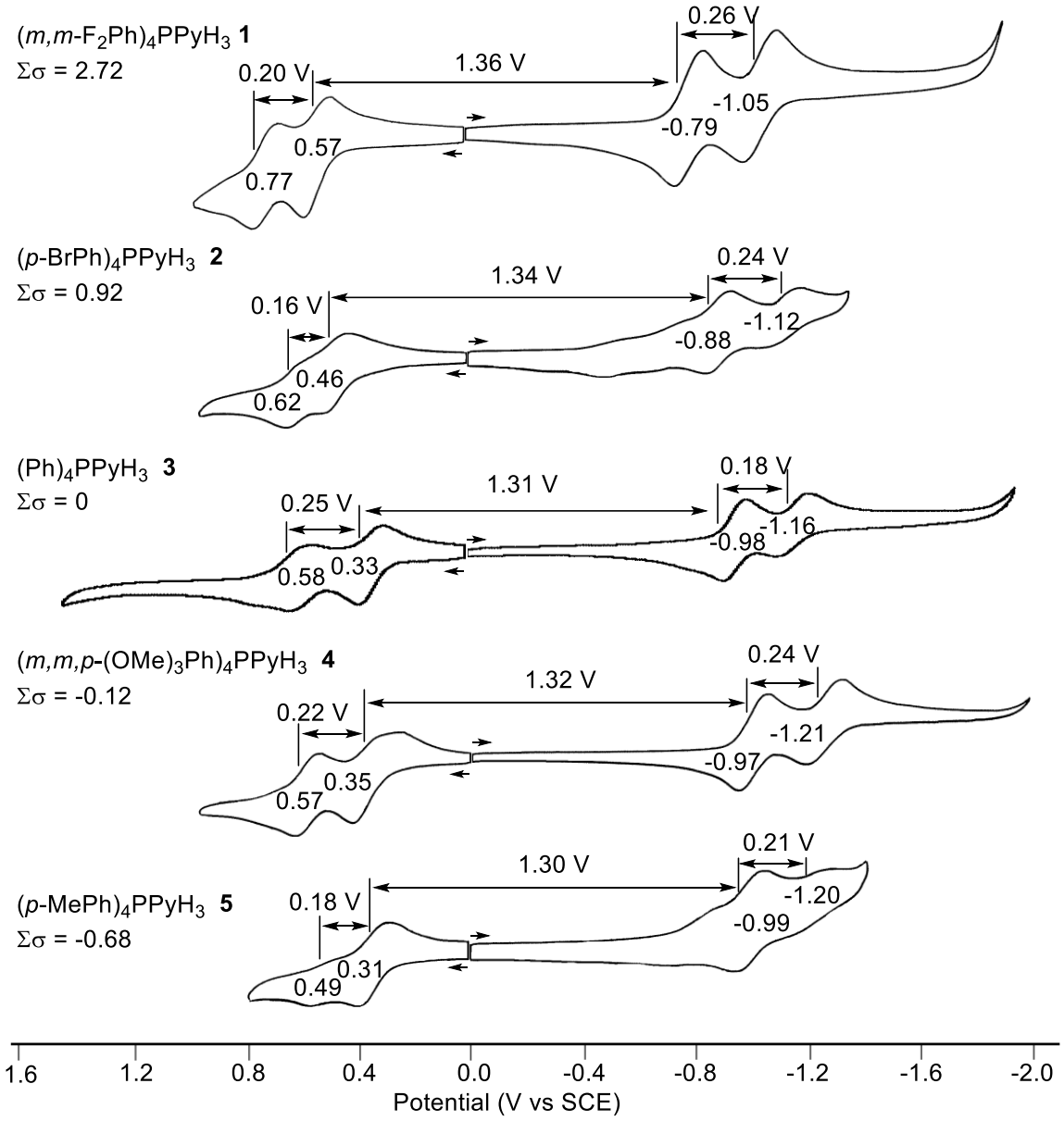

Figure 4-3. Cyclic voltammograms of open-chain pentapyrroles **1-5** in CH_2Cl_2 containing 0.1 M TBAP.

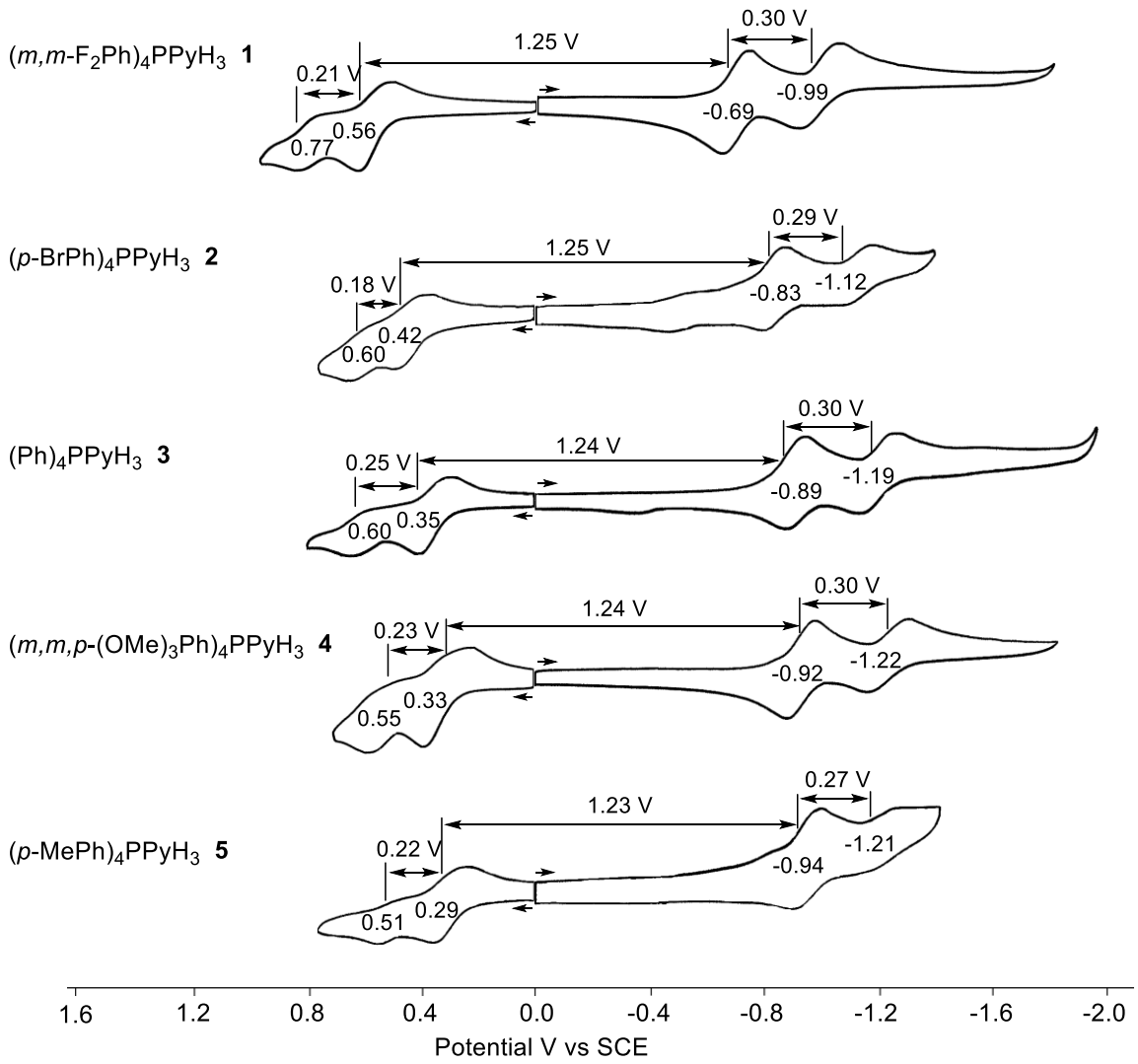

Figure 4-4. Cyclic voltammograms of open-chain pentapyrroles **1-5** in PhCN containing 0.1 M TBAP.

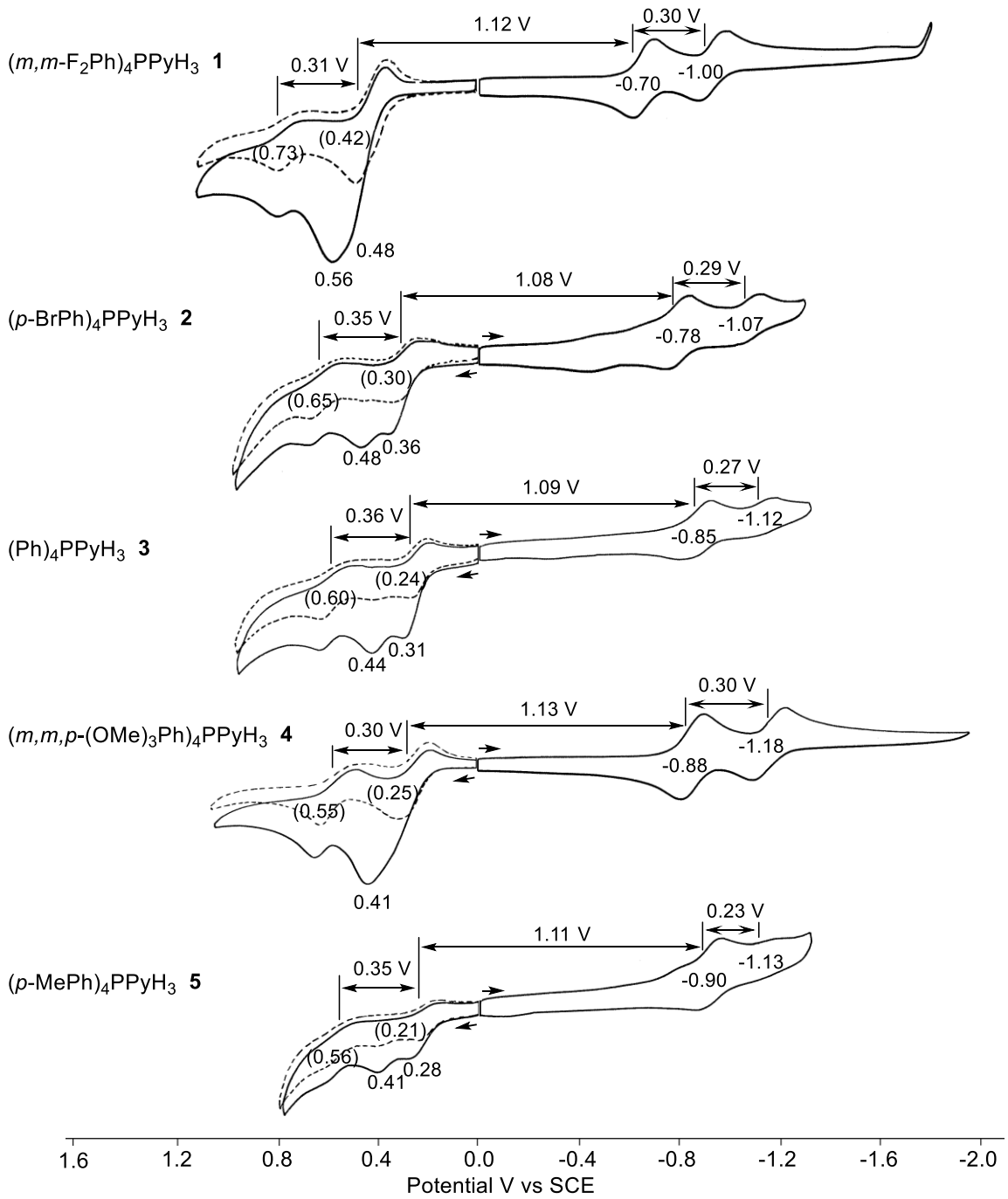

Figure 4-5. Cyclic voltammograms of open-chain pentapyrroles **1-5** in pyridine containing 0.1 M TBAP.

The measured $E_{1/2}$ values for each redox reaction of the open-chain pentapyrroles can be related to the specific electron-donating or electron-withdrawing substituent on the four phenyl rings of the compounds by linear free energy relationships.[5, 8] The relevant correlation is given in Equation 4-1, where ρ is the slope of $E_{1/2}$ vs. Σσ plot[12] and the values of σ are taken from the literature.[13] The larger the value of ρ (given in volts), the larger is the effect of the electron-donating or electron-withdrawing substituents on the measured half wave potentials for a given electron transfer reaction, in this case the two one-electron reductions and two one-electron oxidations of the pentapyrroles.

$$\Delta E_{1/2} = \Sigma\sigma\rho \qquad (4\text{-}1)$$

Examples of linear free energy relationships for the pentapyrroles in the three electrochemical solvents are given in Figures 4-6, 4-7 and 4-8 where the redox potentials in the plots are listed in Table 4-2 for the newly investigated compounds and in Table 4-3 for previously characterized pentapyrroles with different *meso*-phenyl substituents.[5, 6, 8] The values of ρ which were calculated in each solvent from $E_{1/2}$ vs 4σ plots of the type shown in Figure 4-6 are summarized in Table 4-4, which also includes data for structurally related free-base porphyrins possessing four substituted *meso*-phenyl groups.[14]

As shown in the table, the calculated ρ values for the two oxidations of the pentapyrrole are larger in CH_2Cl_2 (76 and 67 mV) than in PhCN (61 and 57 mV) or pyridine (57 and 50 mV) and an opposite trend is seen in pyridine, namely smaller effects of the substituents for oxidation than for reduction. However, the range of ρ

values in Table 4-5 are similar to values observed for numerous porphyrins and corrole redox reactions of tetraaryl derivatives.[14, 15] and this strongly suggests that there is not a significant difference in substituent effects between the electron-donating or electron-withdrawing groups on the four *meso*-phenyl rings of the open chain pentapyrroles and those on the four *meso*-phenyl rings of free-base tetraphenylporphyrin.

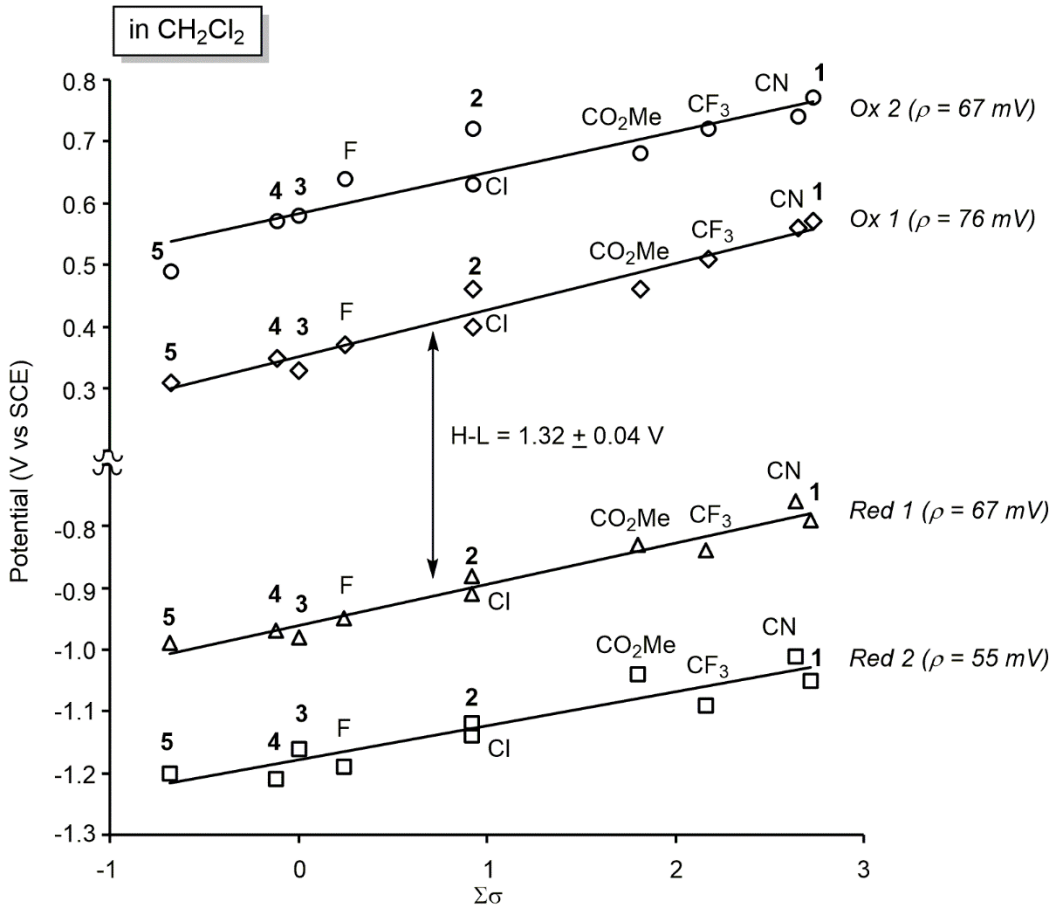

Figure 4-6. Plots of half-wave potentials vs. the sum of Hammett substituent constants ($\Sigma\sigma$) for open-chain pentapyrroles $(XPh)_4PPyH_3$ in CH_2Cl_2 containing 0.1 M TBAP.

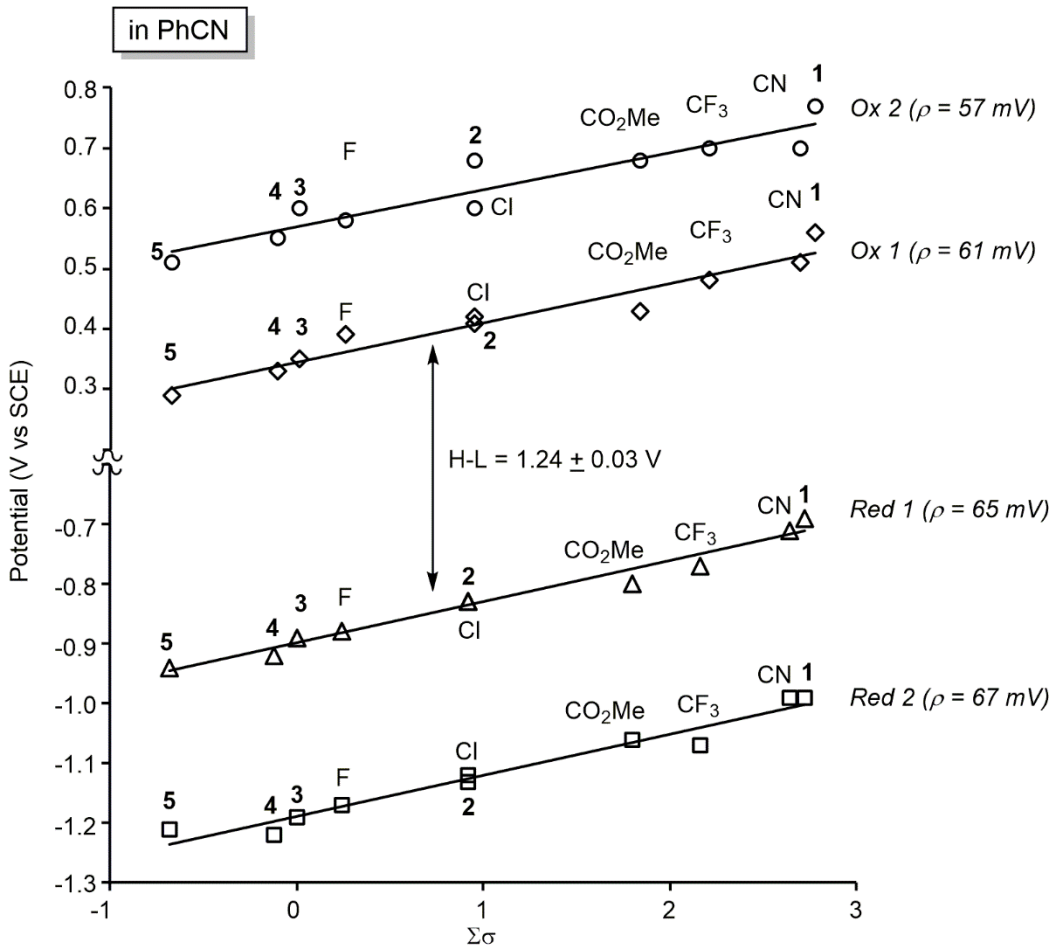

Figure 4-7. Plots of half-wave potentials vs. the sum of Hammett substituent constants (Σσ) for open-chain pentapyrroles $(XPh)_4PPyH_3$ in PhCN containing 0.1 M TBAP. All values are given in Tables 4-1 and 4-2.

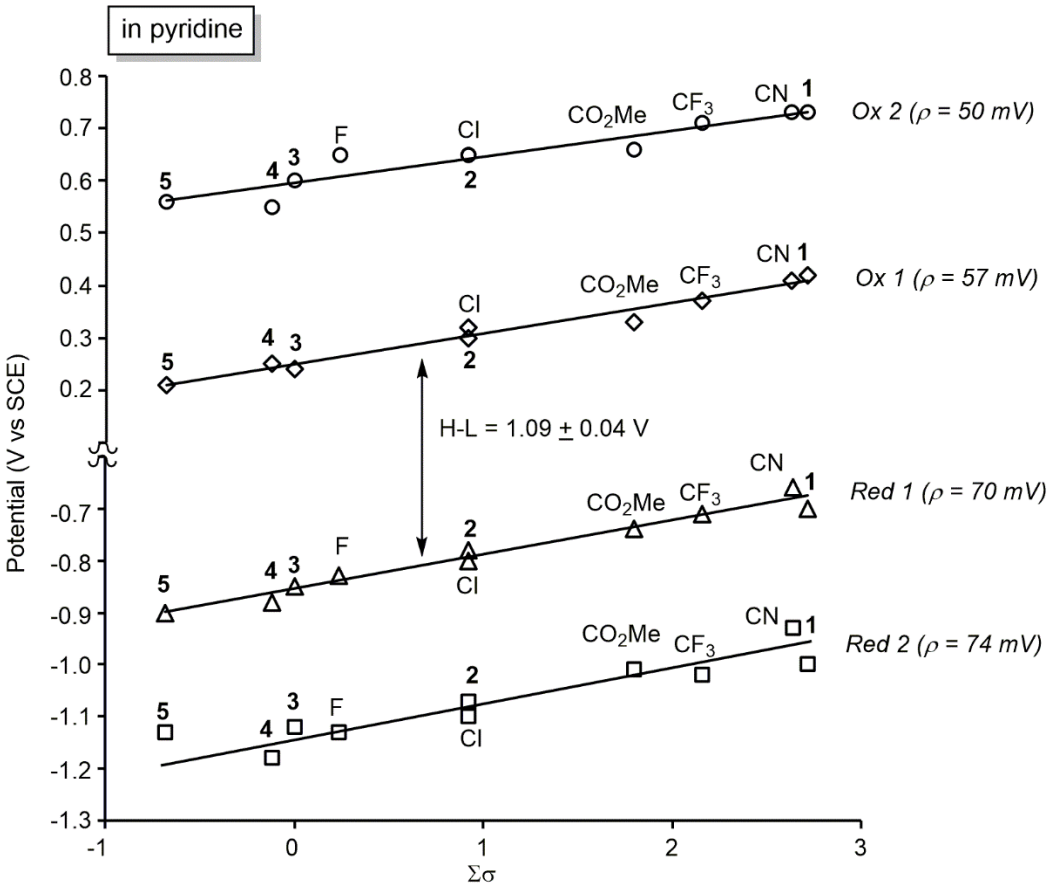

Figure 4-8. Plots of half-wave potentials vs. the sum of Hammett substituents constants (Σσ) for open-chain pentapyrroles $(XPh)_4PPyH_3$ in pyridine containing 0.1 M TBAP. All values are given in Tables 4-1 and 4-2.

Table 4-3. Half-wave potentials ($E_{1/2}$, V vs SCE) of related open-chain pentapyrroles $(XPh)_4PPyH_3$ in CH_2Cl_2, PhCN and pyridine containing 0.1 M TBAP.

Solvent	X	Σσ[a]	$E_{1/2}$ (V vs SCE)						H-L(eV)[b]	ref.
			1st Ox[c]	2nd Ox	ΔE_{ox}	1st Red	2nd Red	ΔE_{red}		
CH_2Cl_2	*p*-CN	2.64	0.56	0.74	0.18	-0.76	-1.01	0.25	1.32	[8]
	p-CF_3	2.16	0.51	0.72	0.21	-0.84	-1.09	0.25	1.35	[8]
	p-CO_2Me	1.80	0.46	0.68	0.22	-0.83	-1.04	0.21	1.29	[8]
	p-Cl	0.92	0.40	0.63	0.23	-0.91	-1.14	0.23	1.31	[5]
	p-F	0.24	0.37	0.64	0.27	-0.95	-1.19	0.24	1.32	[5]
PhCN	*p*-CN	2.64	0.51	0.70	0.19	-0.71	-0.99	0.28	1.22	[8]
	p-CF_3	2.16	0.48	0.70	0.22	-0.77	-1.07	0.30	1.25	[8]
	p-CO_2Me	1.80	0.43	0.68	0.25	-0.80	-1.06	0.26	1.23	[8]
	p-Cl	0.92	0.41	0.68	0.27	-0.83	-1.13	0.30	1.24	[5]
	p-F	0.24	0.39	0.58	0.19	-0.88	-1.17	0.29	1.27	[5]
pyridine	*p*-CN	2.64	0.41	0.73	0.32	-0.66	-0.93	0.27	1.07	[8]
	p-CF_3	2.16	0.37	0.71	0.34	-0.71	-1.02	0.31	1.08	[8]
	p-CO_2Me	1.80	0.33	0.66	0.33	-0.74	-1.01	0.27	1.07	[8]
	p-Cl	0.92	0.32	0.65	0.33	-0.80	-1.10	0.30	1.12	[6]
	p-F	0.24	-	0.65	-	-0.83	-1.13	0.30	-	[6]

[a]Values of σ were taken from reference [13]. [b]The HOMO-LUMO gap (whose value equals to the potential difference between the first oxidation and first reduction). [c]The half-wave potentials of first oxidation were obtained from the second scans.

Table 4-4. Average potential differences between the first two oxidations (ΔE_{ox}), the first two reductions (ΔE_{red}) and the HOMO-LUMO gaps of compounds **1-5** in various solvents.

Solvent	Ave. ΔE_{ox} (V)	Δ Ave. ΔE_{red} (V)	Ave. HOMO-LUMO gap (V)
CH_2Cl_2	0.21 ± 0.04	0.23 ± 0.05	1.32 ± 0.04
PhCN	0.22 ± 0.03	0.29 ± 0.03	1.24 ± 0.03
pyridine	0.33 ± 0.03	0.28 ± 0.03	1.09 ± 0.04

Table 4-5. Plots of $E_{1/2}$ vs. 4σ for the reversible redox reactions of open-chain pentapyrroles of the type $(Ar)_4PPyH_3$ and related free-base *meso*-aryl porphyrins $(Ar)_4PorH_2$ having similar *meso*-phenyl substituents.

Compound	Solvent	ρ (mV)			
		Ox1	Ox2	Red1	Red2
$(Ar)_4PorH_2$[a]	CH_2Cl_2	65	--	73	64
$(Ar)_4PPyH_3$	CH_2Cl_2	76	67	67	55
	PhCN	61	57	65	67
	Pyridine	57	50	70	74[b]

[a]Data for porphyrins were taken from reference [14]. [b]The ρ value was calculated without (*p*-MePh)$_4$PPyH$_3$ **5**.

4.4 Protonation Reaction

The open-chain pentapyrroles can add two protons in a single step as written in Equation 4-2.

$$(Ar)_4PPyH_3 + 2H^+ \overset{\beta_2}{\rightleftharpoons} [(Ar)_4PPyH_5]^{2+} \qquad (4\text{-}2)$$

An example of the spectral changes which occur during protonation of compound **3** is shown in Figure 4-9 and the Hill plot used for calculating the equilibrium constant is given as an inset in the figure. The slope of the diagnostic plot is 2.0 which confirms a two-proton addition to the pyrrole nitrogens of this compound and the presence of well-defined isosbestic points in Figure 4-9 is consistent with the absence of intermediates during the conversion of $(Ph)_4PPyH_3$ to $[(Ph)_4PPyH_5]^{2+}$.

The same types of spectral changes and slopes of 2.0 were seen for all five newly synthesized pentapyrroles and a summary of the calculated equilibrium constants for these and previously characterized pentapyrroles is given in Table 4-6 where the measured $\log\beta_2$ ranges from 11.0 to 8.2, the exact value depending upon substituents on the phenyl rings which influences the basicity of the pyrrole nitrogens. Pentapyrroles with larger $\Sigma\sigma$ values have smaller $\log\beta_2$ values for the two-proton addition reaction. That is to say, the electron-withdrawing groups on the *meso*-phenyl rings make this protonation more difficult, a result which can be explained by the fact that the electron-withdrawing groups on the *meso*-phenyl rings pull electron density from the pyrrole nitrogens, thus making them less basic.

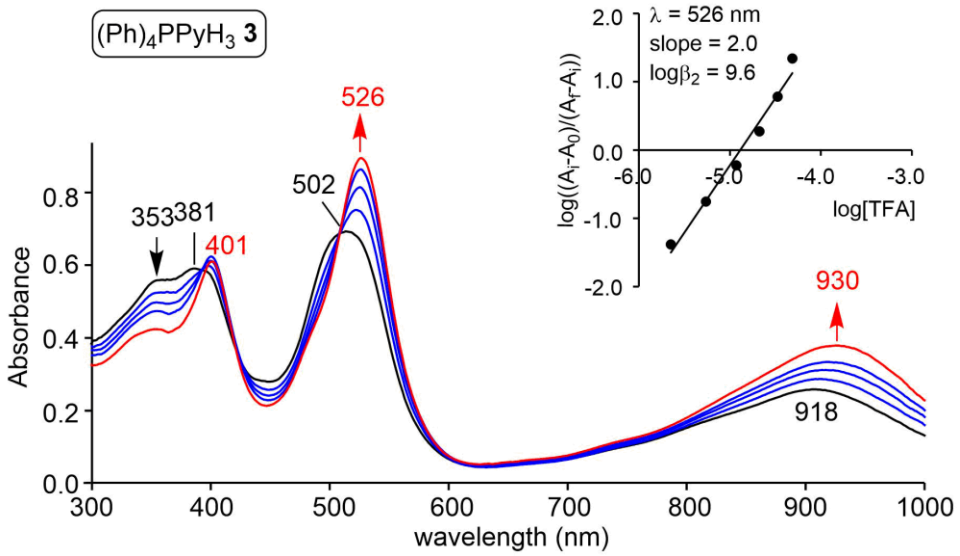

Figure 4-9. UV-vis spectral changes of $(Ph)_4PPyH_3$ **3** during the protonation in CH_2Cl_2 with TFA. The Hill plot for the calculation of equilibrium constant was shown as inset.

We anticipated a linear relationship would exist between the measured $\log\beta_2$ and the $\Sigma\sigma$ for all of the pentapyrroles in Table 4-6 but this was not the case for all compounds (see Figure 4-10), indicating that the basicity of the pyrrole nitrogens (and the measured $\log\beta_2$ values for protonation) were affected not only by the electron-donating or withdrawing properties of the *meso*-phenyl substituents but also by steric hindrance of these groups when it occurred.[5]

The known proton-induced oxidation reaction to generate the close-ring species [8] was also studied for compounds **1-5**. Compounds **1-3** were partially converted to the closed-ring sapphyrin derivatives, but this was not the case for compounds **4** and **5** where no such conversion occurred. The proposed overall mechanism of this proton-induced reaction and side reaction is given in Scheme 4-1.

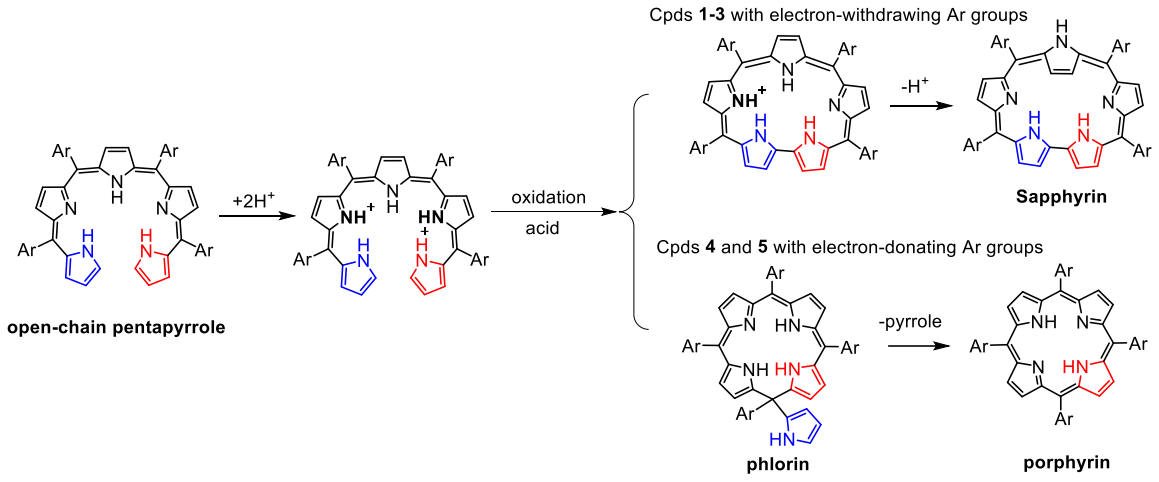

Scheme 4-1. Proposed overall mechanism of proton-induced oxidation reactions of open-chain pentapyrroles.

Table 4-6. UV-vis spectral data of $[(Ar)_4PPyH_5]^{2+}$ and equilibrium constants ($\log\beta_2$) for protonation reactions of open-chain pentapyrroles containing different *meso*-substituents.

X (Ar = XPh)	$\Sigma\sigma^a$	λ/nm of $[(Ar)_4PPyH_5]^{2+}$			$\log\beta_2{}^b$	reference
m,m-F_2 **1**	2.72	404	529	899	8.5	t.w.
p-CN	2.64	411	534	918	8.2	[8]
p-CF_3	2.16	404	530	919	8.5	[8]
p-CO_2Me	1.80	411	536	935	9.1	[8]
p-Br **2**	0.92	407	505	894	9.0	t.w.
o,p-$(Cl)_2$	1.72	403	514	876	8.1	[5]
p-Cl	0.92	404	526	914	9.1	[5]
p-F	0.24	400	524	915	11.0	[5]
H **3**	0.0	401	526	930	9.6	t.w.
m,p,m-$(OMe)_3$ **4**	-0.12	391	535	944	9.8	t.w.
p-Me **5**	-0.68	403	488, 524	926	9.9	t.w.

[a]Values of σ were taken from reference [13]. [b]Values were calculated from the Hill plots. t.w. = this work.

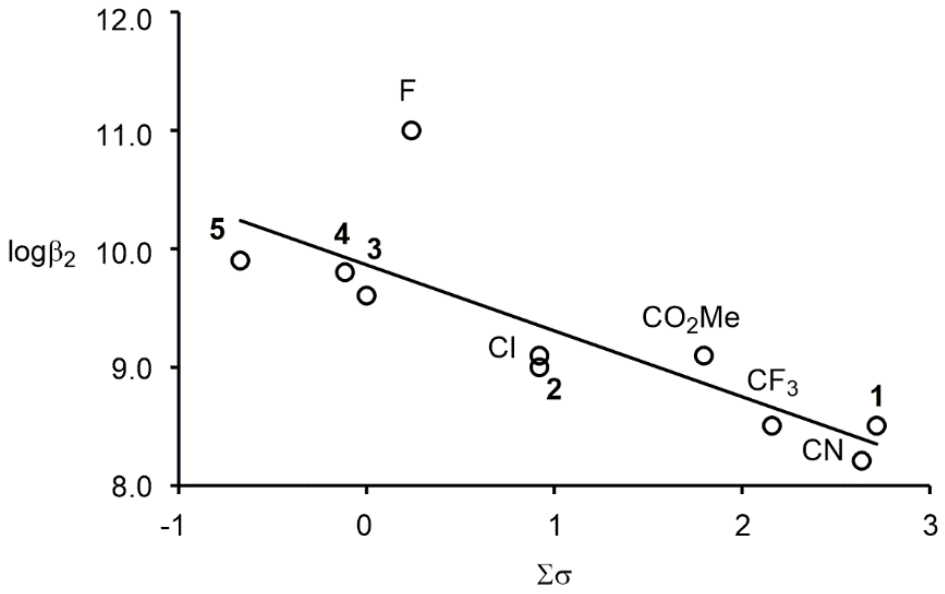

Figure 4-10. Plots of measured $\log\beta_2$ vs. the sum of Hammett substituent constants ($\Sigma\sigma$) for protonation reactions of open-chain pentapyrroles. The data are given in Table 4-6.

4.5 Conclusion

The aryl substituents on the four *meso*-positions of the open-chain pentapyrroles can affect the electron transfer behavior of these pentapyrrolic species. At the same time, it will also change the basicity of the central pyrrole nitrogen. This may result from both the electronic structure (substituent effects) and the molecular configuration (steric effects), the latter of which requires further studies in the future.

4.6 References

[1] Z. Gross, N. Galili, L. Simkhovich, I. Saltsman, M. Botoshansky, D. Blaeser, R. Boese, I. Goldberg, Solvent-Free Condensation of Pyrrole and Pentafluorobenzaldehyde: A Novel Synthetic Pathway to Corrole and Oligopyrromethenes, *Org. Lett.* **1999**, *1*, 599-602.

[2] L. Simkhovich, S. Rosenberg, Z. Gross, Facile synthesis of a novel sapphyrin and its rhodium(I) complex, *Tetrahedron Lett.* **2001**, *42*, 4929-4931.

[3] L. Naumovski, M. Sirisawad, P. Lecane, J. Chen, J. Ramos, Z. Wang, C. Cortez, D. Magda, P. Thiemann, G. Boswell, D. Miles, G. Cho Dong, L. Sessler Jonathan, R. Miller, Tumor localization and antitumor efficacy of novel sapphyrin compounds, *Mol. Cancer Ther.* **2006**, *5*, 2798-2805.

[4] B. Koszarna, D. T. Gryko, Efficient Synthesis of *meso*-Substituted Corroles in a H2O-MeOH Mixture, *J. Org. Chem.* **2006**, *71*, 3707-3717.

[5] M. Yuan, Z. Ou, Y. Fang, S. Huang, Z. Xue, G. Lu, K. M. Kadish, Synthesis, Characterization, Protonation Reactions, and Electrochemistry of Substituted Open-Chain Pentapyrroles and Sapphyrins in Nonaqueous Media, *Inorg. Chem.* **2013**, *52*, 6664-6673.

[6] Z. Ou, D. Meng, M. Yuan, W. Huang, Y. Fang, K. M. Kadish, Deprotonation Reactions and Electrochemistry of Substituted Open-Chain Pentapyrroles and Sapphyrins in Basic Nonaqueous Media, *J. Phys. Chem. B* **2013**, *117*, 13646-13657.

[7] W. Huang, Z. Ou, X. Chen, Z. Xue, G. Lu, H. Wang, J. Xiao, Y. Fang, K. M. Kadish, A facile synthetic route to *meso*-tetraaryl substituted N-5 sapphyrins and first single crystal X-ray analysis confirming the pyrrole inverted structure, *J. Porphyrins Phthalocyanines* **2015**, *19*, 794-802.

[8] W. Shan, N. Desbois, V. Blondeau-Patissier, M. L. Naitana, V. Quesneau, Y. Rousselin, C. P. Gros, Z. Ou, K. M. Kadish, Synthesis, characterization and electrochemistry of open-chain pentapyrroles and sapphyrins with highly electron-withdrawing *meso*-tetraaryl substituents, *Chem. - Eur. J.* **2017**, *23*, 12833-12844.

[9] W. Shan, V. Quesneau, N. Desbois, V. Blondeau-Patissier, M. L. Naitana, Y. Rousselin, C. P. Gros, Z. Ou, K. M. Kadish, Synthesis, electrochemistry, protonation and X-ray analysis of *meso*-aryl substituted open-chain pentapyrroles, *J. Porphyrins Phthalocyanines* **2019**, *23*, 213-222.

[10] J.-Y. Shin, S. S. Hepperle, D. Dolphin, Linear fully conjugated *meso*-aryl pentapyrrins, *Tetrahedron Lett.* **2009**, 6909–6912.

[11] U. G. Wagner, C. Kratky, H. Falk, H. Flödl, Kristallstruktur und Konformation eines linearen Pentapyrrols, *Monatshefte für Chemie* **1987**, *118*, 1185-1194.

[12] P. Zuman, *Substituents Effects in Organic Polarography* **1967**, *Plenum Press: New York*, pp. 23-41.

[13] C. Hansch, A. Leo, R. W. Taft, A survey of Hammett substituent constants and resonance and field parameters, *Chem. Rev.* **1991**, *91*, 165-195.

[14] K. M. Kadish, M. M. Morrison, Solvent and substituent effects on the redox reactions of para-substituted tetraphenylporphyrin, *J. Am. Chem. Soc.* **1976**, *98*, 3326-3328.

[15] K. M. Kadish, E. Van Caemelbecke, G. Royal, Electrochemistry of metalloporphyrins in nonaqueous media, **2000**, *8*, 1-114.

5

Electrochemistry of Bis(pyridine)cobalt (Nitrophenyl)corroles in Nonaqueous Media

5.1 Introduction

Metallocorroles are now an often-studied group of macrocycles because of their unique spectral and electrochemical properties, as well as their potential applications as catalysts for a variety of reactions.[1-11] A rich redox reactivity can be observed for transition-metal corroles, where both metal- and ring-centered reactions have been characterized under a variety of solution conditions. The most-often-studied derivatives have contained cobalt,[3, 11-29] iron,[30-42] or manganese[19, 32, 37, 43-56] central metal ions, which have been characterized in both high and low oxidation states. A conversion between the different oxidation states of the corrole is easy to achieve using electrochemical techniques and has been best demonstrated in the case of cobalt derivatives, where the potentials for reduction or oxidation will systematically vary with changes in the number and types of electron-donating or electron-withdrawing substituents on the macrocycle.[7, 11, 12, 21, 24, 26, 57, 58]

As part of our continuing studies into elucidating the electrochemistry of metallocorroles,[2, 3, 11] a new series of cobalt (nitrophenyl)corroles containing two pyridine ligands were synthesized and electrochemically characterized in dichloromethane, benzonitrile, and pyridine. The structures of these compounds are shown in Chart 5-1 along with a structurally related four-coordinate triarylcorrole, as a reference compound. These cobalt (nitrophenyl)corroles possess not only a redox-active metal center and a redox-active π-ring system but also redox-active nitrophenyl groups, a fact that has not been previously recognized in a number of publications containing electrochemical

studies on *meso*-nitrophenyl-substituted macrocycles. The currently studied compounds differ from our previously investigated cobalt triarylcorroles in that the *meso*-nitrophenyl substituents on the macrocycle carry electron-donating (OCH_3) or electron-withdrawing (F) groups and the central cobalt ion has two axially ligated pyridine molecules, which can remain coordinated or dissociate depending on the concentration of the corrole and the solution conditions. Thus, the aim of this study is not only to examine the electrochemistry of the redox-active *meso*-nitrophenyl groups themselves compared to the previously characterized (nitrophenyl)corroles[24] but also to see how changes in the number of nitrophenyl groups on the macrocycle, the position of the NO_2 group on the *meso*-phenyl rings, or the presence of other electron-donating or electron-withdrawing substituents on this ring might affect redox reactions of the nitrophenyl groups themselves, the cobalt central metal ion, and the corrole macrocycle. The third point is to see how changes in the solvent, oxidation state, or axial coordination of the central metal ion might influence both the redox potentials and the site of electron transfer in these newly synthesized compounds.

Thus, the focus of our current study is to evaluate not only the prevailing redox reactions but also any electronic communication that might occur between the three redoxactive sites on the corrole, i.e., the cobalt metal ion, the corrole π-ring system, and the *meso*-nitrophenyl groups. To accomplish this, the electrochemical behavior of each corrole shown in Chart 5-1 is examined by cyclic voltammetry in several solvents, and in each solvent, the UV-visible spectra of the neutral, electroreduced, and electrooxidized

forms of the corroles are obtained. Each redox reaction is then discussed in terms of the oxidation state of the central cobalt ion, the degree of axial ligand coordination, the properties of the solvent, and the number and types of *meso*-nitrophenyl substituents on the corrole macrocycle.

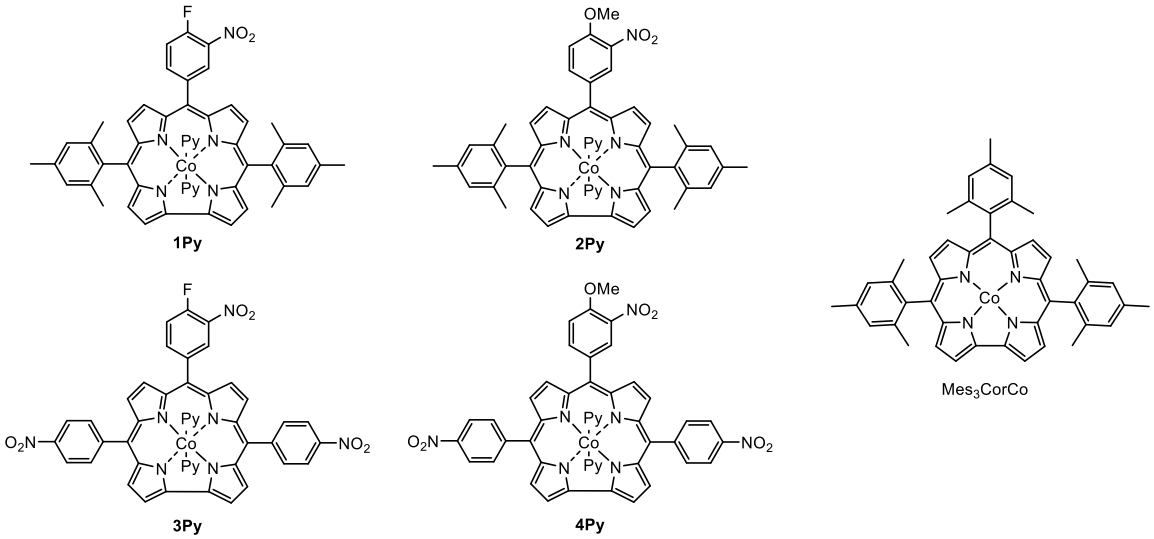

Chart 5-1. Structures of the investigated six-coordinate bis(pyridine)cobalt nitrophenyl corroles **1Py-4Py** and structurally four-coordinate triarylcorrole, Mes_3CorCo.

5.2 UV-Visible Spectra of Bis(pyridine) Complexes 1Py-4Py

In order to correctly analyze the prevailing redox reactions of cobalt (nitrophenyl)corroles **1Py-4Py** under different solution conditions, it was first necessary to evaluate the exact form of the corrole (i.e., four-, five-, or sixcoordinate) in the utilized electrochemical solvents. As will be discussed below, this is illustrated first by comparing the UV-visible spectra of Mes_3CorCo and **1Py-4Py** in binding and nonbinding solvents, followed by a comparison of the UV-visible spectra of each corrole at different concentrations and third by titration of Mes_3CorCo and **1Py-4Py** in CH_2Cl_2 with pyridine.

The UV-visible spectra of Mes_3CorCo and **1Py-4Py** in CH_2Cl_2, PhCN and pyridine are given in Figure 5-1. The spectra in CH_2Cl_2 are presented at high and low concentrations of the corrole (10^{-3} and 10^{-5} M), while the spectra in PhCN and pyridine are given only at a low concentration of 10^{-5} M. The higher concentration (10^{-3} M) corresponds to conditions of the electrochemical and electron paramagnetic resonance (EPR) measurements.

Similar spectral envelopes are seen for each of the five corroles in CH_2Cl_2 or PhCN at a concentration of 10^{-5} M, but there are slight differences in the wavelengths of the absorption bands between the two solvents. For example, Mes_3CorCo at 10^{-5} M in CH_2Cl_2 is characterized by bands at 388 and 543 nm (Figure 5-1a) but by bands at 386 and 554 nm in PhCN (Figure 5-1d). Likewise, compound **3Py** is characterized in CH_2Cl_2 by bands at 380, 432, 565, and 643 nm (Figure 5-1), but these bands are at 382, 429, 570, and 644 nm in PhCN (Figure 5-1d).

However, more significant changes in the number and positions of the absorption bands occur for **1Py-4Py** when the concentration of the corrole in CH_2Cl_2 is increased from 10^{-5} M (Figure 5-1a) to 10^{-3} M (Figure 5-1b). New absorption bands are seen in the 10^{-3} M solutions, which can be associated with the bis(pyridine) adduct, a form of the corrole that is predominant in neat pyridine. For example, compound **1Py** at a concentration of 10^{-3} M in CH_2Cl_2 has new bands at 433, 451, and 619 nm (Figure 5-1b) that are not seen at a concentration of 10^{-5} M in CH_2Cl_2 (Figure 5-1a) but are observed in pyridine at a corrole concentration of 10^{-5} M (Figure 5-1c). Moreover, these bands are more intense in pyridine. This suggests an equilibrium between different axially coordinated forms of the corrole **1Py-4Py** at a concentration of 10^{-3} M in CH_2Cl_2. The bands of compound **1Py** at 433, 451, and 619 nm are assigned to the six-coordinate bis(pyridine) derivative, while those at 380, 424, and 550 nm are assigned to the five-coordinate mono(pyridine) adduct. Bands associated with the bis(pyridine) adduct are also seen for compounds **2Py-4Py** in CH_2Cl_2 at a concentration of 10^{-3} M. The UV-visible spectra of the five- and six-coordinate species of **1Py-4Py** are also similar to the spectra of the mono- and bis(pyridine) adducts of other $(Ar)_3CorCo$ derivatives reported in the literature,[59] where the bis(pyridine) adduct has split Soret bands that are separated by about 15 nm and have equal intensity absorptions.

As will be shown in the following pages, the dissociation of one pyridine ligand from the cobalt center in **1Py-4Py** occurs upon dissolution in CH_2Cl_2. This reaction is given by Equation 5-1, where $(Ar)_3Cor$ represents the corrole macrocycle of **1Py-4Py**.

$$(Ar)_3CorCo(Py)_2 \xrightleftharpoons{\log K_d} (Ar)_3CorCo(Py) + Py \qquad (5\text{-}1)$$

A dissociation of pyridine does not occur for **1Py-4Py** in pure pyridine where the bis(pyridine) adduct is present at different concentrations (10^{-5} M for spectroscopic condition and 10^{-3} M for electrochemical condition). Moreover, the equilibrium in Equation 5-1 is shifted to the left at high concentrations of the corrole in CH_2Cl_2, and the spectra of **1Py-4Py** under these conditions are then characterized by bands associated with a mixture of $(Ar)_3CorCo(Py)$ and $(Ar)_3CorCo(Py)_2$ in solution. As expected, a concentration-dependent equilibrium does not occur for Mes_3CorCo, which lacks an axial pyridine ligand in its synthesized form, and the UV-visible spectra in CH_2Cl_2 are virtually identical at all concentrations between 10^{-3} and 10^{-5} M.

Additional evidence for the concentration dependence of the UV-visible spectra of the (nitrophenyl)corroles is shown in Figure 5-2 for compounds **1Py** and **3Py**, with a comparison made with Mes_3CorCo, where the cell path length (b) times the concentration (c) was kept constant for corrole concentrations of 10^{-5} M (b = 1.0 cm), 10^{-4} M (b = 0.1 cm), and 10^{-3} M (b = 0.01 cm). A clear transition between the two different ligated forms of the corrole is observed in CH_2Cl_2, with a larger amount of the bis(pyridine) adduct being

obtained at a concentration of 10^{-3} M of the corrole for **3Py** compared to **1Py**. Evidence for formation of the bis(pyridine) adduct is given by the decrease in the intensity of the original Soret band at 380 nm with increasing concentration and the concomitant gain in the intensity of the Q band at 618 or 650 nm. This latter absorption band has also been well-characterized in the literature,[18, 22] and is diagnostic of the bis(pyridine) adduct of $(Ar)_3CorCo(Py)_2$. A similar study on related cobalt corroles with coordinated pyridine ligands also showed a concentration dependence of the spectra that was interpreted in terms of the association and dissociation of pyridine.[60]

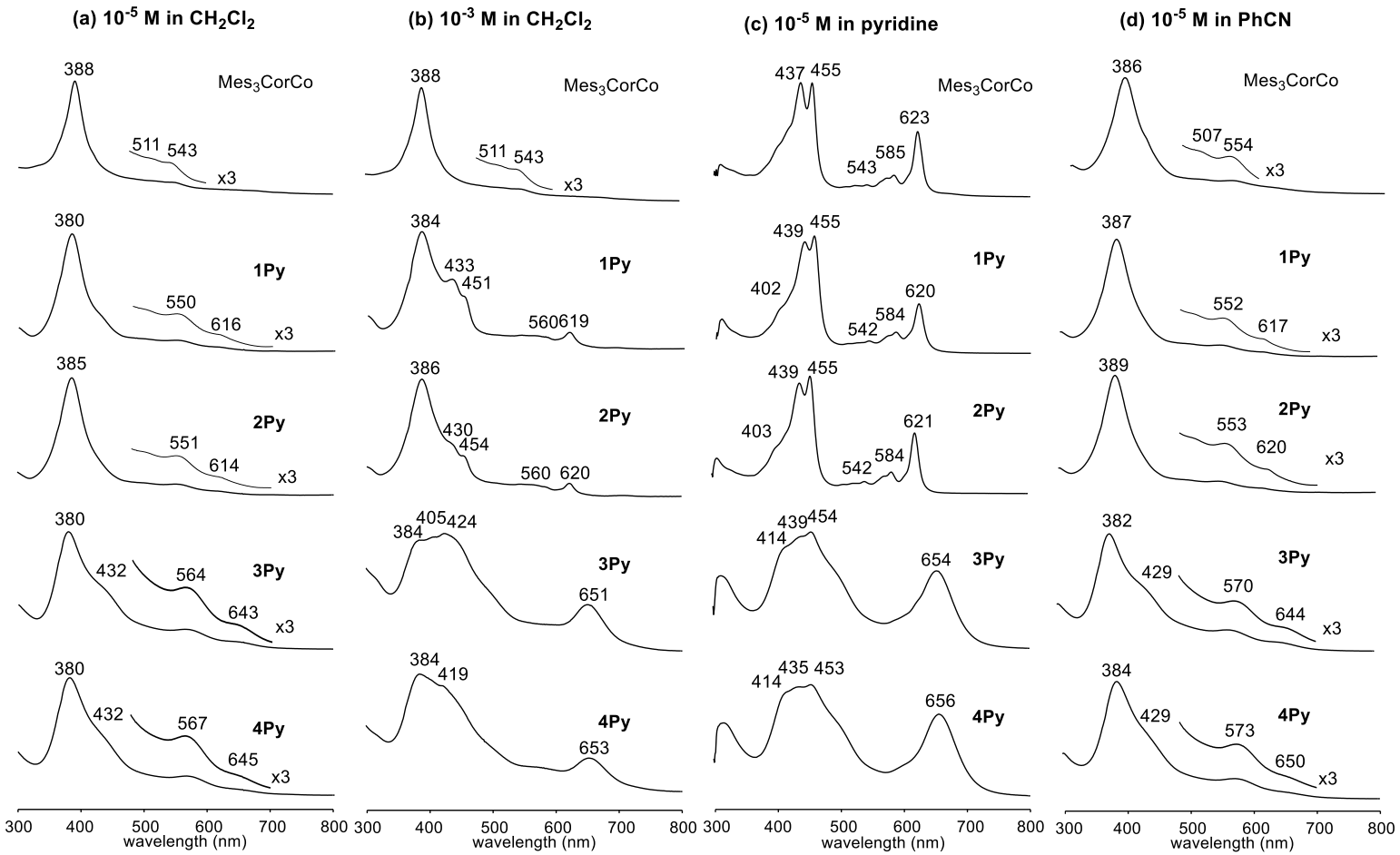

Figure 5-1. UV-visible spectra of Mes_3CorCo and **1Py-4Py** at (a) 10^{-5} M, (b) 10^{-3} M in CH_2Cl_2, (c) 10^{-5} M in pyridine and (d) 10^{-5} M in PhCN.

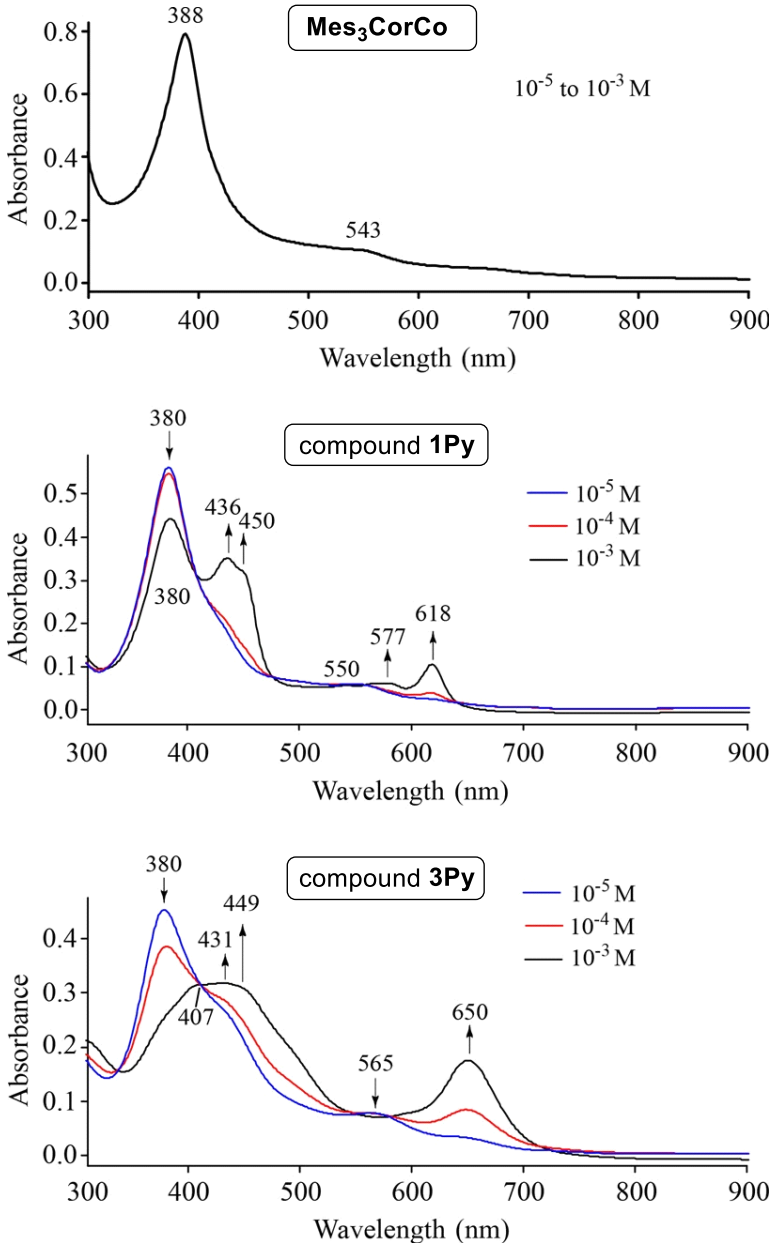

Figure 5-2. UV-visible spectral changes in CH_2Cl_2 upon an increase in the concentration of the corrole for Mes_3CorCo, **1Py** and **3Py**.

Table 5-1. UV-visible spectral data of investigated cobalt corroles **1Py-4Py** in CH_2Cl_2, PhCN and pyridine at a concentration of 10^{-5} M.

solvent	cpd	Wavelength: λ_{max}, nm (ε x 10^{-4} M^{-1} cm^{-1})					
		Soret region			visible region		
CH_2Cl_2	Mes_3CorCo	388 (6.1)			543 (0.7)		
	1Py	380 (6.4)			550 (0.7)		616 (0.3)
	2Py	385 (7.2)			551 (0.8)		614 (0.3)
	3Py	380 (5.9)	432 (3.4)		565 (1.0)		643 (0.4)
	4Py	380 (6.6)	432 (3.7)		567 (1.1)		645 (0.4)
PhCN	Mes_3CorCo	386 (5.3)			554 (0.7)		
	1Py	387 (5.5)			552 (0.6)		617 (0.2)
	2Py	389 (6.1)			553 (0.6)		620 (0.3)
	3Py	382 (5.9)	429 (3.4)		570 (1.1)		644 (0.5)
	4Py	384 (6.2)	429 (3.7)		573 (1.1)		650 (0.4)
pyridine	Mes_3CorCo		437 (5.5)	455 (5.5)	543 (0.7)	585 (1.1)	623 (3.2)
	1Py	402 (2.1)	439 (5.2)	455 (5.4)	542 (0.6)	584 (1.0)	620 (2.3)
	2Py	403 (2.5)	439 (5.9)	455 (6.3)	542 (1.0)	584 (1.2)	621 (3.3)
	3Py	414 (5.1)	439 (5.6)	454 (5.8)			654 (3.9)
	4Py	414 (5.1)	435 (5.4)	453 (5.5)			656 (4.1)

The equilibrium given by Equation 5-1 is further examined by monitoring the spectral changes during titration of **1Py-4Py** with pyridine in CH_2Cl_2. A similar titration was also carried out for the structurally related four-coordinate Mes_3CorCo reference compound.

The titration of Mes_3CorCo with pyridine involves a two-step process. The first step is assigned as a conversion of Mes_3CorCo to $Mes_3CorCo(Py)$ by adding one axial pyridine molecule to the cobalt center. The second step results in the formation of $Mes_3CorCo(Py)_2$ at a higher pyridine concentration. The pyridine addition of each step is confirmed by the diagnostic log-log plot in the figure inset, with the corresponding calculated binding constant $\log K_1 = 6.5$ or $\log K_2 = 2.6$, respectively. The reactions of two steps discussed above are given in Equation 5-2 and 5-3, where Ar = Mesityl in the case of reference compound Mes_3CorCo.

$$(Ar)_3CorCo + Py \xrightleftharpoons{\log K_1} (Ar)_3CorCo(Py) \tag{4-2}$$

$$(Ar)_3CorCo(Py) + Py \xrightleftharpoons{\log K_2} (Ar)_3CorCo(Py)_2 \tag{4-3}$$

The spectral pattern of the mono(pyridine) adduct $Mes_3CorCo(Py)$ is similar to the initial four-coordinate Mes_3CorCo in CH_2Cl_2, but possesses a slightly blue-shifted and decreased intensity Soret band with a shoulder at 416 nm, and a weak Q band, which has shifted from 543 nm for Mes_3CorCo to 551 nm for $Mes_3CorCo(Py)$ (Figure 5-3a). As will be discussed later in the manuscript, a shoulder is also observed at 432 and 429 nm for

compounds **3Py** and **4Py** at a concentration of 10^{-5} M in CH_2Cl_2 and PhCN (Figures 5-1), which is associated with the five-coordinate mono(pyridine) adduct of each corrole.

The UV-visible spectrum of bis(pyridine) adduct $Mes_3CorCo(Py)_2$, formed after the second ligand addition of pyridine titration, is significantly different (Figure 5-3b). The spectrum is characterized by split Soret bands at 434 and 453 nm, in addition to an intense Q band at 621 nm and multiple weaker Q bands at 543-585 nm. Virtually the same UV-visible spectrum is obtained for Mes_3CorCo at 10^{-5} M in pyridine (Figure 5-1c) or 10^{-3} M in pyridine containing 0.1 M TBAP (spectrum not shown). These results, when combined with the similar spectra of $Mes_3CorCo(Py)$ and **1Py-4Py** in CH_2Cl_2 or PhCN at a concentration of 10^{-5} M (Figure 5-1), strongly suggest the dissociation of one pyridine ligand from the cobalt center of **1Py-4Py** when they are dissociated in these two solvents (see Equation 5-1).

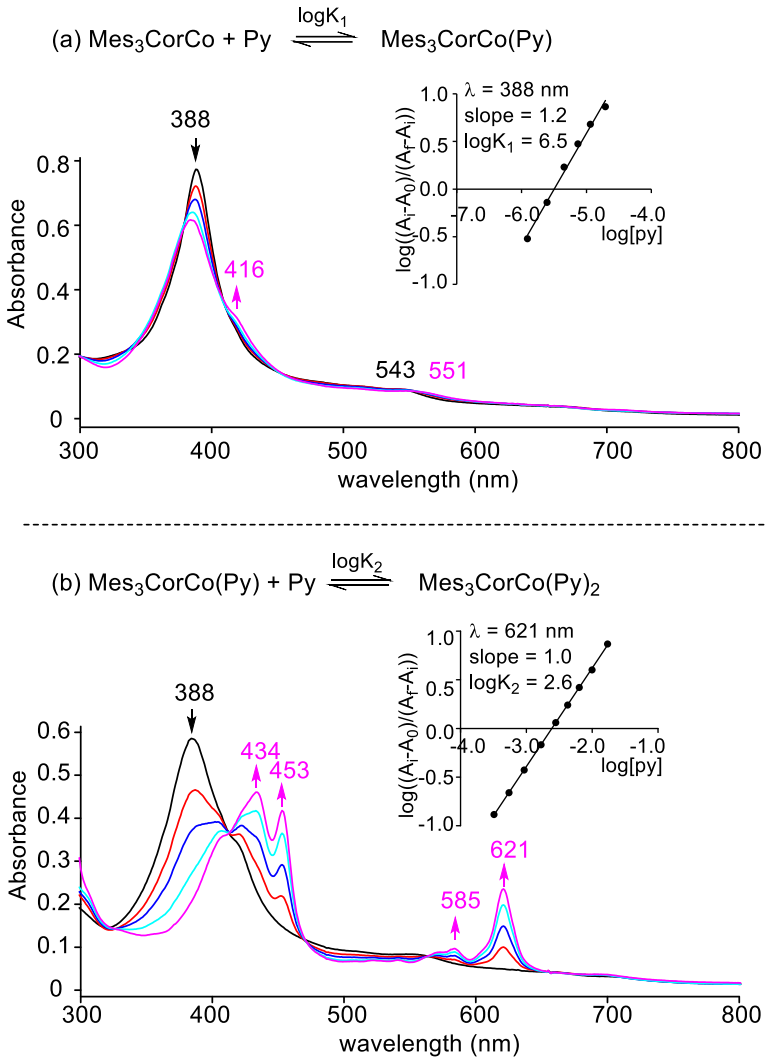

Figure 5-3. UV-visible spectral changes during the (a) first and (b) second pyridine ligand binding to Mes_3CorCo at a concentration of 10^{-5} M in CH_2Cl_2. The inset shows the Hill plot analysis of the data for determining the binding constants.

The spectral changes that occur during the titration of **1Py-4Py** with pyridine in CH_2Cl_2 are also given in Figure 5-4. Unlike the four-coordinate reference compound Mes_3CorCo (shown in Figure 5-3), only a single pyridine molecule can be added to **1Py–4Py**, because these cobalt corrole complexes are initially five-coordinate when dissolved in CH_2Cl_2. The addition of one pyridine ligand to each of the corroles are confirmed by the slope of 1.0 from the Hill plots in the figure insets. Moreover, the final spectrum for each titration is characterized by an intense Q band at 619–656 nm, suggesting the formation of a bis(pyridine) adduct. The observation of isosbestic points in the spectral changes rules out the existence of the intermediate during each titration, and the prevailing ligand binding reaction can be characterized as a conversion of $(Ar)_3CorCo(Py)$ to $(Ar)_3CorCo(Py)_2$, as shown in Equation 5-3 (the reverse of Equation 5-1).

Thus, the data in Figures 5-3 and 5-4 are consistent with the spectroscopic data in Figure 5-1, which show that the initial synthesized six-coordinate bis(pyridine)cobalt (nitrophenyl)corroles are converted to their five-coordinate forms when dissolved in CH_2Cl_2 or PhCN at a concentration of 10^{-5} M.

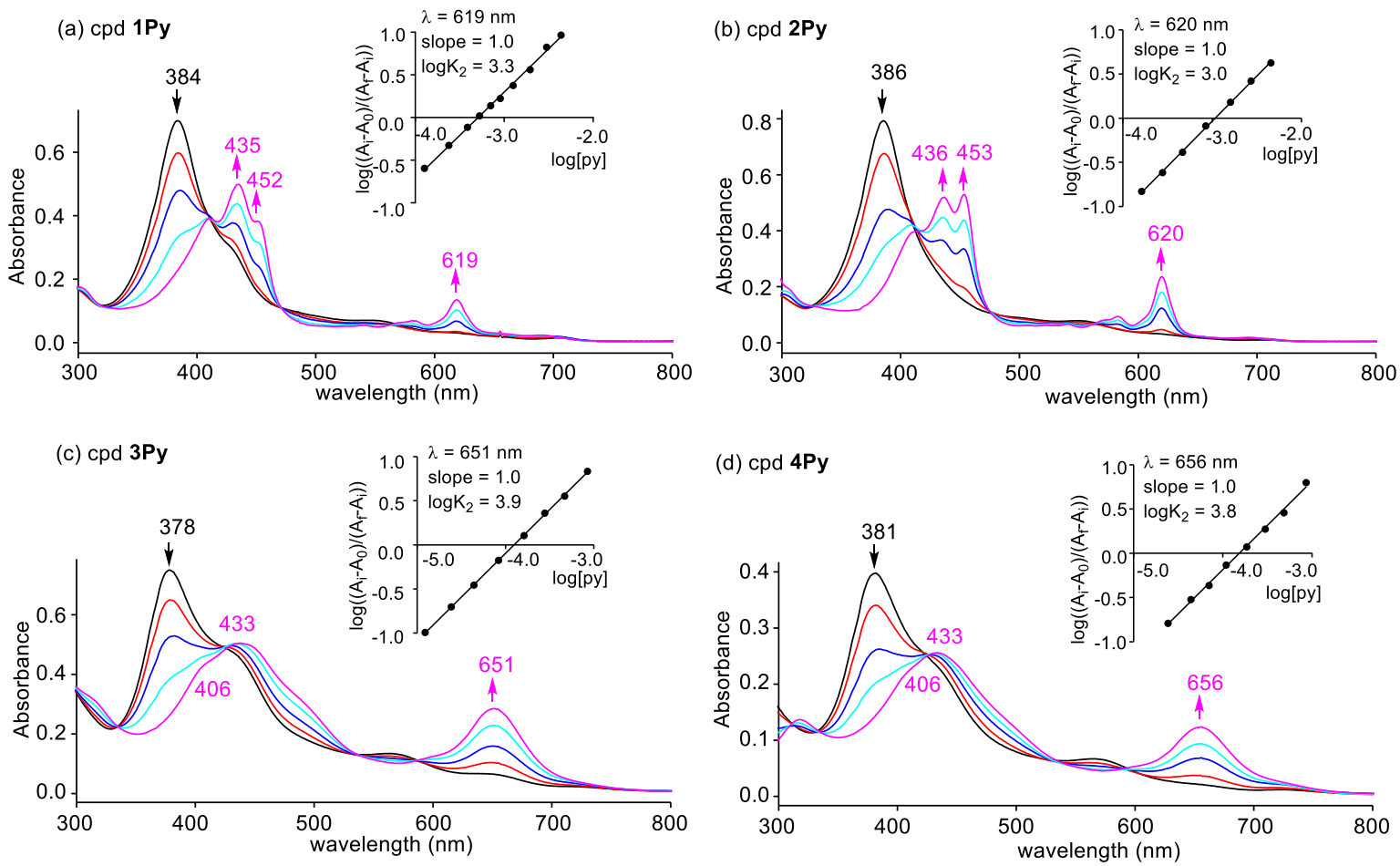

Figure 5-4. UV-visible spectral changes during the second pyridine ligand binding to compounds (a) **1Py**, (b) **2Py**, (c) **3Py**, (d) **4Py** at a concentration of 10^{-5} M in CH_2Cl_2. The inset shows the Hill plot analysis of the data for determining the binding constants.

Table 5-2. Pyridine binding constants of cobalt corrole Mes_3CorCo and **1Py-4Py** in CH_2Cl_2 at a concentration of 10^{-5} M.

	binding constants	
compound	$\log K_1$	$\log K_2$
Mes_3CorCo	6.5	2.6
1Py		3.3
2Py		3.0
3Py		3.9
4Py		3.8

The measured formation constants for the addition of a second pyridine molecule to the five-coordinate mono(pyridine) derivatives of **1Py-4Py** range from $\log K_2 = 3.0$ to 3.9 in CH_2Cl_2. These $\log K_2$ values are summarized in Table 5-2, along with the $\log K_1$ and $\log K_2$ values for Mes_3CorCo under the same solution conditions. Of the five corroles in Table 5-2, compounds **3Py** and **4Py** have the largest $\log K_2$ values and Mes_3CorCo has the smallest, while the $\log K_2$ values for compounds **1Py** and **2Py** are in between. This is consistent with the presence of the electron-withdrawing nitrophenyl groups on the molecule, which leads to an enhanced positive charge on the central metal ion and thus an increased pyridine binding ability.

Finally, it should be pointed out that two different envelopes of UV-visible spectra are seen for the bis(pyridine) adducts of compounds **1Py-4Py** as shown in Figures 5-1 and 5-3. One type is for corroles **1Py** and **2Py**, which possess one *meso*-nitrophenyl group on the macrocycle, and is characterized by a well-defined split Soret band and a sharp Q band. The other is for the bis(pyridine) complexes **3Py** and **4Py**, which possess three *meso*-nitrophenyl groups and have spectra with substantially broadened Soret and Q bands.

5.3 Electrochemistry of Bis(pyridine) Complexes 1Py-4Py

Cyclic voltammograms for **1Py-4Py** are illustrated in Figures 5-5 (CH_2Cl_2), 5-6 (pyridine), and 5-7 (PhCN), and a summary of the measured redox potentials under different solution conditions is given in Table 5-3. Each investigated corrole contains multiple redox-active sites on the molecule, and this is reflected by the large number of oxidation or reduction processes shown by the cyclic voltammograms in the three different solvents.

Two or three one-electron oxidations and three to four reductions are seen for complexes **1Py-4Py**. These processes can involve the conjugated macrocycle or the metal center as well as the redox-active *meso*-nitrophenyl substituents. Earlier electrochemical studies of cobalt corroles have often assigned the oxidation states and sites of electron transfer based on what was known for the related cobalt porphyrins, namely, cobalt(III)/cobalt(II), cobalt(II)/cobalt(I), or cobalt(III)/cobalt(IV) in the case of the metal-centered reactions and π-cation or π-anion radicals when the electrode reaction involves the conjugated macrocycle.[16] However, the site of electron transfer is not so clear in the case of transition-metal corroles, which have been characterized as possessing a noninnocent macrocycle, the most-often-cited examples of which have been given for corrole derivatives containing copper or iron ions.[6, 7, 30, 35, 36, 61-68] Five-coordinate cobalt triarylcorroles were also proposed as containing a noninnocent macrocycle.[7, 59, 69] Thus, the possible noninnocent character of the corrole macrocycle should be considered during analysis of the redox reactions of the currently investigated cobalt corroles. The presence

of the highly electron-withdrawing and redox-active *meso*-nitrophenyl groups on the macrocycles of **1Py-4Py**, as well as the utilized solvents that may strongly bind to the central cobalt ion, should also be taken into account when elucidating neutral, oxidized or reduced state of the investigated cobalt corroles.

To address the above points, our description of the redox reactions for **1Py-4Py** is divided into three sections. The first is that of the redox-active nitrophenyl groups, followed by the electrochemical behavior of Mes_3CorCo under different solution conditions and then the metal- or ring-centered redox reactions of **1Py-4Py**. The reductions of **1Py-4Py** at potentials more negative than -1.5 V are irreversible and involve coupled chemical reactions of either the electroreduced NO_2Ph groups, the corrole macrocycle, or a combination of both. These processes are shown by dashed lines in Figures 5-5 to 5-7 and were not investigated in further detail.

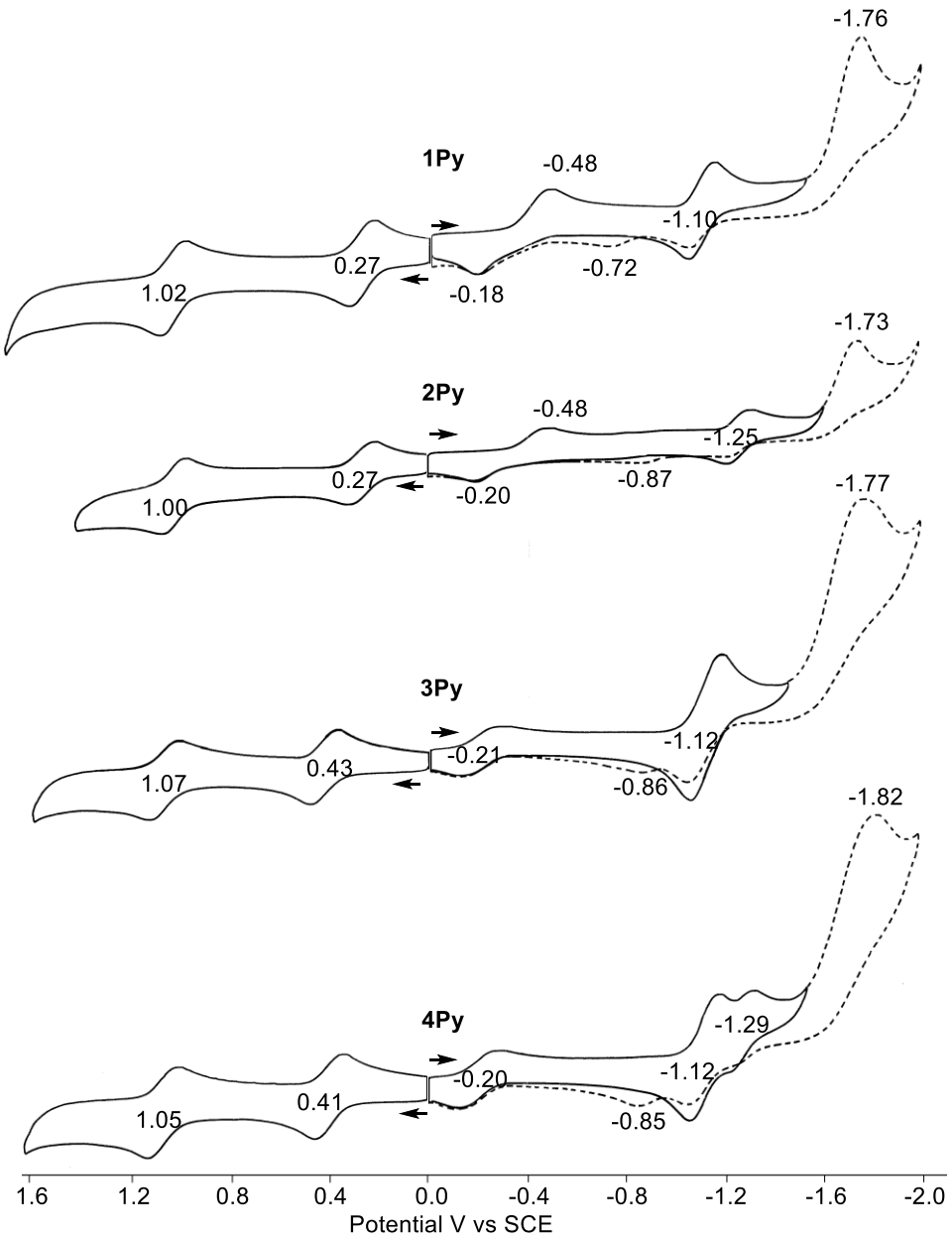

Figure 5-5. Cyclic voltammograms of **1Py-4Py** in CH_2Cl_2 containing 0.1 M TBAP. *The anodic peaks indicated by asterisks are reactions of products formed from the irreversible reduction of nitrophenyl groups located at E_P = -1.73 to -1.82 V. *For each cyclic voltammogram in this thesis, the current (μA) is plotted versus potential (V) with the potential values given in the figure (see Chapter 2 for details).

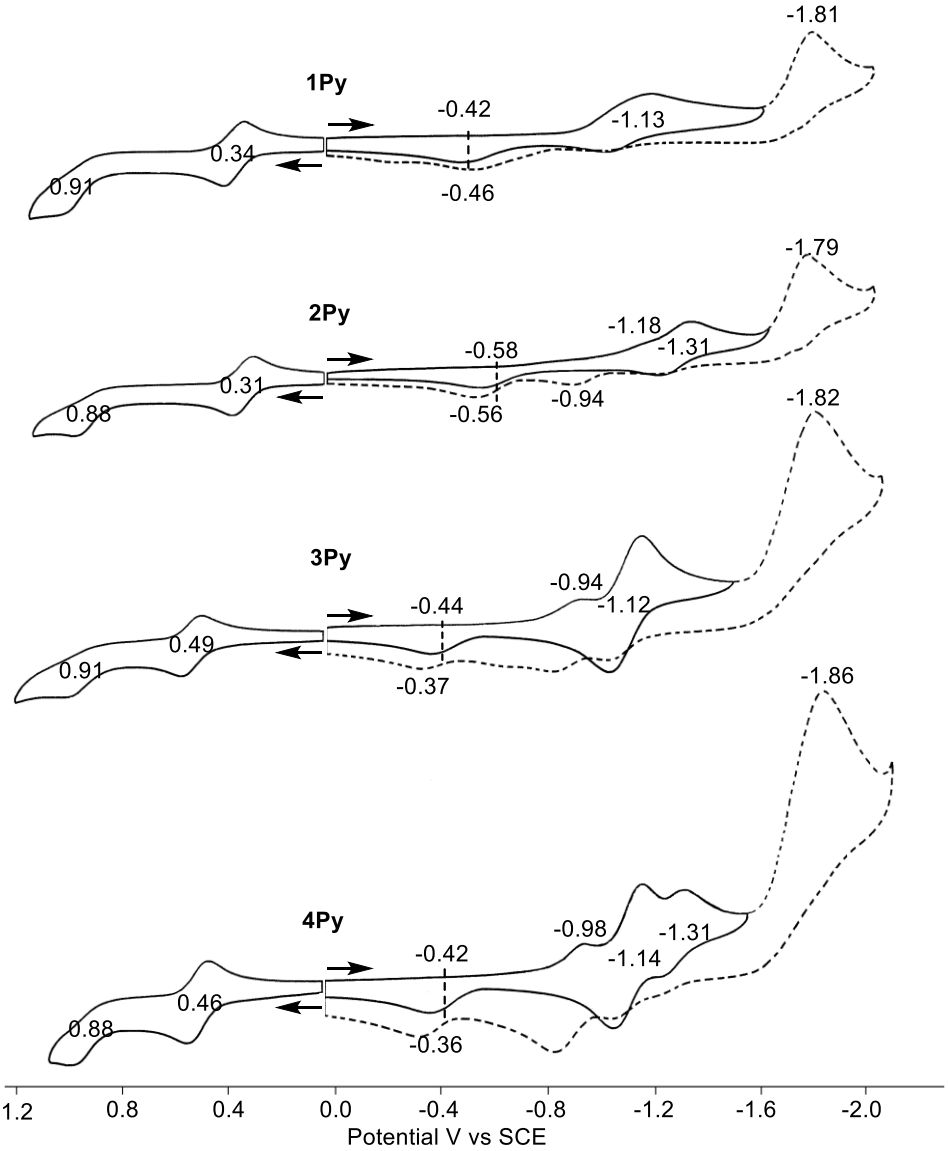

Figure 5-6. Cyclic voltammograms of **1Py-4Py** in pyridine containing 0.1 M TBAP. *The anodic peaks indicated by asterisks are reactions of products formed from the irreversible reduction of nitrophenyl groups located at E_p = -1.81 to -1.86 V.

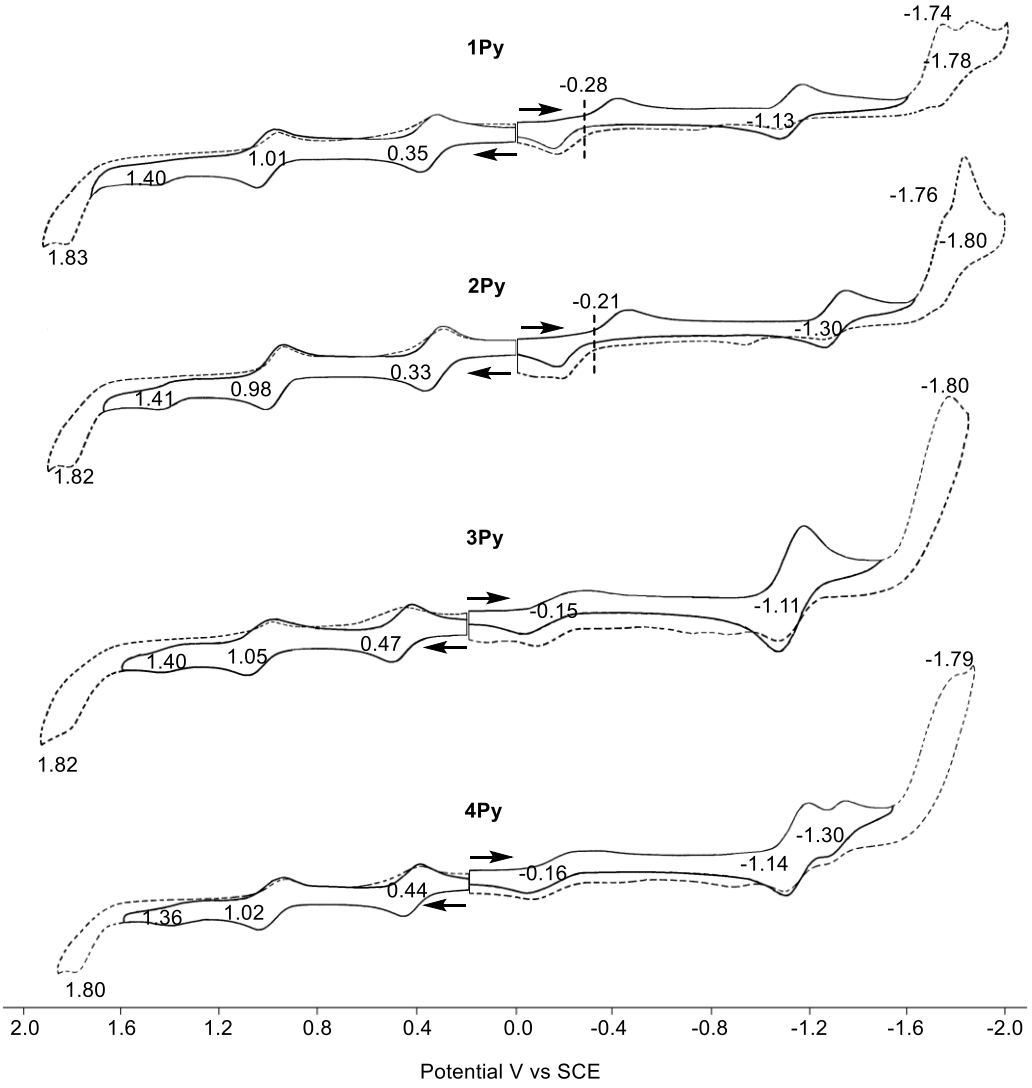

Figure 5-7. Cyclic voltammograms of **1Py-4Py** in PhCN containing 0.1 M TBAP. *The anodic peaks indicated by asterisks are reactions of products formed from the irreversible reduction of nitrophenyl groups located at E_p = -1.74 to -1.80 V.

Table 5-3. Half-wave or peak potentials ($E_{1/2}$ or E_p, V vs SEC) for reductions and the first two oxidations of cobalt corroles in CH_2Cl_2, PhCN, or pyridine (Py) containing 0.1 M TBAP.

solvent	compound	oxidation		reduction			
		Ox 2	Ox 1	Red 1		Red of NO_2Ph (#e)	further Red
				E_{pc}	E_{pa}		
CH_2Cl_2	Mes_3CorCo + 2 eq. Py	0.98	0.15	-0.70	-0.24		-1.78
	1Py	1.02	0.27	-0.48	-0.18	-1.10 (1)	-1.76
	2Py	1.00	0.27	-0.48	-0.20	-1.25 (1)	-1.73
	3Py	1.07	0.43	-0.28	-0.14	-1.12 (3)	-1.77
	4Py	1.05	0.41	-0.27	-0.13	-1.12 (2), -1.29 (1)	-1/82
PhCN	**1Py**	1.01	0.35	-0.41	-0.15	-1.12 (1)	-1.73, -1.78
	2Py	0.98	0.33	-0.45	-0.17	-1.30 (1)	-1.75, -1.84
	3Py	1.05	0.47	-0.26	-0.04	-1.13 (3)	-1.80
	4Py	1.02	0.44	-0.25	-0.05	-1.14 (2), -1.30 (1)	-1.79
pyridine	Mes_3CorCo		0.26	-1.16	-0.70		-1.80
	1Py	0.90	0.34	-1.20	-0.42	-1.14 (1)	-1.81
	2Py	0.88	0.31	-1.18	-0.56	-1.31 (1)	-1.82
	3Py	0.91	0.49	-0.94	-0.42	-1.12 (3)	-1.82
	4Py	0.87	0.46	-0.98	-0.42	-1.14 (2), -1.31 (1)	-1.86

5.4 Reductions of the *Meso*-Nitrophenyl Group(s) in 1Py-4Py

Nitrobenzene can be reversibly reduced by one electron at $E_{1/2}$ = -1.08 V in CH_2Cl_2[40] or in PhCN[70] and -1.12 V in pyridine[70], which produces a relatively stable anion radical that can be further reduced at E_p = -2.00 V via an irreversible process in all solvents.[40, 70] A reversible one-electron reduction was also earlier reported for the NO_2Ph groups on the *meso*-positions of porphyrins or corroles containing various central metal ions. The reported redox potentials of the NO_2Ph groups range from -1.05 to -1.12 V,[24, 33, 40, 43, 44, 51, 71-94] which are independent of either the central metal ion, the number of *meso*-nitrophenyl groups, or the presence of other electron-donating or electron-withdrawing substituents on the macrocycle. The *meso*-nitrophenyl groups of **1Py-4Py** also exhibit similar electrochemical reduction behavior; i.e., they undergo an initial reversible one-electron reduction process located at $E_{1/2}$ = −1.10 to −1.14 V or −1.25 to −1.31 V, depending on another substituent on the nitrophenyl ring, followed by a second irreversible reduction step at E_p = -1.73 to -1.86 V, as shown in Figures 5-5 to 5-7 and Table 5-3.

The invariant values of $E_{1/2}$ for the reversible one-electron reduction of *meso*-nitrophenyl groups on earlier studied metallomacrocycles in CH_2Cl_2, PhCN, or pyridine suggest the lack of an interaction between these redox-active units on the *meso*-positions of the different compounds, be it a porphyrin, a corrole, or another related conjugated system. An electronic interaction between the three nitrophenyl groups across the macrocycle is also not electrochemically observed in the currently studied compounds **3Py** and **4Py**, which both contain three nitrophenyl groups. As shown in Table 5-3 and

Figure 5-5 to 5-7, The *meso*-(4-F-3-NO_2)Ph group on compound **1Py** is reversibly reduced by one electron at -1.10 to -1.13 V in three solvents, and essentially the same value of $E_{1/2}$ is seen in the cyclic voltammogram of compound **3Py** with a single (4-F-3-NO_2)Ph group at the 10 position of corrole macrocycle and two *p*-NO_2Ph groups at the 5 and 15 positions (see Chart 5-1). The reductions for these two different types of nitrophenyl groups are overlapped because the sum values of substituent constants ($\Sigma\sigma$) for two types of nitrophenyl rings are similar, i.e., $\Sigma\sigma = 0.772$ for (4-F-3-NO_2)Ph (σ(*p*-F) = 0.062, σ(*m*-NO_2) = 0.71) and $\Sigma\sigma = 0.778$ for *p*-NO_2Ph (σ(*p*-NO_2) = 0.778).[95] Each phenyl ring of these two types of *meso*-nitrophenyl groups experiences an overall almost identical substituent effect, and therefore the same reduction potential of these two groups is observed. However, this is not the case for compound **4Py**, where separate reduction potentials are observed for the two different nitrophenyl groups on the molecule. The easier reduction (e.g. $E_{1/2}$ = -1.12 V in CH_2Cl_2) occurs for the two *p*-NO_2Ph groups, while the harder reduction (e.g. $E_{1/2}$ = -1.29 V in CH_2Cl_2) occurs for the 5-OMe-3-NO_2)Ph group. This is because the electron-donating OMe substituent shifts the reduction of this nitrophenyl group in a negative direction. Similar reduction potential ($E_{1/2}$ = -1.25 V in CH_2Cl_2) is also observed for the (4-OMe-3-NO_2)Ph group in compound **2Py**.

In summary, the $E_{1/2}$ values of the reversible one-electron reductions for the easiest-to-reduce nitrophenyl groups, (4-F-3-NO_2)Ph and *p*-NO_2Ph, in compounds **1Py, 3Py** and **4Py** range from −1.10 to −1.13 V in the three solvents, while $E_{1/2}$ values for the hardest-to-reduce (4-OMe-3-NO_2)Ph ranges from -1.25 to -1.31 V for compounds **2Py** and

4Py (Table 5-3). It can be concluded that varying the total electronic effect on the nitrophenyl ring, e.g., by adding a second electron-donating or electron-withdrawing substituent, will affect the reduction of this redox-active nitrophenyl group.

As mentioned above, although the half-wave potentials for reduction of the nitrophenyl groups on different metallomacrocycles do not depend upon the specific macrocycle or the specific central metal ion, these substituents do exert a moderate-to-strong electron-withdrawing effect on other redox reactions of the compounds, shifting their potentials in a positive direction by 45-90 mV per NO_2Ph group in the case of porphyrins[71] and by 35-100 mV in the case of corroles.[24, 40, 72] The first oxidation of the currently investigated compounds **1Py-4Py** exhibits a 76 mV potential shift per NO_2Ph group in pyridine and a 80 mV shift per NO_2Ph group in CH_2Cl_2, as shown in Figure 5-8.

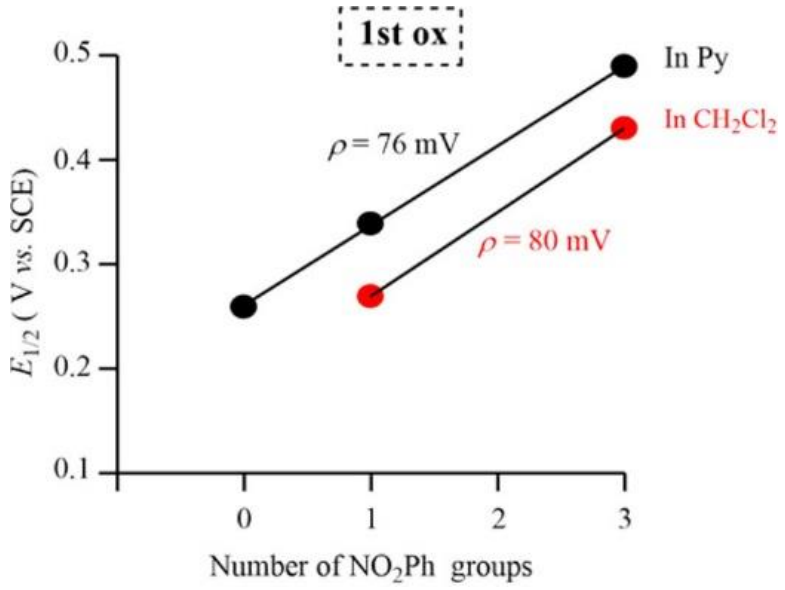

Figure 5-8. Plots of the half-wave potentials for the first oxidation versus number of *meso*-NO_2Ph groups for Mes_3CorCo, **1Py** and **3Py** in pyridine and CH_2Cl_2. The measured $E_{1/2}$ values are given in Table 5-3.

5.5 Electrochemistry of Mes_3CorCo

In order to better understand the electrochemical behavior of the currently investigated bis(pyridine) cobalt corrole complexes in different solution conditions and the effect of ligand binding on the redox reactions, the electrochemical reactions of the four-coordinate Mes_3CorCo were monitored in different solution conditions (Figure 5-9).

As shown in Figure 5-9a, the four-coordinate corrole in CH_2Cl_2 undergoes an initial reversible one-electron reduction located at $E_{1/2}$ = -0.19 V, consistent with an earlier reported potential of $E_{1/2}$ = −0.18 V in CH_2Cl_2.[21] Surprisingly, an identical $E_{1/2}$ value of −0.19 V was also observed for the reversible one-electron reduction of (TPC)Cu under the same solution conditions.[96] This might be perceived as a coincidence were it not for the fact that similar reduction potentials have also been reported for the one-electron reduction of cobalt and copper corroles with other types of macrocycles. Best examples are given for the octaethylcorroles (OEC)Cu ($E_{1/2}$ = -0.34 V) and (OEC)Co ($E_{1/2}$ = -0.30 V) in PhCN,[53] the pentafluorophenylcorroles (TPFPC)Cu[66] ($E_{1/2}$ = 0.21 V) and (TPFPC)Co[21] ($E_{1/2}$ = 0.24 V) in CH_2Cl_2, and the triferrocenylcorroles (TFcC)Cu ($E_{1/2}$ = -0.33 V) and (TFcC)Co ($E_{1/2}$ = -0.30 V) in CH_2Cl_2.[97]

Copper invariably engenders a noninnocent M(II)-corrole$^{\bullet 2-}$ electronic structure, a fact that has been described by a number of laboratories.[6, 7, 35, 53, 61, 62, 64-67, 88, 98-107] This electronic configuration of a metal(II) ion and a corrole cation radical is also assigned to the currently investigated four-coordinate Mes_3CorCo in neat CH_2Cl_2. Studies on (TPFPC)Co and other four-coordinate cobalt corroles indicate that these derivatives are

paramagnetic.[108] Moreover, theoretical calculations of the electronic structure carried out specifically for (TPC)Co and (TPC)Co(Py) strongly suggest a cobalt(II) radical ground state.[7] A noninnocent corrole ligand was also assigned for related five-coordinate $(Ar)_3CorCo(Py)$ derivatives in a recent study by Ghosh and co-workers.[59]

Thus, in the current study, the five-coordinate mono-(pyridine) adduct of $Mes_3CorCo(Py)$ formed in a mixture of CH_2Cl_2/Py and $(Ar)_3CorCo(Py)$ of **1Py-4Py** when they were dissolved in a CH_2Cl_2 solution is assigned as containing a $Co(II)Cor^{\bullet}$ electronic structure. This assignment is also rationalized by our EPR data[70] and gives clear evidence for paramagnetic character of the examined compounds in nonbonding solvents where the five-coordinate mono(pyridine) adduct is largely present.

However, the bis(pyridine) adduct of compounds **1Py-4Py** in neat pyridine is assigned as a cobalt(III) corrole, as suggested by Ghosh based on EPR, NMR, etc.[7] This assignment is also supported by the single-crystal data in the current study for compound **1Py**, which exhibits a short equatorial Co-N distance of ~1.89 Å, indicating an optimum fit with the corrole ligand. It also exhibits Co-Npy distances of ~1.99 Å. These geometry parameters are all indicative of a classic low-spin cobalt(III) description for these complexes.

Although the one-electron reduction of most neutral cobalt corroles has almost always been proposed as involving a cobalt(III) to cobalt(II) process, the fact that identical reduction potentials are observed in CH_2Cl_2 for a number of structurally related copper and cobalt triarylcorroles is totally inconsistent with a metal(III)/metal(II) transition.

Moreover, the reported half-wave potentials for the copper(II)/copper(III) and cobalt(II)/cobalt(III) processes of several structurally related porphyrins have been shown to differ by up to 1.5 V in potential.[109] However, this does not occur for the cobalt and copper triarylcorroles, thus strongly suggesting the same site of electron transfer for these two compounds. This site is proposed as the noninnocent corrole macrocyclic ligand. A cobalt(II) central metal ion is therefore present in the neutral species, and the redox reaction would occur as shown in Equation 5-4.

$$(Ar)_3Cor^{\bullet}Co^{II} + e^- \rightleftharpoons [(Ar)_3CorCo^{II}]^- \qquad (5\text{-}4)$$

Mes_3CorCo also undergoes three reversible one-electron oxidations at $E_{1/2}$ = 0.54, 0.89, and 1.48 V in CH_2Cl_2 containing 0.1 M TBAP. The first oxidation is assigned as a one-electron abstraction from the cobalt center, leading to formation of the cobalt(III) π-cation radical (see Equation 5-5), as supported by EPR and theoretical analysis of the singly oxidized species of a structurally similar compound, $(F_5Ph)Mes_2CorCo$, which is unambiguously assigned as forming a $[(F_5Ph)Mes_2Cor^{\bullet}Co^{III}]^+$ cation radical after the one-electron abstraction.[21] The UV−visible spectrum of electrogenerated $[Mes_3Cor^{\bullet}Co]^+$ is characterized in CH_2Cl_2 by a decrease in the intensity of Soret and Q bands at 383 and 545 nm along with a broad near-IR band at around 670 nm (see a later section). This π-cation-radical-type spectrum of singly oxidized Mes_3CorCo in CH_2Cl_2 also resembles UV-visible spectra obtained for $[(F_5Ph)Mes_2Cor^{\bullet}Co^{III}]^+$ and $[Me_4Ph_5Cor^{\bullet}Co^{III}]^+$, which were both assigned as cobalt(III) corrole cation radicals.[15, 21]

$$(Ar)_3Cor^{\bullet}Co^{II} \rightleftharpoons [(Ar)_3Cor^{\bullet}Co^{III}]^+ + e^- \qquad (5\text{-}5)$$

The second and third oxidations of Mes_3CorCo at 0.89 and 1.48 V in CH_2Cl_2 are both proposed to involve one-electron abstraction from the corrole macrocycle, based on spectroelectrochemical data obtained during these two oxidation processes (see Figure 5-11).

In the solution of CH_2Cl_2 containing 2 eq. of pyridine (Figure 5-9b), the redox-active species is assigned as $Mes_3Cor^{\bullet}Co^{II}(Py)$, as described earlier in this paper. In contrast with the four-coordinate complex that is reversibly reduced by one electron at -0.19 V in CH_2Cl_2, the five-coordinate $Mes_3Cor^{\bullet}Co^{II}(Py)$ undergoes an irreversible reduction at E_{pc} = -0.70 V, owing to dissociation of the Py ligand.

This irreversible reduction is coupled with an oxidation process at E_{pa} = -0.24 V, which corresponds to oxidation of the one-electron-reduced species $[Mes_3CorCo^{II}]^-$. The reduction behavior of the mono(pyridine) adduct of the neutral corrole can be explained via a classical electrochemical EC mechanism (Electron transfer followed by a Chemical reaction), as shown in the top right of Scheme 5-1. This chemical reaction is a dissociation of one pyridine ligand from $[Mes_3CorCo(Py)]^-$ in the CH_2Cl_2/Py mixture and occurs on the forward negative potential scan. A re-association of one pyridine ligand then occurs on the reverse positive scan, giving back the original corrole via another EC mechanism upon oxidation. The re-oxidation peak potential of −0.24 V corresponds to the conversion of four-coordinate $[Mes_3CorCo]^-$ to $[Mes_3CorCo]$, as confirmed by the reversible reduction potential of −0.19 V for Mes_3CorCo in CH_2Cl_2 shown in Figure 5-9a. By way of comparison, the five-coordinate $Ph_3CorCo(PPh_3)$ has been shown to undergo an irreversible reduction

and reoxidation at E_{pc} = -0.73 V and E_{pa} = -0.10 V under the same solution conditions,[24] and this was explained by an "electrochemical EC box mechanism" similar to that described above. As seen in Figure 5-9b, only two oxidations ($E_{1/2}$ = 0.15 and 0.98 V) can be observed for Mes_3CorCo in CH_2Cl_2 containing 2 eq. of pyridine. As will be further described later in the manuscript, the redox-active species under these solution conditions, $Mes_3Cor^{\bullet}Co^{II}(Py)$, is first oxidized to $[Mes_3Cor^{\bullet}Co^{III}(Py)]^+$ and then coordinates one free pyridine ligand in the solution, forming a bis(pyridine)cobalt(III) cation radical, $[Mes_3Cor^{\bullet}Co^{III}(Py)_2]^+$, as shown in the middle left of Scheme 5-1.

The redox-active form of this corrole in neat pyridine is assigned as $Mes_3CorCo^{III}(Py)_2$ based on analysis of the pyridine titration data (Figure 5-3) and an earlier assignment of the cobalt oxidation state. As shown in Figure 5-9c, the first irreversible reduction of $Mes_3CorCo(Py)_2$ occurs at -1.16 V, a value negatively shifted by 460 mV compared to reduction of the five-coordinate $Mes_3CorCo^{III}(Py)$. Reoxidation of the reduction product is located at -0.70 V, a value consistent with the reduction potential of the five-coordinate mono-(pyridine)cobalt corrole in Figure 5-9b. Thus, reduction of the six-coordinate bis(pyridine)cobalt corrole is explained by another box mechanism shown at the bottom of Scheme 5-1.

The starting $(Ar)_3CorCo^{III}(Py)_2$ undergoes an initial one-electron reduction, followed by dissociation of one pyridine ligand to form $[(Ar)_3CorCo^{II}(Py)]^-$. This five-coordinate species is first reoxidized to $(Ar)_3CorCo^{III}(Py)$ and then reassociated with a Py ligand, yielding six-coordinate $(Ar)_3CorCo^{III}(Py)_2$. The first one-electron oxidation of

$Mes_3CorCo^{III}(Py)_2$ is also reversible and located at $E_{1/2}$ = 0.26 V in pyridine containing 0.1 M TBAP. This singly oxidized corrole is assigned as the bis(pyridine) adduct $[Mes_3Cor^{\bullet}Co^{III}(Py)_2]^+$. This is because the one-electron-oxidized species of $[TPFPC]Co^{III}(Py)_2$, structurally similar to $Mes_3CorCo^{III}(Py)_2$, is unambiguously assigned as $[(TPFP)Cor^{\bullet}Co^{III}(Py)_2]^+$ with corrole cationradical character, as supported by the electron paramagnetic resonance (EPR) data.[28] A second oxidation, which is not shown in the figure, is quasi-reversible and located close to the positive potential limit of the solvent.

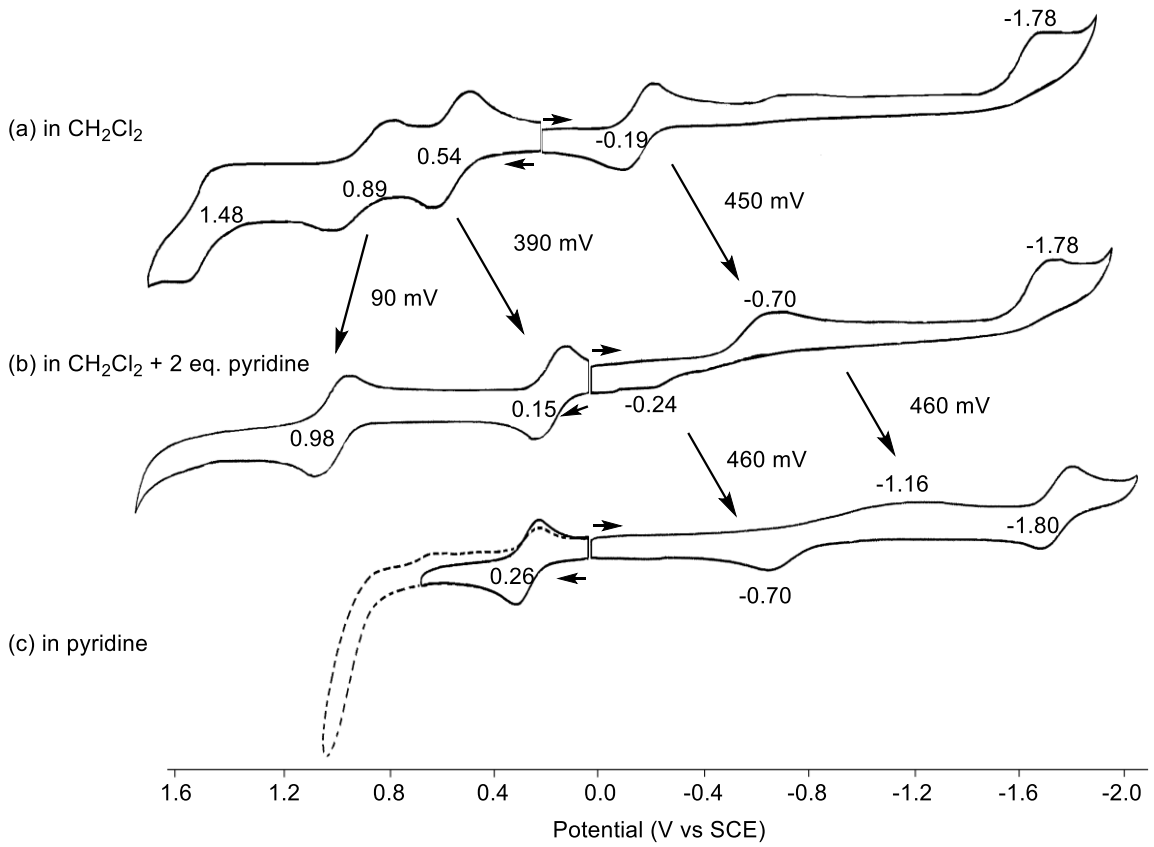

Figure 5-9. Cyclic voltammograms of Mes_3CorCo (a) in CH_2Cl_2, (b) in CH_2Cl_2 with 2 eq. of pyridine, and (c) in pyridine containing 0.1 M TBAP.

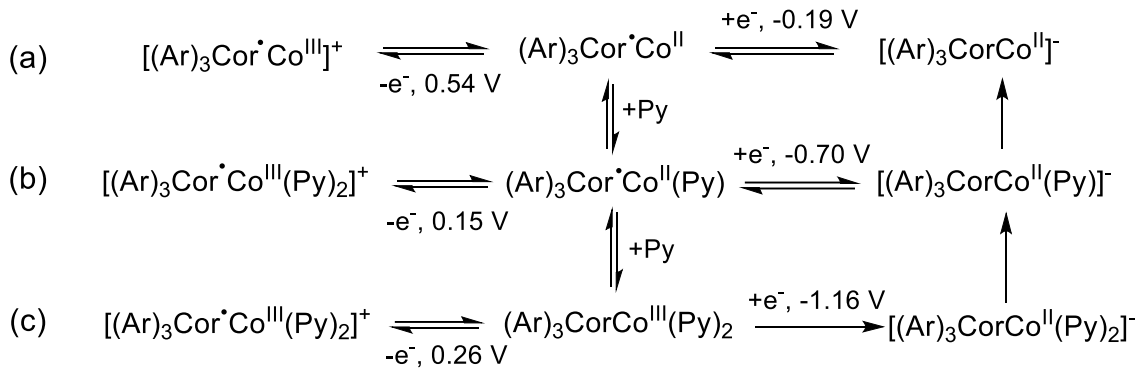

Scheme 5-1. Reaction Mechanism of Mes_3CorCo (a) in CH_2Cl_2, (b) in CH_2Cl_2 with 2 eq. of pyridine, and (c) in pyridine containing 0.1 M TBAP. *The listed potentials are given for Mes_3CorCo and were taken from Figure 5-9.

5.6 Metal- and Ring-Centered Redox Reactions of 1Py-4Py

The redox behavior of compounds **1Py-4Py** in CH_2Cl_2 resembles in part that of Mes_3CorCo in a CH_2Cl_2/pyridine mixture because the redox-active species for each of these corroles is the mono(pyridine) adduct, based on the UV-visible data described earlier in the manuscript. However, large differences do exist, as can be seen in the cyclic voltammograms in Figures 5-6 and 5-9b, where the potential separation between E_{pa} and E_{pc} for the first reduction varies with the number of *meso*-nitrophenyl groups on the corrole, with the separation being 460 mV for $Mes_3CorCo(Py)$, 280-300 mV for compounds **1Py** and **2Py**, and 140 mV for compounds **3Py** and **4Py**. The cyclic voltammetric data for **1Py** and **2Py** suggest that these two $[(Ar)_3Cor^{\bullet}Co^{II}(Py)]$ derivatives are reduced to $[(Ar)_3CorCo^{II}(Py)]^-$ and then lose one pyridine axial ligand to give the four-coordinate complex on the forward sweep (see Scheme 5-1b for $Mes_3CorCo(Py)$). The reverse potential sweep then involves re-oxidation of $[(Ar)_3CorCo^{II}]^-$ to $(Ar)_3Cor^{\bullet}Co^{II}$, followed by re-association of one pyridine ligand to yield the starting compound (again, as shown in Scheme 5-1b). This seems to be not the case for **3Py** and **4Py**, which contain three *meso*-nitrophenyl substituents.

As seen in Figure 5-9, the first one-electron addition of these two corroles is almost reversible, with a peak-to-peak potential separation of 140 mV, strongly suggesting that the one-electron reduction product, $[(Ar)_3CorCo^{II}(Py)]^-$, does not lose its pyridine ligand in CH_2Cl_2 on the cyclic voltammetric time scale. Thus, the reactants and products in the

first reductions of **3Py** and **4Py** would be $(Ar)_3Cor^{\bullet}Co^{II}(Py)$ and $[(Ar)_3CorCo^{II}(Py)]^-$ on the time scale of the cyclic voltammetric measurement, as shown in Equation 5-6.

$$(Ar)_3Cor^{\bullet}Co^{II}(Py) \;+\; e^- \rightleftharpoons [(Ar)_3Cor^{\bullet}Co^{II}(Py)]^- \qquad (5\text{-}6)$$

Evidence for the above oxidation state and coordination number assignments in both Mes_3CorCo and compounds **1Py-4Py** is given in part by UV-visible spectra for the singly oxidized and singly reduced corroles, which were generated in a thin-layer cell under the application of a controlled reducing or oxidizing potential. Examples of these spectra are shown in Figure 5-10 for compound **1Py** in CH_2Cl_2, PhCN, and pyridine containing 0.1 M TBAP. In all three solvents, the first one-electron reduction generates an anionic cobalt(II) corrole that possesses a Soret band at 420 nm in CH_2Cl_2, 427 nm in PhCN, and 423 nm in pyridine. Singly reduced Mes_3CorCo in CH_2Cl_2 also has a Soret band at 420 nm along with two Q bands at 572 and 620 nm, and similar Q-band absorptions are seen for compound **1Py** in CH_2Cl_2 (562 and 622 nm) or PhCN (578 and 620 nm). Furthermore, almost the same UV−visible spectrum is obtained for compound **1Py** in pyridine, where the singly reduced corrole has a Soret band at 423 nm and Q bands at 579 and 621 nm.

The singly oxidized form of compound **1Py** has the same UV−visible spectra in all three solvents. As seen in Table 5-4, this singly oxidized corrole has a split Soret band at 409 and 431 nm in CH_2Cl_2, 410 and 433 nm in PhCN, and 412 and 434 nm in pyridine. All three spectra suggest the oxidation of compound **1Py** to $[(Cor)Co^{III}(Py)_2]^+$. As shown in Scheme 5-1, in the case of a CH_2Cl_2 solution, a second pyridine ligand is added to the

cobalt center of the singly oxidized mono(pyridine) adduct $[CorCo^{III}(Py)]^{+}$, while in pyridine, two pyridine ligands are coordinated before and after electro-oxidation.

The singly reduced form of compound **3** also exhibits similar spectra in these three solvents, which suggests that the same species is generated after the initial one-electron addition on the spectroelectrochemical time scale. This is also the case for the singly oxidized species. A summary of the wavelengths and molar absorptivities of neutral, electro-oxidized, and electro-reduced forms of the corrole derivatives having zero, one, and three *meso*-nitrophenyl groups is given in Table 5-4.

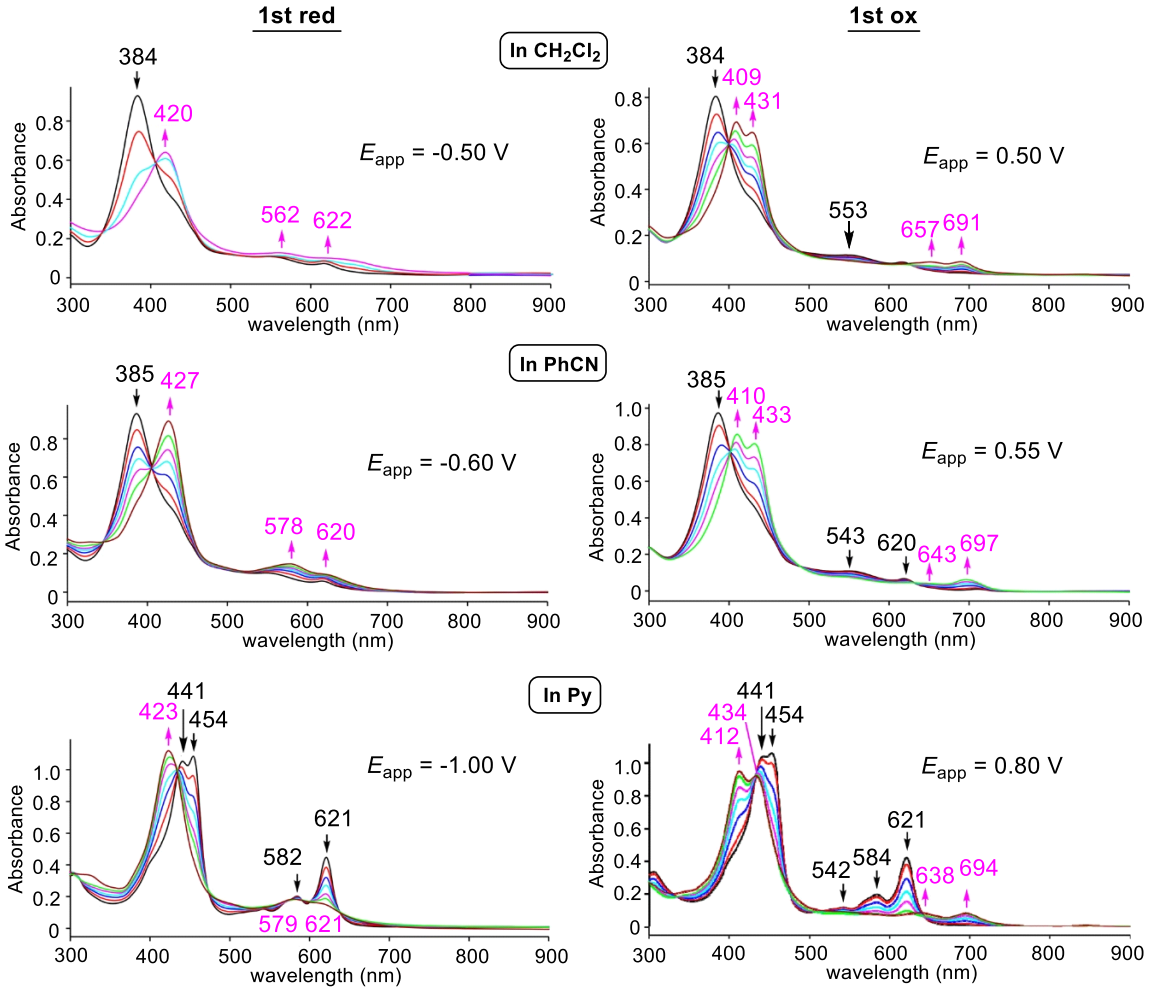

Figure 5-10. UV-visible spectral changes during the first reduction and first oxidation of compound **1Py** in CH_2Cl_2, PhCN, and pyridine containing 0.1 M TBAP.

Table 5-4. UV-visible spectral data of neutral, electrooxidized, and electroreduced forms of Mes_3CorCo, **1**, and **3** different solvents containing 0.1 M TBAP.

compound	solvent	λ_{max}, nm (ε x 10^{-4}, M^{-1} cm^{-1})		
		neutral	singly reduced	singly oxidized
Mes_3CorCo	CH_2Cl_2	388 (6.1), 543 (0.7)	420 (4.4), 572 (1.1), 620 (0.7)	383 (4.3)， 662 (0.6)
	PhCN	386 (5.3), 560 (0.2)	425 (5.0), 578 (0.8), 622 (0.4)	409 (4.8), 419 (4.8), 704 (0.05)
1	CH_2Cl_2	383 (6.4), 435 (2.6), 546 (0.9), 616 (0.7)	420 (4.4), 562 (0.9), 621 (0.6)	409 (5.5), 431 (4.5), 643 (0.2), 691 (0.7)
	PhCN	387 (5.5), 429 (1.9), 546 (0.6), 618 (0.3)	426 (5.3), 576 (0.9), 621 (0.6)	410 (4.8), 433 (4.5), 643 (0.2), 695 (0.4)
	Py	400 (2.1), 440 (5.2), 454 (5.4), 542 (0.6), 578 (0.9), 620 (2.2)	423 (5.6), 579 (1.1), 620 (0.8)	412 (4.6), 434 (4.6), 638 (0.4), 694 (0.4)
3	CH_2Cl_2	383 (6.4), 424 (5.7), 568 (0.1), 652 (0.2)	412 (6.8), 634 (2.6)	437 (8.6), 660 (0.7), 708 (0.6)
	PhCN	382 (5.9),438 (4.0), 570 (1.4), 650 (1.1)	414 (5.2), 605 (2.1)	438 (7.2), 650 (0.8), 713 (0.9)
	Py	414 (5.1), 452 (5.5), 654 (4.0)	414 (6.9), 654 (2.8)	443 (7.0), 654 (2.6)

5.7 Conclusions

A new series of bis(pyridine)cobalt (nitrophenyl)corroles have been synthesized and characterized by spectroscopic and electrochemical methods in three nonaqueous solvents. One of the corroles (compound **1Py**) was also structurally characterized. The bis(pyridine)cobalt (nitrophenyl)corroles are stable when dissolved in pyridine, but one axial ligand dissociates in CH_2Cl_2 or PhCN, giving the five-coordinate corrole, independent of the number of nitrophenyl groups on the macrocycle and the substitution pattern of each nitrophenyl group. This dissociation depends on the concentration and is only complete in a dilute solution of 10^{-5} M corrole. The electronic configuration of the neutral bis(pyridine)cobalt (nitrophenyl)corroles in solution, i.e., $(Ar)_3CorCo^{III}(Py)_2$ or $(Ar)_3Cor^{\bullet}Co^{II}(Py)$, depends on the number of pyridines axially coordinated to the cobalt center but not on the number of the NO_2Ph substituents on the macrocycle.

Compounds **1Py-4Py** can be reduced in three to five electron transfer steps. The first reduction of the investigated compounds gives the singly reduced four-coordinate corrole $[CorCo^{II}]^-$ for compounds **1Py** and **2Py**, which possess one nitrophenyl group in CH_2Cl_2 and PhCN, and the five-coordinate $[CorCo^{II}(Py)]^-$ for **3Py** and **4Py**, which have three nitrophenyl groups in each investigated solvent. For all four corroles, the first reduction at the macrocycle is followed by a reversible one-electron addition at the *meso*-nitrophenyl substituents, with this process being located at $E_{1/2}$ = -1.10 to -1.14 V or -1.25 to -1.31 V, depending on the type of second substituent on the nitrophenyl ring. Irreversible processes beyond -1.5 V are also observed for all four corroles but were not

investigated in this study. Each derivative also undergoes several oxidation processes within the anodic potential limit of the solvent, and for each compound, the first electron abstraction is proposed to yield a π-cation radical and a cobalt(III) metal center with two axially bound pyridine ligands.

The redox-active *meso*-nitrophenyl groups show no evidence of interaction with each other through the conjugated macrocycle, which is probably because the NO_2Ph ring is perpendicular to the corrole macrocycle and thus not in direct conjugation with the corrole π-ring system. However, the electron-withdrawing NO_2Ph groups affect the UV-visible spectra as well as the metal- and ring-centered redox reactions, shifting the potential by ~80 mV in a positive direction per each NO_2Ph group for the first oxidation in pyridine and CH_2Cl_2.

5.8 References

[1] R. Paolesse, *Syntheses of Corroles, Vol. 2*, Academic Press, **2000**, pp. 201-232.

[2] C. Erben, S. Will, K. M. Kadish, *Metallocorroles: Molecular Structure, Spectroscopy and Electronic States, Vol. 2*, Academic Press, **2000**, pp. 233-300.

[3] R. Guilard, J.-M. Barbe, C. Stern, K. M. Kadish, in *The Porphyrin Handbook, Vol. 18* (Eds.: K. M. Kadish, K. M. Smith, R. Guilard), World Scientific Publishing Co. Pte. Ltd., Singapore, **2003**, pp. 303-349.

[4] I. Aviv, Z. Gross, Corrole-Based Applications, *Chem. Commun.* **2007**, 1987-1999.

[5] L. Flamigni, D. T. Gryko, Photoactive Corrole-Based Arrays, *Chem. Soc. Rev.* **2009**, *38*, 1635-1646.

[6] K. E. Thomas, A. B. Alemayehu, J. Conradie, C. M. Beavers, A. Ghosh, The Structural Chemistry of Metallocorroles: Combined X-ray Crystallography and Quantum Chemistry Studies Afford Unique Insights, *Acc. Chem. Res.* **2012**, *45*, 1203-1214.

[7] A. Ghosh, Electronic Structure of Corrole Derivatives: Insights from Molecular Structures, Spectroscopy, Electrochemistry, and Quantum Chemical Calculations, *Chem. Rev.* **2017**, *117*, 3798-3881.

[8] R. Orlowski, D. Gryko, D. T. Gryko, Synthesis of Corroles and Their Heteroanalogs, *Chem. Rev.* **2017**, *117*, 3102-3137.

[9] R. D. Teo, J. Y. Hwang, J. Termini, Z. Gross, H. B. Gray, Fighting Cancer with Corroles, *Chem. Rev.* **2017**, *117*, 2711-2729.

[10] A. Mahammed, Z. Gross, Metallocorroles as Electrocatalysts for the Oxygen Reduction Reaction (ORR), *Isr. J. Chem.* **2016**, *56*, 756-762.

[11] Y. Fang, Z. Ou, K. M. Kadish, Electrochemistry of Corroles in Nonaqueous Media, *Chem. Rev.* **2017**, *117*, 3377-3419.

[12] V. A. Adamian, F. D'Souza, S. Licoccia, M. L. Di Vona, E. Tassoni, R. Paolesse, T. Boschi, K. M. Kadish, Synthesis, Characterization, and Electrochemical Behavior of (5,10,15-Tri-X-phenyl-2,3,7,8,12,13,17,18-octamethylcorrolato)cobalt(III)

Triphenylphosphine Complexes, Where X = p-OCH3, p-CH3, p-Cl, m-Cl, o-Cl, m-F, or o-F, *Inorg. Chem.* **1995**, *34*, 532-540.

[13] S. Will, J. Lex, E. Vogel, V. A. Adamian, E. Van Caemelbecke, K. M. Kadish, Synthesis, Characterization, and Electrochemistry of σ-Bonded Cobalt Corroles in High Oxidation States, *Inorg. Chem.* **1996**, *35*, 5577-5583.

[14] K. M. Kadish, Z. Ou, J. Shao, C. P. Gros, J.-M. Barbe, F. Jerome, F. Bolze, F. Burdet, R. Guilard, Alkyl and Aryl Substituted Corroles. 3. Reactions of Cofacial Cobalt Biscorroles and Porphyrin-Corroles with Pyridine and Carbon Monoxide, *Inorg. Chem.* **2002**, *41*, 3990-4005.

[15] K. M. Kadish, J. Shao, Z. Ou, C. P. Gros, F. Bolze, J.-M. Barbe, R. Guilard, Alkyl- and Aryl-Substituted Corroles. 4. Solvent Effects on the Electrochemical and Spectral Properties of Cobalt Corroles, *Inorg. Chem.* **2003**, *42*, 4062-4070.

[16] R. Guilard, F. Burdet, J.-M. Barbe, C. P. Gros, E. Espinosa, J. Shao, Z. Ou, R. Zhan, K. M. Kadish, Heterobimetallic Complexes of Cobalt(IV) Porphyrin-Corrole Dyads. Synthesis, Physicochemical Properties, and X-ray Structural Characterization, *Inorg. Chem.* **2005**, *44*, 3972-3983.

[17] K. M. Kadish, L. Fremond, Z. Ou, J. Shao, C. Shi, F. C. Anson, F. Burdet, C. P. Gros, J.-M. Barbe, R. Guilard, Cobalt(III) Corroles as Electrocatalysts for the Reduction of Dioxygen: Reactivity of a Monocorrole, Biscorroles, and Porphyrin-Corrole Dyads, *J. Am. Chem. Soc.* **2005**, *127*, 5625-5631.

[18] K. M. Kadish, J. Shao, Z. Ou, L. Fremond, R. Zhan, F. Burdet, J.-M. Barbe, C. P. Gros, R. Guilard, Electrochemistry, Spectroelectrochemistry, Chloride Binding, and O_2 Catalytic Reactions of Free-Base Porphyrin-Cobalt Corrole Dyads, *Inorg. Chem.* **2005**, *44*, 6744-6754.

[19] K. M. Kadish, J. Shao, Z. Ou, R. Zhan, F. Burdet, J.-M. Barbe, C. P. Gros, R. Guilard, Electrochemistry and Spectroelectrochemistry of Heterobimetallic Porphyrin-corrole Dyads. Influence of the Spacer, Metal Ion, and Oxidation State on the Pyridine Binding Ability, *Inorg. Chem.* **2005**, *44*, 9023-9038.

[20] K. M. Kadish, L. Fremond, F. Burdet, J.-M. Barbe, C. P. Gros, R. Guilard, Cobalt(IV) Corroles as Catalysts for the Electroreduction of O_2: Reactions of Heterobimetallic Dyads Containing a Face-to-face Linked Fe(III) or Mn(III) Porphyrin, *J. Inorg. Biochem.* **2006**, *100*, 858-868.

[21] K. M. Kadish, J. Shen, L. Fremond, P. Chen, M. El Ojaimi, M. Chkounda, C. P. Gros, J.-M. Barbe, K. Ohkubo, S. Fukuzumi, R. Guilard, Clarification of the Oxidation State of Cobalt Corroles in Heterogeneous and Homogeneous Catalytic Reduction of Dioxygen, *Inorg. Chem.* **2008**, *47*, 6726-6737.

[22] Z. Ou, A. Lu, D. Meng, S. Huang, Y. Fang, G. Lu, K. M. Kadish, Molecular Oxygen Reduction Electrocatalyzed by *meso*-Substituted Cobalt Corroles Coated on Edge-Plane Pyrolytic Graphite Electrodes in Acidic Media, *Inorg. Chem.* **2012**, *51*, 8890-8896.

[23] B. Mondal, K. Sengupta, A. Rana, A. Mahammed, M. Botoshansky, S. G. Dey, Z. Gross, A. Dey, Cobalt Corrole Catalyst for Efficient Hydrogen Evolution Reaction from H_2O under Ambient Conditions: Reactivity, Spectroscopy, and Density Functional Theory Calculations, *Inorg. Chem.* **2013**, *52*, 3381-3387.

[24] B. Li, Z. Ou, D. Meng, J. Tang, Y. Fang, R. Liu, K. M. Kadish, Cobalt Triarylcorroles Containing One, Two or Three Nitro Groups. Effect of NO_2 Substitution on Electrochemical Properties and Catalytic Activity for Reduction of Molecular Oxygen in Acid Media, *J. Inorg. Biochem.* **2014**, *136*, 130-139.

[25] J. Tang, Z. Ou, L. Ye, M. Yuan, Y. Fang, Z. Xue, K. M. Kadish, *Meso*-dichlorophenyl Substituted Co(III) Corrole: A Selective Electrocatalyst for the Two-electron Reduction of Dioxygen in Acid Media, X-ray Crystal Structure Analysis and Electrochemistry, *J. Porphyrins Phthalocyanines* **2014**, *18*, 891-898.

[26] J. Sun, Z. Ou, R. Guo, Y. Fang, M. Chen, Y. Song, K. M. Kadish, Synthesis and Electrochemistry of Cobalt Tetrabutanotriarylcorroles. Highly Selective Electrocatalysts for Two-Electron Reduction of Dioxygen in Acidic and Basic Media, *J. Porphyrins Phthalocyanines* **2016**, *20*, 456-464.

[27] Y. Wang, Z. Ou, Y. Fang, R. Guo, J. Tang, Y. Song, K. M. Kadish, Synthesis and Electrochemistry of A_2B Type Mono- and Bis-cobalt Triarylcorroles and Their Electrocatalytic Properties for Reduction of Dioxygen in Acid Media, *J. Porphyrins Phthalocyanines* **2016**, *20*, 1284-1295.

[28] J. H. Palmer, A. Mahammed, K. M. Lancaster, Z. Gross, H. B. Gray, Structures and Reactivity Patterns of Group 9 Metallocorroles, *Inorg. Chem.* **2009**, *48*, 9308-9315.

[29] A. Mahammed, M. Botoshansky, Z. Gross, Chlorinated Corroles, *Dalton Trans.* **2012**, *41*, 10938-10940.

[30] H.-K. Norheim, J. Capar, R. F. Einrem, K. J. Gagnon, C. M. Beavers, H. Vazquez-Lima, A. Ghosh, Ligand Noninnocence in FeNO Corroles: Insights from β-Octabromocorrole Complexes, *Dalton Trans.* **2016**, *45*, 681-689.

[31] H. L. Buckley, L. K. Rubin, M. Chrominski, B. J. McNicholas, K. H. Y. Tsen, D. T. Gryko, J. Arnold, Corroles That "Click": Modular Synthesis of Azido- and Propargyl-Functionalized Metallocorrole Complexes and Convergent Synthesis of a Bis-corrole Scaffold, *Inorg. Chem.* **2014**, *53*, 7941-7950.

[32] L. Ye, Z. Ou, D. Meng, M. Yuan, Y. Fang, K. M. Kadish, Electrochemistry of Fe(IV) and Mn(IV) corroles containing *meso*-dichlorophenyl substituents and the use of these compounds as catalysts for the electroreduction of dioxygen in acid media, *Turk. J. Chem.* **2014**, *38*, 994-1005, 1012 pp.

[33] P. Singh, I. Saltsman, A. Mahammed, I. Goldberg, B. Tumanskii, Z. Gross, Iron Complexes of Tris(4-nitrophenyl)corrole, with Emphasis on the (Nitrosyl)iron Complex, *J. Porphyrins Phthalocyanines* **2012**, *16*, 663-673.

[34] M. Eckshtain, I. Zilbermann, A. Mahammed, I. Saltsman, Z. Okun, E. Maimon, H. Cohen, D. Meyerstein, Z. Gross, Superoxide Dismutase Activity of Corrole Metal Complexes, *Dalton Trans.* **2009**, 7879-7882.

[35] E. Steene, A. Dey, A. Ghosh, β-Octafluorocorroles, *J. Am. Chem. Soc.* **2003**, *125*, 16300-16309.

[36] E. Steene, T. Wondimagegn, A. Ghosh, Resonance Raman Spectroscopy and Density Functional Theoretical Calculations of Manganese Corroles. A Parallelism Between High-Valent Metallocorroles and Metalloporphyrins, Relevant to Horseradish Peroxidase and Chloroperoxidase Compound I and II Intermediates, *J. Inorg. Biochem.* **2002**, *88*, 113-118.

[37] E. Steene, T. Wondimagegn, A. Ghosh, Electrochemical and Electronic Absorption Spectroscopic Studies of Substituent Effects in Iron(IV) and Manganese(IV) Corroles. Do the Compounds Feature High-Valent Metal Centers or Noninnocent Corrole Ligands? Implications for Peroxidase Compound I and II Intermediates, *J. Phys. Chem. B* **2001**, *105*, 11406-11413.

[38] E. Van Caemelbecke, S. Will, M. Autret, V. A. Adamian, J. Lex, J.-P. Gisselbrecht, M. Gross, E. Vogel, K. M. Kadish, Electrochemical and Spectral Characterization of Iron Corroles in High and Low Oxidation States: First Structural Characterization of an Iron(IV) Tetrapyrrole π Cation Radical, *Inorg. Chem.* **1996**, *35*, 184-192.

[39] M. Autret, S. Will, E. V. Caemelbecke, J. Lex, J.-P. Gisselbrecht, M. Gross, E. Vogel, K. M. Kadish, Synthesis and Electrochemistry of Iron(III) Corroles Containing a Nitrosyl Axial Ligand. Spectral Characterization of $[(OEC)Fe^{III}(NO)]_n$ where n = 0, 1, 2, or -1 and OEC is the Trianion of 2,3,7,8,12,13,17,18-Octaethylcorrole, *J. Am. Chem. Soc.* **1994**, *116*, 9141-9149.

[40] S. Nardis, M. Stefanelli, P. Mohite, G. Pomarico, L. Tortora, M. Manowong, P. Chen, K. M. Kadish, F. R. Fronczek, G. T. McCandless, K. M. Smith, R. Paolesse, β-Nitro Derivatives of Iron Corrolates, *Inorg. Chem.* **2012**, *51*, 3910-3920.

[41] J. Grodkowski, P. Neta, E. Fujita, A. Mahammed, L. Simkhovich, Z. Gross, Reduction of Cobalt and Iron Corroles and Catalyzed Reduction of CO2, *J. Phys. Chem. A* **2002**, *106*, 4772-4778.

[42] L. Simkhovich, A. Mahammed, I. Goldberg, Z. Gross, Synthesis and Characterization of Germanium, Tin, Phosphorus, Iron, and Rhodium Complexes of

Tris(pentafluorophenyl)Corrole, and the Utilization of the Iron and Rhodium Corroles as Cyclopropanation Catalysts, *Chem. - Eur. J.* **2001**, *7*, 1041-1055.

[43] B. Gao, Z. Ou, X. Chen, S. Huang, B. Li, Y. Fang, K. M. Kadish, Spectroelectrochemical Characterization of *Meso* Triaryl-Substituted Mn(IV), Mn(III) and Mn(II) corroles. Effect of Solvent and Oxidation State on UV-Visible Spectra and Redox Potentials in Nonaqueous Media, *J. Porphyrins Phthalocyanines* **2014**, *18*, 1131-1144.

[44] P. Singh, G. Dutta, I. Goldberg, A. Mahammed, Z. Gross, Expected and Unexpected Transformations of Manganese(III) Tris(4-nitrophenyl)corrole, *Inorg. Chem.* **2013**, *52*, 9349-9355.

[45] P. Chen, M. El Ojaimi, C. P. Gros, J.-M. Barbe, R. Guilard, J. Shen, K. M. Kadish, Electrochemistry and Spectroelectrochemistry of Bismanganese Biscorroles Dyads, *J. Porphyrins Phthalocyanines* **2011**, *15*, 188-196.

[46] P. Chen, M. El Ojaimi, C. P. Gros, P. Richard, J.-M. Barbe, R. Guilard, J. Shen, K. M. Kadish, Electrochemistry and Spectroelectrochemistry of Bismanganese Porphyrin-Corrole Dyads, *Inorg. Chem.* **2011**, *50*, 3479-3489.

[47] A. Kumar, I. Goldberg, M. Botoshansky, Y. Buchman, Z. Gross, Oxygen Atom Transfer Reactions from Isolated (Oxo)manganese(V) Corroles to Sulfides, *J. Am. Chem. Soc.* **2010**, *132*, 15233-15245.

[48] H. Y. Liu, L. Chen, F. Yam, H. Y. Zhan, X. Ying, X. L. Wang, H. F. Jiang, C. K. Chang, Reductive Demetalation of Manganese Corroles: the Substituent Effect, *Chin. Chem. Lett.* **2008**, *19*, 1000-1003.

[49] J. Shen, M. El Ojaimi, M. Chkounda, C. P. Gros, J.-M. Barbe, J. Shao, R. Guilard, K. M. Kadish, Solvent, Anion, and Structural Effects on the Redox Potentials and UV-visible Spectral Properties of Mononuclear Manganese Corroles, *Inorg. Chem.* **2008**, *47*, 7717-7727.

[50] Z. Ou, C. Erben, M. Autret, S. Will, D. Rosen, J. Lex, E. Vogel, K. M. Kadish, Manganese(III) and Manganese(IV) Corroles: Synthesis, Spectroscopic, Electrochemical and X-ray Structural Characterization, *J. Porphyrins Phthalocyanines* **2005**, *9*, 398-412.

[51] J. Fryxelius, G. Eilers, Y. Feyziyev, A. Magnuson, L. Sun, R. Lomoth, Synthesis and Redox Properties of A [*Meso*-Tris(4-Nitrophenyl)corrolato]Mn(III) Complex, *J. Porphyrins Phthalocyanines* **2005**, *9*, 379-386.

[52] N. Y. Edwards, R. A. Eikey, M. I. Loring, M. M. Abu-Omar, High-Valent Imido Complexes of Manganese and Chromium Corroles, *Inorg. Chem.* **2005**, *44*, 3700-3708.

[53] K. M. Kadish, V. A. Adamian, E. Van Caemelbecke, E. Gueletii, S. Will, C. Erben, E. Vogel, Electrogeneration of Oxidized Corrole Dimers. Electrochemistry of (OEC)M Where M = Mn, Co, Ni, or Cu and OEC is the Trianion of 2,3,7,8,12,13,17,18-Octaethylcorrole, *J. Am. Chem. Soc.* **1998**, *120*, 11986-11993.

[54] G. Golubkov, J. Bendix, H. B. Gray, A. Mahammed, I. Goldberg, A. J. DiBilio, Z. Gross, High-Valent Manganese Corroles and the First Perhalogenated Metallocorrole Catalyst, *Angew. Chem., Int. Ed.* **2001**, *40*, 2132-2134.

[55] H. Lei, A. Han, F. Li, M. Zhang, Y. Han, P. Du, W. Lai, R. Cao, Electrochemical, Spectroscopic and Theoretical Studies of A Simple Bifunctional Cobalt Corrole Catalyst for Oxygen Evolution and Hydrogen Production, *Phys. Chem. Chem. Phys.* **2014**, *16*, 1883-1893.

[56] H.-Y. Liu, M. H. R. Mahmood, S.-X. Qiu, C. K. Chang, Recent Developments in Manganese Corrole Chemistry, *Coord. Chem. Rev.* **2013**, *257*, 1306-1333.

[57] K. M. Kadish, B. C. Han, A. Endo, Electrochemistry of Five- and Six-Coordinate σ-Bonded Cobalt Porphyrins. Reactions of (TPP)Co(C_2H_5)(py) and (TPP)Co(R) where TPP is the Dianion of Tetraphenylporphyrin and R = CH_3, C_2H_5, or CH_2Cl, *Inorg. Chem.* **1991**, *30*, 4502-4506.

[58] K. M. Kadish, E. Wang, Electrochemistry of Metalloporphyrins in Nonaqueous Media, *Yingyong Huaxue* **1986**, *3*, 1-7.

[59] S. Ganguly, J. Conradie, J. Bendix, K. J. Gagnon, L. J. McCormick, A. Ghosh, Electronic Structure of Cobalt-Corrole-Pyridine Complexes: Noninnocent Five-Coordinate Co(II) Corrole-Radical States, *J. Phys. Chem. A* **2017**, *121*, 9589-9598.

[60] A. Mahammed, I. Giladi, I. Goldberg, Z. Gross, Synthesis and Structural Characterization of A Novel Covalently-Bound Corrole Dimer, *Chemistry* **2001**, *7*, 4259-4265.

[61] M. Schwalbe, D. K. Dogutan, S. A. Stoian, T. S. Teets, D. G. Nocera, Xanthene-Modified and Hangman Iron Corroles, *Inorg. Chem.* **2011**, *50*, 1368-1377.

[62] C. M. Lemon, M. Huynh, A. G. Maher, B. L. Anderson, E. D. Bloch, D. G. Nocera, D. C. Powers, Electronic Structure of Copper Corroles, *Angew. Chem., Int. Ed.* **2016**, *55*, 2176-2180.

[63] P. Yadav, M. Sankar, X. Ke, L. Cong, K. M. Kadish, Highly Reducible π-Extended Copper Corroles, *Dalton Trans.* **2017**, *46*, 10014-10022.

[64] A. B. Alemayehu, E. Gonzalez, L. K. Hansen, A. Ghosh, Copper Corroles Are Inherently Saddled, *Inorg. Chem.* **2009**, *48*, 7794-7799.

[65] B. Van Oort, E. Tangen, A. Ghosh, Electronic Structure of Transition Metal-Isocorrole Complexes: A First Quantum Chemical Study, *Eur. J. Inorg. Chem.* **2004**, 2442-2445.

[66] Z. Ou, J. Shao, H. Zhao, K. Ohkubo, I. H. Wasbotten, S. Fukuzumi, A. Ghosh, K. M. Kadish, Spectroelectrochemical and ESR Studies of Highly Substituted Copper Corroles, *J. Porphyrins Phthalocyanines* **2004**, *8*, 1236-1247.

[67] A. Ghosh, T. Wondimagegn, A. B. J. Parusel, Electronic Structure of Gallium, Copper, and Nickel Complexes of Corrole. High-Valent Transition Metal Centers versus Noninnocent Ligands, *J. Am. Chem. Soc.* **2000**, *122*, 5100-5104.

[68] S. Ganguly, L. J. Giles, K. E. Thomas, R. Sarangi, A. Ghosh, Ligand Noninnocence in Iron Corroles: Insights from Optical and X-ray Absorption Spectroscopies and Electrochemical Redox Potentials, *Chem. - Eur. J.* **2017**, *23*, 15098-15106.

[69] S. Ganguly, D. Renz, L. J. Giles, K. J. Gagnon, L. J. McCormick, J. Conradie, R. Sarangi, A. Ghosh, Cobalt- and Rhodium-Corrole-Triphenylphosphine Complexes Revisited: The Question of a Noninnocent Corrole, *Inorg. Chem.* **2017**, *56*, 14788-14800.

[70] X. Jiang, M. L. Naitana, N. Desbois, V. Quesneau, S. Brandes, Y. Rousselin, W. Shan, W. R. Osterloh, V. Blondeau-Patissier, C. P. Gros, K. M. Kadish, Electrochemistry of Bis(pyridine)cobalt (Nitrophenyl)corroles in Nonaqueous Media, *Inorg. Chem.* **2018**, *57*, 1226-1241.

[71] Y. Fang, X. Jiang, Z. Ou, C. Michelin, N. Desbois, C. P. Gros, K. M. Kadish, Redox Properties of Nitrophenylporphyrins and Electrosynthesis of Nitrophenyl-linked Zn Porphyrin Dimers or Arrays, *J. Porphyrins Phthalocyanines* **2014**, *18*, 832-841.

[72] D. Bhattacharya, P. Singh, S. Sarkar, Synthesis, X-structure and Solvent Induced Electronic States Tuning of *Meso*-tris(4-nitrophenyl)corrolato-copper Complex, *Inorg. Chim. Acta* **2010**, *363*, 4313-4318.

[73] S. M. LeCours, S. G. DiMagno, M. J. Therien, Exceptional Electronic Modulation of Porphyrins through *meso*-Arylethynyl Groups. Electronic Spectroscopy, Electronic Structure, and Electrochemistry of [5,15-Bis[(aryl)ethynyl]-10,20-diphenylporphinato]zinc(II) Complexes. X-ray Crystal Structures of [5,15-Bis[(4'-fluorophenyl)ethynyl]-10,20-diphenylporphinato]zinc(II) and 5,15-Bis[(4'-methoxyphenyl)ethynyl]-10,20-diphenylporphyrin, *J. Am. Chem. Soc.* **1996**, *118*, 11854-11864.

[74] N. M. Rowley, L. J. Yellowlees, P. R. Ashton, T. A. Hamor, C. J. Jones, N. Spencer, J. A. McCleverty, G. S. Beddard, T. M. Feehan, N. T. H. White, S. S. Kurek, E. J. L. McInnes, N. N. Payne, Synthesis and Photochemistry of Amido-Linked, Peripherally-Molybdenated Tetraphenylporphyrins, *Inorg. Chem.* **1996**, *35*, 7526-7534.

[75] M. A. Schiavon, L. S. Iwamoto, A. G. Ferreira, Y. Iamamoto, M. V. B. Zanoni, M. d. D. Assis, Synthesis and Characterization of A Novel Series of *Meso*-(Nitrophenyl) and *Meso*-(Carboxyphenyl) Substituted Porphyrins, *J. Braz. Chem. Soc.* **2000**, *11*, 458-466.

[76] H. T. Uyeda, Y. Zhao, K. Wostyn, I. Asselberghs, K. Clays, A. Persoons, M. J. Therien, Unusual Frequency Dispersion Effects of the Nonlinear Optical Response in Highly Conjugated (Polypyridyl)metal-(Porphinato)zinc(II) Chromophores, *J. Am. Chem. Soc.* **2002**, *124*, 13806-13813.

[77] H. Koga, T. Arai, T. Hamada, S. Sakaki, Application of Metalloporphyrins and Methylviologen-Pendent Iron Porphyrin to Reduction of Diphenylsulfoxide, *J. Mol. Catal. A: Chem.* **2003**, *200*, 223-228.

[78] Y. Li, J.-S. Huang, G.-B. Xu, N. Zhu, Z.-Y. Zhou, C.-M. Che, K.-Y. Wong, Spectral, Structural, and Electrochemical Properties of Ruthenium Porphyrin Diaryl and Aryl(alkoxycarbonyl) Carbene Complexes: Influence of Carbene Substituents, Porphyrin Substituents, and Trans-Axial Ligands, *Chem. - Eur. J.* **2004**, *10*, 3486-3502.

[79] E. Annoni, M. Pizzotti, R. Ugo, S. Quici, T. Morotti, M. Bruschi, P. Mussini, Synthesis, Electronic Characterization and Significant Second-Order Non-Linear Optical Responses of *Meso*-Tetraphenylporphyrins and Their ZnII Complexes Carrying A Push or Pull Group in the β-Pyrrolic Position, *Eur. J. Inorg. Chem.* **2005**, 3857-3874.

[80] Y. Inokuma, Z. S. Yoon, D. Kim, A. Osuka, *Meso*-Aryl-Substituted Subporphyrins: Synthesis, Structures, and Large Substituent Effects on Their Electronic Properties, *J. Am. Chem. Soc.* **2007**, *129*, 4747-4761.

[81] K. Heinze, A. Reinhart, Structural and Photophysical Ptudies of Trans-AB2C-Substituted Porphyrin Ligands and Their Zinc and Copper Complexes, *Dalton Trans.* **2008**, 469-480.

[82] C.-F. Lo, S.-J. Hsu, C.-L. Wang, Y.-H. Cheng, H.-P. Lu, E. W.-G. Diau, C.-Y. Lin, Tuning Spectral and Electrochemical Properties of Porphyrin-Sensitized Solar Cells, *J. Phys. Chem. C* **2010**, *114*, 12018-12023.

[83] K. Rajesh, A. K. Rahiman, K. S. Bharathi, S. Sreedaran, V. Gangadevi, V. Narayanan, Spectroscopic, Redox and Biological Studies of Push-pull Porphyrins and Their Metal Complexes, *Bull. Korean Chem. Soc.* **2010**, *31*, 2656-2664.

[84] B. A. Iglesias, M. Hoerner, H. E. Toma, K. Araki, 5-(1-(4-Phenyl)-3-(4-Nitrophenyl)triazene)-10,15,20-Triphenylporphyrin: A New Triazene-Porphyrin Dye and Its Spectroelectrochemical Properties, *J. Porphyrins Phthalocyanines* **2012**, *16*, 200-209.

[85] C. A. Joseph, M. S. Lee, A. V. Iretskii, G. Wu, P. C. Ford, Substituent Effects on Nitrosyl Iron Corrole Complexes Fe(Ar3C)(NO), *Inorg. Chem.* **2006**, *45*, 2075-2082.

[86] Y. Gao, J. Liu, M. Wang, Y. Na, B. Aakermark, L. Sun, Synthesis and Characterization of Manganese and Copper Corrole Xanthene Complexes as Catalysts for Water Oxidation, *Tetrahedron* **2007**, *63*, 1987-1994.

[87] L. M. Reith, M. Koenig, C. Schwarzinger, W. Schoefberger, BiIII-Corroles: A Versatile Platform for the Synthesis of Functionalized Corroles, *Eur. J. Inorg. Chem.* **2012**, *2012*, 4342-4349.

[88] H. Lei, H. Fang, Y. Han, W. Lai, X. Fu, R. Cao, Reactivity and Mechanism Studies of Hydrogen Evolution Catalyzed by Copper Corroles, *ACS Catal.* **2015**, *5*, 5145-5153.

[89] G. Lu, J. Li, X. Jiang, Z. Ou, K. M. Kadish, Europium Triple-Decker Complexes Containing Phthalocyanine and Nitrophenyl-Corrole Macrocycles, *Inorg. Chem.* **2015**, *54*, 9211-9222.

[90] A. Atifi, M. D. Ryan, Electrochemistry and Spectroelectrochemistry of 1,4-Dinitrobenzene in Acetonitrile and Room-Temperature Ionic Liquids: ion-Pairing Effects in Mixed Solvents, *Anal. Chem.* **2014**, *86*, 6617-6625.

[91] A. Liska, P. Lhotak, J. Ludvik, Electrochemical Reduction and Intramolecular Electron Communication of Nitro Substituted Thiacalix[4]arenes, *Electroanalysis* **2016**, *28*, 2861-2865.

[92] S. Ooi, T. Tanaka, A. Osuka, Synthesis and Characterization of cis-A2B-Type *meso*-Triaryl-Substituted Corroles, *Eur. J. Org. Chem.* **2015**, *2015*, 130-134.

[93] V. S. Shetti, U. R. Prabhu, M. Ravikanth, Synthesis and Studies of Thiacorroles, *J. Org. Chem.* **2010**, *75*, 4172-4182.

[94] P. J. Sintic, W. E, Z. Ou, J. Shao, J. A. McDonald, Z.-L. Cai, K. M. Kadish, M. J. Crossley, J. R. Reimers, Control of the Site and Potential of Reduction and Oxidation Processes in π-Expanded Quinoxalinoporphyrins, *Phys. Chem. Chem. Phys.* **2008**, *10*, 268-280.

[95] C. Hansch, A. Leo, R. W. Taft, A Survey of Hammett Substituent Constants and Resonance and Field Parameters, *Chem. Rev.* **1991**, *91*, 165-195.

[96] P. Yadav, P. Rathi, M. Sankar, Facile Generation of A2B Corrole Radical Using Fe(III) Salts and Its Spectroscopic Properties., *ACS Omega* **2017**, *2*, 959-965.

[97] G. Pomarico, P. Galloni, F. Mandoj, S. Nardis, M. Stefanelli, A. Vecchi, S. Lentini, D. O. Cicero, Y. Cui, L. Zeng, K. M. Kadish, R. Paolesse, 5,10,15-Triferrocenylcorrole Complexes, *Inorg. Chem.* **2015**, *54*, 10256-10268.

[98] C. Brueckner, R. P. Brinas, J. A. Krause-Bauer, X-ray Structure and Variable Temperature NMR Spectra of [*meso*-Triarylcorrolato]copper(III), *Inorg. Chem.* **2003**, *42*, 4495-4497.

[99] I. Luobeznova, L. Simkhovich, I. Goldberg, Z. Gross, Electronic Structures and Reactivities of Corrole-Copper Complexes, *Eur. J. Inorg. Chem.* **2004**, *2004*, 1724-1732.

[100] M. Broring, F. Bregier, T. E. Consul, C. Hell, M. C. Holthausen, Revisiting the Electronic Ground State of Copper Corroles, *Angew. Chem., Int. Ed.* **2007**, *46*, 445-448.

[101] J. L. Fillol, Z. Codola, I. Garcia-Bosch, L. Gomez, J. J. Pla, M. Costas, Efficient Water Oxidation Catalysts Based on Readily Available Iron Coordination Complexes, *Nat. Chem.* **2011**, *3*, 807-813.

[102] M. Stefanelli, F. Mandoj, M. Mastroianni, S. Nardis, P. Mohite, F. R. Fronczek, K. M. Smith, K. M. Kadish, X. Xiao, Z. Ou, P. Chen, R. Paolesse, Amination Reaction on Copper and Germanium β-Nitrocorrolates, *Inorg. Chem.* **2011**, *50*, 8281-8292.

[103] S. M. Barnett, K. I. Goldberg, J. M. Mayer, A Soluble Copper-Bipyridine Water-Oxidation Electrocatalyst, *Nat. Chem.* **2012**, *4*, 498-502.

[104] M. J. Rose, H. B. Gray, J. R. Winkler, Hydrogen Generation Catalyzed by Fluorinated Diglyoxime-Iron Complexes at Low Overpotentials, *J. Am. Chem. Soc.* **2012**, *134*, 8310-8313.

[105] M. K. Coggins, M.-T. Zhang, Z. Chen, N. Song, T. J. Meyer, Single-Site Copper(II) Water Oxidation Electrocatalysis: Rate Enhancements with HPO42- as a Proton Acceptor at pH 8, *Angew. Chem., Int. Ed.* **2014**, *53*, 12226-12230.

[106] D. J. Graham, D. G. Nocera, Electrocatalytic H2 Evolution by Proton-Gated Hangman Iron Porphyrins, *Organometallics* **2014**, *33*, 4994-5001.

[107] P. Zhang, M. Wang, Y. Yang, T. Yao, L. Sun, A Molecular Copper Catalyst for Electrochemical Water Reduction with a Large Hydrogen-Generation Rate Constant in Aqueous Solution, *Angew. Chem., Int. Ed.* **2014**, *53*, 13803-13807.

[108] D. K. Dogutan, S. A. Stoian, R. McGuire, M. Schwalbe, T. S. Teets, D. G. Nocera, Hangman Corroles: Efficient Synthesis and Oxygen Reaction Chemistry, *J. Am. Chem. Soc.* **2011**, *133*, 131-140.

[109] Y. Fang, M. O. Senge, E. Van Caemelbecke, K. M. Smith, C. J. Medforth, M. Zhang, K. M. Kadish, Impact of Substituents and Nonplanarity on Nickel and Copper Porphyrin Electrochemistry: First Observation of a CuII/CuIII Reaction in Nonaqueous Media, *Inorg. Chem.* **2014**, *53*, 10772-10778.

6

Mono-DMSO Ligated Cobalt (Nitrophenyl)corroles: Electrochemical and Spectral Characterization

6.1 Introduction

Numerous cobalt corroles have been characterized with respect to their spectral, electrochemical and catalytic properties.[1-32] The cobalt central metal ion of structurally related porphyrins has been shown to exist in multiple oxidation states,[33, 34] but this may not be the case for the corroles which may contain a non-innocent macrocyclic ligand and a Co(II) rather than Co(III) central metal ion in the air stable form of the compound.[30-32] Whatever the oxidation state of the central metal ion, cobalt corroles still exhibit a rich redox reactivity which can be systematically tuned by changes in the peripheral and/or axial substituents on the molecule.

Cobalt corroles containing two pyridine axial ligands and one or three nitrophenyl (NO_2Ph) substituents on the meso-positions of the macrocycle were recently synthesized and characterized by electrochemical studies in CH_2Cl_2, PhCN and pyridine, [35] and the same series of compounds with a single bound DMSO axial ligand are now synthesized and electrochemically investigated in CH_2Cl_2 and DMSO. The structures of these compounds are shown in Chart 6-1.

Different from the earlier studied bis-py cobalt nitrophenylcorroles,[36] the currently investigated compounds have only one DMSO ligand on the cobalt ion in the solid state. However, under conditions of the electrochemical measurements, the synthesized mono-DMSO five-coordinate derivatives will form tetra- or hexa-coordinated complexes in solution, depending upon the concentration of the corrole, the specific solution conditions and the application of an applied oxidizing or reducing

potential. This is investigated in the current study where the neutral, singly-reduced and singly-oxidized corroles are spectroscopically characterized and the data utilized to assign both the degree of axial coordination and the site of electron transfer.

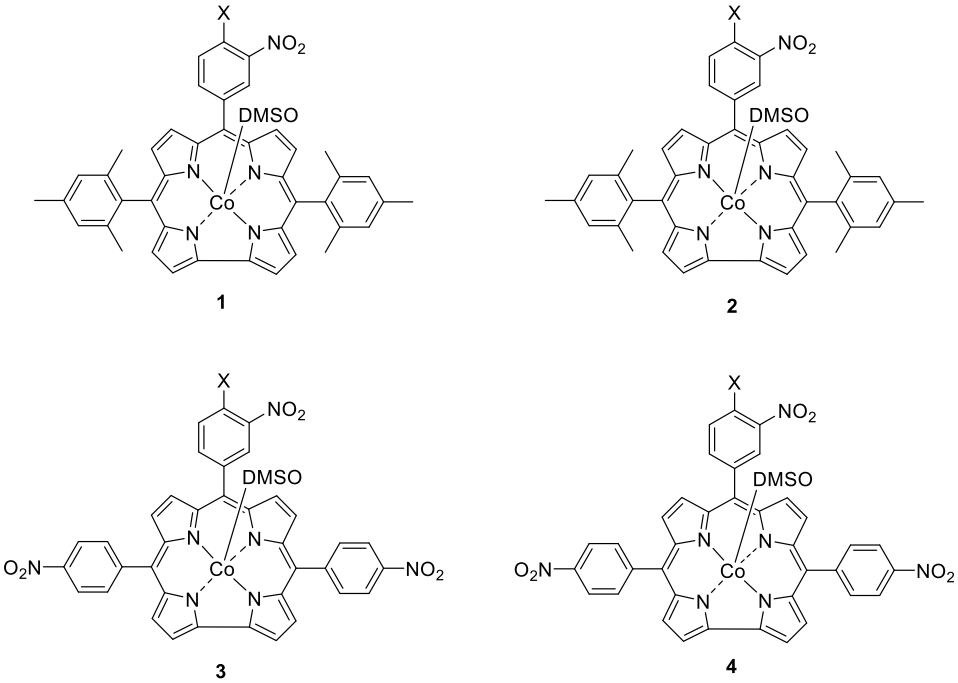

Chart 6-1. Structures of mono-DMSO ligated cobalt (nitrophenyl)corroles **1-4**.

6.2 UV-visible Characterization

The air-stable cobalt corroles **1-4** contain one DMSO axial ligand in their synthesized form. However, to correctly analyze the prevailing redox reactions under different solution conditions, it was necessary to first examine any changes, which might occur in axial coordination when the synthesized five-coordinate compounds were dissolved in the utilized electrochemical solvents. For example, the bound DMSO axial ligand might dissociate from the cobalt center of **1-4** when dissolved in CH_2Cl_2 solutions, while in DMSO a second DMSO solvent molecule might bind to the cobalt center, giving the six-coordinate bis-DMSO complex in this solvent.

The above possibilities were examined by first recording the UV-visible spectra of the four-coordinate reference corrole Mes_3CorCo in CH_2Cl_2 or DMSO and then comparing the resulting spectral data to that of the nitrophenyl corroles **1-4** under the same solution conditions. Examples of the measured spectra are illustrated in Figure 6-1 and a summary of the data is given in Table 6-1.

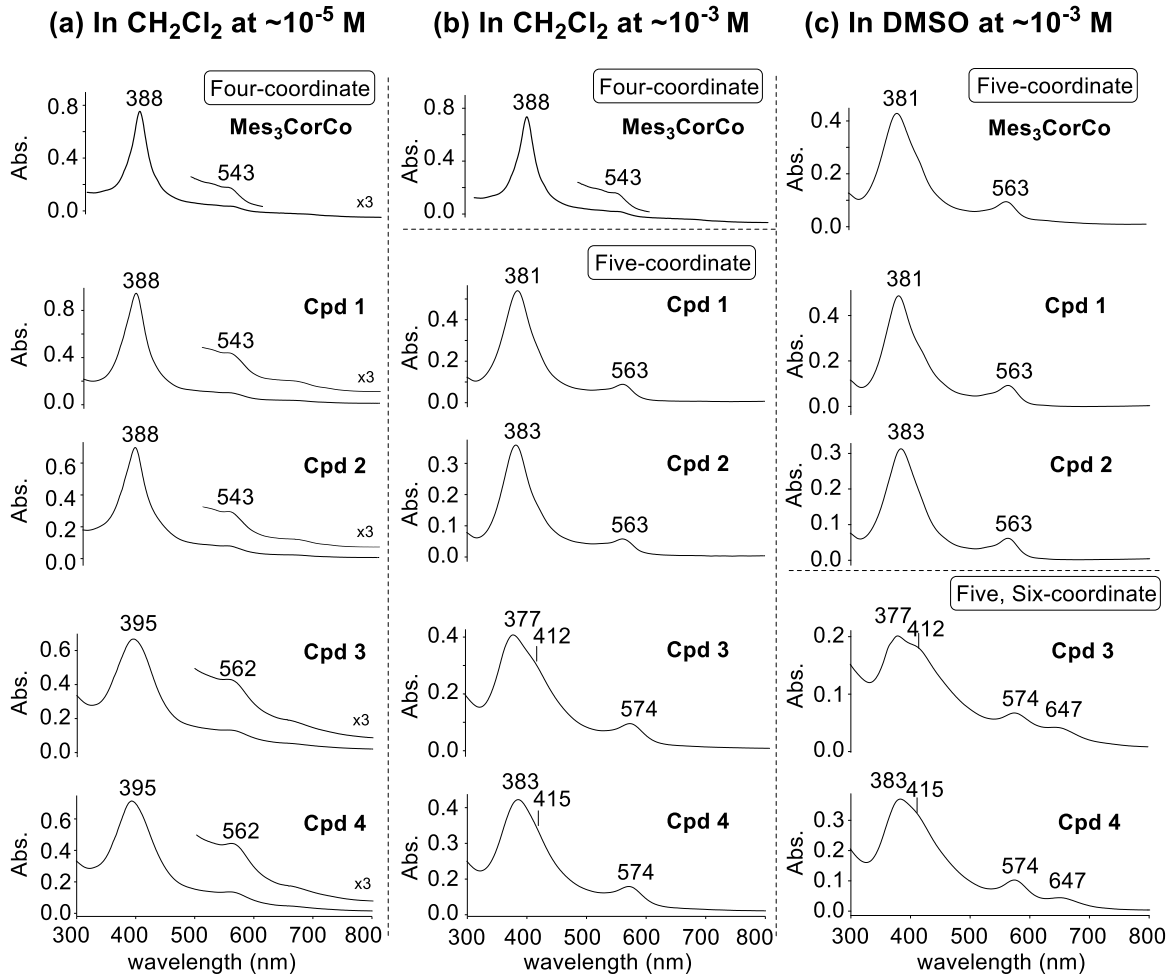

Figure 6-1. UV-visible spectra of Mes_3CorCo and **1-4** in CH_2Cl_2 and DMSO with proposed coordination.

Table 6-1. UV-visible spectra (λ_{max}, $\varepsilon \times 10^{-4}$ M^{-1} cm^{-1}) of Mes_3CorCo and **1-4** in CH_2Cl_2 and DMSO.

compound	λ_{max}, nm ($\varepsilon \times 10^{-4}$ M^{-1} cm^{-1})					
	in CH_2Cl_2 (10^{-5} M)		in CH_2Cl_2 (10^{-3} M)		in DMSO (10^{-3} M)	
	Soret band	visible band	Soret band	visible band	Soret band	visible band
Mes_3CorCo	388 (6.1)	543 (0.7)	388 (6.1)	543 (0.7)	381 (6.1)	563 (1.3)
1	388 (7.6)	543 (0.9)	381 (7.4)	563 (1.2)	381 (6.5)	563 (1.4)
2	388 (7.8)	543 (0.9)	383 (7.2)	563 (1.2)	383 (6.3)	563 (1.3)
3	395 (4.8)	562 (0.9)	377 (3.9), 412[s]	574 (0.8)	377 (4.0), 412[s]	574 (1.2), 647 (0.7)
4	395 (5.5)	562 (1.0)	383 (5.5), 415[s]	574 (1.1)	383 (5.0), 415[s]	574 (1.4), 647 (0.7)

[s]Shoulder bands.

Different absorption bands are observed for Mes_3CorCo[19] in CH_2Cl_2 and DMSO. The spectrum of 10^{-5} or 10^{-3} M corrole in CH_2Cl_2 is characterized by a sharp Soret band at 388 nm and a single Q band at 543 nm, while a 10^{-3} M solution of the corrole in DMSO has a broadened and blue-shifted Soret band at 381 nm and red-shifted Q band at 563 nm. The spectrum of Mes_3CorCo in both CH_2Cl_2 solutions is assigned to the original synthesized four-coordinate derivative while a five-coordinate DMSO adduct is proposed to exist in DMSO solutions. This assignment was confirmed by an electrochemically monitored titration of Mes_3CorCo in CH_2Cl_2 with DMSO as described on the following pages.

The UV-visible spectra for a 10^{-5} M concentration of corroles **1** and **2** are identical to each other in CH_2Cl_2, and they are also identical to the spectrum of four-coordinate Mes_3CorCo (Figure 6-1a) under the same solution conditions. This similarity can only be accounted for by a loss of the single axially bound DMSO solvent molecule from **1** and **2** in dilute solutions of CH_2Cl_2. This ligand dissociation, shown in Equation 6-1, does not occur for **1** and **2** in CH_2Cl_2 at a higher corrole concentration of 10^{-3} M. Under these conditions, the UV-visible spectra are characterized by bands at 381-383 nm and 563 nm. These wavelengths are identical to those obtained for the same compounds in neat DMSO, where the five-coordinate corroles are present in the bulk of solution.

$$(Ar)_3CorCo(DMSO) \rightleftharpoons (Ar)_3CorCo + DMSO \qquad (6\text{-}1)$$

In contrast to the two mono-nitrophenyl corroles (**1** and **2**), three distinct spectral patterns are seen for compounds **3** and **4** under the different solution conditions of

Figure 6-1. The first is in CH_2Cl_2 for a 10^{-5} M concentration of these corroles, both of which have bands at 395 and 562 nm and are assigned as characteristic of the four-coordinate corrole, which has lost one DMSO ligand. The second spectral pattern is for compounds **3** and **4** at a 10^{-3} M concentration in CH_2Cl_2 where there is a blue shift of the Soret band absorption and a red shift of the Q band upon increasing the concentration from 10^{-5} to 10^{-3} M. This change in position of the absorption bands with change in concentration is similar to what occurs for compounds **1** and **2** and is assigned as a conversion of the four- to the five-coordinate form of corrole as labelled in Figure 6-1.

The third spectral pattern for compounds **3** and **4** is obtained in DMSO, where the spectra can be described as a composite overlapping of two absorbing species, one with bands identical to that for the five-coordinate corroles in Figure 6-1b (λ_{max} = 377 or 383 and 574 nm) and the other which has red-shifted Soret and Q bands located at 412-415 and 647 nm. These latter red-shifted bands are assigned to the six-coordinate corroles **3** and **4**, which are generated by the binding of a second axial DMSO ligand as shown in Equation 6-2.

$$(Ar)_3CorCo(DMSO) + DMSO \rightleftharpoons (Ar)_3CorCo(DMSO)_2 \qquad (6\text{-}2)$$

A more detailed concentration dependence study of the UV-visible spectra for **1-4** in CH_2Cl_2 is given in Figure 6-2 for corrole concentrations between 10^{-3} and 10^{-6} M and parallels the concentration dependence shown in Figure 6-1. No such concentration dependence is observed in DMSO where the same UV-visible spectrum is obtained for each corrole over the above concentration range (Figure 6-3).

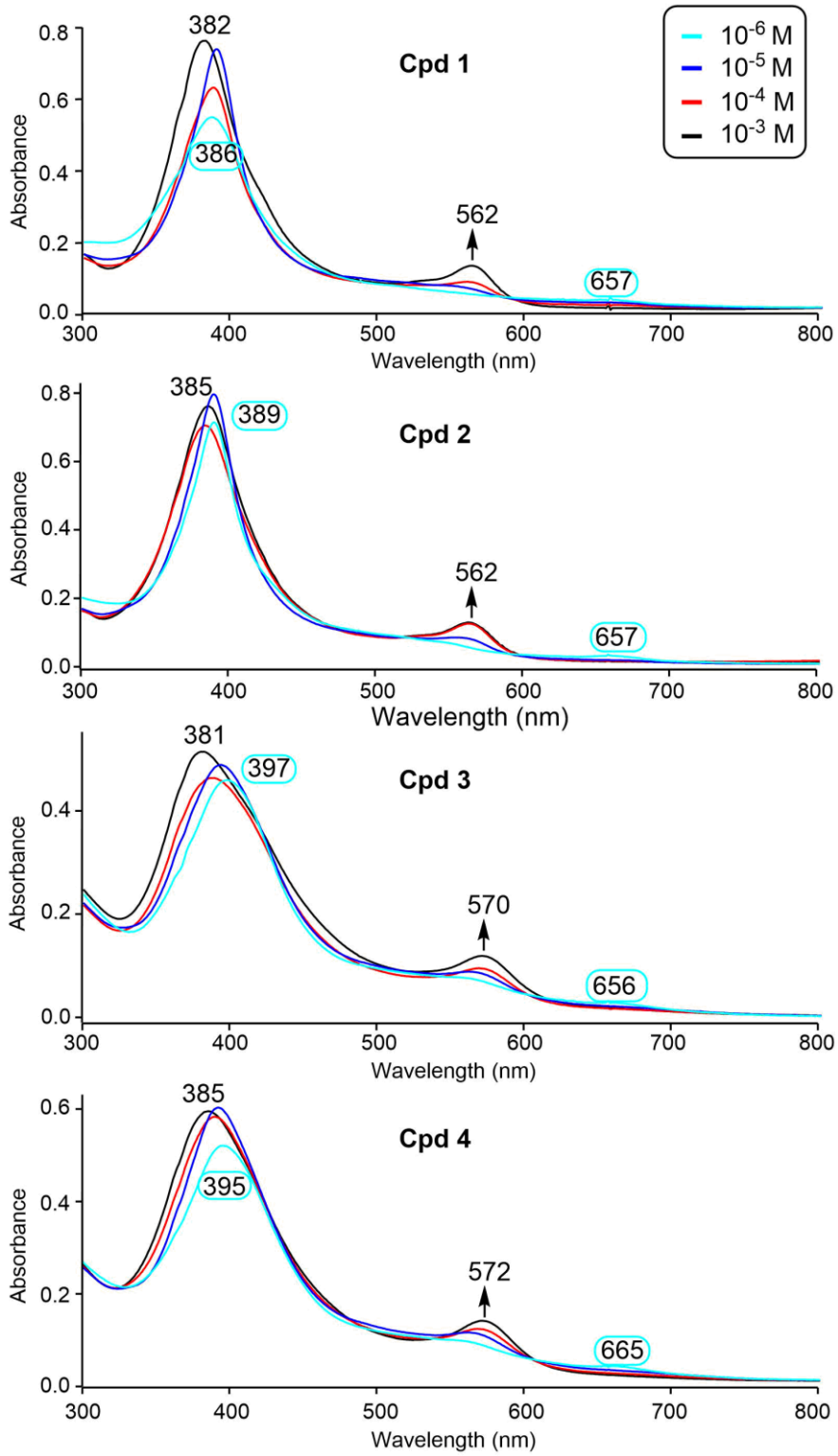

Figure 6-2. Changes in absorbance (A) of compounds **1-4** at concentrations ranging from 10^{-6} M to 10^{-3} M in CH_2Cl_2 while cell path length (b) times concentration (c) constant.

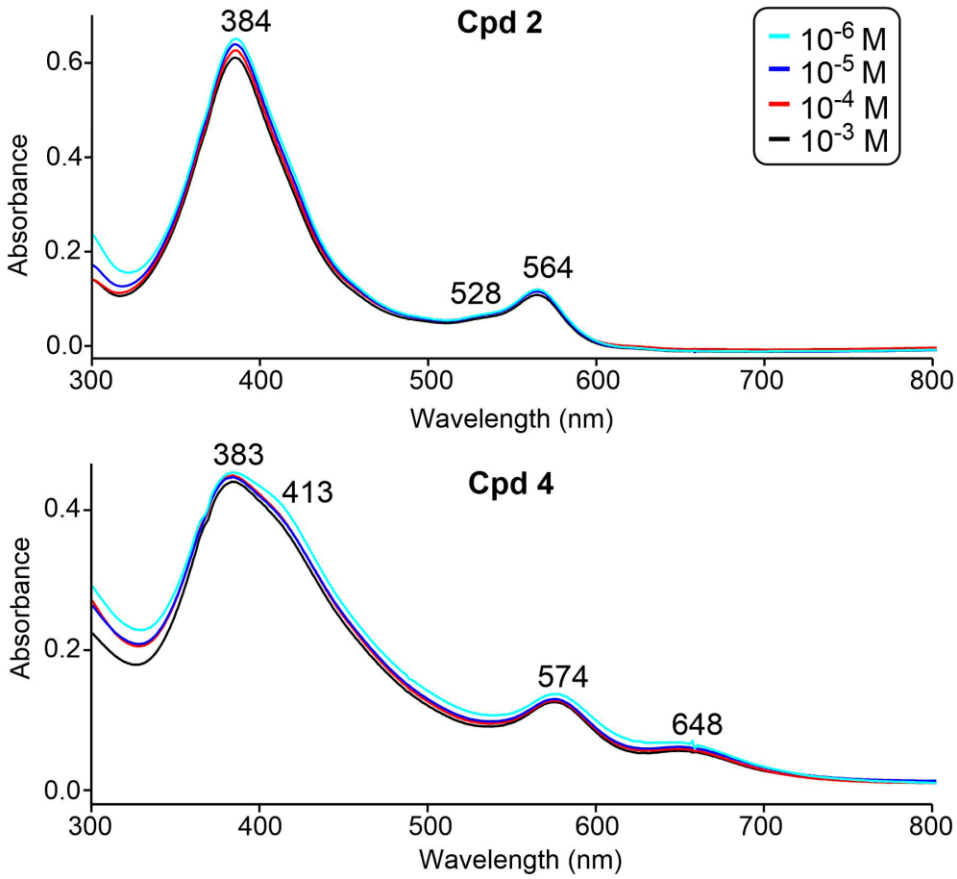

Figure 6-3. Changes in absorbance (A) of compounds **2** and **4** at concentrations ranging from 10^{-6} M to 10^{-3} M in DMSO while cell path length (b) times concentration (c) constant.

6.3 Electrochemistry

The redox reactions of **1-4** and Mes_3CorCo were investigated in CH_2Cl_2, DMSO and DMSO/CH_2Cl_2 mixtures containing 0.1 M TBAP. Examples of cyclic voltammograms under the first two solution conditions are shown in Figures 6-4 and 6-5, and a summary of the measured potentials is given in Table 6-2.

The reference compound Mes_3CorCo exhibits two one-electron reductions and three reversible one-electron oxidations in CH_2Cl_2. The first reversible reduction at $E_{1/2}$ = -0.19 V was previously assigned as a one-electron addition to the corrole macrocycle of $Mes_3Cor^{\bullet}Co^{II}$ forming a Co(II) corrole with an intact macrocycle. The first oxidation at $E_{1/2}$ = 0.54 V in this solvent was assigned as a one-electron abstraction from the Co(II) center to give a Co(III) π-cation radical.[35] Compounds **1-4** also exhibit three reversible one-electron oxidations in CH_2Cl_2 in addition to three or four reductions as shown in Figure 6-4. The reductions of these corroles at potentials more negative than -1.0 V all involve the electroactive *meso*-NO_2Ph substituents on the corrole macrocycle and were described in a previous publication.[35] These reactions are not discussed in further detail in the present study.

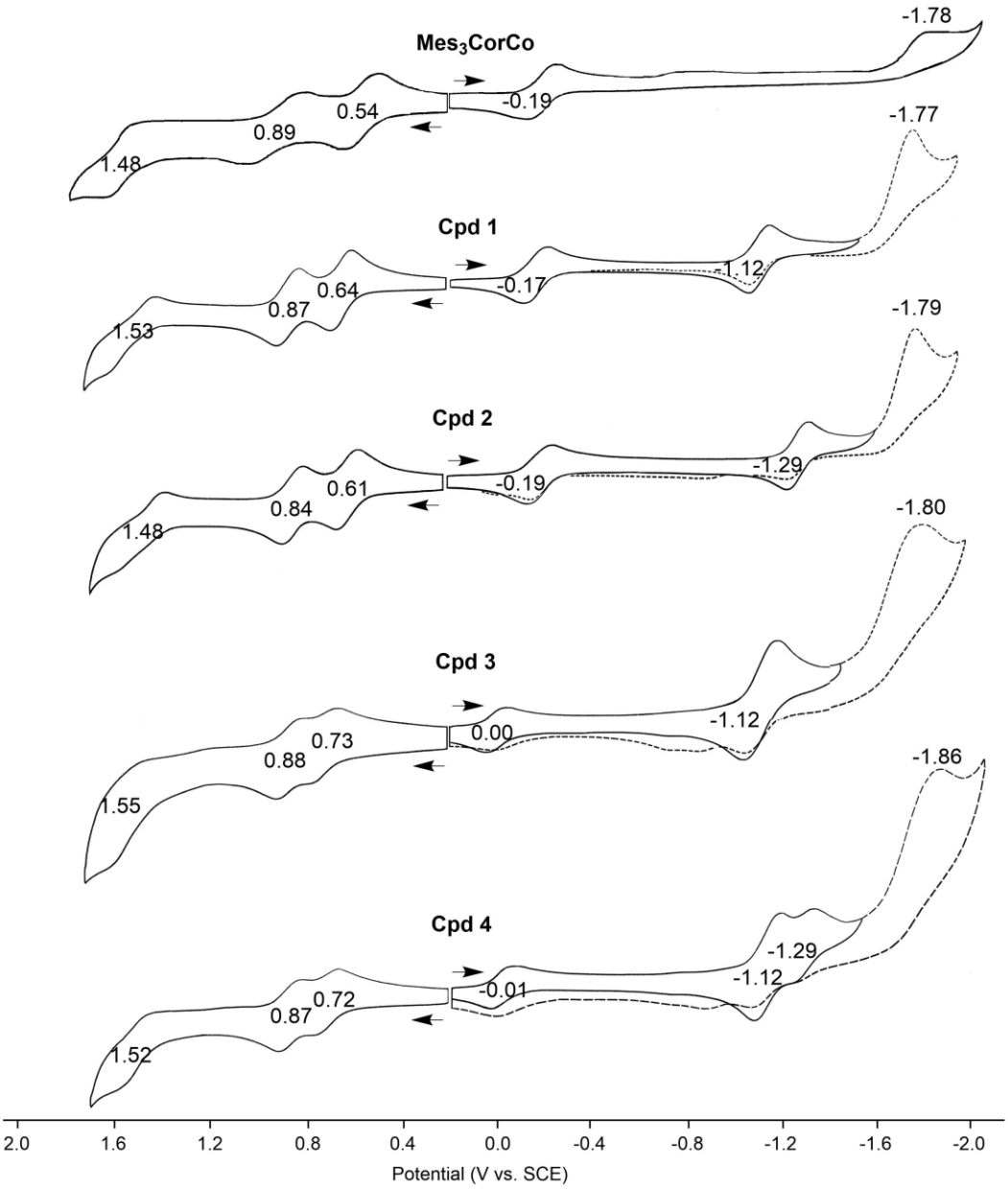

Figure 6-4. Cyclic voltammograms of Mes_3CorCo and **1-4** (~10^{-3} M) in CH_2Cl_2 containing 0.1 M TBAP. Reversible reductions are shown by solid line.

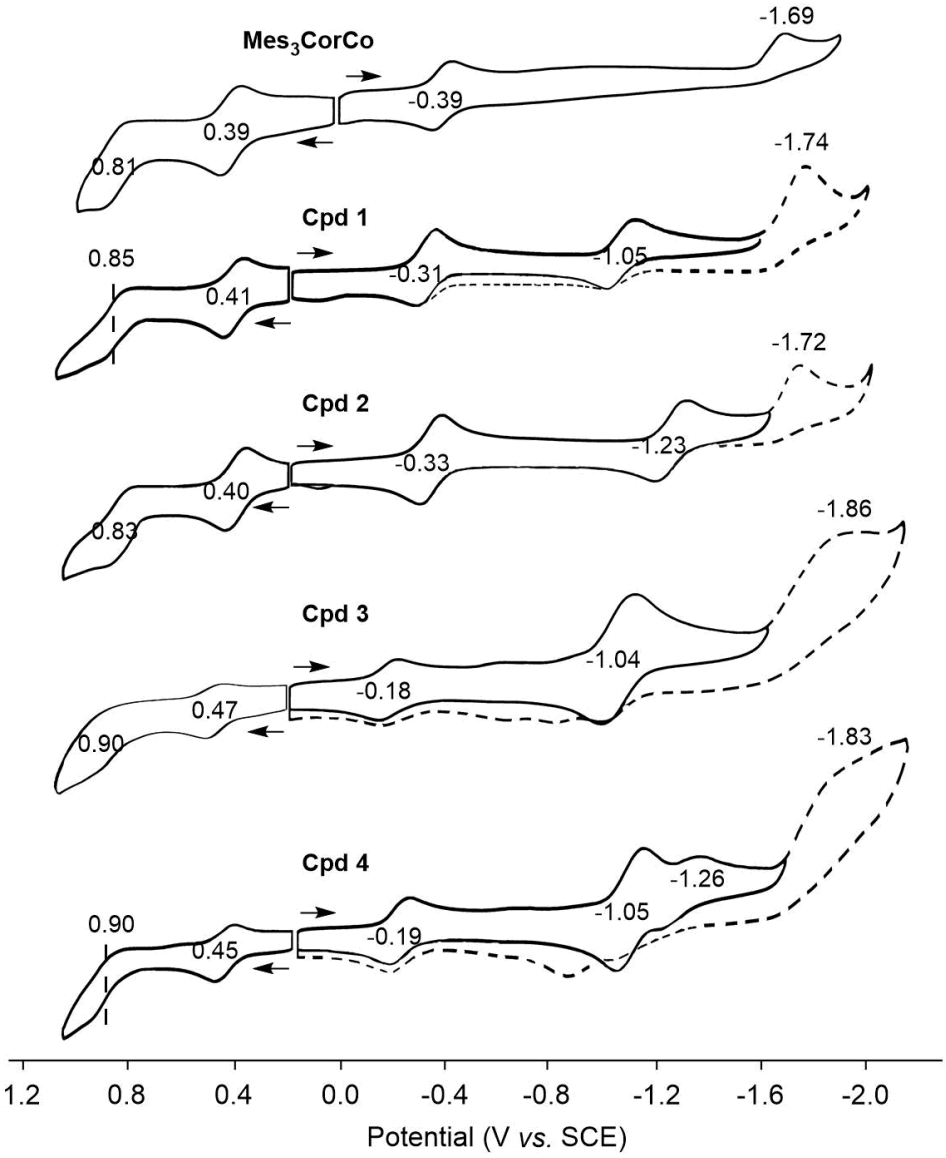

Figure 6-5. Cyclic voltammograms of Mes_3CorCo and **1-4** (~10^{-3} M) in DMSO containing 0.1 M TBAP. Reversible reductions are shown by solid line.

Table 6-2. Half-wave or peak potentials ($E_{1/2}$ or E_p, V vs. SCE) of Mes_3CorCo and **1-4** in CH_2Cl_2 and DMSO, containing 0.1 M TBAP.

Solvent	Compound	Oxidation			Reduction		
		3rd	2nd	1st	1st	NO_2Ph (# of e^-)	3rd
CH_2Cl_2	Mes_3CorCo	1.48	0.89	0.54	-0.19	-	-1.78[a]
	1	1.52	0.85	0.63	-0.17	-1.12 (1)	-1.83[a]
	2	1.52	0.85	0.63	-0.21	-1.29 (1)	-1.88[a]
	3	1.58	0.92	0.73	-0.01	-1.12 (3)	-1.94[a]
	4	1.54	0.87	0.72	0.01	-1.12 (2), -1.29 (1)	-1.90[a]
DMSO	Mes_3CorCo		0.81	0.39	-0.39	-	-1.69[a]
	1		0.85	0.41	-0.31	-1.05 (1)	-1.74[a]
	2		0.83	0.40	-0.33	-1.23 (1)	-1.72[a]
	3		0.90	0.47	-0.18	-1.04 (3)	-1.86[a]
	4		0.90	0.45	-0.19	-1.05 (2), -1.26 (1)	-1.83[a]

[a]Irreversible peak potential at a scan rate of 0.1 V/s.

When changing the solvent from CH_2Cl_2 to DMSO, the first reversible reduction and first reversible oxidation of each corrole are shifted negatively in potential by 120 to 270 mV, but much smaller changes in $E_{1/2}$ are seen for the other redox reactions as seen in Figure 6-5 and Table 6-2. For example, the first reduction of Mes_3CorCo shifts from $E_{1/2}$ = -0.19 V in CH_2Cl_2 to -0.39 V in DMSO while the first oxidation shifts from $E_{1/2}$ = +0.54 V to +0.39 V with the change of solvent. A third reduction cannot be seen in DMSO due to the positive potential limit of the solvent.

The easier oxidation and harder reduction for all the corroles in DMSO as compared to CH_2Cl_2 can be accounted for by a change in the number of axially coordinated ligands either before or after electron transfer. This was investigated in the current study by electrochemically monitoring the shifts of potential in a CH_2Cl_2 solvent as DMSO was progressively added to the solution. This data was then analyzed using equations described in the literature for calculating binding constants of related iron porphyrins,[37] and enabled us to elucidate the number of DMSO molecules bound to the neutral, singly-oxidized and singly-reduced forms of the corrole.

An example of how the cyclic voltammograms changed for Mes_3CorCo in CH_2Cl_2 containing different amounts of added DMSO is given in Figure 6-6. As seen in this figure, the first reduction and first oxidation both shift in a negative direction with increasing additions of DMSO to the solvent, going from -0.19 and +0.54 V in CH_2Cl_2 prior to the addition of DMSO to -0.48 and +0.45 V in a CH_2Cl_2 solution containing 400 eq. of added DMSO.

The loss or gain of bound DMSO molecules during the electron transfer was determined from plots of the measured $E_{1/2}$ values vs. log[DMSO], an example of which is given in Figure 6-7. As seen in the figure, both redox reactions show a linear correlation between the measured $E_{1/2}$ values and log [DMSO] with slopes of -55 and -57 mV for first reduction and first oxidation respectively. These slopes are close to the theoretical Nernstian value of -59 mV, consistent with a dissociation or association of one DMSO axial ligand during the reduction and oxidation, respectively. These electrode reactions are shown in Equations 6-3 and 6-4 where one DMSO molecule is bound to the central metal ion of the neutral corrole.

$$(Ar)_3Cor\bullet Co^{II}(DMSO) + e^- \rightleftharpoons [(Ar)_3CorCo^{II}]^- + DMSO \quad (6\text{-}3)$$

$$(Ar)_3Cor\bullet Co^{II}(DMSO) + DMSO \rightleftharpoons [(Ar)_3Cor\bullet Co^{III}(DMSO)_2]^+ + e^- \quad (6\text{-}4)$$

The binding constant for adding one DMSO molecule to the cobalt center of neutral Mes_3CorCo was calculated as logK = 5.6 using $E_{1/2}$ values for the first reduction of the unligated corrole in CH_2Cl_2 (-0.19 V) and that of the mono-ligated corrole in the CH_2Cl_2/DMSO mixtures (see Figures 6-6 and 6-7). Similar electrochemically monitored titrations with DMSO were also carried out for compounds **1** and **3** in CH_2Cl_2 and plots of $E_{1/2}$ *vs.* log [DMSO] for the first oxidation and the first reduction are given in Figure 6-8. In each case, the slope of the $E_{1/2}$ vs. log[DMSO] plots varied between -55 to -59 mV for each ten-fold increase in the DMSO concentration, thus providing conclusive evidence for the loss of one DMSO axial ligand from the pentacoordinate species during reduction and the addition of one DMSO ligand upon oxidation as shown in Eqs. 3 and 4.

Although the UV-visible spectra for **3** and **4** in Figure 6-1c suggest the presence of an equilibrium between the five- and six-coordinate corroles in neat DMSO, no evidence for a six-coordinate DMSO adduct was seen for these neutral corroles in the electrochemical titration experiments which examined the redox reactions in CH_2Cl_2 containing 10^{-3} to 10^{-5} M DMSO.

As described earlier in the manuscript and also in an earlier publication,[35] the measured values of $E_{1/2}$ will depend upon a number of factors, the most important of which are the number of electron-withdrawing *meso*-nitrophenyl substituents on the corrole macrocycle, and the number of axially bound solvent molecules on the cobalt center before and after electron transfer. The values of $E_{1/2}$ should also systematically vary with the magnitude of the solvent binding constants for a series of structurally related corroles.

Unfortunately, these linear free energy relationships become more complex because of competing effects, which shift $E_{1/2}$ in opposite directions. Specifically, an increase in number of electron-withdrawing NO_2Ph groups leads on one hand to a positive shift of all redox potentials due to electronic effects, and on the other hand to a negative shift of redox potentials with increase in the solvent binding constants as the cobalt center upon going from 0 to 3 NO_2Ph groups on the corrole.

Nonetheless, additional information can be obtained from plots of $E_{1/2}$ vs. the number of NO_2Ph groups on the corroles. Such a correlation is shown in Figure 6-9 where the slope of $E_{1/2}$ vs. the number of NO_2Ph groups is 27 mV for the first oxidation in

DMSO as compared to 70 mV for the first reduction in this solvent and 61-63 mV for the same two redox redox reactions in CH_2Cl_2. The substituent effect of the *meso*-nitrophenyl groups on $E_{1/2}$ for first oxidation in DMSO is diminished as compared to the other electron transfer reactions because the potentials are strongly influenced by the binding of a second DMSO molecule to the electrogenerated corroles in this solvent.

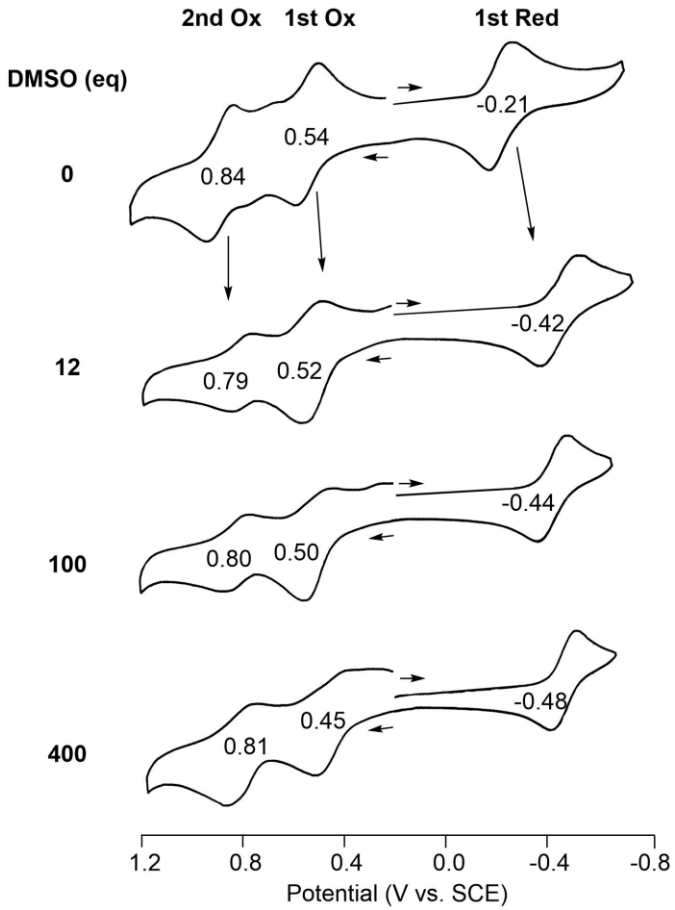

Figure 6-6. Cyclic voltammograms of Mes_3CorCo in CH_2Cl_2 containing 0.1 M TBAP and up to 400 eq. of DMSO.

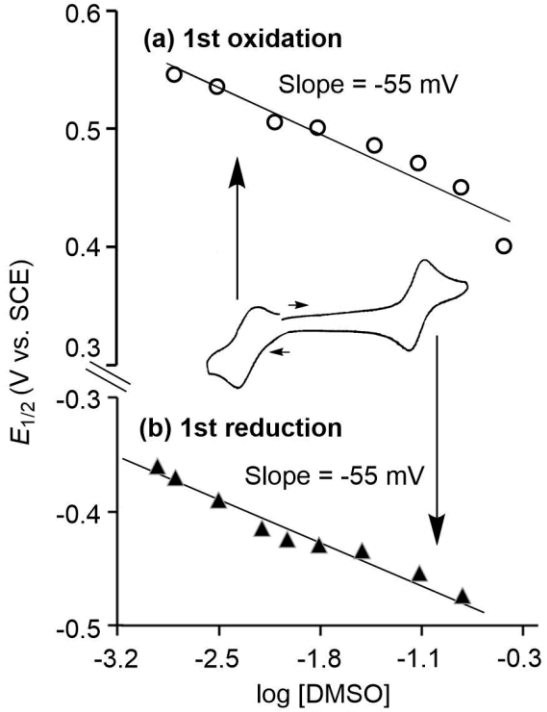

Figure 6-7. Plot of $E_{1/2}$ vs. log[DMSO] for (a) the first oxidation and (b) the first reduction of Mes_3CorCo (7.9×10^{-4} M) in CH_2Cl_2.

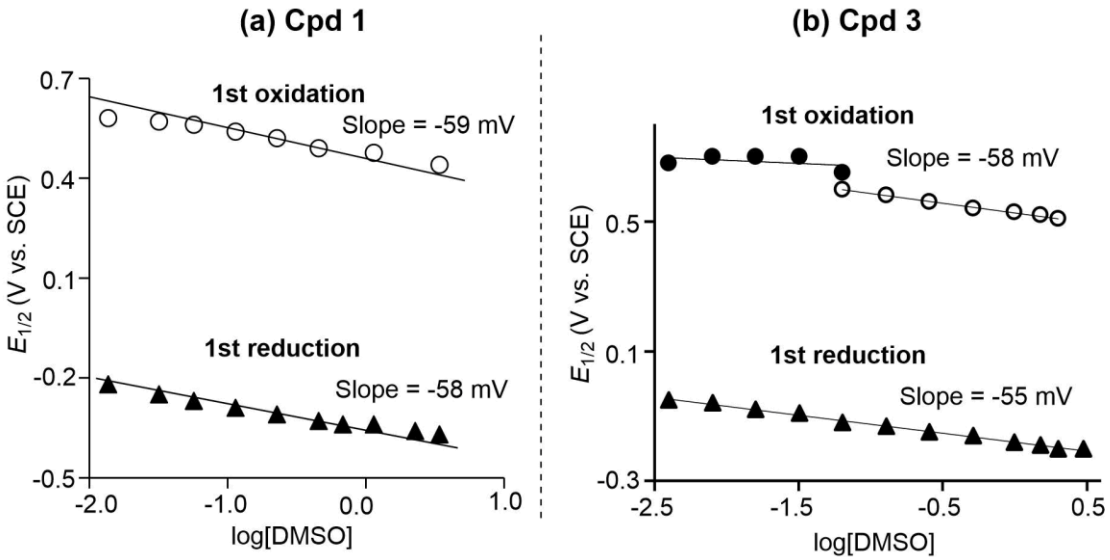

Figure 6-8. Plot of $E_{1/2}$ vs. log[DMSO] for the first oxidation and the first reduction of (a) compound **1** and (b) compound **3** in CH_2Cl_2.

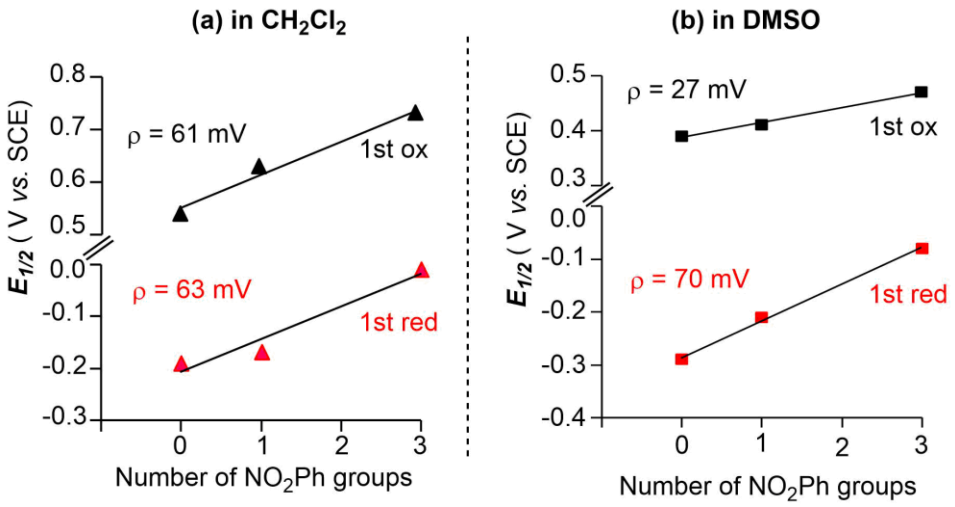

Figure 6-9. Plots of half-wave potentials $E_{1/2}$ for the first oxidation and the first reduction vs. number of *meso*-NO_2Ph groups for Mes_3CorCo, compounds **1** and **3** in (a) CH_2Cl_2 and (b) DMSO containing 0.1 M TBAP. The measured $E_{1/2}$ are given in Table 6-2.

6.4 Spectroscopic Characterization of Oxidation and Reduction Products

In summary, four different forms of the neutral, singly-oxidized and singly-reduced corroles can be definitely identified in CH_2Cl_2 solutions under conditions of the electrochemical experiments, but a fifth form, $[(Ar)_3Cor^{\bullet}Co^{III}(DMSO)]^+$, is also possible in this solvent for the singly-oxidized derivatives **1-4** which possess one DMSO axial ligand in their neutral form when added to solution. Three different DMSO-complexed forms of the corrole in different oxidation states can be identified in DMSO or in CH_2Cl_2/DMSO mixtures and the electrochemical conversion between each of these is shown in Scheme 6-1 where the neutral corrole is represented as $(Ar)_3Cor^{\bullet}Co^{II}$ or $(Ar)_3Cor^{\bullet}Co^{II}(DMSO)$, the singly-reduced corrole as $[(Ar)_3CorCo^{II}]^-$ and the singly-oxidized corrole as $[(Ar)_3Cor^{\bullet}Co^{III}]^+$, $[(Ar)_3Cor^{\bullet}Co^{III}(DMSO)_2]^+$ and possibly $[(Ar)_3Cor^{\bullet}Co^{III}(DMSO)]$.

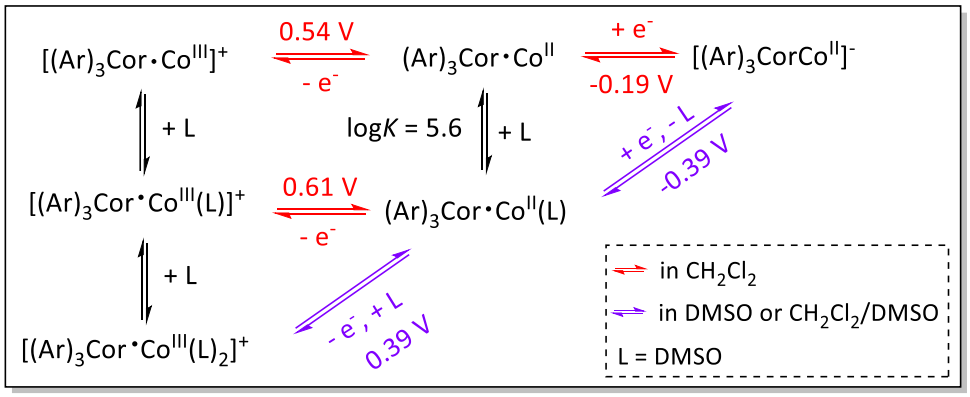

Scheme 6-1. Electron-transfer mechanism for the first reduction and the first oxidation of Mes_3CorCo and **1-4** in CH_2Cl_2, DMSO or CH_2Cl_2/DMSO mixtures containing 0.1 M TBAP. The potentials are given for Mes_3CorCo or compound **1**.

Each of the above singly-oxidized and singly-reduced species in Scheme 6-1 was spectroscopically characterized using thin-layer UV-visible spectroelectrochemistry, examples of which are given in Figures 6-10 and 6-11.

The plots in Figure 6-7 indicate formation of a singly-reduced four-coordinate cobalt corrole $[(Ar)_3CorCo^{II}]^-$ and, as seen in Figure 6-10, almost identical spectra are obtained after the controlled potential addition of one electron in the thin-layer cell, independent of the solvent. For example, the major Soret band of $[(Ar)_3CorCo^{II}]^-$ is located as 419-420 nm for Mes_3CorCo, at 417-421 nm for compound **1** and at 409-412 nm for compound **3**, the small differences between the λ_{max} values being assigned as due to solvent effects, and not to differences in axial coordination.

Each of the singly reduced corroles in Figure 6-10 also has similar Q band absorptions in the two solvents. These bands are well-defined in the case of $[Mes_3CorCo]^-$ and $[\mathbf{1}]^-$ but broad and overlapping in the case of $[\mathbf{3}]^-$. This broadening might be attributed to an aggregation of the singly reduced corrole **3**.

Unlike the reduction, three different DMSO-coordinated forms of the corrole are possible upon oxidation and these are formulated as $[(Ar)_3Cor^{\bullet}Co^{III}(DMSO)_x]^+$ where x = 0, 1 or 2. The corrole with x = 0 is obtained after oxidation of Mes_3CorCo in CH_2Cl_2 while the bis-DMSO adduct (x = 2) is obtained after oxidation of **1-4** in both DMSO and CH_2Cl_2/DMSO mixtures. A singly-oxidized Co(III) corrole with one bound DMSO axial ligand (x = 1) is also probable for compounds **1**-**4** in CH_2Cl_2 since the initial synthesized corroles contain a single DMSO axial ligand when added to solution.

The spectral pattern after oxidation of compound **1** in CH_2Cl_2 is similar to that of $[Mes_3CorCo]^+$ (Figure 6-10a) but sufficient differences exist between the positions of the spectral bands to suggest that $[\mathbf{1}]^+$, with absorption at 387 and 647 nm, contains a single axially coordinated DMSO molecule; while $[Mes_3CorCo]^+$, which lacks a DMSO axial ligand, has bands at 383 and 670 nm.

The spectra of the electrogenerated $[(Ar)_3Cor^{\bullet}Co^{III}(DMSO)_2]^+$ derivatives in DMSO are characterized in Figure 6-10b by a broad Soret band at 409 to 429 nm and a NIR band close to 700 nm. Almost the same spectral pattern was earlier reported for the related bis-pyridine derivative $[(Ar)_3Cor^{\bullet}Co^{III}(py)_2]^+$, which possesses a split Soret band at 409 to 443 nm and a Q band at 691 to 713 nm in CH_2Cl_2, PhCN or pyridine, the exact value depending upon the electrochemical solvent and the number of *meso*-nitrophenyl substituents on the macrocycle.[35]

Overall, quite different absorption spectra are seen for the singly-oxidized corroles in CH_2Cl_2 as compared to DMSO, the most notable difference being an 18-26 nm blue shift of the Soret band in CH_2Cl_2 and a 30-55 nm blue shift in λ_{max} for the less intense absorption in the Q band region of the spectrum.

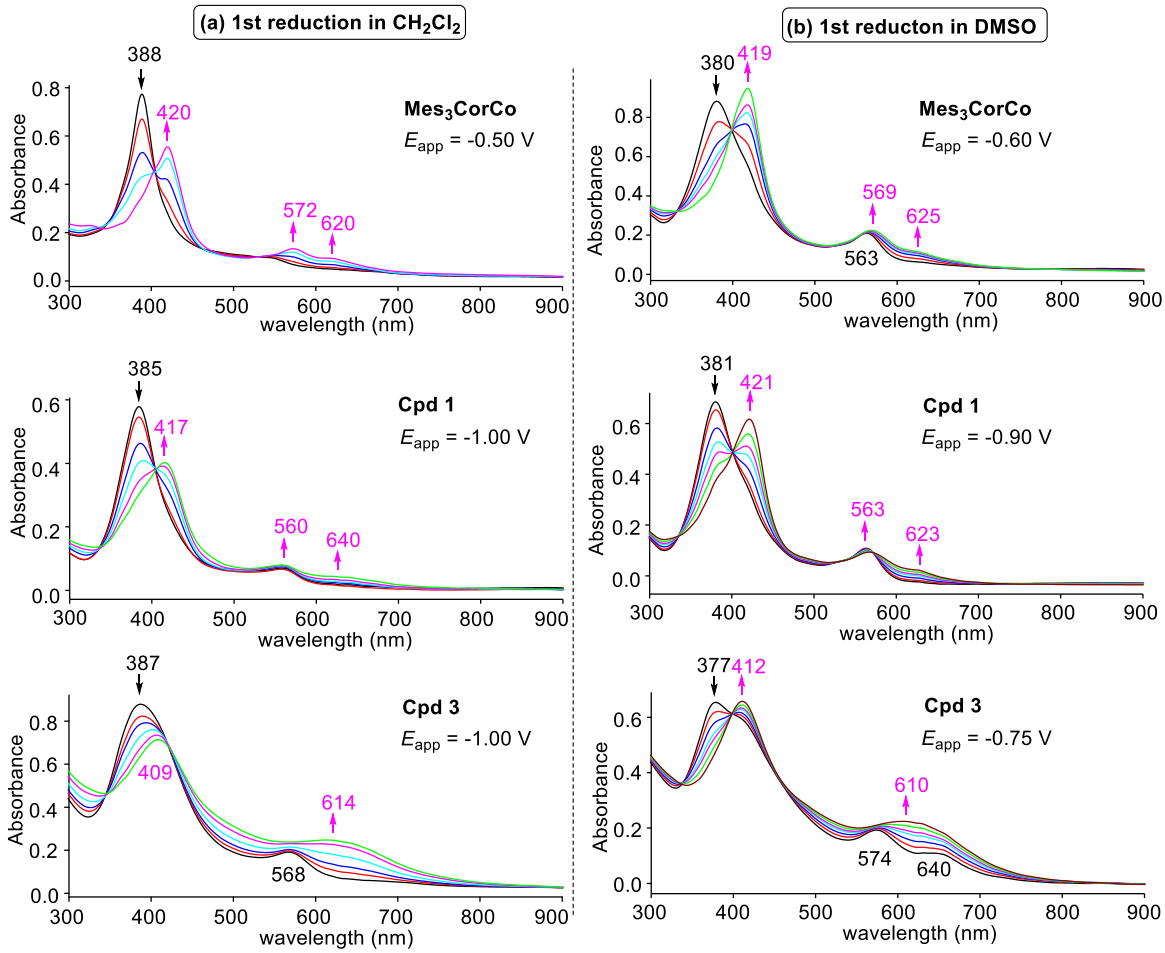

Figure 6-10. UV-visible spectral changes of the first reduction for Mes_3CorCo, compounds **1** and **3** (a) in CH_2Cl_2 and (b) in DMSO containing 0.1 M TBAP.

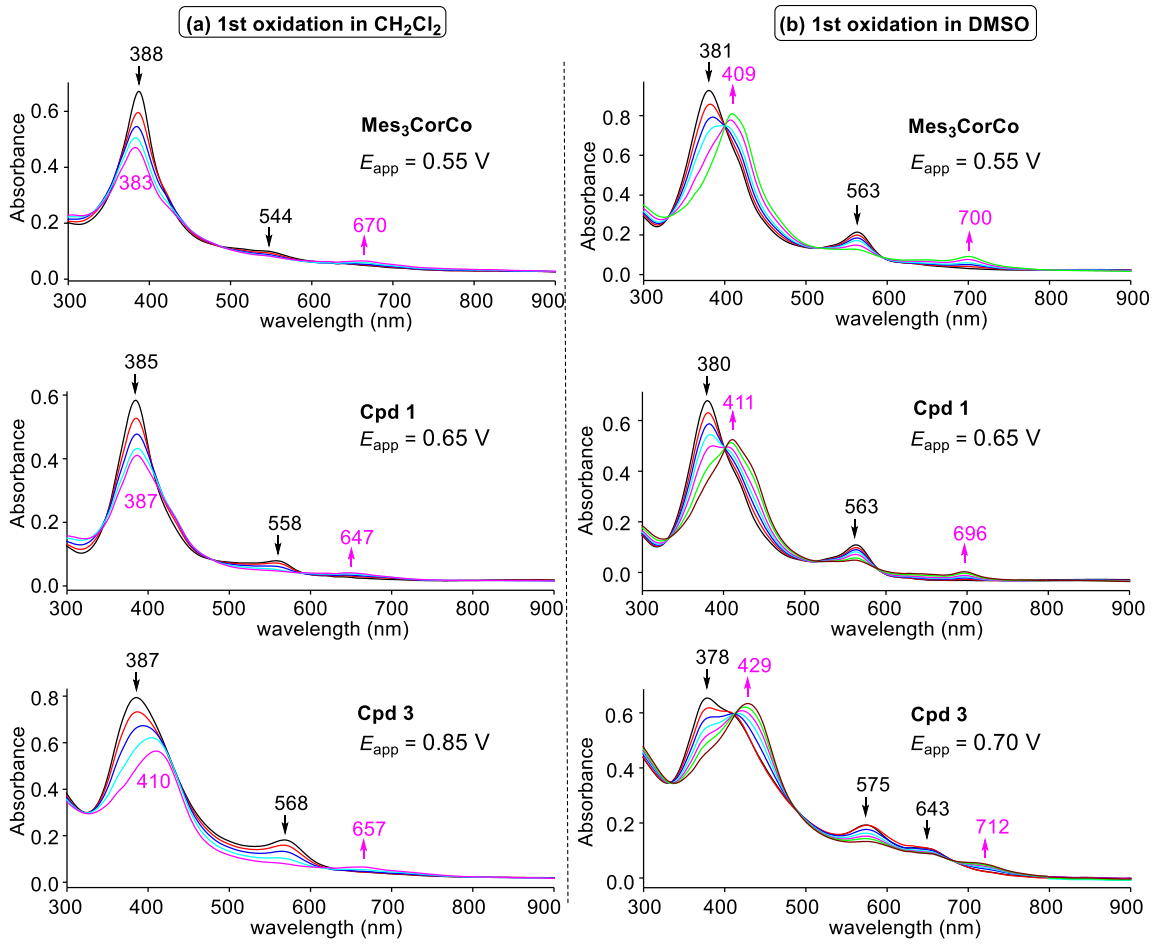

Figure 6-11. UV-visible spectral changes of the first oxidation for Mes_3CorCo, compounds **1** and **3** (a) in CH_2Cl_2 and (b) in DMSO containing 0.1 M TBAP.

5.5 Reactions under a CO Atmosphere

The binding of carbon monoxide was previously examined for a number of four-coordinate corroles in CH_2Cl_2 where a single CO molecule was able to complex to the cobalt center of the neutral compound.[38] We wished to know if mono-CO adducts would also be obtained for the currently investigated corroles containing nitrophenyl substituents, where the redox active species in solution is assigned as $(Ar)_3Cor^{\bullet}Co^{II}(DMSO)$ or $(Ar)_3Cor^{\bullet}Co^{II}$, depending upon the specific *meso*-substituents and the compound concentration in solution. We anticipated that if CO binds to compounds **1-4** in CH_2Cl_2, it would first displace the ligated DMSO, and then dissociate upon a one electron addition or one electron abstraction as reported for other cobalt corroles in this non-complexing solvent.[38] This possibility was examined by first examining the UV-visible spectra of **1-4** under CO and then recording the electrochemistry under these conditions.

The UV-visible spectral data for compounds **1-4** at a concentration of 10^{-3} M in CH_2Cl_2 under a CO atmosphere are shown in Figure 6-12 and Table 6-3. In each case, the shape of the spectrum is comparable to the corresponding spectra for the same corroles under N_2 (Figure 6-1b) and is assigned to a five-coordinate derivative under the electrochemical conditions.

Examples of the resulting cyclic voltammograms under a CO and N_2 atmosphere are given in Figure 6-13 (Mes_3CorCo) and Figure 6-14 (compounds **1-4**). In the case of Mes_3CorCo, the $E_{1/2}$ for the first reduction under CO is shifted negatively by 240 mV as

compared to the same reduction under N_2 while a similar $\Delta E_{1/2}$ of 230 mV is seen for the first oxidation under N_2 or CO but the shift is in a positive direction as seen in the figure.

For each corrole, the difference between $E_{1/2}$ of the first reduction under N_2 and that under CO is identical in magnitude but opposite in sign to what is seen for the first oxidation. This result would be expected when CO were lost from both the singly-reduced and singly-oxidized forms of the corrole as shown in Scheme 6-2. Moreover, the magnitude of the $\Delta E_{1/2}$ would be proportional to the magnitude of the CO binding constant and, as seen in Figure 11, this value decreases systematically with increase in the electron-withdrawing substituents on the *meso*-positions of the macrocycle, namely: Mes_3CorCo (240 mV) > **2** (170 mV) > **1** (150 mV) > **4** (120 mV) > **3** (100 mV) in the case of reduction. A similar trend with almost the same values of $\Delta E_{1/2}$ is seen for oxidation.

In summary, a similar behavior is seen for compounds **1-4** under N_2 or CO and the overall mechanism for reduction is given in Scheme 6-3 where the displacement of DMSO by CO is shown to occur prior to reduction.

Finally, it should be pointed out that the $E_{1/2}$ for the first reduction of Mes_3CorCo under CO (-0.43 V) is about 70 mV less negative than the half wave potential for the first reduction of the same compound in CH_2Cl_2 containing 1.0 M of added DMSO (-0.50 V) and this would suggest one order of magnitude smaller binding constant for CO to the cobalt center of Mes_3CorCo. This latter value was measured as logK = 5.6 from the data in Figures 6-6 and 6-7, suggesting an approximate CO binding constant of logK = 4.6.

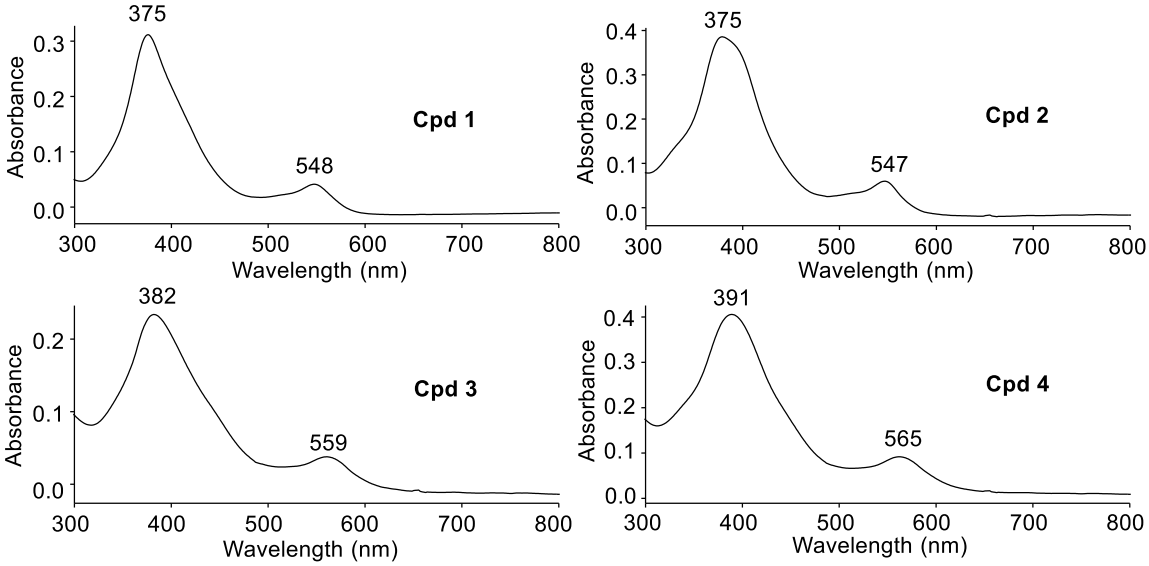

Figure 6-12. UV-visible spectra of compounds **1-4** (~10^{-3} M) in CH_2Cl_2 under CO.

Table 6-3. UV-visible spectra (λ_{max}, $\varepsilon \times 10^{-4}$ M^{-1} cm^{-1}) of compounds **1-4** under CO in CH_2Cl_2 containing 0.1 M TBAP.

cpd	λ_{max}, nm ($\varepsilon \times 10^{-4}$ M^{-1} cm^{-1})	
1	374 (5.1)	547 (1.0)
2	378 (5.2)	547 (1.1)
3	382 (4.6)	558 (1.1)
4	387 (5.1)	559 (1.2)

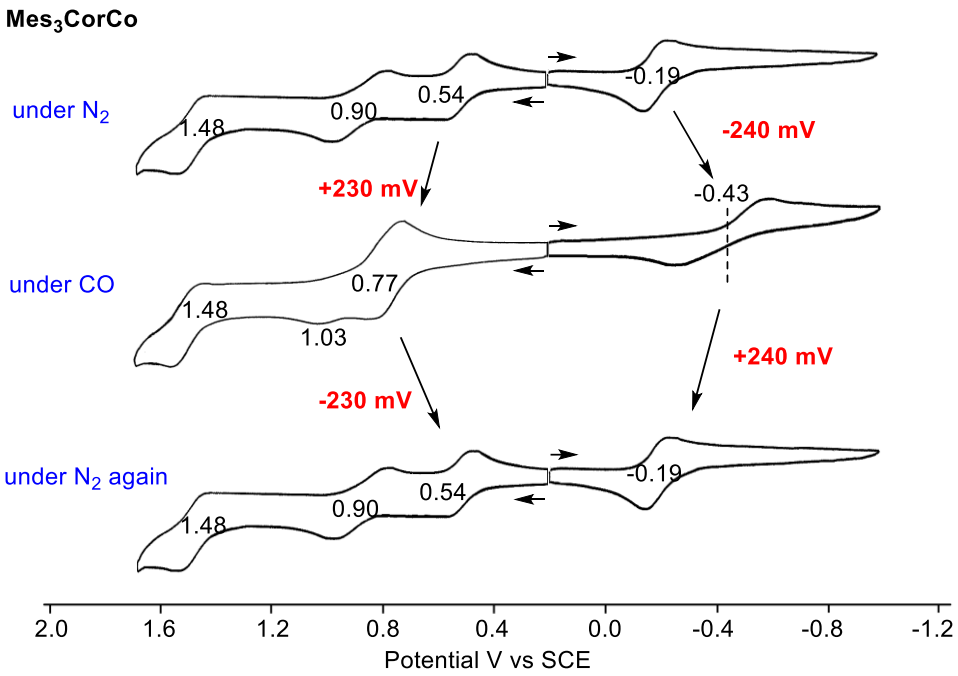

Figure 6-13. Cyclic voltammograms of Mes_3CorCo in CH_2Cl_2 under N_2 and CO.

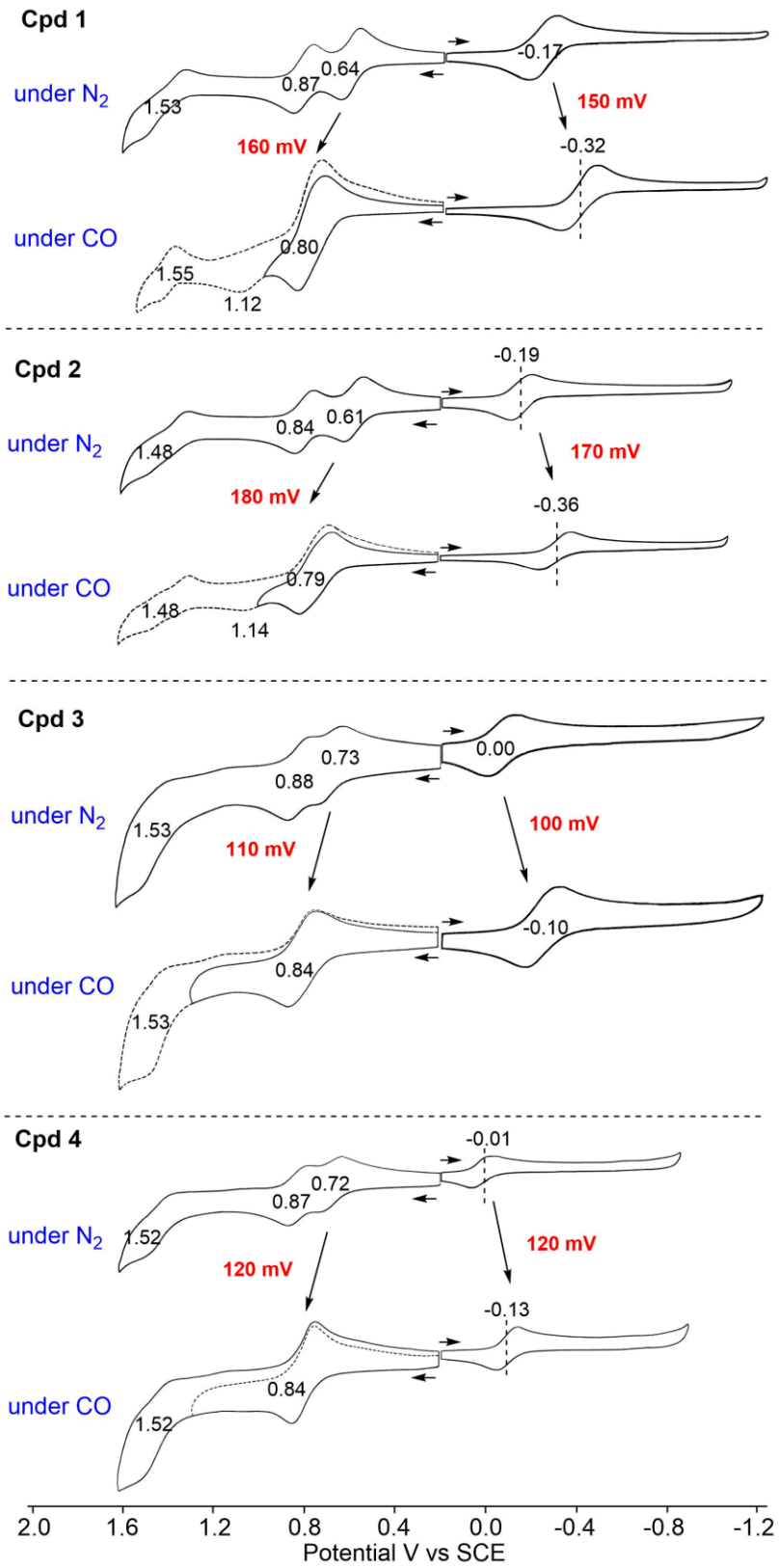

Figure 6-14. Cyclic voltammograms of compounds **1-4** in CH_2Cl_2 under N_2 and CO.

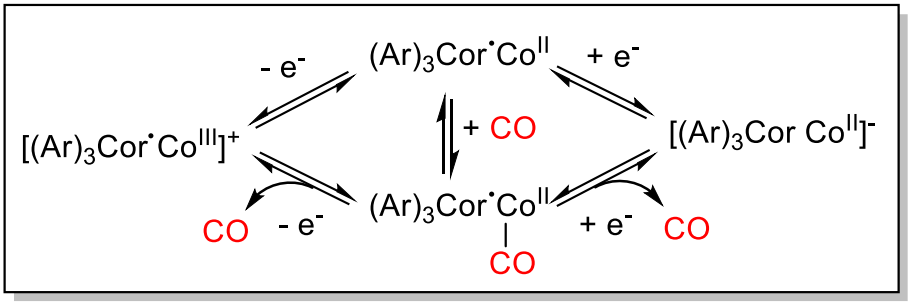

Scheme 6-2. Proposed mechanism for the first reduction and first oxidation of Mes_3CorCo in CH_2Cl_2 under CO.

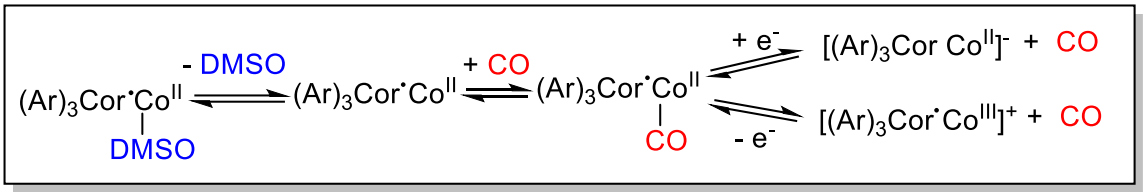

Scheme 6-3. Proposed mechanism for the first reduction and first oxidation of compounds **1-4** in CH_2Cl_2 under CO.

6.6 Conclusions

In summary, we have characterized the electrochemistry and spectroscopic properties of mono-DMSO ligated nitrophenylcorroles in CH_2Cl_2, DMSO and CH_2Cl_2/DMSO mixtures. The first one-electron reduction generates a four-coordinate Co(II) corrole under all solution conditions while the first one-electron oxidation generates a four-, five- or six-coordinate Co(III) corrole π-cation radical as determined by a monitoring of the reactions using UV-visible spectroelectrochemistry. Further studies of the UV-visible spectra after oxidation of different corroles in different solvents and with different axial ligands may be needed but the current spectral data obtained in DMSO, CH_2Cl_2 and pyridine prior to that[35] seems to provide diagnostic information which is sufficient for assigning the coordination number of the singly-oxidized and singly-reduced species.

The binding constant of DMSO to four-coordinate Mes_3CorCo was calculated as logK = 5.6 in CH_2Cl_2, and this value was about one order of magnitude larger than the binding constant for carbon monoxide to the same corrole in this solvent. Carbon monoxide was also show to coordinate to the nitrophenylcorroles **1-4** in CH_2Cl_2, resulting in a shift of potentials towards a harder first reduction and a harder first oxidation, the magnitude of shift depending upon the CO binding constant. Exact values of logK were not determined for this reaction, but the relative values for each examined corrole could be obtained and these decreased with increase in the overall electron-withdrawing properties of *meso*-substituents on the macrocycle.

6.7 References

[1] M. Autret, S. Will, E. V. Caemelbecke, J. Lex, J.-P. Gisselbrecht, M. Gross, E. Vogel, K. M. Kadish, Synthesis and Electrochemistry of Iron(III) Corroles Containing a Nitrosyl Axial Ligand. Spectral Characterization of $[(OEC)Fe^{III}(NO)]_n$ where n = 0, 1, 2, or -1 and OEC is the Trianion of 2,3,7,8,12,13,17,18-Octaethylcorrole, *J. Am. Chem. Soc.* **1994**, *116*, 9141-9149.

[2] E. Vogel, S. Will, A. S. Tilling, L. Neumann, J. Lex, E. Bill, A. X. Trautwein, K. Wieghardt, Metallocorroles with Formally Tetravalent Iron, *Angew. Chem.* **1994**, *106*, 771-775

[3] V. A. Adamian, F. D'Souza, S. Licoccia, M. L. Di Vona, E. Tassoni, R. Paolesse, T. Boschi, K. M. Kadish, Synthesis, Characterization, and Electrochemical Behavior of (5,10,15-Tri-X-phenyl-2,3,7,8,12,13,17,18-octamethylcorrolato)cobalt(III) Triphenylphosphine Complexes, Where X = p-OCH_3, *p*-CH_3, *p*-Cl, *m*-Cl, *o*-Cl, *m*-F, or *o*-F, *Inorg. Chem.* **1995**, *34*, 532-540.

[4] S. Will, J. Lex, E. Vogel, V. A. Adamian, E. Van Caemelbecke, K. M. Kadish, Synthesis, Characterization, and Electrochemistry of σ-Bonded Cobalt Corroles in High Oxidation States, *Inorg. Chem.* **1996**, *35*, 5577-5583.

[5] E. Van Caemelbecke, S. Will, M. Autret, V. A. Adamian, J. Lex, J.-P. Gisselbrecht, M. Gross, E. Vogel, K. M. Kadish, Electrochemical and Spectral Characterization of Iron Corroles in High and Low Oxidation States: First Structural Characterization of an Iron(IV) Tetrapyrrole π Cation Radical, *Inorg. Chem.* **1996**, *35*, 184-192.

[6] S. Cai, F. A. Walker, S. Licoccia, NMR and EPR Investigations of Iron Corrolates: Iron(III) Corrolate p Cation Radicals or Iron(IV) Corrolates?, *Inorg. Chem.* **2000**, *39*, 3466-3478.

[7] E. Steene, T. Wondimagegn, A. Ghosh, Electrochemical and Electronic Absorption Spectroscopic Studies of Substituent Effects in Iron(IV) and Manganese(IV) Corroles. Do the Compounds Feature High-Valent Metal Centers or Noninnocent

Corrole Ligands? Implications for Peroxidase Compound I and II Intermediates, *J. Phys. Chem. B* **2001**, *105*, 11406-11413.

[8] K. M. Kadish, Z. Ou, J. Shao, C. P. Gros, J.-M. Barbe, F. Jerome, F. Bolze, F. Burdet, R. Guilard, Alkyl and Aryl Substituted Corroles. 3. Reactions of Cofacial Cobalt Biscorroles and Porphyrin-Corroles with Pyridine and Carbon Monoxide, *Inorg. Chem.* **2002**, *41*, 3990-4005.

[9] R. Guilard, J.-M. Barbe, C. Stern, K. M. Kadish, in *The Porphyrin Handbook, Vol. 18* (Eds.: K. M. Kadish, K. M. Smith, R. Guilard), World Scientific Publishing Co. Pte. Ltd., Singapore, **2003**, pp. 303-349.

[10] K. M. Kadish, J. Shao, Z. Ou, C. P. Gros, F. Bolze, J.-M. Barbe, R. Guilard, Alkyl- and Aryl-Substituted Corroles. 4. Solvent Effects on the Electrochemical and Spectral Properties of Cobalt Corroles, *Inorg. Chem.* **2003**, *42*, 4062-4070.

[11] C. Brueckner, R. P. Brinas, J. A. Krause-Bauer, X-ray Structure and Variable Temperature NMR Spectra of [meso-Triarylcorrolato]copper(III), *Inorg. Chem.* **2003**, *42*, 4495-4497.

[12] I. Luobeznova, L. Simkhovich, I. Goldberg, Z. Gross, Electronic Structures and Reactivities of Corrole-Copper Complexes, *Eur. J. Inorg. Chem.* **2004**, *2004*, 1724-1732.

[13] Z. Ou, J. Shao, H. Zhao, K. Ohkubo, I. H. Wasbotten, S. Fukuzumi, A. Ghosh, K. M. Kadish, Spectroelectrochemical and ESR Studies of Highly Substituted Copper Corroles, *J. Porphyrins Phthalocyanines* **2004**, *8*, 1236-1247.

[14] R. Guilard, F. Burdet, J.-M. Barbe, C. P. Gros, E. Espinosa, J. Shao, Z. Ou, R. Zhan, K. M. Kadish, Heterobimetallic Complexes of Cobalt(IV) Porphyrin-Corrole Dyads. Synthesis, Physicochemical Properties, and X-ray Structural Characterization, *Inorg. Chem.* **2005**, *44*, 3972-3983.

[15] K. M. Kadish, L. Fremond, Z. Ou, J. Shao, C. Shi, F. C. Anson, F. Burdet, C. P. Gros, J.-M. Barbe, R. Guilard, Cobalt(III) Corroles as Electrocatalysts for the Reduction of Dioxygen: Reactivity of a Monocorrole, Biscorroles, and Porphyrin-Corrole Dyads, *J. Am. Chem. Soc.* **2005**, *127*, 5625-5631.

[16] K. M. Kadish, J. Shao, Z. Ou, L. Fremond, R. Zhan, F. Burdet, J.-M. Barbe, C. P. Gros, R. Guilard, Electrochemistry, Spectroelectrochemistry, Chloride Binding, and O_2 Catalytic Reactions of Free-Base Porphyrin-Cobalt Corrole Dyads, *Inorg. Chem.* **2005**, *44*, 6744-6754.

[17] K. M. Kadish, J. Shao, Z. Ou, R. Zhan, F. Burdet, J.-M. Barbe, C. P. Gros, R. Guilard, Electrochemistry and Spectroelectrochemistry of Heterobimetallic Porphyrin-corrole Dyads. Influence of the Spacer, Metal Ion, and Oxidation State on the Pyridine Binding Ability, *Inorg. Chem.* **2005**, *44*, 9023-9038.

[18] K. M. Kadish, L. Fremond, F. Burdet, J.-M. Barbe, C. P. Gros, R. Guilard, Cobalt(IV) Corroles as Catalysts for the Electroreduction of O_2: Reactions of Heterobimetallic Dyads Containing a Face-to-face Linked Fe(III) or Mn(III) Porphyrin, *J. Inorg. Biochem.* **2006**, *100*, 858-868.

[19] K. M. Kadish, J. Shen, L. Fremond, P. Chen, M. El Ojaimi, M. Chkounda, C. P. Gros, J.-M. Barbe, K. Ohkubo, S. Fukuzumi, R. Guilard, Clarification of the Oxidation State of Cobalt Corroles in Heterogeneous and Homogeneous Catalytic Reduction of Dioxygen, *Inorg. Chem.* **2008**, *47*, 6726-6737.

[20] J. H. Palmer, A. Mahammed, K. M. Lancaster, Z. Gross, H. B. Gray, Structures and Reactivity Patterns of Group 9 Metallocorroles, *Inorg. Chem.* **2009**, *48*, 9308-9315.

[21] D. Astruc, Ferrocenyl Dendrimers: Multi-electron Redox Reagents and Their Applications, *New J. Chem.* **2011**, *35*, 764-772.

[22] Z. Ou, A. Lu, D. Meng, S. Huang, Y. Fang, G. Lu, K. M. Kadish, Molecular Oxygen Reduction Electrocatalyzed by meso-Substituted Cobalt Corroles Coated on Edge-Plane Pyrolytic Graphite Electrodes in Acidic Media, *Inorg. Chem.* **2012**, *51*, 8890-8896.

[23] A. Mahammed, M. Botoshansky, Z. Gross, Chlorinated Corroles, *Dalton Trans.* **2012**, *41*, 10938-10940.

[24] B. Mondal, K. Sengupta, A. Rana, A. Mahammed, M. Botoshansky, S. G. Dey, Z. Gross, A. Dey, Cobalt Corrole Catalyst for Efficient Hydrogen Evolution Reaction from

H_2O under Ambient Conditions: Reactivity, Spectroscopy, and Density Functional Theory Calculations, *Inorg. Chem.* **2013**, *52*, 3381-3387.

[25] B. Li, Z. Ou, D. Meng, J. Tang, Y. Fang, R. Liu, K. M. Kadish, Cobalt Triarylcorroles Containing One, Two or Three Nitro Groups. Effect of NO_2 Substitution on Electrochemical Properties and Catalytic Activity for Reduction of Molecular Oxygen in Acid Media, *J. Inorg. Biochem.* **2014**, *136*, 130-139.

[26] J. Tang, Z. Ou, L. Ye, M. Yuan, Y. Fang, Z. Xue, K. M. Kadish, Meso-dichlorophenyl Substituted Co(III) Corrole: A Selective Electrocatalyst for the Two-electron Reduction of Dioxygen in Acid Media, X-ray Crystal Structure Analysis and Electrochemistry, *J. Porphyrins Phthalocyanines* **2014**, *18*, 891-898.

[27] J. Sun, Z. Ou, R. Guo, Y. Fang, M. Chen, Y. Song, K. M. Kadish, Synthesis and Electrochemistry of Cobalt Tetrabutanotriarylcorroles. Highly Selective Electrocatalysts for Two-Electron Reduction of Dioxygen in Acidic and Basic Media, *J. Porphyrins Phthalocyanines* **2016**, *20*, 456-464.

[28] Y. Wang, Z. Ou, Y. Fang, R. Guo, J. Tang, Y. Song, K. M. Kadish, Synthesis and Electrochemistry of A_2B Type Mono- and Bis-cobalt Triarylcorroles and Their Electrocatalytic Properties for Reduction of Dioxygen in Acid Media, *J. Porphyrins Phthalocyanines* **2016**, *20*, 1284-1295.

[29] Y. Fang, Z. Ou, K. M. Kadish, Electrochemistry of Corroles in Nonaqueous Media, *Chem. Rev.* **2017**, *117*, 3377-3419.

[30] A. Ghosh, Electronic Structure of Corrole Derivatives: Insights from Molecular Structures, Spectroscopy, Electrochemistry, and Quantum Chemical Calculations, *Chem. Rev.* **2017**, *117*, 3798-3881.

[31] S. Ganguly, D. Renz, L. J. Giles, K. J. Gagnon, L. J. McCormick, J. Conradie, R. Sarangi, A. Ghosh, Cobalt- and Rhodium-Corrole-Triphenylphosphine Complexes Revisited: The Question of a Noninnocent Corrole, *Inorg. Chem.* **2017**, *56*, 14788-14800.

[32] S. Ganguly, J. Conradie, J. Bendix, K. J. Gagnon, L. J. McCormick, A. Ghosh, Electronic Structure of Cobalt-Corrole-Pyridine Complexes: Noninnocent Five-Coordinate Co(II) Corrole-Radical States, *J. Phys. Chem. A* **2017**, *121*, 9589-9598.

[33] K. M. Kadish, The electrochemistry of metalloporphyrins in nonaqueous media, *Prog. Inorg. Chem.* **1986**, *34*, 435-605.

[34] K. M. Kadish, B. C. Han, A. Endo, Electrochemistry of Five- and Six-Coordinate σ-Bonded Cobalt Porphyrins. Reactions of (TPP)Co(C_2H_5)(py) and (TPP)Co(R) where TPP is the Dianion of Tetraphenylporphyrin and R = CH_3, C_2H_5, or CH_2Cl, *Inorg. Chem.* **1991**, *30*, 4502-4506.

[35] X. Jiang, M. L. Naitana, N. Desbois, V. Quesneau, S. Brandes, Y. Rousselin, W. Shan, W. R. Osterloh, V. Blondeau-Patissier, C. P. Gros, K. M. Kadish, Electrochemistry of Bis(pyridine)cobalt (Nitrophenyl)corroles in Nonaqueous Media, *Inorg. Chem.* **2018**, *57*, 1226-1241.

[36] X. Jiang, M. L. Naitana, N. Desbois, V. Quesneau, S. Brandes, Y. Rousselin, W. Shan, W. R. Osterloh, V. Blondeau-Patissier, C. P. Gros, K. M. Kadish, Electrochemistry of Bis(pyridine)cobalt (Nitrophenyl)corroles in Nonaqueous Media, *Inorg Chem* **2018**.

[37] K. M. Kadish, in *Iron Porphyrin, Part 2* (Eds.: A. B. P. Lever, H. B. Gray), Addison Wesley, Reading, Massachusetts, **1983**, pp. 161-249.

[38] R. Guilard, C. P. Gros, F. Bolze, F. Jerome, Z. Ou, J. Shao, J. Fischer, R. Weiss, K. M. Kadish, Alkyl and Aryl Substituted Corroles. 1. Synthesis and Characterization of Free Base and Cobalt Containing Derivatives. X-ray Structure of (Me4Ph5Cor)Co(py)2, *Inorg. Chem.* **2001**, *40*, 4845-4855.

7

Cobalt Corroles with Bis-Ammonia or Mono-DMSO Axial Ligands. Electrochemical, Spectroscopic Characterizations and Ligand Binding Properties

7.1 Introduction

Metallocorroles are now an often-studied group of macrocycles because of their unique spectral and electrochemical properties and their potential applications as catalysts for a variety of reactions. Although corroles show many similarities with porphyrins, their distinctive structural, spectroscopic and photophysical properties as well as their specific coordination chemistry and particular chemical reactivity places these macrocycles in a distinctive position among members of the porphyrinoid family.[1-7] Particularly, cobalt corroles exhibit a rich redox chemistry which depends on both the type of macrocycle and axial coordination at the cobalt metal center.[2] We have shown that solvents such as DMSO or pyridine as well as diatomic molecules such as CO will strongly coordinate to the cobalt center of the neutral corrole, leading not only to changes in electron density at the metal ion, but also in some cases to a change of metal and ligand oxidation state.[8] Electron-withdrawing groups anchored at the periphery of the macrocyclic core will also change electron density at the cobalt central metal ion, thus directly affecting the magnitude and degree of axial coordination.[9]

Recently, we reported the synthesis and electrochemical characterization of nitrophenyl-substituted cobalt corroles axially ligated DMSO or pyridine molecules in their air stable form.[8, 9] The current manuscript is an expansion of these studies and characterizes in greater detail the properties of cobalt corroles with a single DMSO axial ligand or two NH_3 axial ligands in their air stable form. A schematic representation of the investigated compounds is given in Chart 7-1. It is worthy to note that the hexa-

coordinated bis-ammonia cobalt corrole could easily give access to the tetra-coordinated cobalt corrole *e.g.* without any axial ligand (Scheme 7-1). The removal of the two coordinated ammonia molecules can be done under vacuum at 80 °C or by dissolving the complex in dichloromethane and bubbling N_2 gas. Since now many years, we have been interested in the selective CO binding for detection of CO traces at the sub-ppm level in the atmosphere by using SAW sensors functionalized by cobalt corroles. This new pathway allows us the smooth and easy access to the active species (*e.g.* the tetra-coordinated form of various A_3- and A_2B-cobalt corroles) for further CO binding.

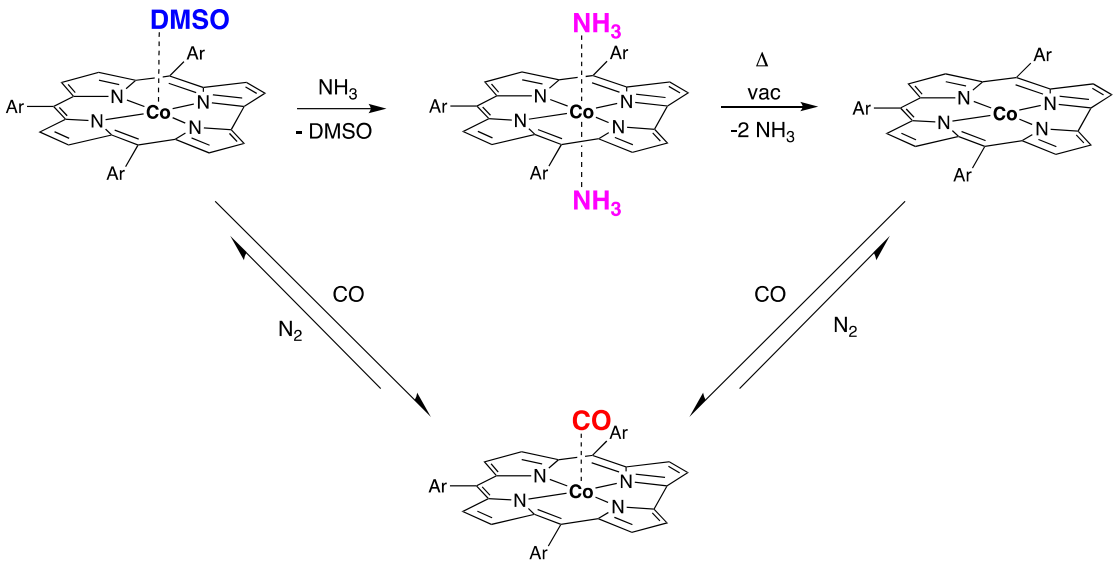

Scheme 7-1. From pentacoordinate to hexacoordinate cobalt corroles; easy access to the tetra-coordinated species.

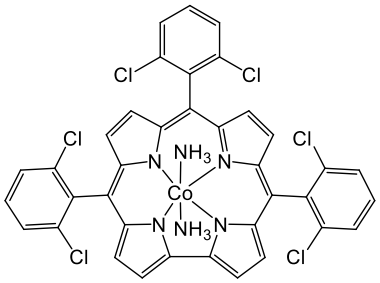

$(Cl_2Ph)_3CorCo(NH_3)_2$ **1NH$_3$**

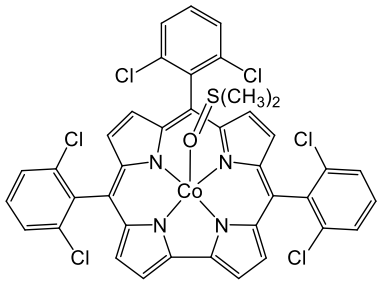

$(Cl_2Ph)_3CorCo(DMSO)$ **1DMSO**

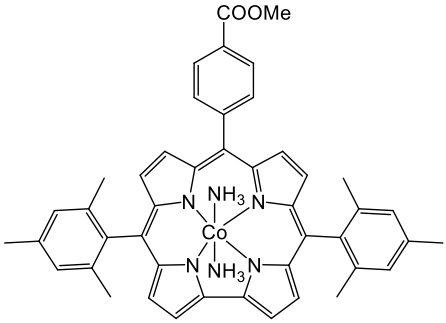

$(COOMePh)Mes_2CorCo(NH_3)_2$ **2NH$_3$**

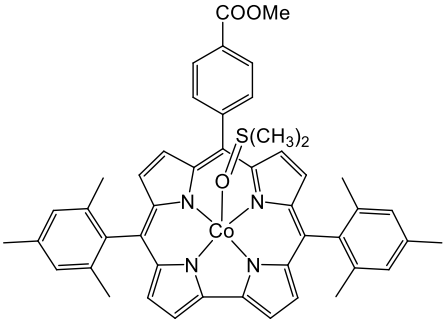

$(COOMePh)Mes_2CorCo(DMSO)$ **2DMSO**

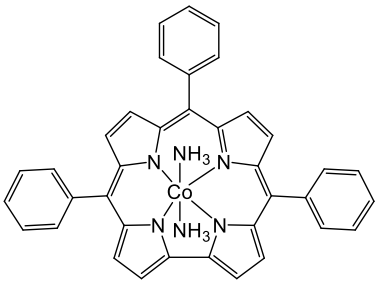

$(Ph)_3CorCo(NH_3)_2$ **3NH$_3$**

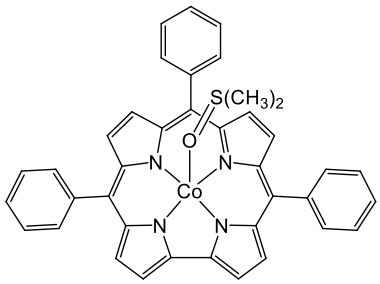

$(Ph)_3CorCo(DMSO)$ **3DMSO**

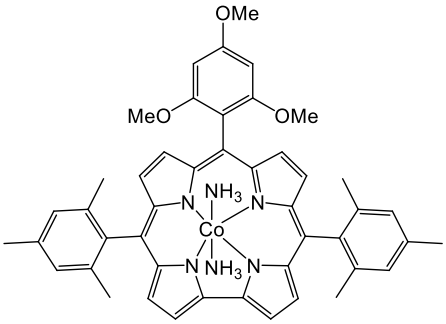

$((OMe)_3Ph)Mes_2CorCo(NH_3)_2$ **4NH$_3$**

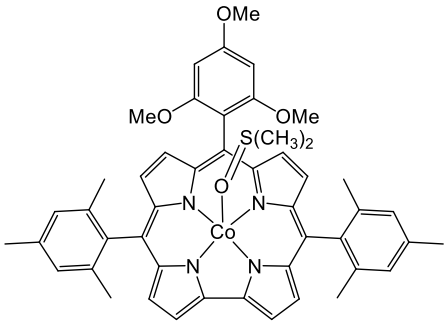

$((OMe)_3Ph)Mes_2CorCo(DMSO)$ **4DMSO**

Chart 7-1. Structures of the investigated bis-ammonia and mono-DMSO *meso*-aryl cobalt corroles.

7.2 Synthesis of Cobalt Corrole Complexes

The eight cobalt corroles **1DMSO-4DMSO** and **1NH$_3$-4NH$_3$** were prepared according to the synthetic procedure shown in Scheme 7-2. The A$_3$- and A$_2$B- free-base corroles **1H-4H** were synthesized according to published procedures described by Gryko and co-workers,[10, 11] and metallated with Co(OAc)$_2$ in DMSO to give the cobalt complexes 1DMSO-4DMSO, each with a single DMSO molecule as axial ligand. These mono-DMSO adducts were then treated with an aqueous ammonia solution to give the bis-ammonia derivatives 1NH$_3$-4NH$_3$ in 79-94% yield.

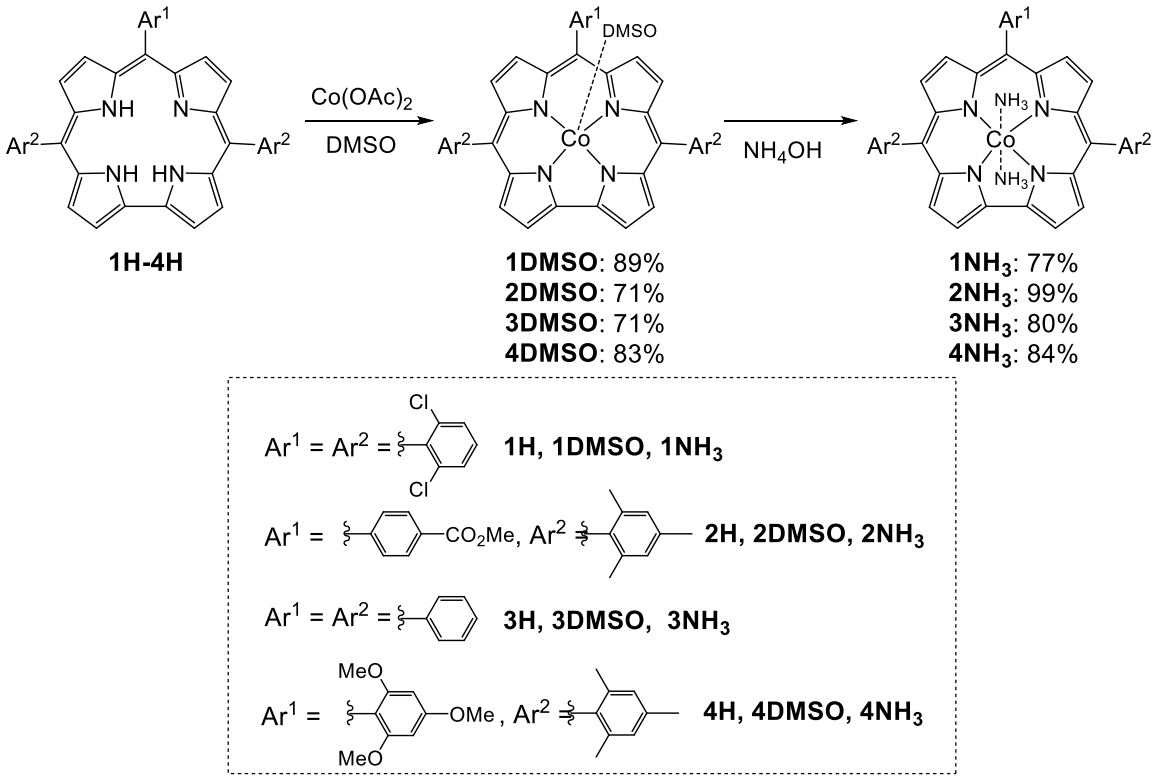

Scheme 7-2. Synthesis of mono-DMSO and bis-NH_3 cobalt corroles.

7.3 UV−Visible Spectroscopic Characterization

The axial coordination of the cobalt corrole can be easily monitored by UV-vis spectroscopy (Figure 7-1). The penta-coordinated cobalt corroles are both characterized by an moderate absorption at 553 and 570 nm in the visible region for **1CO** and **1DMSO**, respectively. **.**

The six coordinate bis-NH_3 cobalt corrole **1-NH_3** is characterized by an intense absorption band at 616 nm and a split Soret band at 438 and 452 nm, showing a strong red-shift in comparison with the tetra-coordinated cobalt corroles, which display a Soret band at 390 nm.

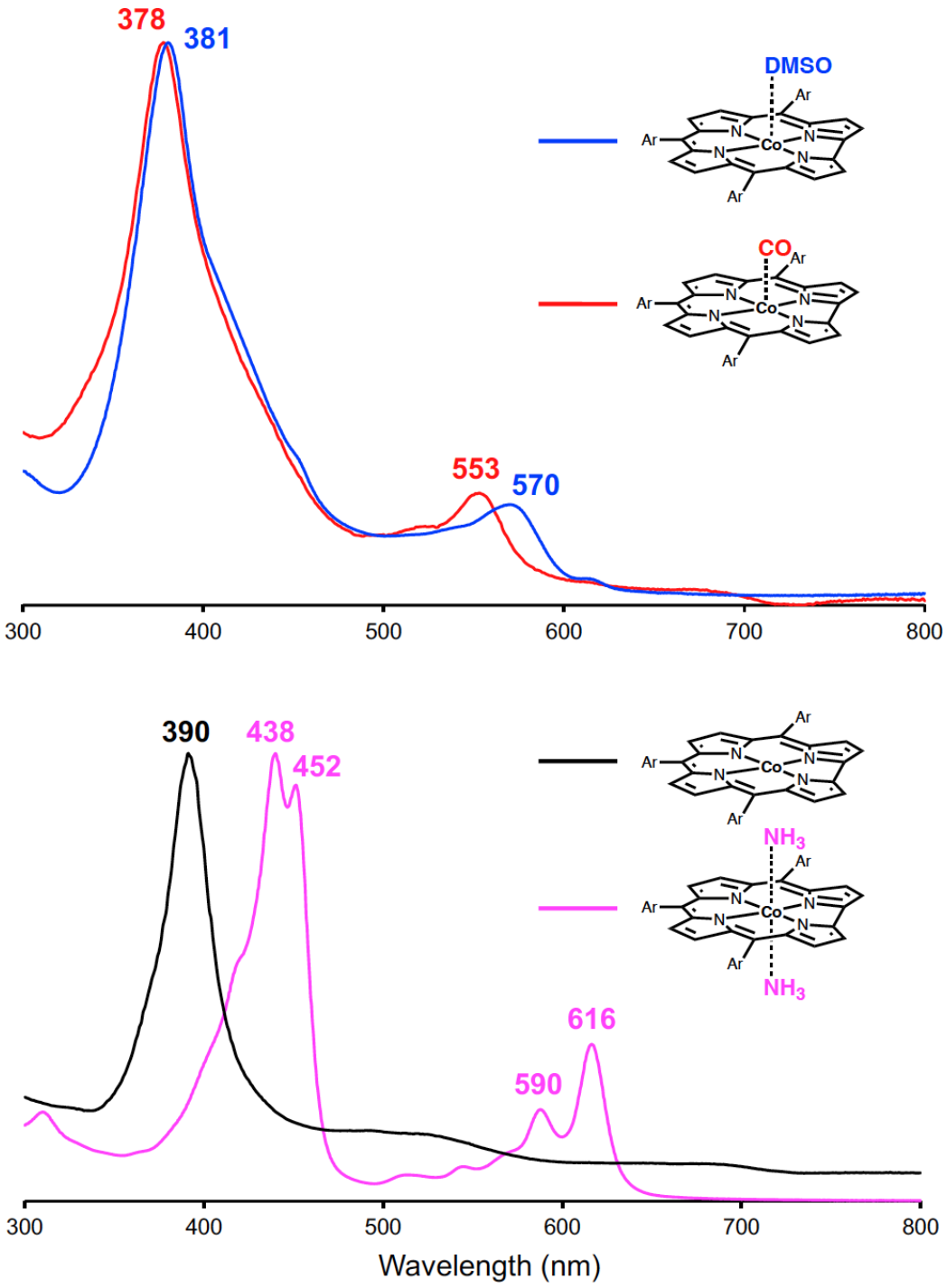

Figure 7-1. UV-visible spectra (in CH_2Cl_2) of cobalt corrole **1** as function of the axial coordination (DMSO, NH_3, CO or nothing).

UV-visible spectra of **1DMSO-4DMSO** were measured at a concentration of 10^{-3} M in both CH_2Cl_2 and DMSO containing 0.1 M TBAP (Figure 7-2). In CH_2Cl_2 the spectra of the four corroles are characterized by a Soret band at 379-387 nm and a single less intense band at 562-566 nm. There is also a shoulder on the Soret band at about 414-417 nm. These spectra are similar to previously reported spectra for a related series of mono-DMSO ligated cobalt nitrophenylcorroles under the same solution conditions.[9]

Similar spectral patterns are seen for **2DMSO, 3DMSO** and **4DMSO** in the two solvents but this is not the case for **1DMSO** as seen in Figure 7-2. The spectrum in CH_2Cl_2 (Figure 7-2a) is assigned to the mono-DMSO adduct while in the DMSO solvent a mixture of the five- and six-coordinated derivatives are proposed to exist, the hexa-coordinate DMSO adduct having bands at 417, 442, 453 and 618 nm as described on the following pages. It should be noted that **1DMSO** is the only cobalt corrole among the currently investigated compounds which possesses electron-withdrawing substituents on the *meso*-phenyl rings and this seems to facilitate the binding of a second DMSO molecule to the cobalt center of the neutral compound. Stronger pyridine binding constants were also earlier reported for cobalt corroles with electron-withdrawing substituents on the *meso*-phenyl rings.[9]

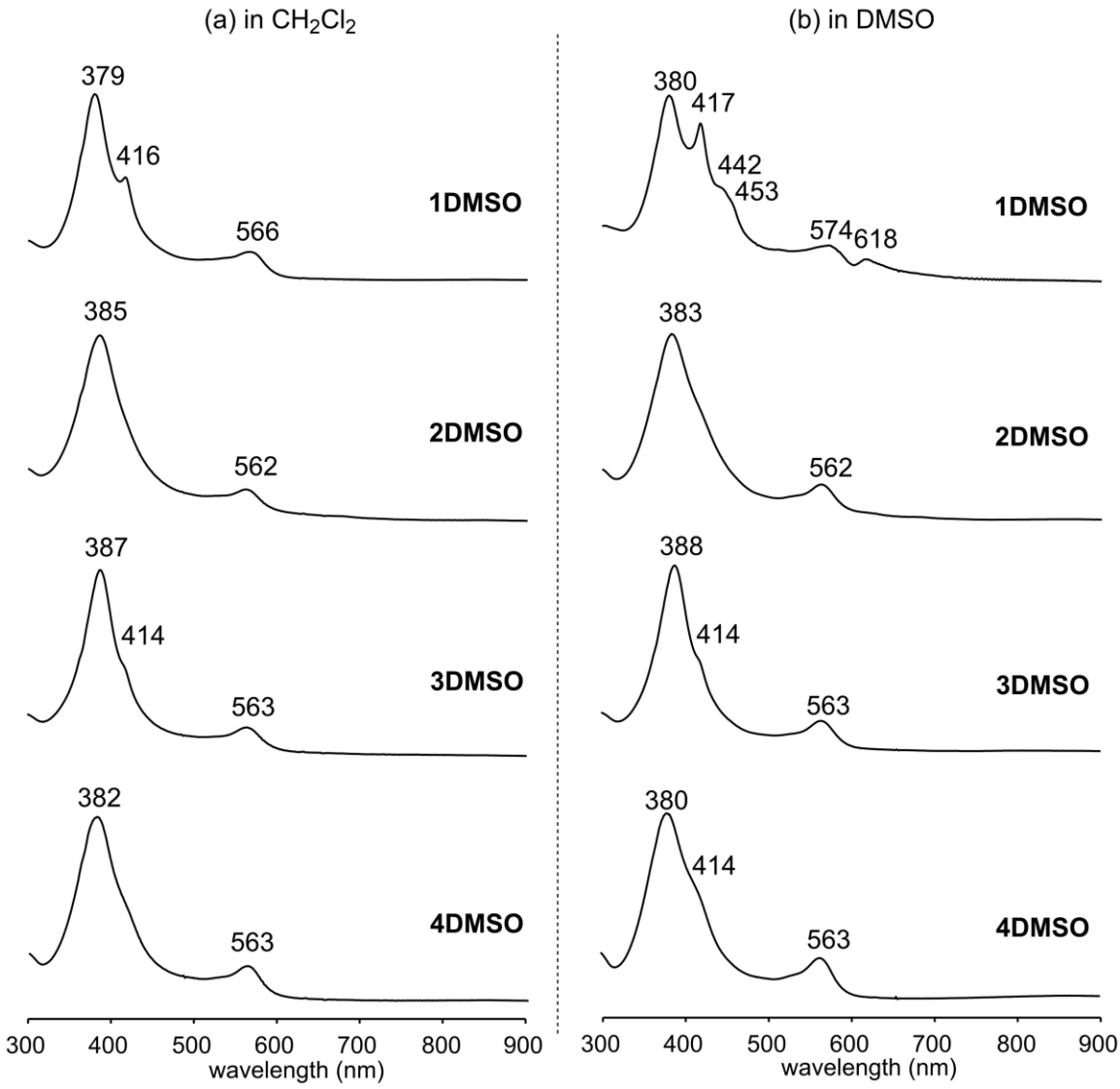

Figure 7-2. UV-visible spectra of **1DMSO**-**4DMSO** at 10^{-3} M concentration in (a) CH_2Cl_2 and (b) DMSO containing 0.1 M TBAP.

UV-visible spectra of the bis-ammonia complexes **1NH$_3$-4NH$_3$** were also measured at a concentration of 1 x 10^{-3} M under two solution conditions, one being CH_2Cl_2 containing 0.1 M TBAP and the other CH_2Cl_2 containing 0.1 M TBAP and 1% (v/v) NH_4OH which produces NH_3 in solution. Examples of the corrole spectra in the two solvents are shown in Figure 7-3 and a summary of the spectral data for **1NH$_3$–4NH$_3$** in CH_2Cl_2 containing 1% NH_4OH is given in Table 7-1.

As seen in Figure 7-3b, the UV-visible spectrum of each bis-NH_3 derivative is characterized by a split Soret band and two or three visible bands, the most intense of which is located at 615-628 nm. The band at 615-629 nm is considered as a marker band for the hexa-coordinated Co(III) corrole and the overall spectral patterns of the **1NH$_3$** to **4NH$_3$** derivatives are similar to spectral patterns earlier reported for structurally related cobalt corroles containing two axially bound pyridine ligands.[9]

The same UV-vis spectrum is obtained for **1NH$_3$** in CH_2Cl_2 with and without 1% NH_4OH, both spectra being consistent with spectra of the initial synthesized bis-NH_3 adduct in toluene (see Experimental). In contrast, different spectra are seen for **2NH$_3$ to 4NH$_3$** corroles in CH_2Cl_2 with and without 1% NH_4OH. The largest variation between the two solution conditions is observed in the Soret region of the spectrum, where bands assigned to a five-coordinate corrole are observed for the synthesized bis-NH_3 derivatives **2, 3** and **4** but not for compound **1.** The fact that identical spectra are obtained for **1NH$_3$** in the CH_2Cl_2 with and without added NH_3 suggests that this corrole has a stronger affinity for NH_3 than the other investigated derivatives and that dissociation of the bound NH_3

axial ligand does not readily occur in CH_2Cl_2. This observation is consistent with the poorest electron density of **1NH$_3$** due to the electron-withdrawing effect of the halogen atoms located at the periphery of the corrole, that is corroborated with magnitude of the pyridine binding constant to the corroles **1DMSO** to **4DMSO**, as described on the following pages.

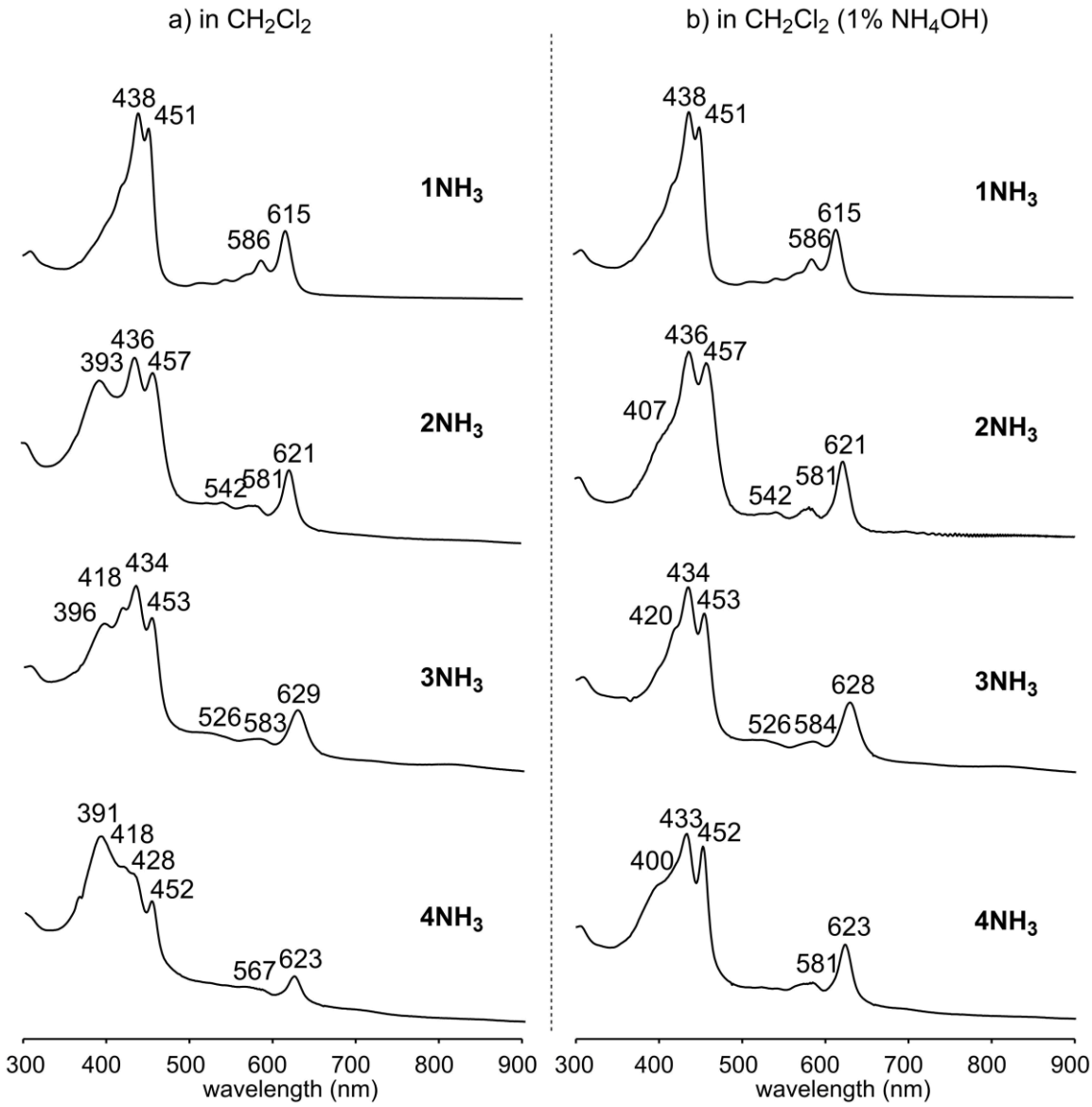

Figure 7-3. UV-visible spectra of **1NH$_3$**-**4NH$_3$** at 10^{-3} M concentration in (a) CH_2Cl_2 and (b) CH_2Cl_2 with 1% (v/v) NH_4OH containing 0.1 M TBAP.

Table 7-1. UV-visible spectral data of investigated cobalt corroles under different solution conditions.

solution condition	cpd	Wavelength: λ_{max}, nm ($\varepsilon \times 10^{-4}$ M^{-1} cm^{-1})						
		Soret region				visible region		
CH_2Cl_2	**1DMSO**	379 (7.2)	416 (4.1)[s]			566 (1.3)		
	2DMSO	385 (6.4)				562 (1.3)		
	3DMSO	387 (7.1)	414 (3.6)[s]			563 (1.3)		
	4DMSO	382 (7.2)				563 (1.6)		
CH_2Cl_2 (1% NH_4OH)	**1NH$_3$**		417 (5.0)	438 (8.3)	451 (7.6)		586 (1.9)	615 (3.2)
	2NH$_3$		407 (2.3)	436 (4.1)	457 (3.9)	541 (0.6)	581 (0.7)	621 (1.7)
	3NH$_3$		420 (3.9)	434 (4.9)	453 (4.2)	526 (1.1)	584 (1.1)	628 (2.1)
	4NH$_3$		400 (4.2)	433 (5.6)	452 (5.2)		581 (1.4)	623 (2.4)

[s]Shoulder peaks.

7.4 Pyridine Binding Ability

The relative intensity of the diagnostic six-coordinate absorption band at 615-623 nm for compounds **1NH$_3$** to **4NH$_3$** in Figure 7-3a follows the order **1NH$_3$** > **2NH$_3$** > **3NH$_3$** > **4NH$_3$** and provides an approximate measure of the extent of NH_3 dissociation from the bis-NH_3 adducts in CH_2Cl_2 at a corrole concentration of 10^{-3} M. The band intensity follows the order **1** > **2** > **3** > **4** and this would also be the relative order of the NH_3 binding strength for the examined bis-NH_3 derivatives in the CH_2Cl_2 solvent.

We could not evaluate the magnitude of the NH_3 binding constants to the four-coordinate corroles in the current study but we could measure binding constants for the stepwise addition of two pyridine molecules to the mono-DMSO adducts in CH_2Cl_2. This was done by monitoring changes in the UV-visible spectra during a titration of each corrole with pyridine, giving results of the type shown in Figure 7-4 for the stepwise conversion of **1DMSO**-**4DMSO** to their respective six-coordinate, bis-pyridine form.

Equilibrium constants for addition of a single pyridine axial ligand to the mono-DMSO adducts could not be easily measured given the small differences in spectra between the initial corrole reactant and the mono-pyridine adduct but much larger spectral changes are associated with formation of the bis-pyridine derivatives and well-defined log-log plots could be obtained as shown by the insets in Figure 7-4b.

The binding constant for addition of a second pyridine molecule to **1DMSO** was measured as $\log K_2 = 3.6$ and this $\log K_2$ value systematically decreased to 2.1, 1.5 and 1.1 for **2DMSO**, **3DMSO** and **4DMSO**, respectively (remark: define to which equilibrium K_2

corresponds). These values are given in Table 7-2 along with $\log K_2 = 2.6$ for addition of a second pyridine molecule to $Mes_3CorCo(py)$, as reported in an earlier study.[9]

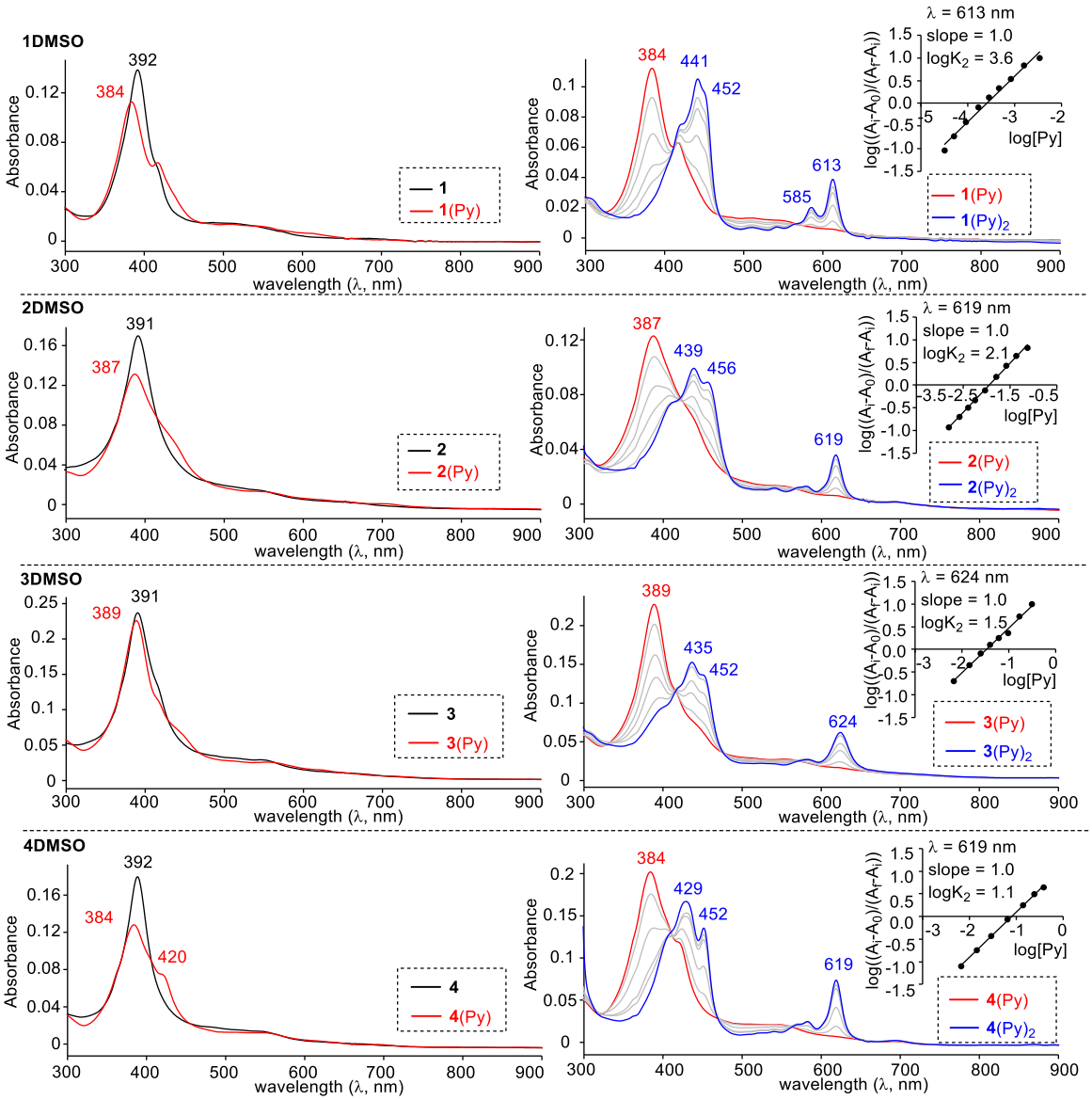

Figure 7-4. UV-visible spectral changes of **1DMSO-4DMSO** (at ~10^{-5} M) in CH_2Cl_2 upon addition of pyridine to solution.

Table 7-2. Pyridine binding constants, logK, for cobalt corroles in CH_2Cl_2.

Compound	$\log K_1$	$\log K_2$	ref
(*o,o*-Cl_2Ph)$_3$CorCo **1**	-	3.6	tw
(*p*-COOMePh)Mes_2CorCo **2**	-	2.1	tw
(Ph)$_3$CorCo **3**	-	1.5	tw
(*o,o,p*-(OMe)$_3$Ph)Mes_2CorCo **4**	-	1.1	tw
(*m*-NO_2-*p*-FPh)(*p*-NO_2Ph)$_2$CorCo	-	3.9	[12]
(*m*-NO_2-*p*-OMePh)(*p*-NO_2Ph)$_2$CorCo	-	3.8	[12]
(*m*-NO_2-*p*-FPh)Mes_2CorCo	-	3.3	[12]
(*m*-NO_2-*p*-OMePh)Mes_2CorCo	-	3.0	[12]
Mes_3CorCo	6.5	2.6	[12]

tw = this work

7.5 Electrochemistry

Redox properties of the synthesized corroles were investigated by cyclic voltammetry under different solution conditions. As previously demonstrated for a related series of derivative,[9] the synthesized mono-ligated DMSO cobalt corroles are invariably characterized by facile and reversible one-electron reductions in CH_2Cl_2 or DMSO (Figure 7-9 and 7-10). This contrasts with what is seen for the hexa-coordinated bis-pyridine derivatives where the first reduction in pyridine is irreversible and occurs at much more negative potentials.[12] The difference in redox behavior between what is seen in CH_2Cl_2 , DMSO or pyridine was explained as being due to a different site of electron transfer and a different electronic configuration of the redox active form of the molecule in solution, the mono-DMSO adducts being assigned as containing a Co(II) center and a non-innocent easily reduced macrocyclic ligand in CH_2Cl_2 or DMSO as compared to a Co(III) center and a hard to reduce innocent macrocyclic ligand in pyridine where the first reduction involves a metal-centered Co(III)/(II) process followed by a loss of one or both axial ligands after electron transfer. In other word, the reversibility of the first reduction process and the small electronic effect of the ligand on the potential values are in accordance with a Co(II) center and a non-innocent macrocycle.

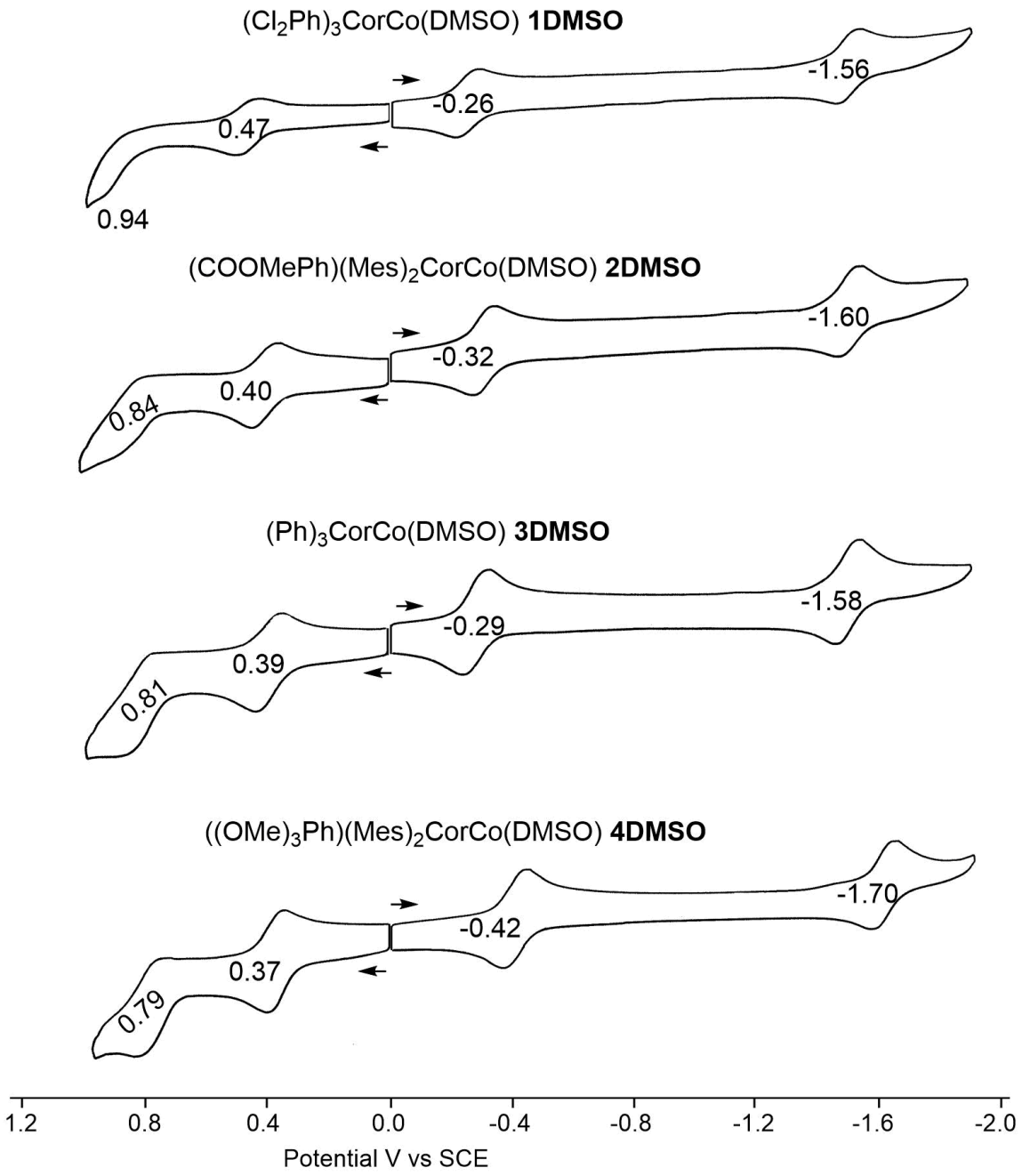

Figure 7-5. Cyclic voltammograms of cobalt corrole complexes **1DMSO-4DMSO** (~10^{-3} M) in DMSO containing 0.1 M TBAP.

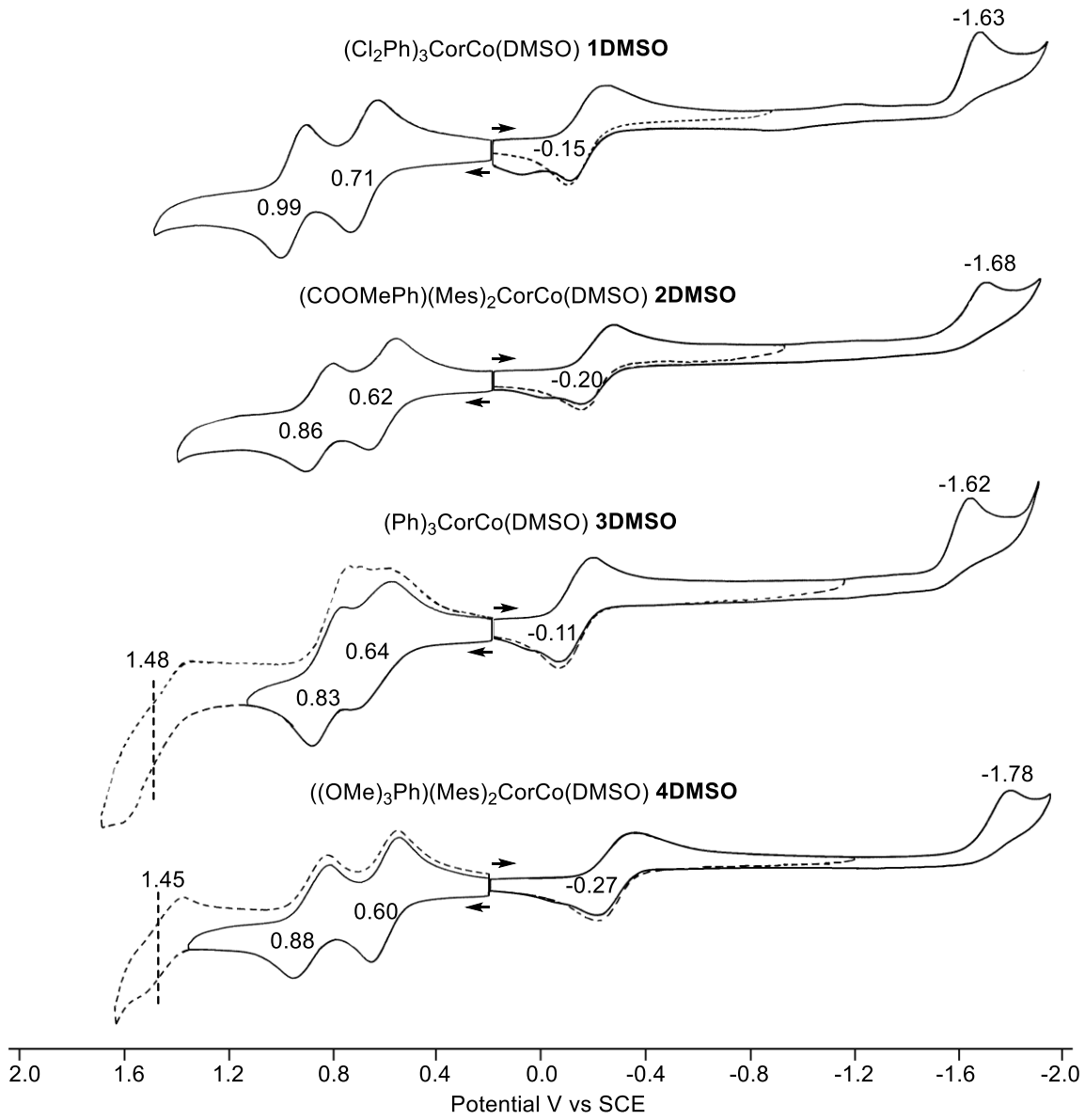

Figure 7-6. Cyclic voltammograms of cobalt corrole complexes **1DMSO-4DMSO** (~10^{-3} M) in CH_2Cl_2 containing 0.1 M TBAP.

The difference in axial coordination and ligand innocence or non-innocence also manifests itself in a difference of half wave potentials for the first one-electron oxidation, this process being easiest (more negative potential) for oxidation of the cobalt bis-pyridine derivatives in pyridine and harder (more positive potential) for oxidation of the four- or five-coordinate cobalt corroles in CH_2Cl_2 or DMSO.[9]

We anticipated observing facile one electron reductions for the newly synthesized mono-DMSO derivatives in the current study and this is indeed the case as shown by the cyclic voltammograms measured in DMSO (Figure 7-5) or CH_2Cl_2 (Figure 7-6).

1DMSO-4DMSO in DMSO (Figure 7-5) undergo two reductions and two oxidations within the negative and positive potential limits of the solvent. The first one-electron reduction is located at $E_{1/2}$ = -0.26 to -0.42 V and the second at -1.56 to -1.70 V. The first one-electron oxidation ranges from $E_{1/2}$ = 0.37 to 0.47 V depending upon the *meso*-substituent and the absolute difference in potential between the first reversible reduction and first reversible oxidation of each compound (the HOMO-LUMO gap) varies from 0.72 to 0.79 V in DMSO, a range of values slightly smaller than the measured HOMO-LUMO gaps in CH_2Cl_2 where the potential separation ranges from 0.75 to 0.87 V (See examples of cyclic voltammograms in Figure 7-11 and summary of half wave potentials in Table 7-3).

The binding of NH_3 to the neutral and singly oxidized cobalt corroles **1** to **4** is stronger than the binding of DMSO to the same series of compounds in CH_2Cl_2 and this is reflected in large negative shifts of potential for the first one electron abstraction, the

measured $E_{1/2}$ values ranging from 0.30 V for 1NH_3 to 0.05 V for 4NH_3 as seen in Figure 8. Like potentials for electron abstraction from the mono-DMSO adducts, the measured half wave potentials for oxidation of the bis-NH_3 derivatives shift negatively with increasing electron-donating character of substituents on the three *meso*-phenyl rings of the macrocycle. However, it should be noted that the substituent effect of the *meso*-phenyl groups is larger for the bis-NH_3 ligated Co(III) corroles than for the five-coordinate derivatives (perhaps containing a Co(II) center and a non-innocent ligand), resulting in an increasing difference in $E_{1/2}$ values between the first reduction oxidation of the same corrole with different axial ligands, from 170 mV in the case of compound **1** (0.47 V in DMSO and 0.30 V in CH_2Cl_2) to 320 mV for compound **4** (0.37 vs 0.05 V).

The oxidation of (Cor)Co$(NH_3)_2$ to [(Cor)Co$(NH_3)_2]^+$ occurs in the absence of coupled chemical reactions but this is not the case for the reduction where a dissociation of one or both NH_3 axial ligands is proposed to occur prior to electron transfer, thus leading to several competing reduction pathways, one for the six-coordinate complex which is the most difficult to reduce and located at $E_{1/2}$ values more negative than -1.0 V vs SCE and the others for the five- and/or four-coordinate species which generate the Co(II) corrole at potentials as positive as -0.07 to -0.26 V as seen in Figure 7-7.

Evidence for dissociation of the NH_3 ligand(s) prior to electron transfer is given in part by the shape of the current voltage curves which is consistent with a coupled chemical reaction prior to electron transfer (an electrochemical CE mechanism), in part by the fact that the first (ill-defined) reduction potentials of the bis-NH_3 complexes in Figure

7-7 are almost identical to the well-defined $E_{1/2}$ values for the same cobalt corroles bearing a single DMSO axial ligand in their synthesized air stable form (Figure 7-7), namely, -0.19/-0.20 V for **2NH$_3$** and **2DMSO**, -0.11 V for 3NH$_3$ and 3DMSO and -0.26/-0.27 V for **4NH$_3$** and **4DMSO** (see Figure 7-7 and Table 7-3), and in part by the current voltage curves for **1NH$_3$** to **4NH$_3$** obtained in CH_2Cl_2 containing excess NH_3 added in the form of NH_4OH.

Examples of cyclic voltammograms under these later solution conditions are given in Figure 7-8 for **2NH$_3$**, **3NH$_3$** and **4NH$_3$**. For all three corroles, the half wave potentials of the two oxidations are the same as in the CH_2Cl_2 solvent without added NH_3 (Figure 7-7), consistent with proposed $[(Cor)Co(NH_3)_2]^{0/+}$ redox process. However, when NH_3 is added to solution, a diminished current intensity is seen in the first reduction peak as the equilibrium is shifted towards the harder to reduce bis-ligated form of the corrole in solution.

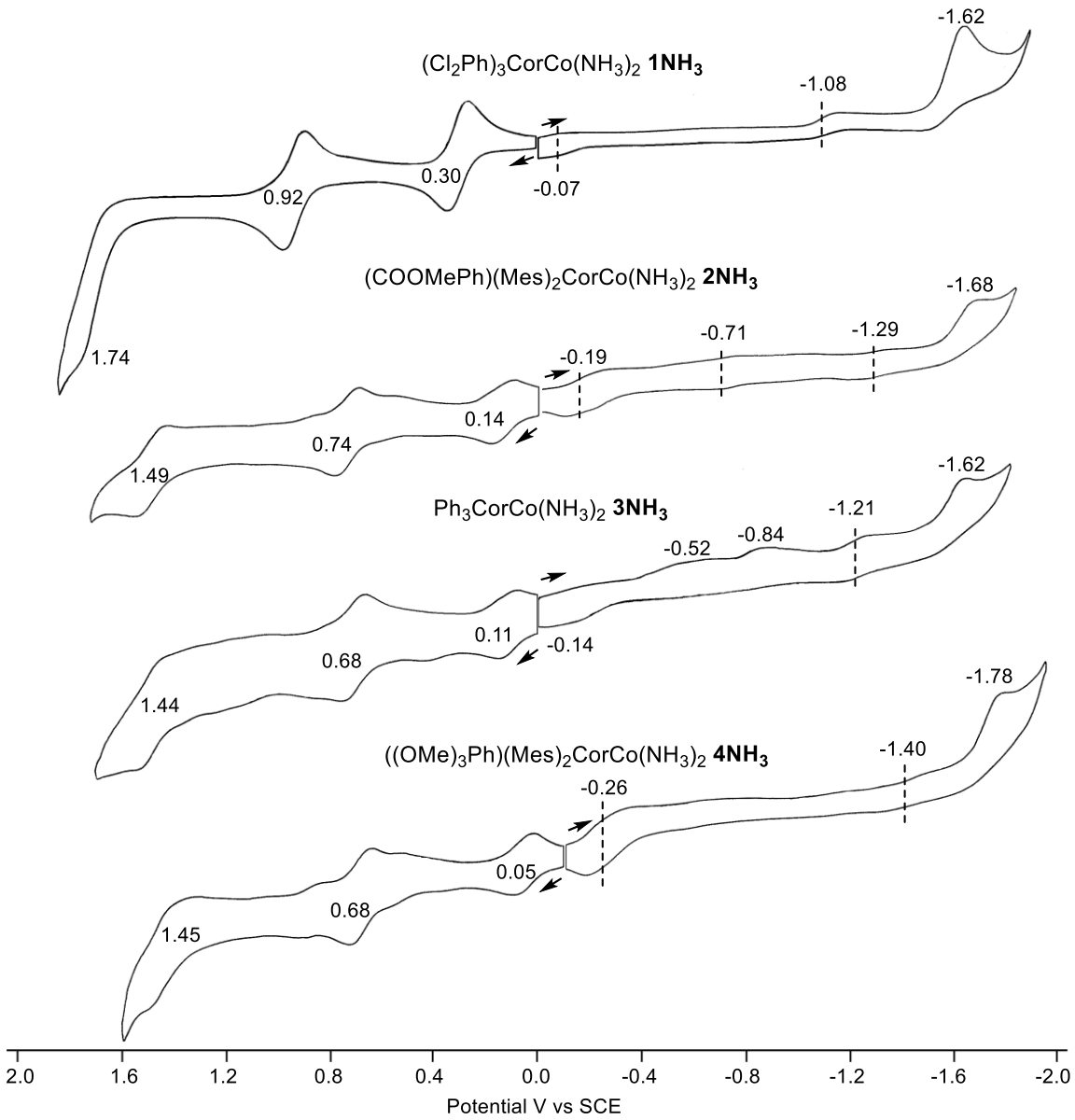

Figure 7-7. Cyclic voltammograms of cobalt corrole complexes **1NH$_3$-4NH$_3$** (~10^{-3} M) in CH_2Cl_2 containing 0.1 M TBAP.

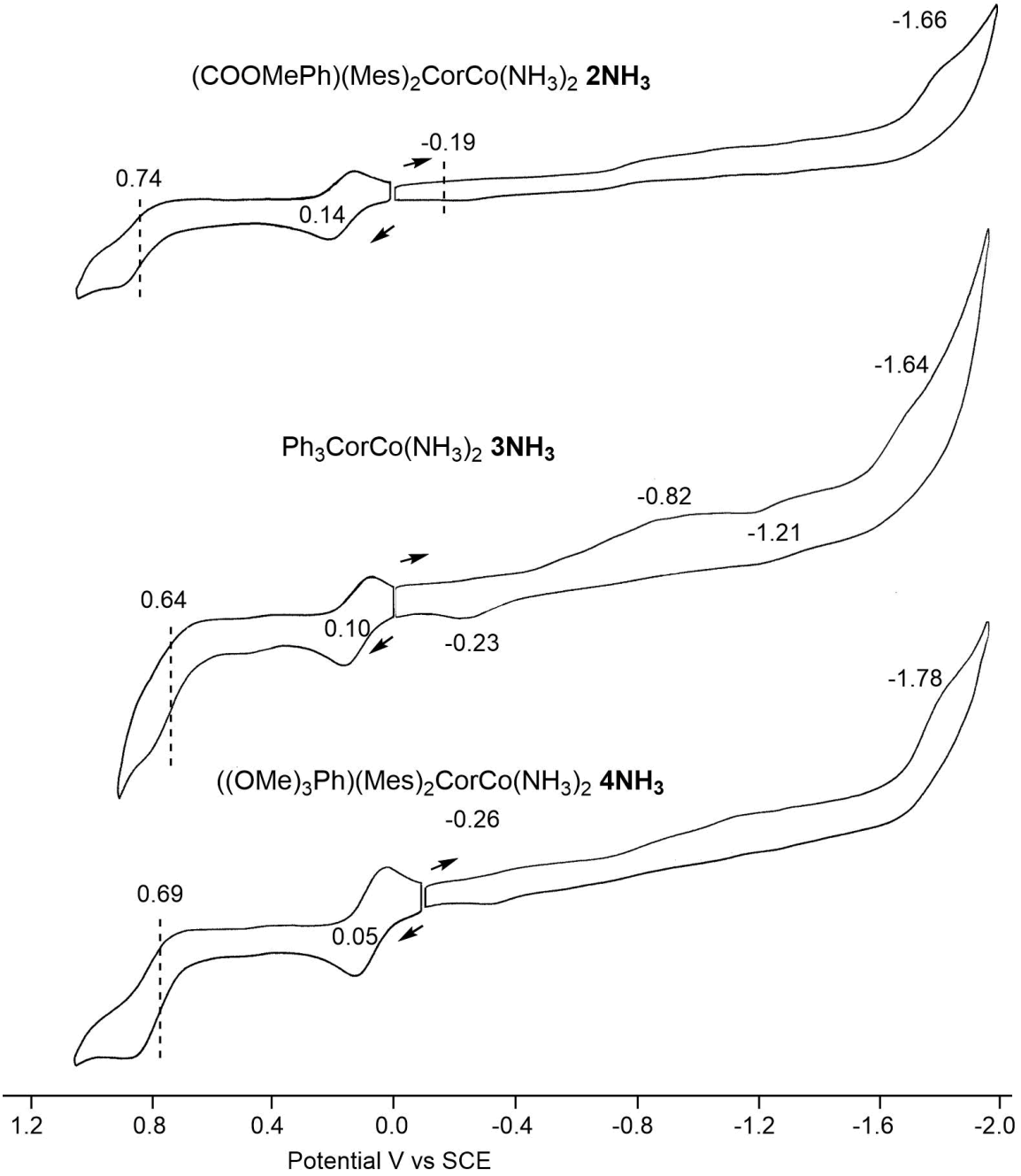

Figure 7-8. Cyclic voltammograms of cobalt corrole complexes **1NH$_3$-4NH$_3$** (~10^{-3} M) in CH_2Cl_2 with 1% (v/v) NH_4OH containing 0.1 M TBAP.

Table 7-3. Half-Wave or Peak Potentials ($E_{1/2}$ or E_p, V vs. SCE) for Reductions and the first two oxidations of cobalt corroles in different solution conditions containing 0.1 M TBAP (sweep rate: 100 mV/s).

solution condition	cpd	Wavelength (λ_{max}, nm)					
		oxidation			reduction		
CH_2Cl_2	**1NH$_3$**	1.74	0.92	0.30	-0.07	-1.08	-1.62[a]
	2NH$_3$	1.49	0.74	0.14	-0.19	-1.29	-1.68[a]
	3NH$_3$	1.44	0.68	0.11	-0.14[b]	-1.21	-1.62[a]
	4NH$_3$	1.45	0.68	0.05	-0.26	-1.40	-1.78[a]
CH_2Cl_2 (*v*/*v* 1% NH_4OH)	**1NH$_3$**		-	-	-	-	-
	2NH$_3$		0.74	0.14	-0.19		-1.66[a]
	3NH$_3$		0.64	0.10	-0.23[b]	-1.21	-1.64[a]
	4NH$_3$		0.69	0.05	-0.26		-1.78[a]

As mentioned above, the average HOMO-LUMO gap of the four mono-DMSO adducts **1DMSO** to **4DMSO** decreases from 825 mV in CH_2Cl_2 (Figure 7-5) to 705 mV in DMSO (Figure 7-6) and the gap decreases even further for the bis-NH_3 adducts where the separation between the first oxidation and first reduction is 330 mV for **2NH$_3$** in CH_2Cl_2 and 310 mV for **4NH$_3$** under the same solution conditions (see Figure 7-7). In each case, the decrease in the measured gap is attributed for the most part to a shift of the HOMO towards an easier oxidation, the measured $E_{1/2}$ value for the one electron abstraction varying from a reversible potential of 0.59 V to 0.37 V and then to 0.19 V for **4DMSO** in CH_2Cl_2, DMSO and pyridine, respectively, and then to 0.05 V for **4NH$_3$** in CH_2Cl_2 as shown graphically in Figure 7-9.

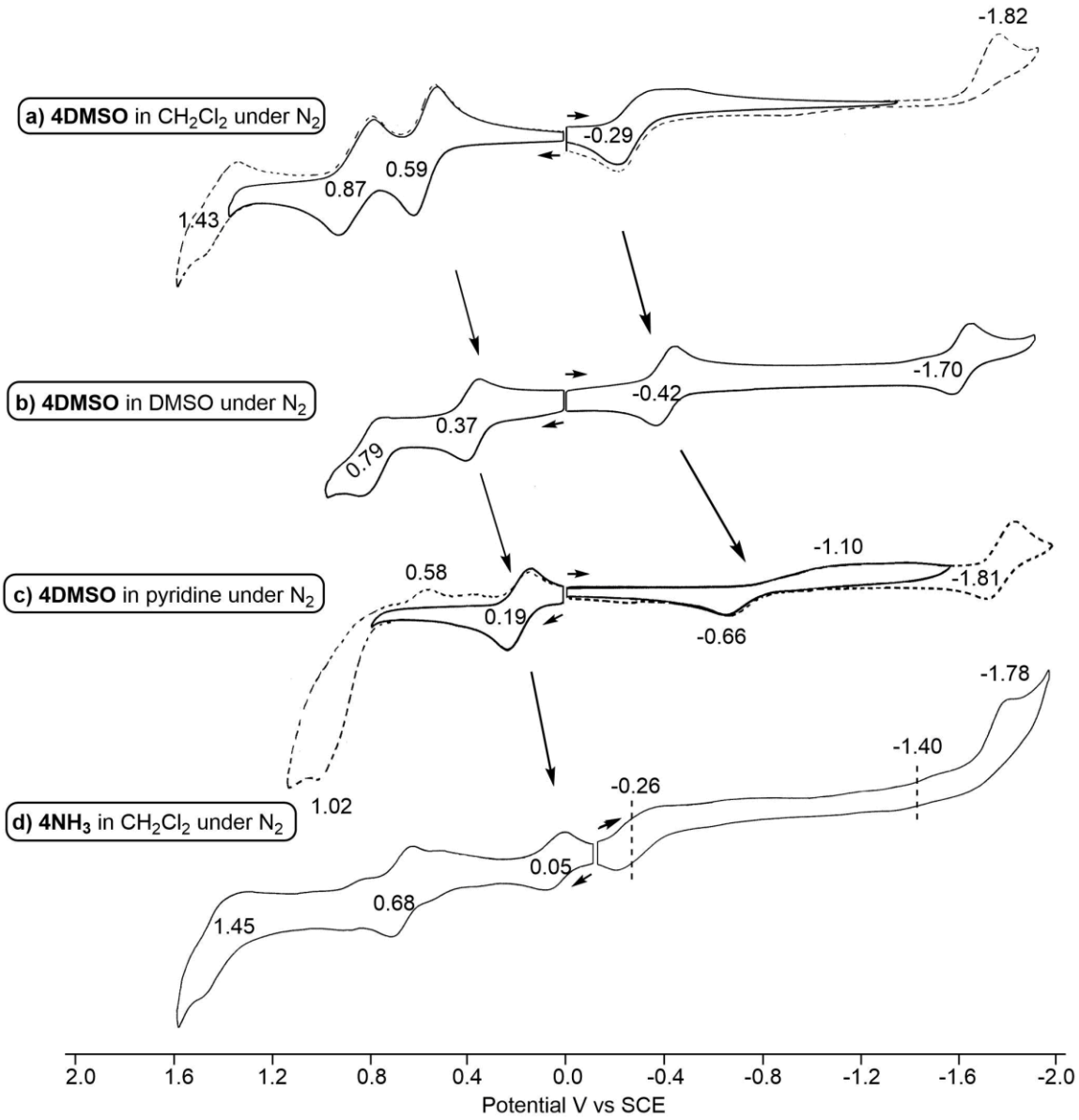

Figure 7-9. Cyclic voltammograms of cobalt corrole **4** with different ligands in different solvent conditions containing 0.1 M TBAP.

7.6 Spectroelectrochemistry

The singly oxidized and singly reduced forms of mono-DMSO and bis-ammonia corroles were characterized by thin-layer UV-visible spectroelectrochemistry and examples of the resulting spectral changes are illustrated in Figure 7-10 for compounds **4DMSO** and **4NH$_3$** under different solution conditions.

The spectral changes obtained during reduction of **4DMSO** are essentially independent of solvent as shown in Figure 7-10b where the Soret band of the neutral corrole shifts from 379/381 to 420/421 nm and the single visible band at 561/563 nm of the unreduced compound is replaced by two visible bands located between 570 and 618 nm after the addition of one electron. The spectrum of [**4DMSO**]$^-$ is assigned as containing an unligated Co(II) central metal ion and virtually the same UV-visible spectrum is obtained after the reduction of **4NH$_3$ in** CH_2Cl_2 under an N_2 or NH_3 atmosphere, thus suggesting a similar unligated square planar Co(II) electroreduction product. However, as mentioned earlier in the manuscript, a partial dissociation of one or both NH_3 ligands occurs for **4NH$_3$** when dissolved in CH_2Cl_2 under N_2 but the original bis-NH_3 adduct can be easily regenerated under an NH_3 atmosphere or when NH_4OH is added to solution. This is shown by the spectral data in Figure 10 where the initial spectrum of **4NH$_3$** under N_2 is identical to that of four- or five-coordinate **4DMSO** species but converts to that of the original bis-NH_3 adduct when NH_3 gas is bubbled through the solution. Under these conditions, the neutral six-coordinate complex is characterized by a split Soret band at 432 and 452 nm and an intense six-coordinate marker band at 624 nm as shown in Figure 7-

10. This spectrum is assigned to the Co(III) corrole which is then converted to its Co(II) form after controlled potential reduction at -1.00 V in the thin layer cell.

The same spectral product is obtained after the one electron oxidation of **4NH$_3$** under N_2 or NH_3 and this species, with a split Soret band between 403 and 419 nm and a broad Q band between 600 and 725 nm is assigned as a six-coordinate Co(III) π–cation radical. Singly oxidized **4DMSO** has a similar spectrum in DMSO which is assigned to the bis-DMSO Co(III) π cation radical but this spectrum differs substantially from the spectrum of singly oxidized **4DMSO** in CH_2Cl_2.

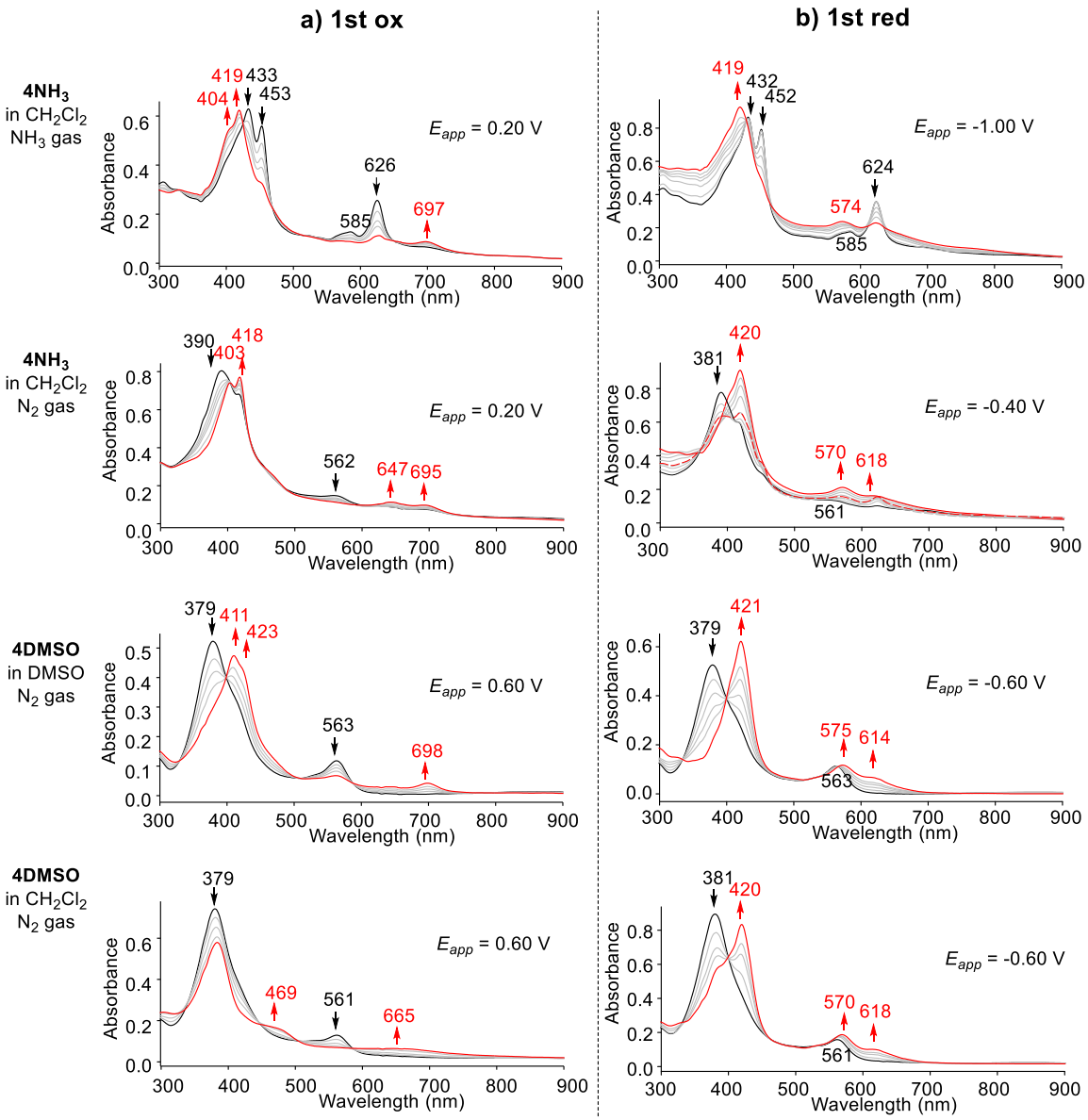

Figure 7-10. UV-visible spectral changes during (a) the first oxidations and (b) the first reductions for **4DMSO** under controlled potentials in different solution condition containing 0.1 M TBAP.

7.7 Conclusion

In summary, we have characterized the electrochemistry and spectroscopic properties of mono-DMSO and bis-ammoniac cobalt corroles in CH_2Cl_2, DMSO and CH_2Cl_2/NH_4OH mixtures. Interestingly, the ligated DMSO axial ligand can be replaced by two ammonia molecules, shifting from a penta-ccordinated cobalt corrole to a hexa-coordinated one. The two ammonia molecules can be further removed to smoothly access to the tetra-coordinated cobalt corrole, an active form able to selectively bind carbon monoxide. A DFT computational study[13] has further confirmed the formation of penta-coordinated cobalt corroles in the case of DMSO and CO derivatives and the formation of hexa-coordinated cobalt corroles in the case of ammonia and pyridine cobalt corroles, in agreement with the electrochemical studies and the spectroscopic data.

7.8 References

[1] J. F. B. Barata, M. G. P. M. S. Neves, M. A. F. Faustino, A. C. Tomé, J. A. S. Cavaleiro, Strategies for Corrole Functionalization, *Chemical Reviews* **2017**, *117*, 3192-3253.

[2] Y. Fang, Z. Ou, K. M. Kadish, Electrochemistry of Corroles in Nonaqueous Media, *Chemical Reviews* **2017**, *117*, 3377-3419.

[3] A. Ghosh, Electronic Structure of Corrole Derivatives: Insights from Molecular Structures, Spectroscopy, Electrochemistry, and Quantum Chemical Calculations, *Chemical Reviews* **2017**, *117*, 3798-3881.

[4] R. Orłowski, D. Gryko, D. T. Gryko, Synthesis of Corroles and Their Heteroanalogs, *Chemical Reviews* **2017**, *117*, 3102-3137.

[5] R. Paolesse, S. Nardis, D. Monti, M. Stefanelli, C. Di Natale, Porphyrinoids for Chemical Sensor Applications, *Chemical Reviews* **2017**, *117*, 2517-2583.

[6] R. D. Teo, J. Y. Hwang, J. Termini, Z. Gross, H. B. Gray, Fighting Cancer with Corroles, *Chemical Reviews* **2017**, *117*, 2711-2729.

[7] W. Zhang, W. Lai, R. Cao, Energy-Related Small Molecule Activation Reactions: Oxygen Reduction and Hydrogen and Oxygen Evolution Reactions Catalyzed by Porphyrin- and Corrole-Based Systems, *Chemical Reviews* **2017**, *117*, 3717-3797.

[8] X. Jiang, W. Shan, N. Desbois, V. Quesneau, S. Brandès, E. Van Caemelbecke, W. R. Osterloh, V. Blondeau-Patissier, C. P. Gros, K. M. Kadish, Mono-DMSO Ligated Cobalt Nitrophenylcorroles: Electrochemical and Spectral Characterization *New J. Chem.* **2018**, *42*, 8220-8229.

[9] X. Jiang, M. Naitana, N. Desbois, V. Quesneau, S. Brandès, Y. Rousselin, W. Shan, W. R. Osterloh, V. Blondeau-Patissier, C. P. Gros, K. M. Kadish, Electrochemistry of Cobalt Nitrophenylcorroles in Nonaqueous Media, *Inorg. Chem.* **2018**, *57*, 1226-1241.

[10] D. T. Gryko, B. Koszarna, *Org. Biomol. Chem.* **2003**, *1*, 350.

[11] B. Koszarna, D. T. Gryko, Efficient Synthesis of meso-Substituted Corroles in a H2O−MeOH Mixture, *J. Org. Chem.* **2006**, *71*, 3707-3717.

[12] X. Jiang, M. L. Naitana, N. Desbois, V. Quesneau, S. Brandes, Y. Rousselin, W. Shan, W. R. Osterloh, V. Blondeau-Patissier, C. P. Gros, K. M. Kadish, Electrochemistry of Bis(pyridine)cobalt (Nitrophenyl)corroles in Nonaqueous Media, *Inorg. Chem.* **2018**, *57*, 1226-1241.

[13] V. Quesneau, W. Shan, N. Desbois, S. Brandes, Y. Rousselin, M. Vanotti, V. Blondeau-Patissier, M. Naitana, P. Fleurat-Lessard, E. Van Caemelbecke, K. M. Kadish, C. P. Gros, Cobalt Corroles with Bis-Ammonia or Mono-DMSO Axial Ligands. Electrochemical, Spectroscopic Characterizations and Ligand Binding Properties, *Eur. J. Inorg. Chem.* **2018**, *2018*, 4265-4277.

8

Ligand Noninnocence in Cobalt Dipyrrin-Bisphenols: Spectroscopic, Electrochemical and Theoretical Insights Indicating an Emerging Analogy with Corroles

8.1 Introduction

The free-base dipyrrin-bisphenols ($DPPH_3$, Chart 8-1), an emerging class of hybrid pyrrole-based ligands, are of interest for a variety of reasons,[1-9] perhaps most notably for the fact that several DPPM derivatives (M = Co,[1, 2] Ni,[1] Cu[3] or Pt[4]) have been found to exist as metal-radical assemblies, i.e., as $(DPP^{\bullet 2-})M^{II}$, as opposed to $(DPP^{3-})M^{III}$. Both in terms of their formally trianionic character and their propensity to yield noninnocent metal-radical assemblies, $DPPH_3$ ligands resemble free-base corroles ($CorH_3$, Chart 8-1), a class of tetrapyrrole ligands whose chemistry has grown dramatically over the last two decades.[10-13] Herein we report a detailed electrochemical, spectroscopic, and quantum chemical study of cobalt DPP complexes that provides strong support for a DPP-corrole analogy, indeed a simple case of an isolobal analogy,[14] which in time may prove to be a significant driver of new discoveries in the DPP field.

Until now, there have been two major studies of four-coordinate (abbr. as 4c) DPPCo derivatives.[1, 2] The authors of one paper,[1] Thomas and coworkers, formulated the neutral cobalt dipyrrin-bisphenols as $(DPP^{\bullet 2-})Co^{II}$ and the corresponding singly oxidized complex as $(DPP^{-})Co^{II}$ (both reasonable formulations, in our view), while in another paper,[2] the authors mainly focused on the catalytical reactivity of the DPPCo complexes. These authors, however, did not characterize the anionic states of the compounds after oxidation or reduction, nor did they explore the axial ligation chemistry of the complexes. As part of this work, we have synthesized three DPPCo derivatives **1-3** as four-coordinate complexes in the solid state and investigated their electrochemical and

spectroscopic properties in four different nonaquaous solvents, one of which is noncoordinating (CH_2Cl_2), and three of which are coordinating (PhCN, DMSO and pyridine). The three compounds are depicted in Chart 8-2 and referred to hereafter as (F_5Ph)DPPCo **1**, (Ph)DPPCo **2**, and **(**Mes)DPPCo **3**, where F_5Ph, Ph, and Mes refer to pentafluorophenyl, phenyl, and mesityl groups at the *meso*-position of the DPP ligand, respectively. By examining three different DPPCo derivatives under different solution conditions, we are able to document the rich coordination chemistry of the DPPCo complexes, which have previously been examined only in one noncoordinating solvent, CH_2Cl_2.[1]

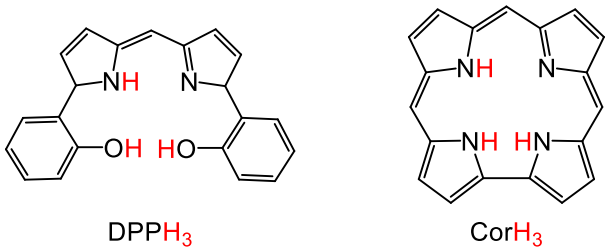

DPPH_3 — dipyrrin-bisphenol

CorH_3 — corrole

Chart 8-1. Structures of free-base dipyrrin-bisphenol and corrole ligands.

Like cobalt porphyrins[15, 16] and corroles,[12, 17, 18] the DPPCo complexes examined are expected to undergo several reduction and oxidation processes involving the cobalt center, the DPP π-system or a combination of the two. Here we have used a comprehensive set of UV-visible spectroelectrochemical measurements to characterize the neutral, cationic, and anionic states of the complexes. The measurements underscore the importance of axial ligands, which greatly influences whether a given redox process occurs in a metal- or ligand-centered manner. Density functional theory calculations (DFT) with three different exchange-correlation functionals on (Ph)DPPCo 2 (Chart 8-2) were also carried out and provide additional detail on the nature of the low-energy states of the complex for the various charge and coordination states.

Our results indicate extensive parallels between the low-energy states of DPPCo and CorCo complexes.[19, 20] These similarities may foreshadow important applications of the DPP derivatives in areas where metallocorroles already play a significant role, examples been in catalytic group transfer chemistry[21] (such as epoxidations,[22, 23] aziridinations[24, 25] and cyclopropanations[26]) and chemical sensing of small molecules such as carbon monoxide[27-29] or nitrite[30].

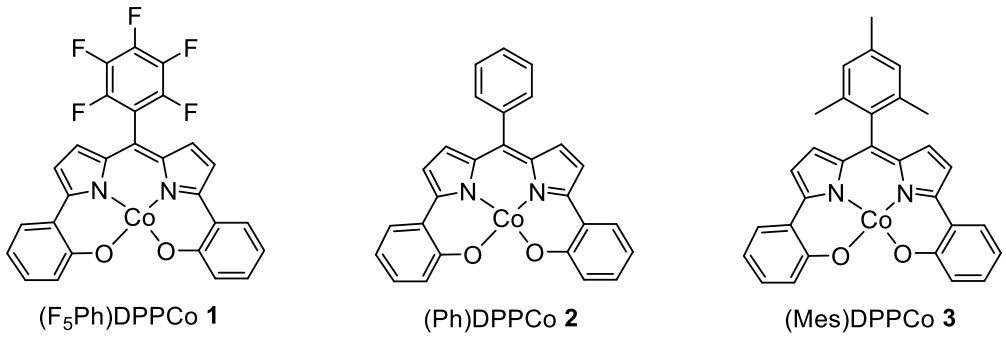

Chart 8-2. Structures of the investigated DPPCo complexes **1-3**.

8.2 Synthesis and Characterization

The DPP complexes **1-3** were synthesized via modification of a previously reported protocol.[2] The synthetic route is shown in Scheme 8-1. Acid-catalyzed condensation of 2-(2-methoxyphenyl)-pyrrole and aldehyde in methylene chloride, followed by subsequent oxidation with DDQ afforded the dipyrrin precursor.[31] Deprotection of the phenol moieties with BBr_3 then quantitatively afforded the free base dipyrrin-bisphenol precursors ($DPPH_3$).[6] The target DPPCo complexes **1-3** were prepared by reaction of $DPPH_3$ with $Co(OAc)_2{\cdot}4H_2O$.

H^1 NMR spectra and MS measurements were carried out to confirm the structures reported in Chart 8-1. A perfect match was observed between the experimental HR-MS spectra of compounds **1-3** and the simulated ionic patterns. ESI mass spectra have been also registered in the presence of pyridine or in the presence of $NH_3{\cdot}H_2O$. In both cases, the molecular peaks corresponding to the hexacoordinated species (e.g. bis-py and bis-NH_3 species) are clearly observed proving that DPPCo complexes **1-3** can also lead to hexacoordinated species in the presence of NH_3 or pyridine as previously reported in the case of cobalt corrole complexes.[32]

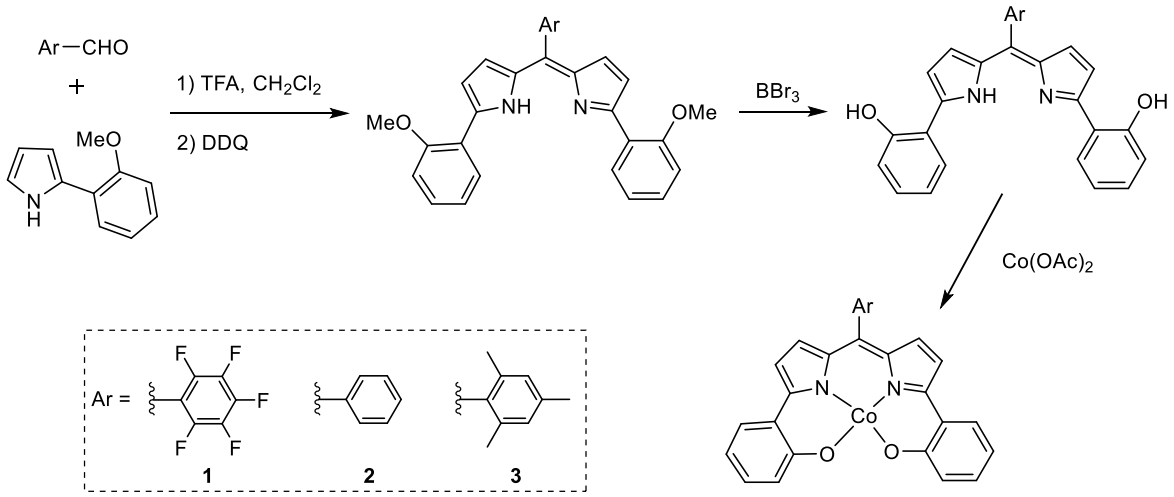

Scheme 8-1. Synthetic route to obtain DPPCo **1-3**.

8.3 UV-Visible Spectroscopy

Before carrying out the redox reactions, the UV-visible spectrum of each neutral compound **1-3** was measured in one noncoordinating solvent (CH_2Cl_2) and three coordinating solvents (PhCN, DMSO and pyridine). Examples of the obtained spectra are given in Figure 1 for a 10^{-3} M solution of compounds **1-3** in four solvents containing 0.1 M TBAP, and a summary of the spectral data under these conditions is given in Table 8-1.

Each spectrum is characterized by an intense band at 311 to 329 nm, two to three intense overlapping bands at 554 to 693 nm and one less intense band at wavelengths between these two major absorption peaks. For example, all three investigated compounds have bands at 414 to 473 nm in PhCN, DMSO or pyridine, but this band is not seen in the noncoordinating CH_2Cl_2 solvent. In addition, the major visible bands of compounds **1-3** in the three coordinating solvents are red-shifted as compared to the corresponding bands in CH_2Cl_2. The magnitude of the wavelength shift as compared to CH_2Cl_2 is 4 to 9 nm in PhCN, 13 to 49 nm in DMSO and 39 to 69 nm in pyridine. The first intense band is at similar wavelengths in CH_2Cl_2, PhCN and DMSO (around 316 nm, 320 nm and 312 nm for compounds **1-3**, respectively), but this band is red-shifted by 5 to 13 nm in pyridine as compared to the other solvents. Considering the known solvent binding ability of the cobalt metal center in similar compounds,[17, 18, 33] those red shift and the appearance of the additional band might correspond to axial coordination of a solvent molecule at the cobalt center in the DPPCo complex.

Moreover, as seen in Figure 8-1, the UV-visible spectra of compounds **2** and **3**, which have *meso*-phenyl and mesityl groups, are almost identical to each other in the same solvent. These spectra differ from that of (F_5Ph)DPPCo **1** which has a highly electron-withdrawing *meso*-F_5Ph group and is characterized by visible bands which are 21 to 43 nm red-shifted as compared to compounds **2** and **3**, the exact value depending upon the specific solvent.

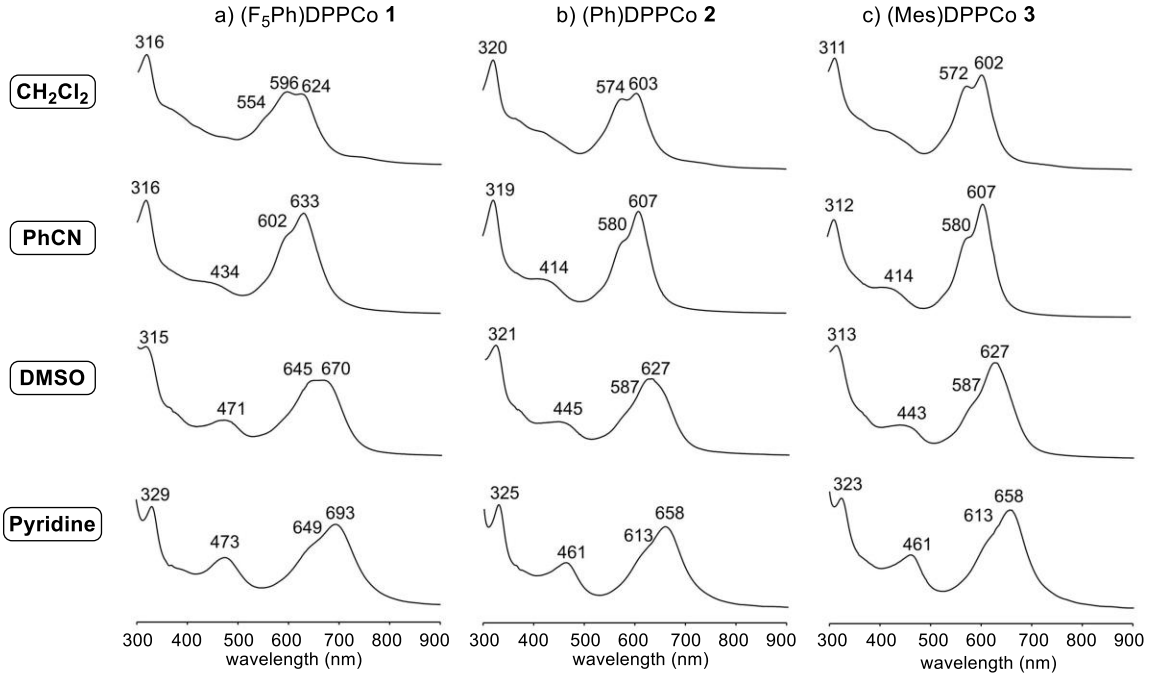

Figure 8-1. UV-visible spectra of **1-3** (~10^{-3} M) in four solvents containing 0.1 M TBAP.

Table 8-1. UV-vis spectral data for **1-3** (~10^{-3} M) in CH_2Cl_2, PhCN, DMSO or pyridine containing 0.1 M TBAP.

solvent	*meso*-substituent	cpd	λ_{max}, nm (ε ×10^{-4} M^{-1} cm^{-1})			
			Soret region		visible region	
CH_2Cl_2	F_5Ph	**1**	316 (1.6)	-	596 (1.2)	624 (1.2)
	Ph	**2**	320 (1.8)	-	574 (1.1)	603 (1.2)
	Mes	**3**	311 (1.8)	-	572 (1.4)	602 (1.6)
PhCN	F_5Ph	**1**	316 (1.5)	434 (0.5)	602 (1.1)	633 (1.4)
	Ph	**2**	319 (1.4)	414 (0.5)	580 (0.9)	607 (1.3)
	Mes	**3**	312 (1.5)	414 (0.5)	580 (1.2)	607 (1.7)
DMSO	F_5Ph	**1**	315 (1.5)	471 (0.5)	645 (1.1)	670 (1.1)
	Ph	**2**	321 (1.6)	445 (0.5)	587 (0.7)	627 (1.1)
	Mes	**3**	313 (1.5)	443 (0.5)	587 (0.8)	627 (1.3)
Py	F_5Ph	**1**	329 (1.4)	473 (0.7)	649 (0.9)	693(1.2)
	Ph	**2**	325 (1.5)	461 (0.7)	613 (0.8)	658 (1.2)
	Mes	**3**	323 (1.4)	461 (0.6)	613 (0.7)	658 (1.2)

8.4 UV-visible Spectroscopic Monitored Titration

In order to investigate the possible binding of the solvent molecules to DPPCo, the UV-visible spectral changes of (Mes)DPPCo **3** in CH_2Cl_2 were measured during the titration with DMSO and pyridine. The binding constants were calculated as $\log K_1 = 1.51$ and 6.55, respectively, for the addition of a single solvent molecule using non-linear curve fitting.[32] A second set of spectral changes were not observed under the experimental conditions on the timescale of both titrations. The major absorption bands of the DPP derivatives in the neat solvents (627 nm in DMSO, 658 nm in pyridine) are red-shifted compared to those of the last spectra during the titration (18 nm shift from 609 nm in the DMSO titration, 54 nm shift from 604 nm in the pyridine titration). This contracts with what is seen in neat PhCN (at 607 nm), where the major absorption band at the end of the titration is the same as in the neat PhCN. This indicates that five-coordinate (abbr. as 5c) species are the major derivatives of DPPCo compounds in PhCN and in the solution mixture at the end of both titration experiments, while six-coordinate (abbr. as 6c) species can exist in neat DMSO and neat pyridine.

Interestingly, when measuring the UV-visible spectrum of compounds **1-3** in pyridine, a slow transformation was observed to occur between two different forms of the DPPCo complexes. To study the kinetics of this transformation, the UV-visible spectral changes of compounds **1-3** in pyridine were recorded as a function of time and kinetic plots were constructed in order to determine the reaction order of the transformation. Examples of the spectral changes and corresponded plots are given in Figure 8-2.

As seen in Figure 8-2a, the initial spectrum of (Mes)DPPCo **3** when dissolved in pyridine has two major bands at 580 and 607 nm, but after 90 min the most intense band has shifted from 607 to 658 nm while the less intense band has disappeared. The initial spectrum is assigned as a five-coordinate (abbr. as 5c) form of DPPCo and the final spectrum as a six-coordinate (abbr. as 6c) form. Well-defined isosbestic points can be seen at 506 and 624 nm in Figure 8-2, which indicate the absence of a spectrally detectable intermediate between the 5c and 6c forms on the timescale of the measurement. The changes in absorbance at 607 nm for state 5c and at 658 nm for state 6c are plotted vs. time in Figure 8-2b while Figure 8-2c shows a plot of ln[5c] *vs.* time, which was calculated from the absorbance band at 607 nm. As shown in Figure 8-2c, there is a linear relationship between the natural logarithm of the calculated concentration of 5c reactant *vs.* time, with a slope of -0.07. The linearity of the slope indicates that this transformation process involves a first order chemical reaction.

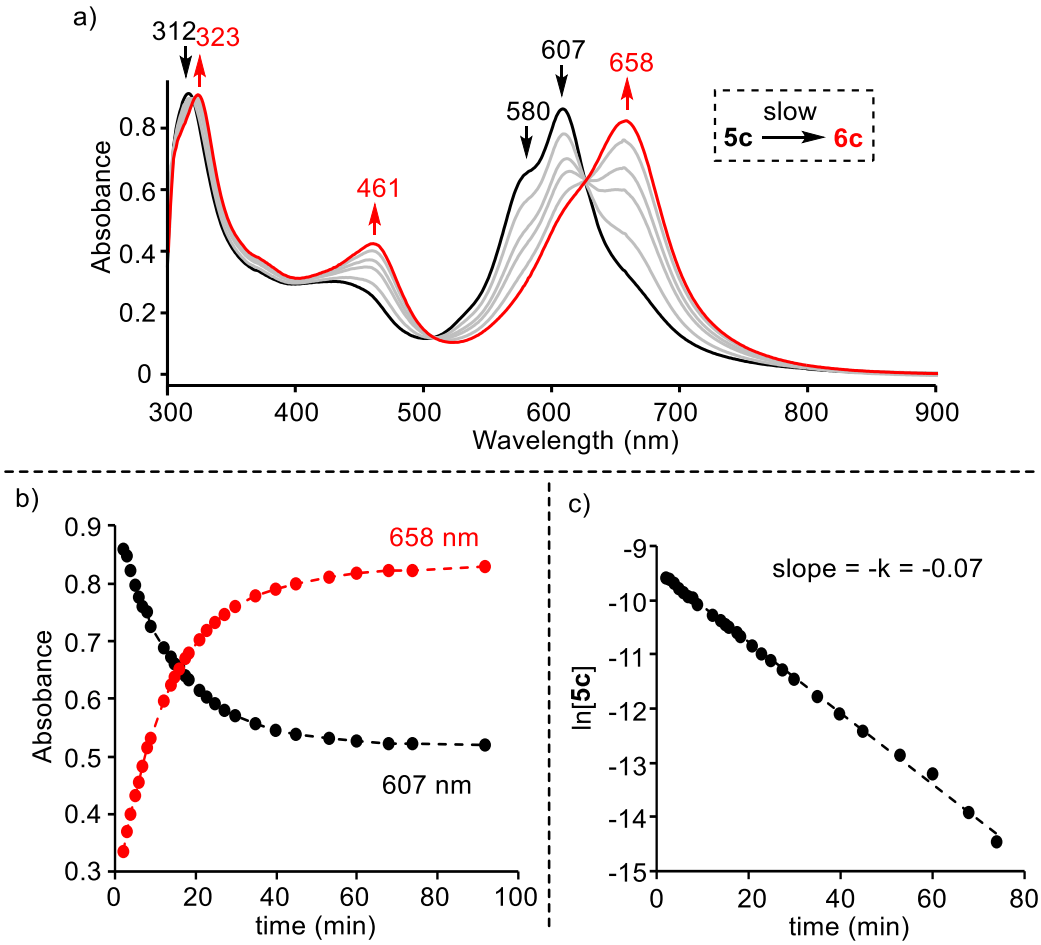

Figure 8-2. (a) UV-visible spectral changes of (Mes)DPPCo **3** (~10^{-5} M) in pyridine, from t = 0 (assigned as five-coordinate, abbr. as 5c) to 90 min (assigned as six-coordinate, abbr. as 6c) after dissolving the compound in solution, (b) plot of the absorbance at 607 nm and 658 nm versus time (min) and (c) correlation between the natural logarithm of concentration of the initial five-coordinate (5c) compound **3** versus time (min).

Similar transformations also can be seen for compounds **1** and **2**, and a summary of the spectral data under different solution conditions are given in Table 8-2, along with the calculated rate constants for the conversion between two states of compounds **1-3**.

As shown in Table 8-2 and Figure 8-2, the major visible bands of **1-3** are red shifted by 50 to 61 nm during the transformation from 5c to 6c. Red shifts are also seen for the other bands. The reaction rate constant for compound **3** which has an electron-donating (mesityl) group on the *meso*-position is 0.07, which is much smaller than the 0.24 for compound **2** (Ph) and 0.18 for compound **1** (F_5Ph). The electron-donating group decreases the rate of the transformation processes.

Table 8-2. Spectral data for compounds **1-3** (~10^{-5} M) in pyridine and CH_2Cl_2/pyridine mixture and slopes of the kinetic plots.

compound	solution condition	CN[a]	λ_{max}, nm ($\varepsilon \times 10^{-4}$ M^{-1} cm^{-1})				slope = -k[b]
			Soret region		visible region		
(F_5Ph)DPPCo **1**	CH_2Cl_2/2000 eq. Py.	5c	316	464	600	627	
	neat Py (initial)	5c	316	464	604	632	
	neat Py (final)	6c	329	473	649	693	-0.18
(Ph)DPPCo **2**	CH_2Cl_2/2000 eq. Py	5c	320	435	575	604	
	neat Py (initial)	5c	320	435	583	608	
	neat Py (final)	6c	325	461	613	658	-0.24
(Mes)DPPCo **3**	CH_2Cl_2/2000 eq. Py	5c	312	430	575	604	
	neat Py (initial)	5c	312	430	580	607	
	neat Py (final)	6c	323	461	613	658	-0.07

[a]CN = coordination number, five-coordinate is abbr. as 5c and six-coordinate as 6c. [b]Conversions between two forms only occurs in neat pyridine.

Considering the possible equilibrium between $(DPP^{\bullet 2-})Co^{II}$ and $(DPP^{3-})Co^{III}$, the slow conversion from 5c to 6c can be proposed to involve a change of the electronic configurations as shown in Scheme 8-2. The 5c form can be assigned to the five-coordinate complex $(DPP^{\bullet 2-})Co^{II}(Py)$ while 6c form would correspond to six-coordinate complex $(DPP^{3-})Co^{III}(Py)_2$. All the data suggests the following reactions in Scheme 8-2.

To confirm the axial ligation of two pyridine molecule on the DPPCo complexes, TGA analysis and H^1 NMR spectroscopy were measured for the chemically synthesized bis-pyridine ligated $(F_5Ph)DPPCo(Py)_2$ **1**$(Py)_2$, which are given in the publication.[32]

According to the TGA analysis, the measured weight loss (Δm) of the bis-ligated compounds is 21.0% as compared to a calculated value 22.3% for two pyridine molecules. More evidence is given in the DFT calculations section in the same paper.[32]

Notably, 6c species can also partially exist in neat DMSO as mentioned above. However, the complete transformation from 5c (with one axial DMSO molecule) to 6c species (with two axial DMSO molecules) was not observed, either in neat DMSO, or during titration of DMSO in CH_2Cl_2. A transformation from 5c to 6c was also not observed on the experimental timescale during the titration with pyridine.

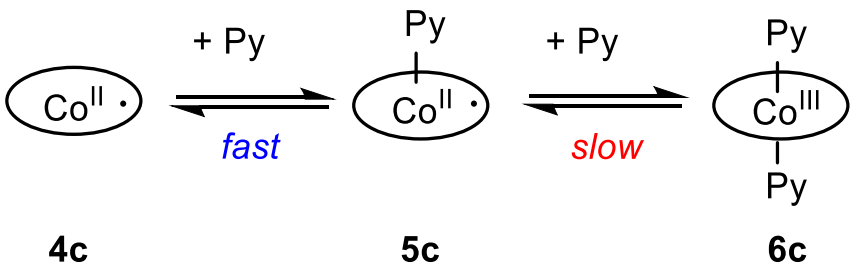

Scheme 8-2. Transformations among 4c, 5c and 6c forms of compounds **1-3**.

8.5 Electrochemistry

8.5.1 General Redox Reactions

The first step in characterizing electrochemistry of compounds **1-3** was to obtain cyclic voltammograms in the coordinating and noncoordinating solvents, and then to relate changes in the observed redox potentials to changes in the spectroscopic properties of the neutral, electroreduced and electrooxidized forms of the compounds. As described on the following pages, two major reductions and two major oxidations can be observed for DPP derivatives as schematically shown in Scheme 8-3.

The DPPCo complex with *t*-butyl groups was earlier reported to undergo two reversible oxidations and one reversible reduction in CH_2Cl_2 containing 0.1 M TBAP, all three of which were assigned to electron transfers at the DPP ligand.[1] However, the currently examined DPPCo complexes **1-3** show three or four oxidations and several reductions, the exact number depending upon the specific electrochemical solvent. An example of the cyclic voltammograms for compound **1** in the four utilized solvents is given in Figure 8-3 and a summary of measured potentials for the major redox reactions of these three complexes is given in Table 8-3.

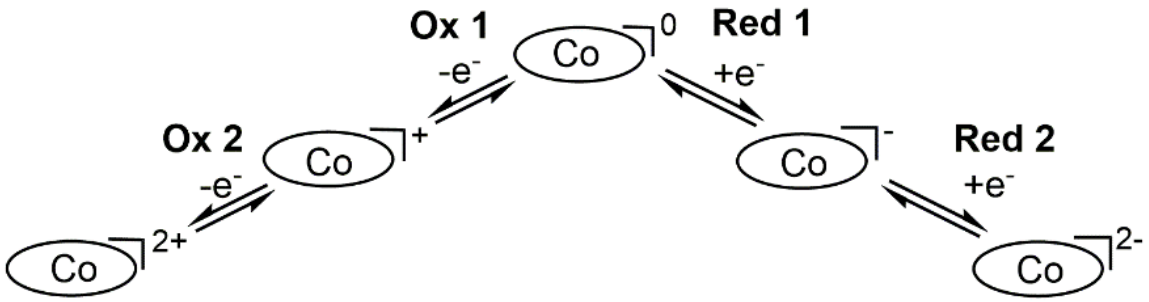

Scheme 8-3. Major redox reactions of DPPCo complexes.

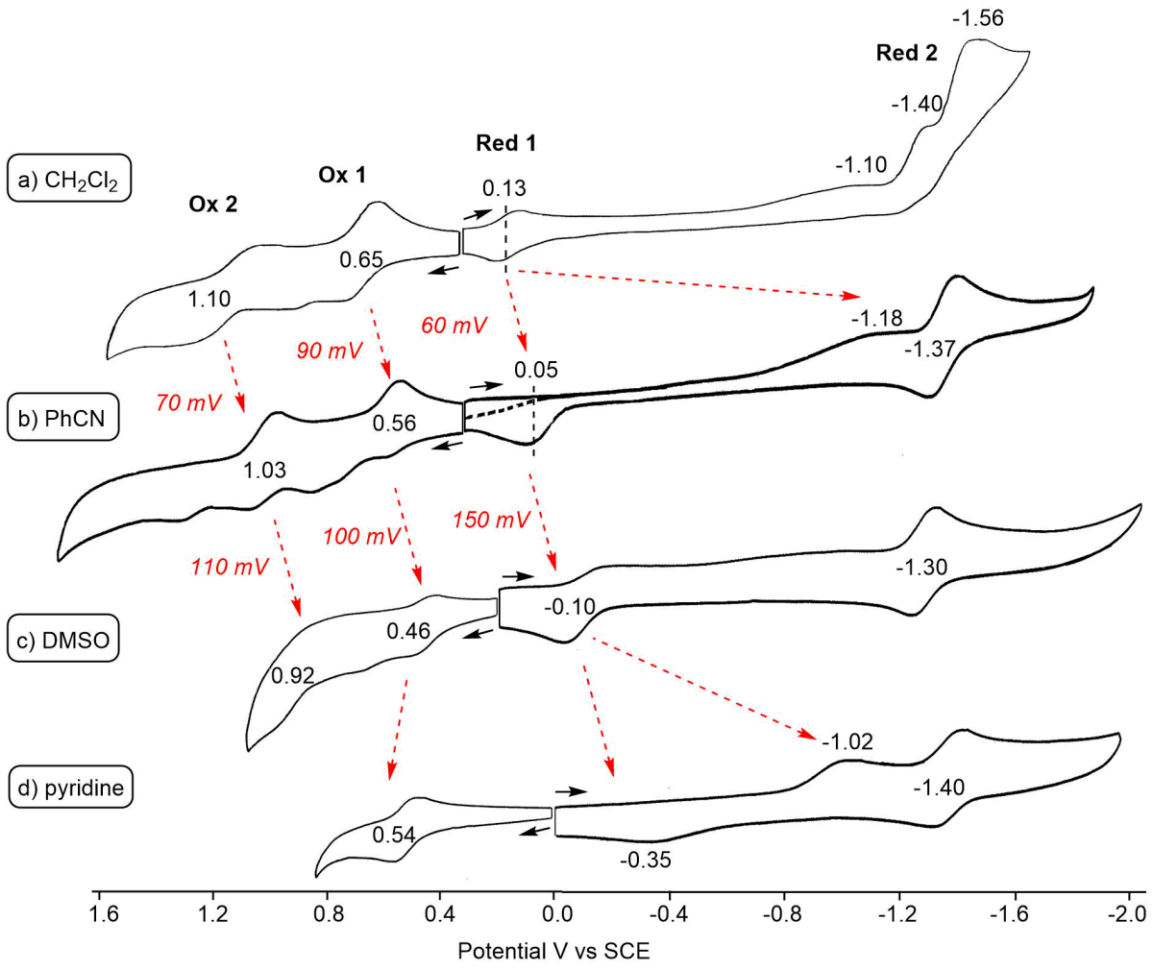

Figure 8-3. Cyclic voltammograms of compound **1** for the redox reactions in (a) CH_2Cl_2, (b) PhCN, (c) DMSO and (d) pyridine containing 0.1 M TBAP.

Table 8-3. Half-wave or peak potentials ($E_{1/2}$ or E_p, V vs. SCE) of DPPCo complexes **1-3** in four solvents containing 0.1 M TBAP.

solvent	*meso*-substituent	cpd	Potential (V vs SCE)			
			Ox 2	Ox 1	Red 1	Red 2
CH_2Cl_2	F_5Ph	**1**	1.10	0.65	0.13	-1.40[a]
	Ph	**2**	1.00	0.57	0.08	-1.46[a]
	Mes	**3**	1.04	0.56	0.07	-1.52[a]
PhCN	F_5Ph	**1**	1.03	0.56[b]	0.05	-1.37
	Ph	**2**	1.01	0.51[b]	0.04	-1.51
	Mes	**3**	1.02	0.51[b]	0.02	-1.55
DMSO	F_5Ph	**1**	0.91	0.46	-0.10	-1.30
	Ph	**2**	0.85	0.44	-0.13	-1.43
	Mes	**3**	0.83	0.41	-0.13	-1.46
Py	F_5Ph	**1**		0.54	-1.02[a]	-1.40
	Ph	**2**		0.48	-1.12[a]	-1.52
	Mes	**3**		0.49	-1.16[a]	-1.55

[a]Peak potentials (E_{pc}) for irreversible redox processes; [b]Potentials were taken from multiple scans at a scan rate of 500 mV/s.

8.5.2 Solvent Effect on Redox Potentials

As shown in Figure 8-3, the first reduction of compound **1,** labeled as Red 1, shifts from $E_{1/2}$ = 0.13 V in CH_2Cl_2, to 0.05 V in PhCN and then to -0.10 V in DMSO. Similar positive shifts of potentials are also seen for two major oxidations of compound **1** as well as for the related redox reactions of compounds **2** and **3**. As seen in Figure 8-3, the cyclic voltammogram of compound **1** in pyridine is quite different from the cyclic voltammograms in the other three solvents, namely, there is one reversible oxidation at $E_{1/2}$ = 0.54 V, one irreversible reduction at E_p = -1.02 V and one reversible reduction at $E_{1/2}$ = -1.40 V. The earlier described spectroscopic data of compounds **1-3** in pyridine suggests the binding of two Py axial ligands and a proposed electron configuration of $(DPP^{3-})Co^{III}(Py)_2$. This is consistent with the electrochemical behavior of the three compounds in this solvent.

8.4.3 Effect of *Meso*-Substituents

In all four solvents, compound **1** is easier to reduce and harder to oxidize than compounds **2** and **3** due to the highly electron-withdrawing F_5Ph- group on the *meso*-position of the dipyrrin ligand. For example, in CH_2Cl_2, the $E_{1/2}$ for the first reduction is shifted positively by 50 mV as compared with the same electrode reactions of compound **2**, while an 80 mV positive shift is seen for the first oxidation of compound **1**. The substituent effect is even larger for the second reduction in all four solvents. The difference in $E_{1/2}$ between the second reductions of compounds **1** and **2** ranges from 60 to 130 mV depending upon the solvent.

8.5.4 "Extra" Reductions in CH_2Cl_2.

Unlike in other solvents, the second reduction of compounds **1-3** in CH_2Cl_2 is irreversible and an additional irreversible reduction is observed at more negative potential. A similar irreversibility is also seen upon reduction of Co(II) porphyrins[15, 34] and electrogenerated Co(II) corroles[35] in CH_2Cl_2, and this was explained by a chemical reaction between the low oxidation state electon-reduction product and the CH_2Cl_2 solvent.

Cyclic voltammograms illustrating the reduction of compound **1** under different solution conditions are given in Figure 8-4. As seen in the figure, an extra reduction is not observed at -60 °C in CH_2Cl_2 as compared to what is seen at room temperature and it is also not observed in PhCN where the doubly reduced dipyrrin complexes are stable. The cyclic voltammogram at -60 °C in CH_2Cl_2 is quite similar to the one in PhCN, providing evidence for a reaction of the doubly reduced species with the CH_2Cl_2 solvent.

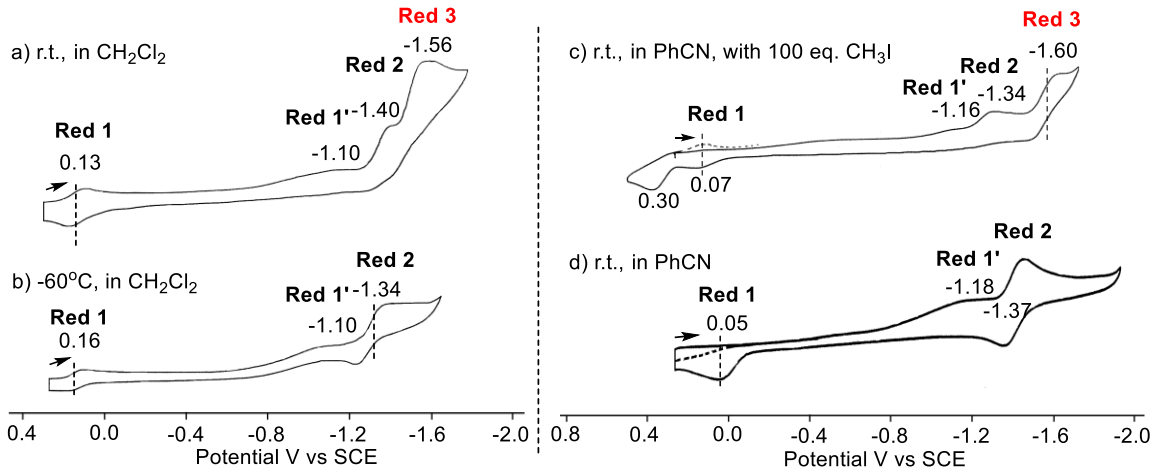

Figure 8-4. Cyclic voltammograms of compound **1** (~10^{-3} M) under different solution conditions: (a) at room temperature (r.t.), (b) at -60 °C in CH_2Cl_2, (c) at r.t. in PhCN containing 100 eq. of added CH_3I and (d) in PhCN without CH_3I.

8.6 Spectroelectrochemical Studies

The spectral changes that occurred during each redox reaction were monitored by UV-visible spectroelectrochemistry in the different solvents. Examples of the time-resolved spectral changes for compound **1** are given in Figure 8-5 and the proposed mechanism for all major redox reactions of this compound is given in Scheme 8-4.

Although spectra of the neutral compounds vary with change of solvent, the spectra of the one-electron reduced species (Figure 8-5b) are almost independent of solvent and are characterized by bands at 626-639 nm and 362-374 nm. The similarity in UV-visible spectra after the first electron addition of each compound under different solution conditions indicates that the electrophilic properties (binding properties) of the four investigated solvents has little to no effect on the one-electron reduced species. According to the previous study on a related cobalt dipyrrin complex,[1] the reactant in the first reduction can be assigned as $(DPP^{\bullet 2-})Co^{II}$, which would then be reduced to $(DPP^{3-})Co^{II}$ as shown in Scheme 8-4.

The spectra of the two-electron reduced species (Figure 8-7c) are also identical to each other in PhCN, DMSO and pyridine but not in CH_2Cl_2 where, as indicated by the CV curves, a chemical reaction occurs between the doubly reduced DPP derivatives and the solvent. During the second reduction, the intense visible bands of the one-electron reduced species at 626 to 639 nm decrease in intensity while new bands grow in at 511 to 515 nm. The decrease in intensity of the major absorption bands indicates a loss of conjugation in the DPP ligand upon the second electron addition. At the same time, new

bands at 803 to 809 nm are seen in the spectra when measured in PhCN, DMSO or pyridine, and those bands can be considered as diagnostic criteria for a redox reaction involving the ligand.

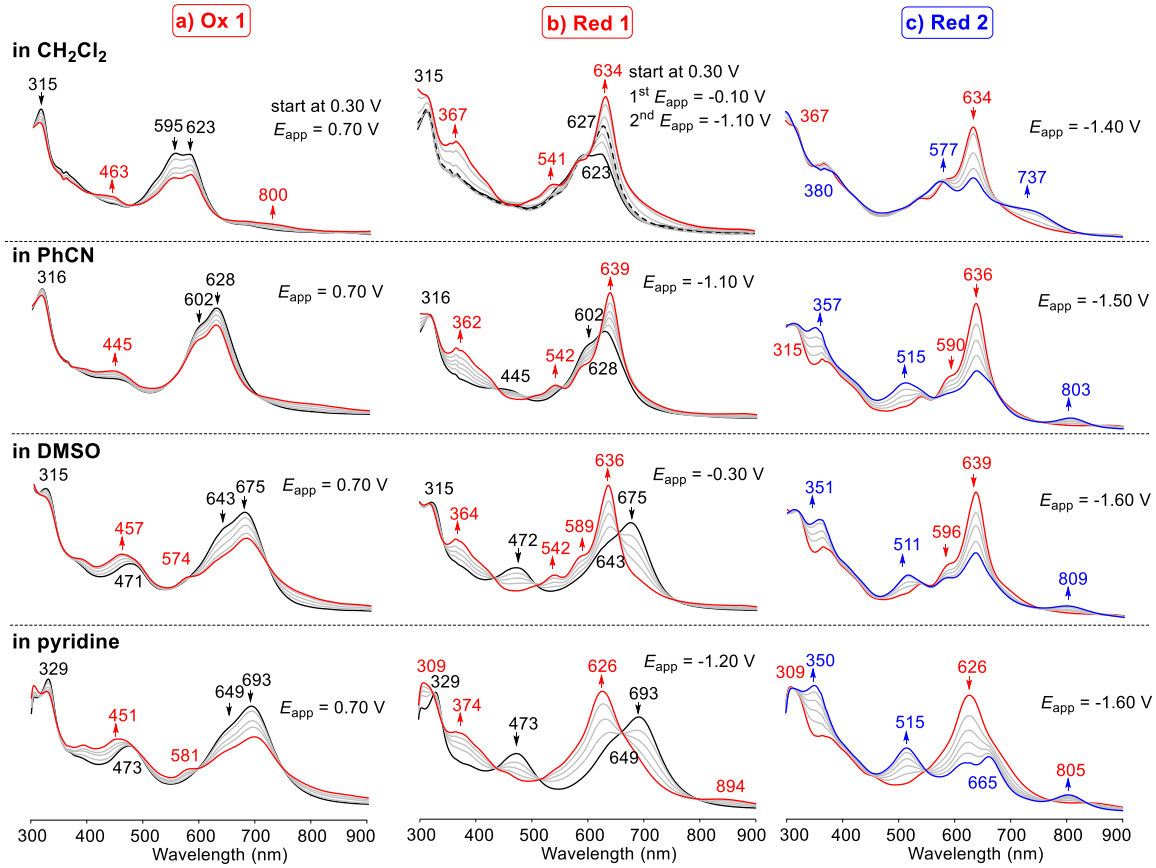

Figure 8-5. UV-vis spectral changes of compound **1** during (a) the first oxidation, (b) the first reduction and (c) the second reduction in four different solvents.

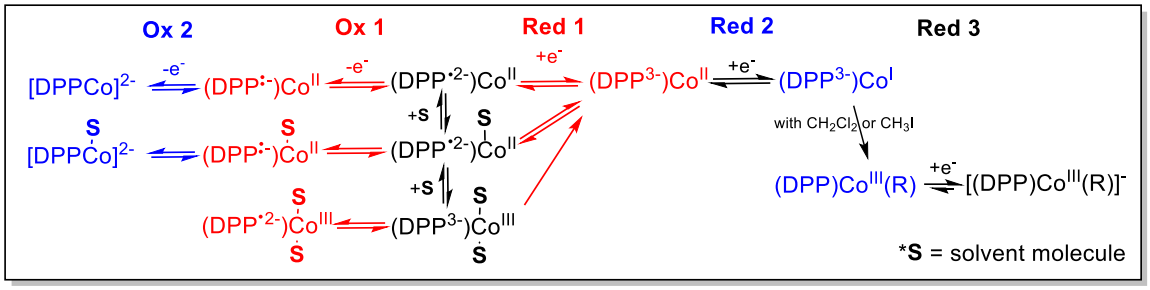

Scheme 8-4. Proposed mechanism for redox reactions of DPPCo complexes **1-3** in different solvents. (S = PhCN or DMSO for 5c complexes, S = pyridine for 6c complexes)

8.7 Conclusions

In summary, three cobalt dipyrrin-bisphenol complexes with different *meso*-aryl substituents have been synthesized, and their spectroscopic and electrochemical properties characterized in both noncoordinating and coordinating solvents. The various charge, spin, and axial ligation states have also been examined by means of DFT calculations, as given in the reference.[32] The experimental and computational studies, together, afford detailed insights into the question of ligand noninnocence in the DPPCo complexes.

The facile reduction potentials ($E_{1/2}$ ~ 0.0 V vs. SCE) of the complexes in noncoordinating (CH_2Cl_2) and weakly coordinating solvents (PhCN and DMSO) are suggestive of a $(DPP^{\bullet 2-})Co^{II}$ formulation for the neutral complexes, a conclusion which is consistent with the DFT calculations.[32] This contrasts with what is seen in pyridine where the complexes are reduced at significantly more negative potentials ($E_{1/2}$ ~ -1.0 V), thus indicating a 6c low-spin Co(III) center that is quite resistant to reduction. The fact that the one-electron reduced state exhibits similar optical spectra in all four solvents appears to indicate a common 4c or 5c $(DPP^{3-})Co^{II}$ state throughout, again consistent with the DFT calculations.[32] Our spectral studies do not allow a definitive assignment of the cationic states. DFT calculations,[32] however, indicate a $(DPP^{-})Co^{II}$ state, with a doubly oxidized DPP ligand, for the 5c complexes and a $(DPP^{\bullet 2-})Co^{III}$ state, with a low-spin Co(III) center for the 6c complexes. A ferromagnetically coupled, $S = 1$ $(DPP^{\bullet 2-})Co^{II}$ description for the

5c monopyridine complex also provides an explanation for the observed slow binding of a second pyridine ligand leading to the 6c low-spin Co(III) bispyridine complex.

The $(DPP^{\bullet 2-})Co^{II}$, $(DPP^{3-})Co^{II}$, and $(DPP^{-})Co^{II}$ formulations of the neutral, anionic, and cationic states of the 5c complexes exactly parallel the $(DPP^{\bullet 2-})Co^{II}$, $(DPP^{3-})Co^{II}$, and $Co^{II}DPP^{-}$ formulations proposed for the analogous charged states of 5c CorCo monopyridine adducts.[19] The ground-state $(DPP^{\bullet 2-})Co^{II}$ description is analogous to that proposed for CorCo, CorCo(PPh_3) and CorCo(CO), as well as to that of MnCl, FeCl, FeNO, $Fe_2(\mu\text{-}O)$, Cu and Pt corrole derivatives.[11] These extensive parallels between DPP and corrole potentially presage a bright future for transition metal DPP complexes in areas such as catalytic transformations and small molecule sensing, where metallocorroles are already playing a significant role.

8.8 References

[1] A. Kochem, L. Chiang, B. Baptiste, C. Philouze, N. Leconte, O. Jarjayes, T. Storr, F. Thomas, Ligand-Centered Redox Activity in Cobalt(II) and Nickel(II) Bis(phenolate)-Dipyrrin Complexes, *Chem. Eur. J.* **2012**, *18*, 14590-14593.

[2] Y. Feng, L. A. Burns, L.-C. Lee, C. D. Sherrill, C. W. Jones, Co(III) Complexes of Tetradentate X3L Type Ligands: Synthesis, Electronic Structure, and Reactivity, *Inorg. Chim. Acta* **2015**, *430*, 30-35.

[3] L. Lecarme, A. Kochem, L. Chiang, J. Moutet, F. Berthiol, C. Philouze, N. Leconte, T. Storr, F. Thomas, Electronic Structure and Reactivity of One-Electron-Oxidized Copper(II) Bis(phenolate)-Dipyrrin Complexes, *Inorg. Chem.* **2018**, *57*, 9708-9719.

[4] M. Yamamura, H. Takizawa, Y. Gobo, T. Nabeshima, Stable neutral radicals of planar N2O2-type dipyrrin platinum complexes: hybrid radicals of the delocalized organic π-orbital and platinum d-orbital, *Dalton Trans* **2016**, *45*, 6834-6838.

[5] L. Lecarme, L. Chiang, J. Moutet, N. Leconte, C. Philouze, O. Jarjayes, T. Storr, F. Thomas, The structure of a one-electron oxidized Mn(III)-bis(phenolate)dipyrrin radical complex and oxidation catalysis control via ligand-centered redox activity, *Dalton Trans.* **2016**, *45*, 16325-16334.

[6] J. Deschamps, Y. Chang, A. Langlois, N. Desbois, C. P. Gros, P. D. Harvey, The First Example of Cofacial Bis(dipyrrins), *New J. Chem.* **2016**, *40*, 5835-5845.

[7] N. Sakamoto, C. Ikeda, M. Yamamura, T. Nabeshima, Structural Interconversion and Regulation of Optical Properties of Stable Hypercoordinate Dipyrrin-Silicon Complexes, *J. Am. Chem. Soc.* **2011**, *133*, 4726-4729.

[8] C. Ikeda, S. Ueda, T. Nabeshima, Aluminium Complexes of N2O2-type Dipyrrins: the First Hetero-multinuclear Complexes of Metallo-dipyrrins with High Fluorescence Quantum Yields, *Chem. Commun.* **2009**, 2544-2546.

[9] S. El Ghachtouli, K. Wojcik, L. Copey, F. Szydlo, E. Framery, C. Goux-Henry, L. Billon, M.-F. Charlot, R. Guillot, B. Andrioletti, A. Aukauloo, Dipyrrinphenol-Mn(III)

Complex: Synthesis, Electrochemistry, Spectroscopic Characterization and Reactivity, *Dalton Trans.* **2011**, *40*, 9090-9093.

[10] J. H. Palmer, Transition Metal Corrole Coordination Chemistry. A Review Focusing on Electronic Structural Studies, *Struct. Bonding* **2012**, *142*, 49-90.

[11] A. Ghosh, Electronic Structure of Corrole Derivatives: Insights from Molecular Structures, Spectroscopy, Electrochemistry, and Quantum Chemical Calculations, *Chem. Rev.* **2017**, *117*, 3798-3881.

[12] Y. Fang, Z. Ou, K. M. Kadish, Electrochemistry of Corroles in Nonaqueous Media, *Chem. Rev.* **2017**, *117*, 3377-3419.

[13] R. Guilard, J.-M. Barbe, C. Stern, K. M. Kadish, New Developments in Corrole Chemistry: Special Emphasis on Face-to-face Bismacrocycles, **2003**, *18*, 303-349.

[14] R. Hoffmann, Building Bridges Between Inorganic and Organic Chemistry, *Prix Nobel* **1982**, 173-205.

[15] X. Ke, R. Kumar, M. Sankar, K. M. Kadish, Electrochemistry and Spectroelectrochemistry of Cobalt Porphyrins with π-Extending and/or Highly Electron-Withdrawing Pyrrole Substituents. In Situ Electrogeneration of σ-Bonded Complexes, *Inorg. Chem.* **2018**, *57*, 1490-1503.

[16] K. M. Kadish, E. Van Caemelbecke, G. Royal, in *Porphyrin Handbook, Vol. 8* (Eds.: K. M. Kadish, K. M. Smith, R. Guilard), Academic Press, **2000**, pp. 1-114.

[17] X. Jiang, W. Shan, N. Desbois, V. Quesneau, S. Brandes, E. Van Caemelbecke, W. R. Osterloh, V. Blondeau-Patissier, C. P. Gros, K. M. Kadish, Mono-DMSO ligated cobalt nitrophenylcorroles: electrochemical and spectral characterization, *New J. Chem.* **2018**, *42*, 8220-8229.

[18] X. Jiang, M. L. Naitana, N. Desbois, V. Quesneau, S. Brandes, Y. Rousselin, W. Shan, W. R. Osterloh, V. Blondeau-Patissier, C. P. Gros, K. M. Kadish, Electrochemistry of Bis(pyridine)cobalt (Nitrophenyl)corroles in Nonaqueous Media, *Inorg. Chem.* **2018**, *57*, 1226-1241.

[19] S. Ganguly, J. Conradie, J. Bendix, K. J. Gagnon, L. J. McCormick, A. Ghosh, Electronic Structure of Cobalt-Corrole-Pyridine Complexes: Noninnocent Five-Coordinate Co(II) Corrole-Radical States, *J. Phys. Chem. A* **2017**, *121*, 9589-9598.

[20] S. Ganguly, D. Renz, L. J. Giles, K. J. Gagnon, L. J. McCormick, J. Conradie, R. Sarangi, A. Ghosh, Cobalt- and Rhodium-Corrole-Triphenylphosphine Complexes Revisited: The Question of a Noninnocent Corrole, *Inorg. Chem.* **2017**, *56*, 14788-14800.

[21] Z. Gross, L. Simkhovich, N. Galili, First Catalysis by Corrole Metal Complexes: Epoxidation, Hydroxylation, Cyclopropanation, *Chem. Commun.* **1999**, 599-600.

[22] A. Mahammed, H. B. Gray, A. E. Meier-Callahan, Z. Gross, Aerobic Oxidations Catalyzed by Chromium Corroles, *J. Am. Chem. Soc.* **2003**, *125*, 1162-1163.

[23] S. H. Wang, B. S. Mandimutsira, R. Todd, B. Ramdhanie, J. P. Fox, D. P. Goldberg, Catalytic Sulfoxidation and Epoxidation with a Mn(III) Triazacorrole: Evidence for A "Third Oxidant" in High-Valent Porphyrinoid Oxidations, *J. Am. Chem. Soc.* **2004**, *126*, 18-19.

[24] L. Simkhovich, Z. Gross, Iron(IV) Corroles Are Potent Catalysts for Aziridination of Olefins by Chloramine-T, *Tetrahedron Lett.* **2001**, *42*, 8089-8092.

[25] M. J. Zdilla, M. M. Abu-Omar, Mechanism of Catalytic Aziridination with Manganese Corrole: The Often Postulated High-Valent Mn(V) Imido Is Not the Group Transfer Reagent, *J. Am. Chem. Soc.* **2006**, *128*, 16971-16979.

[26] L. Simkhovich, A. Mahammed, I. Goldberg, Z. Gross, Synthesis and Characterization of Germanium, Tin, Phosphorus, Iron, and Rhodium Complexes of Tris(pentafluorophenyl)corrole, and the Utilization of the Iron and Rhodium Corroles as Cyclopropanation Catalysts, *Chem. - Eur. J.* **2001**, *7*, 1041-1055.

[27] R. Guilard, C. P. Gros, F. Bolze, F. Jerome, Z. Ou, J. Shao, J. Fischer, R. Weiss, K. M. Kadish, Alkyl and Aryl Substituted Corroles. 1. Synthesis and Characterization of Free Base and Cobalt Containing Derivatives. X-ray Structure of (Me4Ph5Cor)Co(py)2, *Inorg. Chem.* **2001**, *40*, 4845-4855.

[28] J.-M. Barbe, G. Canard, S. Brandes, F. Jerome, G. Dubois, R. Guilard, Metallocorroles as Sensing Components for Gas Sensors: Remarkable Affinity and Selectivity of Cobalt(III) Corroles for CO vs. O2 and N2, *Dalton Trans.* **2004**, 1208-1214.

[29] H. Vazquez-Lima, J. Conradie, A. Ghosh, Metallocorrole Interactions with Carbon Monoxide, Nitric Oxide, and Nitroxyl - A DFT Study of Low-Energy Bound States, *Inorg. Chem.* **2016**, *55*, 8248-8250.

[30] S. Yang, Y. Wo, M. E. Meyerhoff, Polymeric Optical Sensors for Selective and Sensitive Nitrite Detection Using Cobalt(III) Corrole and Rhodium(III) Porphyrin as Ionophores, *Anal. Chim. Acta* **2014**, *843*, 89-96.

[31] R. D. Rieth, N. P. Mankad, E. Calimano, J. P. Sadighi, Palladium-catalyzed Cross-coupling of Pyrrole Anions with Aryl Chlorides, Bromides, and Iodides, *Org. Lett.* **2004**, *6*, 3981-3983.

[32] W. Shan, N. Desbois, S. Pacquelet, B. Stephane, Y. Rousselin, J. Conradie, A. Ghosh, C. P. Gros, K. M. Kadish, Ligand Noninnocence in Cobalt Dipyrrin-Bisphenols: Spectroscopic, Electrochemical, and Theoretical Insights Indicating an Emerging Analogy with Corroles, *Inorg. Chem.* **2019**, Ahead of Print.

[33] V. Quesneau, W. Shan, N. Desbois, S. Brandes, Y. Rousselin, M. Vanotti, V. Blondeau-Patissier, M. Naitana, P. Fleurat-Lessard, E. Van Caemelbecke, K. M. Kadish, C. P. Gros, Cobalt Corroles with Bis-Ammonia or Mono-DMSO Axial Ligands. Electrochemical, Spectroscopic Characterizations and Ligand Binding Properties, *Eur. J. Inorg. Chem.* **2018**, *2018*, 4265-4277.

[34] K. M. Kadish, X. Q. Lin, B. C. Han, Chloride-binding Reactions and Electrochemistry of (Tetraphenylporphyrinato)cobalt and Chloro(tetraphenylporphyrinato)cobalt in Dichloromethane, *Inorg. Chem.* **1987**, *26*, 4161-4167.

[35] K. M. Kadish, J. Shen, L. Fremond, P. Chen, M. El Ojaimi, M. Chkounda, C. P. Gros, J.-M. Barbe, K. Ohkubo, S. Fukuzumi, R. Guilard, Clarification of the Oxidation State of

Cobalt Corroles in Heterogeneous and Homogeneous Catalytic Reduction of Dioxygen, *Inorg. Chem.* **2008**, *47*, 6726-6737.